MECHANICAL PROPERTIES OF GRANULAR
MATERIALS AS RELATED TO LOADS
IN CYLINDRICAL GRAIN
SILOS

By

Lawrence O. Gumbe, Ph.D.

The Ohio State University, 1987

Professor Gordon L. Nelson, Adviser

Physical quantities thought to be pertinent to the
development of loads in cylindrical silos filled with
granular materials were identified. The principles of
similitude and dimensional analysis were used to formulate,
organize, and analyze data from experiments in order to
arrive at prediction equations for loads in silos.

Dimensionless Π-terms were used for the prediction
equation. Experiments were carried out to investigate the
validity of Janssen's constant, k, the ratio of the
horizontal to the vertical pressure in granular materials
en-masse. It was concluded that k is not an independent
material property.

The study revealed that particle size (λ), height-to-
diameter ratio (H/D), relaxation modulus (E(t))

1

and grain depth (z) are pertinent to the development of pressures in grain filled silos. Inertial effects were found to be unimportant to the development of pressures in silos. The phenomenon of dynamic overpressure in emptying silos was observed.

MECHANICAL PROPERTIES OF GRANULAR

MATERIALS AS RELATED TO

LOADS IN CYLINDRICAL

GRAIN SILOS

DISSERTATION

Presented in Partial Fulfillment of the Requirements for

the Degree of Doctor of Philosophy in the Graduate

School of The Ohio State University

By

Lawrence Otweyo-Migire Gumbe

B.Sc., (Hons) University of Nairobi

M.Sc., Cranfield Institute of Technology

★ ★ ★ ★ ★

The Ohio State University

1987

Reading Committee: Approved by:

G.L. Nelson, Ph.D.

S.K. Chaturvedi, Ph.D.

F.L. Herum, Ph.D.   Gordon L. Nelson, Adviser
                                             Dept. of Agricultural
                                                  Engineering

To Ezra Owiti Gumbe

... a great lover of

Education

'Elimu ni Bahari'

ACKNOWLEDGMENTS

VITA

July 28, 1957 .... Born, Kisumu, Kenya

July, 1980 .... B.Sc. (Hons) University of
                                  Nairobi, Engineering
                                  (Agricultural)

July-October, 1980 .... Coffee Factory Engineer,
                                  Ministry of Agriculture,
                                  Nairobi, Kenya

October, 1981 .... M.Sc., Cranfield Institute
                                  of Technology, England

October, 1981 .... Member of the Agricultural
                                  Engineering Faculty,
                                  University of Nairobi,
                                  Kenya

September, 1984 .... On deputation to the
                                  Department of Agricultural
                                  Engineering, The Ohio
                                  State University,
                                  Columbus, Ohio

FIELDS OF STUDY

Agricultural Engineering:

Professor G.L. Nelson

Professor C. Hansen

Civil Engineering:

Professor S.K. Chaturvedi

Professor K.W. Bedford

Engineering Mechanics:

Professor A.E. Engin

Professor A. Gilat

Professor N. Katsube

Professor J.K. Lee

Education:

Professor R.K. Barrick

Finite Element Method:

Professor J.K. Lee

Mathematics:

Professor D. Burghelea

Statistics:

    Professor W.I. Notz

    Professor J.D. Powers

Mechanical Engineering:

    Professor M.A. Drake

    Professor M.J. Moran

Computer and Information Science:

    Professor J.S. Ely

TABLE OF CONTENTS

LIST OF TABLES

LIST OF FIGURES

LIST OF PLATES

INTRODUCTION

The irregularity of harvest yields, and the unequal
distribution of cereals throughout the world, has resulted
in unequal consumption of cereals (54). This has led to
building up of stocks in order to assure more uniform
supply. The recent tragic famines in Africa, and other
parts of the third world, have led to urgent efforts to
increase food production -- especially grains. These
efforts will be futile if good storage is not provided for
the increased harvest. According to the Kenya government,
"Sessional Paper No. 4 on National Food Policy," (1981)
about 30% of all grain harvested in Kenya is lost through
bad storage practices (18).

The obvious choice for grain storage on the large scale
necessary for modern expanded agricultural production, is
the silo, which, according to Reimbert and Reimbert (54),
…"does away with the burdensome use of sacks and reduces
labor costs." Containers for the storage of bulk solids
are called bins, bunkers, silos, and tanks (15). The terms
"bin," "silos" and "bunkers" have different meanings in
different parts of the world and may vary from author to

1

author (43). In the United States the term "bin" generally includes both silos and bunkers, silos being deep bins and bunkers shallow bins (41). The word "silo" originated in the Greek language as "siros" meaning a pit to store grain and over the centuries has managed to retain this particular emphasis (65). Today, the complete reference is more general, including below and above ground storage of a variety of materials and objects (48). The silo is ideally suited for storage of bulk material like grains, as it acts as a storage device, provides protection to and from the environment, and allows for a relatively problem free unloading system using a rather inexpensive motive force, gravity (65).

The physical properties of materials stored in silos and bunkers influence the flowability of the material and the forces that the material applies to the silo walls and bottom (58). The major problem in structural design of silos is to predict, with reasonable accuracy, the loads that these structures will be required to withstand during their service life. The mechanics of granular materials, even for reasonably homogeneous and noncohesive materials, are little understood (65). At present, the state-of-the-art of grain bin design utilizes a less than satisfactory approach to the determination of horizontal and vertical sidewall pressures (69). Indeed, a recent survey in Sweden found that about 25% of concrete bins have

vertical cracks (11). It is believed that some of the structural failures in bins have been caused by the increased stresses and strains developed in the bin wall when the bin contents are being removed from the lower part of the bin. This phenomenon is known as dynamic overpressure in grain bins (63). Literature on the subject contains a great deal of experimental evidence that internal lateral grain pressures on bin walls during emptying of granular material from the bin bottom can be much greater than the static lateral pressure (63). There is controversy as to the pertinent physical quantities of granular materials that influence lateral and vertical pressures in silos. This has resulted in the development of different silo design codes in various countries. There is little agreement among the various codes of practice as to the magnitudes and distributions of pressures, especially dynamic pressures.

The identification of a complete set of physical quantities, affecting magnitude and distribution of pressures in silos, would greatly aid the development of prediction equations for silo loads. The use of the principles of dimensional analysis in the design and operation of model tests and the interpretation of model test results would further illuminate this area of study.

OBJECTIVES

The need for the identification of a complete set of pertinent physical quantities affecting grain silo pressures, and the use of similitude theory in experimental design in the development of adequate mathematical models for silo pressures is outlined in the introduction above. The principal objectives of this study are:

(1) To identify the physical quantities influencing pressures (loads) in grain silos.

(2) Using dimensional analysis, to arrive at the qualitative form of prediction equations for loads in grain silos.

(3) Using similitude theory and experimental data obtained from tests on model bins to develop prediction equations for loads in grain silos.

(4) To investigate the validity of "k", the ratio of the horizontal to vertical pressure as used in the Janssen's equation for predicting loads in grain silos.

2. LITERATURE REVIEW

Early silo designers, not recognizing the importance of vertical friction between stored material and the silo wall, assumed that lateral pressures vary hydrostatically (58). Experiments by Roberts (17) on models and full-sized silos showed that this is incorrect because some of the weight of the stored material is transferred to the wall by friction. Janssen confirmed this conclusion and in 1895 published a theory that accounts for wall friction (74). Airy proposed another method of computing wall pressures (17). A considerable amount of work by various experimenters followed, and Ketchum summarized the state of art in a book published in 1909 (15). These methods, which take into account wall friction, provide means for computing

    (i) Pressure of stored material against vertical walls, sloping surfaces, and flat bottoms;

    (ii) Friction forces and wall compressive forces; and

    (iii) Vertical pressures at various depths in the stored material itself.

5

Some of these methods give static pressure only (58).
Design pressures are usually estimated by modifying the
computed static pressures to account for material movement,
eccentric discharge, and other pressure affecting
conditions, or by the use of analytical methods intended to
give design pressures directly.

2.1 Methods of Computing Static Pressures

Static, or more appropriately, initial pressure
theories can be categorized into three distinct methods
(65).

  (i)   The method of sliding wedges of material,
        developed by Coulomb (1776) but applied to silos
        by Airy (1897)

 (ii)   The method of differential slices as proposed by
        Janssen (1895) and used to some degree by
        Reimbert (1955).

(iii)   Characteristic or numerical methods in the
        solution of the equilibrium equations obtained
        from differential volumes, used by Sokolovski
        (1954) but applied to two-dimensional bins by
        Horne and Nedderman (1976).

These methods are based on equilibrium of the stored
material in a static condition (56). Elastic interaction
with the bin structure is not considered, nor is strain
energy in either the stored material or the structure.

These analytical methods agree with test measurements with varying degrees of accuracy. A sample of the methods described above is discussed below.

2.1.1   The Method of Sliding Wedges

This method, developed by Coulomb in (1776) appeared to have appealed to Airy only (1897). Airy's analysis resulted in the questionable prediction that horizontal pressures reach a maximum at some intermediate level and then begin to decrease. This was because Airy neglected the contribution of one of the walls in his force balance. Hancock (65) and Nedderman (1974) (65) corrected Airy's method and have shown it to be a viable technique, although the relative complexity of the solution renders it unsuitable for design purposes. The wedge method remains best suited for analyzing shallow bins and retaining walls (see Figures 2.1.1 and 2.1.2).

For bunker

Lateral pressure at depth Y:

$$P = \frac{1}{2}\gamma y^2 \left[\frac{1}{\sqrt{\mu(\mu+\mu')} + \sqrt{1+\mu^2}} \right]^2 \tag{2.1}$$

where $\mu = \tan \phi$, ϕ = angle of internal friction

8
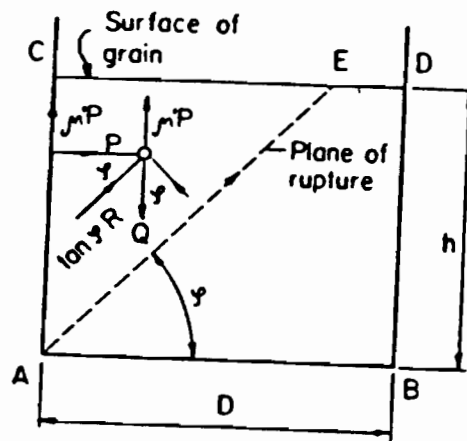
Figure 2.1a.   Dimensions for use in Airy's equation for
               bunker (Safarian and Harris, 1985)
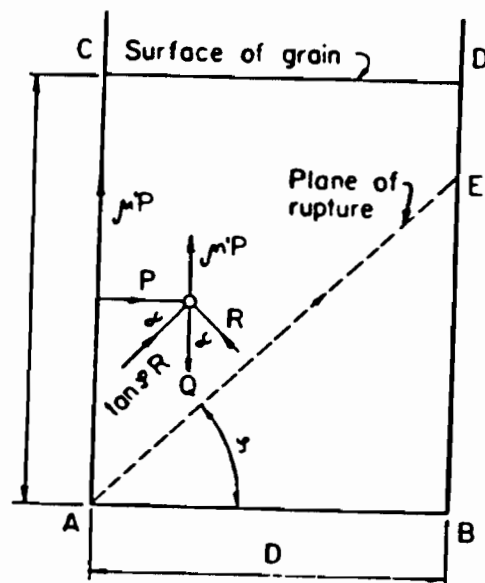
Figure 2.1b.   Dimensions for use in Airy's equation for
               silos (Safarian and Harris, 1985)

μ' = material-bin coefficient of static friction

Vertical pressure at depth Y:

q = P/k$\qquad\qquad$(2.2)

k = ratio of horizontal to vertical pressure

For silos

Lateral pressure at depth Y:

$$P = \frac{\gamma D}{\mu + \mu'}\left[1 - \sqrt{\frac{1 - \mu^2}{\frac{2y}{D}(\mu+\mu') + 1 - \mu\mu'}}\right]\qquad (2.3)$$

Vertical pressure at depth Y:

q = P/k

2.1.2 Janssen's Method

H.A. Janssen (1895) developed equations for computing lateral and vertical pressures of granular materials in deep silos. In deriving the equation, he made the following assumptions:

   (i)   Vertical pressures are uniform throughout horizontal planes.

   (ii) Horizontal pressures are uniform over the perimeter of a cross section.

   (iii) The ratio of the horizontal to the vertical pressure, k, is uniform.

Janssen's method is based on static equilibrium of a thin horizontal layer of stored material, as shown in Figure 2.

Top of fill

Y

dy

Silo

Hopper
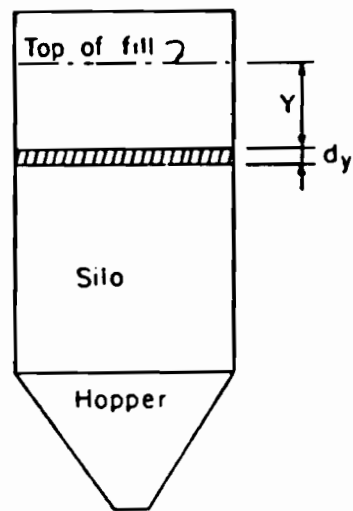
(a)
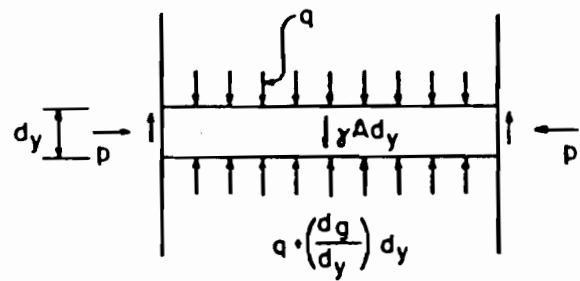
(b)   Horizontal lamina

p   = Horizontal pressure between wall
       and stored material, assumed
       uniform around perimeter U

$\gamma A d_y$ = Lamina weight

μp = Friction force per unit area of
       wall in contact with lamina

Upward and downward pressures are
assumed uniform over entire area.

Figure 2.2.   Horizontal lamina for derivation of Janssen's equation (Safarian and Harris, 1985)

Equating the summation of vertical forces to zero gives

$$qA + \gamma A dy = A[q + dy\frac{dq}{dy}] + \mu'p(Udy)$$

in which

q = static vertical pressure at depth Y

A = area of horizontal cross section through the silo

U = perimeter of cross section

p = pressure of stored material against walls at depth

  Y below surface of stored material

γ = unit weight of stored material

μ'= coefficient of friction between wall and material.

Substituting kP for p, and "hydraulic radius" R for A/U and

rearranging, the differential equation of equilibrium

becomes

$$dq/dy = \gamma - \frac{\mu'k}{R}q$$

The solution of this equation is the Janssen formula for

vertical pressure at depth Y:

$$q = \frac{\gamma R}{\mu'k}[1 - exp(\mu'ky/R)] \qquad (2.4)$$

Koenen (1896) improved Janssen's method by introducing the

term

$$k = \frac{(1 - sin\phi)}{(1 + sin\phi)}$$

where ϕ= internal angle of friction of the material or

simply

$$k = \tan^2(45° - \phi/2)$$

which is the Rankine coefficient for active earth pressure - the ratio of horizontal to vertical pressure. Thus Janssen's equation for horizontal pressure is:

$$p = \frac{\gamma R}{\mu'}[1 - \exp(-\mu'kY/R)] \qquad (2.5)$$

The vertical wall friction force is μp per unit area of wall at depth Y. Vertical friction forces at the wall-grain interface cause vertical internal force in the wall: compression if the wall is supported from below, tension if supported from above. Integrating from the top of the stored material to depth Y, the vertical force in the wall (per unit of wall perimeters) at depth Y is:

$$V_y = \mu' \int pdY = \gamma R[Y - \frac{R}{\mu'k} (1 - \exp(-\mu kY/R))] \qquad (2.6)$$

The above equation makes no assumption as to shape of silo cross section. If the cross section is circular, then the hydraulic radius is:

$$R = area/perimeter = (\pi D^2/4)/(\pi D) = D/4$$

in which D is the inside diameter.

For a square silo of side length a, R = area/perimeter = a/4. For regular polygonal silos a slightly conservative approximation is R = De/4 where De is the diameter of a

circle whose area equals that of the polygon.

A rectangular silo with side lengths a and b will have different pressures on short and long sides. A common procedure is to let R = a/4 when computing pressure on the short side, and for the long side to assume R = a'/4 where:

$$a' = \frac{2ab}{a+b} \qquad (2.7)$$

An alternate a' suggested by Reimbert is to use

$$a' = \frac{2ab - a^2}{b} \qquad (2.8)$$

The silo designer needs to know the total vertical force applied to the wall by friction from the stored material. This vertical force from above at any depth Y, is equal to the weight of those materials minus the upward force from vertical pressure q. Per unit length of wall, the friction force from above is

$$V = R(\gamma Y - q) \qquad (2.9)$$

A state of controversy surrounds the k value, the horizontal to vertical pressure ratio. A discussion of this is included in Section 2.4.

2.1.3 The Reimbert Method

Marcel and André Reimbert (25) presented a method for computing static pressure due to stored material in 1953 and 1954. Their method recognizes that at large depth Y,
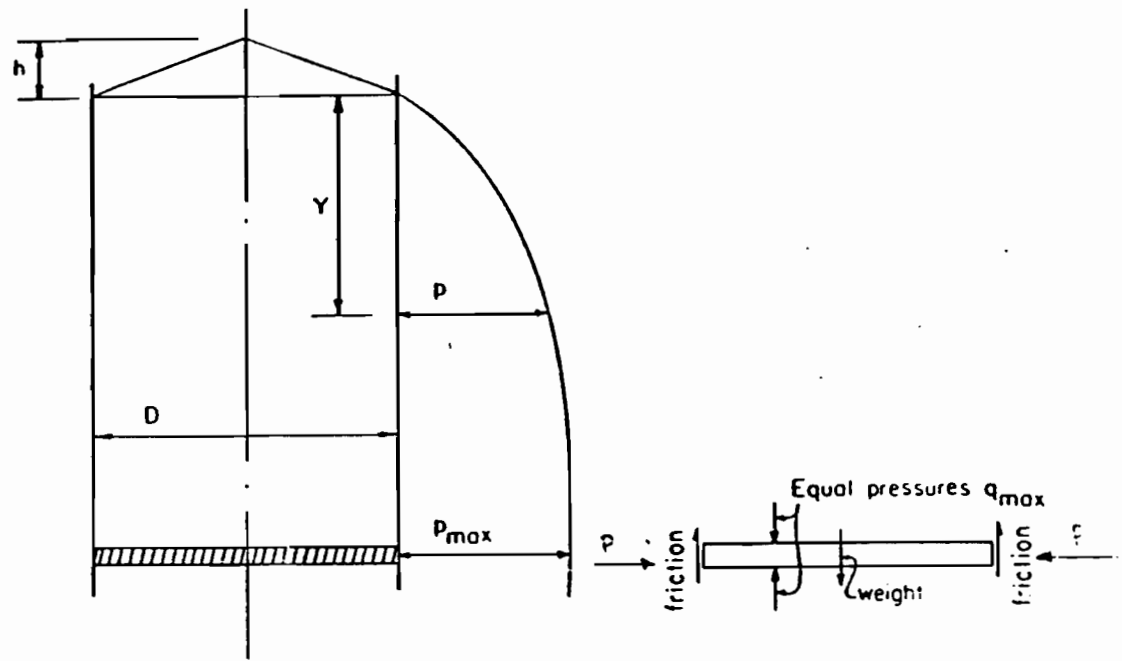
Figure 2.3a & Figure 2.3b.   Lamina of stored material
                    for derivation of Reimbert's Equation
                    (Safarian and Harris, 1985)
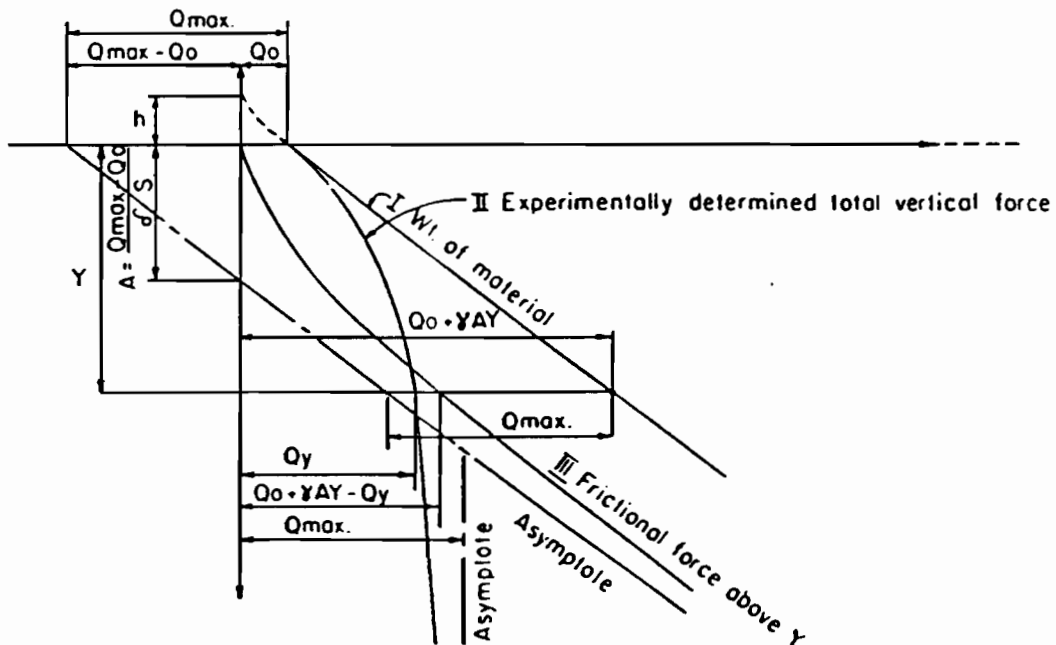
Figure 2.4.   Curves of lateral and vertical pressure
              and wall friction used in deriving Reimbert's
              Equation (Safarian and Harris, 1985)

vertical axis (26). This can be shown by noting that for large Y-values, the first derivative dP/dY, approaches zero (25, 26). At that depth the lateral pressure reaches a maximum, shown as p_{max} in Figure 2.3a. A lamina of material at this depth shows in Figure 2.3b. It has equal vertical pressure above and below. Consequently, the lamina weight is exactly balanced by wall friction, or:

$$\gamma A dy = \mu' \ p_{max} U dy$$

where U = perimeter

Thus:

$$P_{max} = \gamma R / \mu' \qquad (2.10)$$

in which R is the hydraulic radius A/U. Vertical pressure at this location is

$$q_{max} = P_{max}/k = \gamma R / (\mu' k) \qquad (2.11)$$

Allowing for a cone of material at the top of the silo, the total weight of material above depth Y is,

$$\gamma A Y + \gamma A h / 3$$

Curve I, Figure 2.4 represents the total weight graphically. If there were no frictional force it would exactly equal the resultant vertical pressure on the top of a lamina at depth Y. Curve III is a representation of the total friction force on the walls above depth Y, and curve II the total vertical force on top of the lamina.

Therefore,

Vertical force (Curve II) =

Weight (Curve I) - Total friction (Curve III)

M. and A. Reimbert showed experimentally that the shape of Curve III is closely expressed by the form

$$z = \frac{a_1 Y^2 + a_2 Y + a_3}{b_1 y + b_2}$$

(2.12)

Using the five boundary conditions in Figure 2.4, they evaluated five constants in (2.12) above. The Reimbert equation thus derived, comes from experimental data unlike the purely theoretical Janssen's equation.

The Reimbert equations for static pressure are listed below (20):

Vertical pressure at depth Y below stored material surface:

$$q = \gamma \left[Y \left(Y\frac{Y}{c} + 1 \right)^{-2} + \frac{h}{3} \right]$$

(2.13)

Lateral static pressure at depth Y:

$$p = P_{max} \left[1 - \left(\frac{Y}{c} + 1 \right)^{-2} \right]$$

(2.14)

For circular silos the term p_{max} and c (characteristic abscissa) in the above equation are:

abscissa) in the above equation are:

$$p_{max} = a/D(4\mu')$$ (2.15)

$$C = \frac{D}{4\mu'k} - \frac{h}{3}$$ (2.16)

2.1.4 Characteristic or Numerical Methods

This approach encompasses a number of methods that formulate the equilibrium equation using a differential volume rather than a cross-sectional slice and therefore the solutions are labeled "exact" (32). This is a very subjective description because often the initial assumptions, such as the adoption of particular failure criteria, are more important than the method of solution (32).

Figure 2.5 shows the standard elemental volume for plane strain conditions. The resulting equilibrium equations are

$$\frac{\partial \sigma_z}{\partial z} + \frac{\partial \tau_{xz}}{\partial x} = \gamma \qquad \frac{\partial \sigma_x}{\partial x} + \frac{d\tau_{zx}}{\partial z} = 0$$ (2.17)

The equation was numerically solved by Sokolovski (1954) for a retained soil mass using the method of characteristics. Being statically indeterminate, Sokolovskii adopted Mohr-Coulomb failure criteria, in solving the problem:
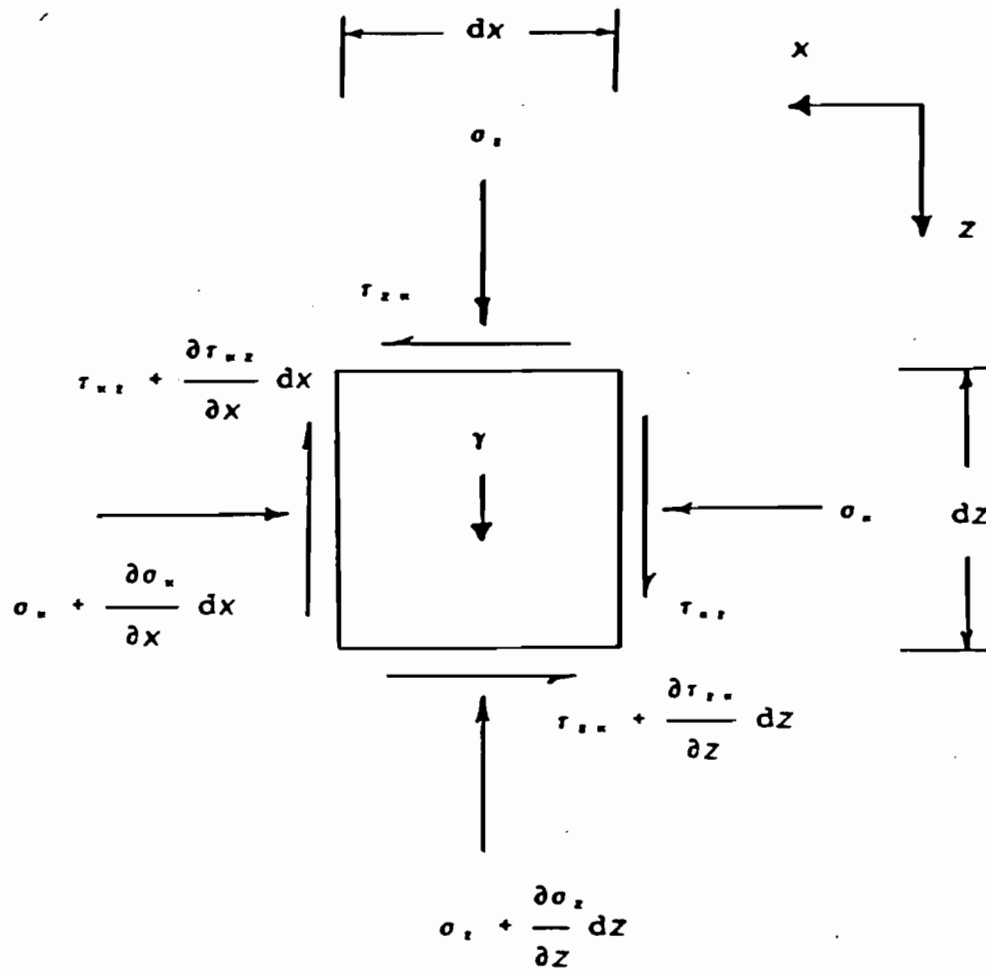
Figure 2.5. Average values of stress on a material
element (plain strain) (Smith, 1983)

$$\sigma_z = p(1 + \sin\theta \cos2\psi) \qquad\qquad (2.18a)$$

$$\sigma_x = p(1 - \sin\theta \cos2\psi) \qquad\qquad (2.18b)$$

$$\tau_{zx} = -\tau_{xz} = p \sin\theta \cos2\psi \qquad\qquad (2.18c)$$

where p is the average of the principal stresses and ψ is the angle of rotation of the principal plane.

This criterion assumes that throughout the mass, the material is in a state of incipient active failure. Given appropriate boundary conditions such as surcharge at the material's surface and the frictional relationship at the bin walls (or a line of symmetry at the bin center line), a numerical soution can proceed along a mesh of characteristics that intersect one another at the angle

$\pi/2 - \phi$ (32).

Horne and Nedderman found that the solution followed a modified-Janssen solution (32) that tended to similar values with increasing depth. At shallow depths, however, and depending on the amount of surcharge, this "exact" solution yielded distinct variation in the rate of change of material pressures that forced the pressure curve to oscillate about the modified-Janssen solution. A characteristic, propagated from an upper corner (where the boundary conditions are discontinuous), will cause a discontinuity in the stress derivatives where it intersects
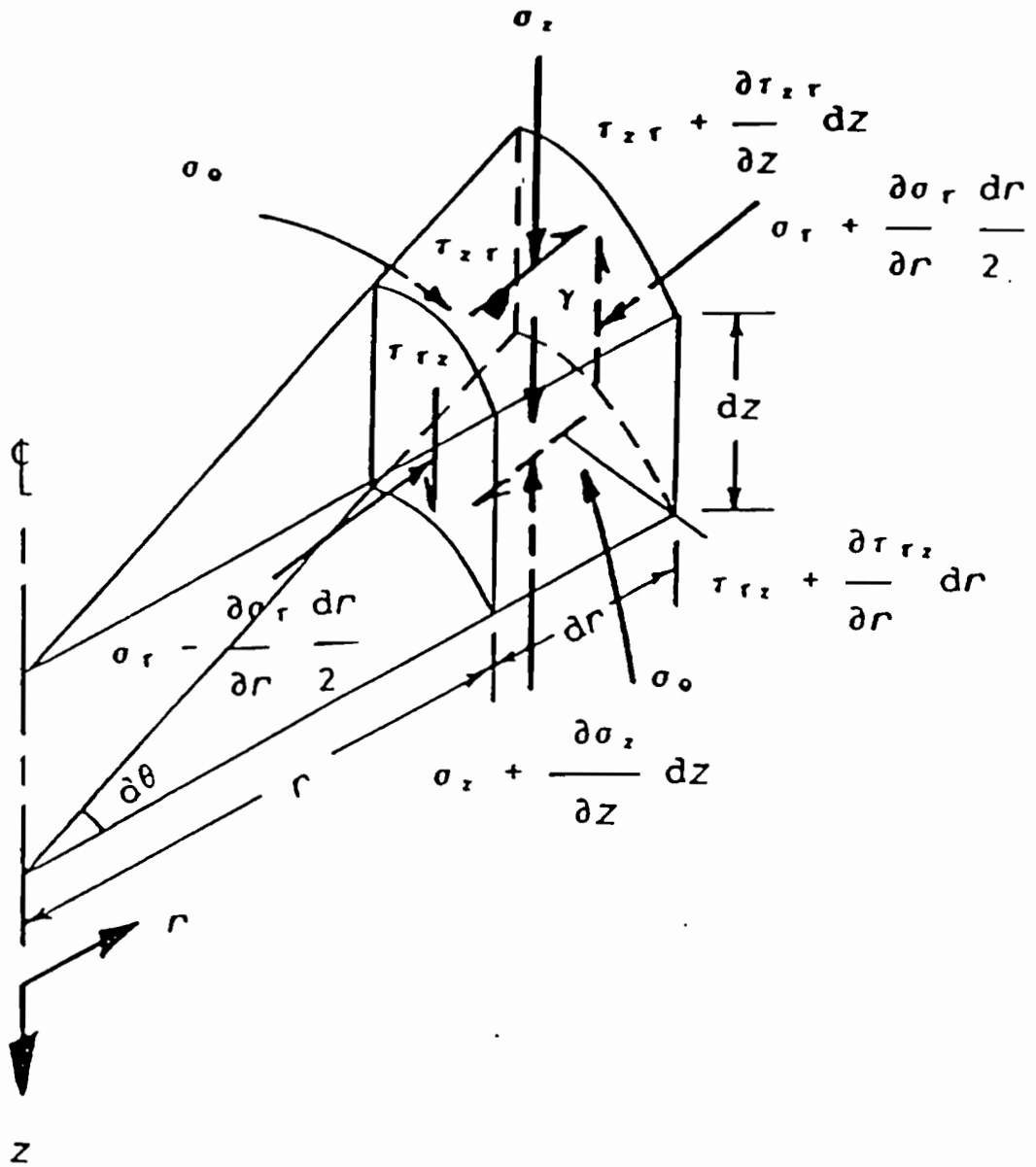
Figure 2.6.   Average values of stress on a material
element (axisymmetry) (Smith, 1983)

the far walls. Lvin (1970) suggested that vertical
pressures are not uniform over a horizontal cross-section
and he sought to remedy this by equilibrating vertical
forces on a differential ring element (as opposed to
Janssen's disc-shaped element). He therefore formulated
his equilibrium equations on what essentially is the free
body in Figure 2.6. The equilibrium equations are:

$$\frac{\partial \sigma_z}{\partial z} + \frac{\partial \tau_{rz}}{\partial r} + \frac{\tau_{rz}}{r} = \gamma \qquad (2.19a)$$

$$\frac{\partial \sigma_r}{\partial r} + \frac{\partial \tau_{zr}}{\partial r} + \frac{\sigma_r - \sigma_\theta}{r} = 0 \qquad (2.19b)$$

The complete solution describes a family of curves, of
which Janssen's solution is one in which p is uniform at
a special depth. The upper bound of this family provides
for a variation in lateral pressure over a cross-section,
and therefore has the potential to more accurately describe
these pressures. Lvin made one questionable assumption in
arriving at a solution for this upper bound curve (32).
For vertical equilibrium in Equation 2.19a he used

$$\tau_{rz} = \mu'k\sigma_z \qquad (2.20)$$

This gave

$$\frac{\partial \sigma_z}{\partial z} + \mu'k \left[\frac{\partial \sigma_z}{\partial r} + \frac{\sigma_z}{r} \right] = \gamma \qquad (2.21)$$

In fact the equation (2.20) only holds true at the wall. At the center line of a bin, vertical shear becomes zero as required by symmetry.

Lvin's solution is unique in that it consists of two regions, the upper region of a cylinder exhibiting a parabolic increase in pressure that becomes a tangent to the usual maximum lateral pressure common to the lower region, where it remains constant. The parabolic increase is described by

$$P(z) = \gamma k z \left[1 - \frac{\mu k z}{4R} \right] \qquad (2.22)$$

The region of constant pressure begins at

$$z_c = \frac{D}{2\mu k}$$

Substituting z_c for z in the lateral pressure formula,

$$P(z_c) = \frac{\gamma k D}{2\mu'k} \left(\frac{1}{2}\right) = \frac{\gamma R}{\mu'} \qquad (2.23)$$

which again is the maximum expected value for horizontal pressure.

2.2 Dynamic Pressures

During the filling or emptying of silos, i.e., during dynamic conditions, observed pressures far exceed those for static conditions. S.A. Tachtamishev (1938, 1939) is

credited with being the first person to conduct accurate experiments on full-size industrial silos, revealing the type of flow occurring during withdrawal and its effect on pressure (21). Working in Baku (U.S.S.R.), he reported that during emptying of the silos, the lateral pressure was two to three times as large as that calculated by Janssen's method. Flow within silos is generally classified into two distinct and limiting patterns: mass flow and funnel flow. Mass flow occurs when the flow channel boundary coincides with the storage vessel's walls. Funnel flow occurs when the flow channel boundary is within the contained material. There is disagreement about the magnitude and location of the dynamic overpressures during emptying (18). The results of numerous research reports vary considerably as do the recommendations expressed in several design codes. Dynamic overpressures ranging from 1.3 to 4.0 times the static pressures have been reported. There has been little work done to quantitatively describe the two flows, i.e., mass and funnel. Jenike et al. (1973) are among the very few researchers to have presented an analytical technique that rationally attempts to predict levels of overpressure in a mass flow situation and which has been corroborated by experimental findings. A review of methods for calculating dynamic overpressures is given below, after a review of flow patterns in silos.

2.2.1 Flow Patterns

As pointed out above, flow of stored material from silos takes place in two distinct patterns. Because loads and stresses are related to flow patterns, the flow pattern should be considered in silo design.

2.2.1.1 Mass-Flow Silos

In mass flow the hopper is sufficiently steep and smooth to cause flow of all solids during emptying. Mass flow will occur if three conditions are met:

1. The outlet must be large enough for the material to flow without arching.

2. The flow-control device must permit material to flow through the entire opening area.

3. The hopper must be smooth enough and steep enough to allow the material to slide, thus expanding the flow channel upward until it meets the vertical walls of the silo.

2.2.1.2 Funnel-Flow Silos

Funnel flow occurs when the hopper is not sufficiently steep and smooth to force material to slide along the walls, or when the outlet of a mass-flow bin is not fully effective. In a funnel flow silo, solids flow towards the outlet through a channel that forms within stagnant material. In funnel flow, with non-free flowing solids,
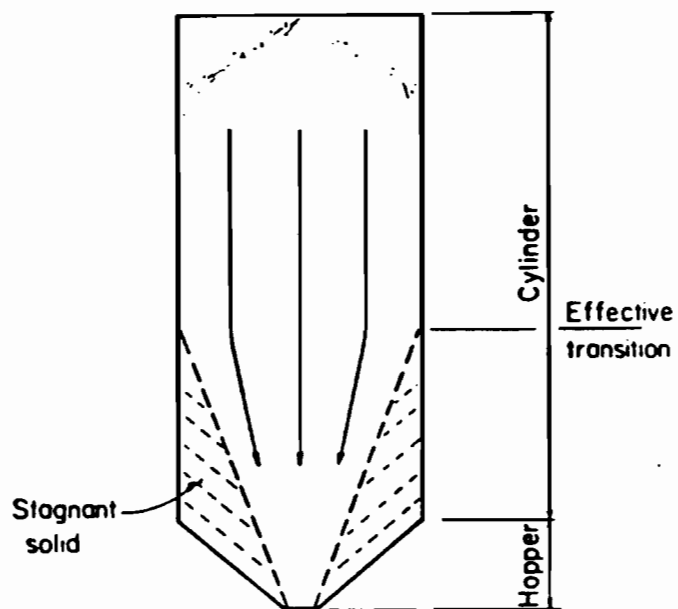
(b) Funnel flow
(or core flow)
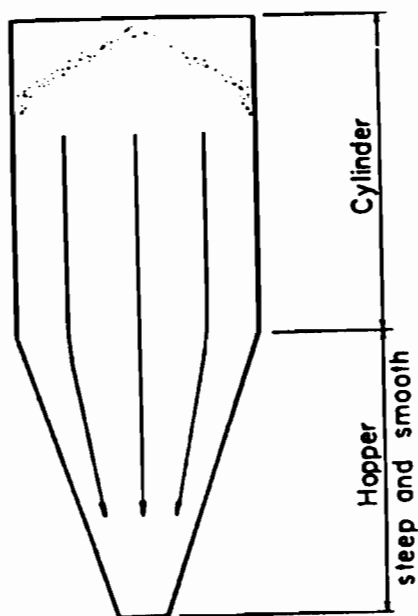
(a) Mass flow

Figure 2.7. Mass flow and funnel flow (Safarian and Harris, 1985)

the flow channel expands upward from the outlet to a diameter that approximates the largest dimension of the effective outlet. Figure 2.8 below shows charts by Jenike that may be used to predict whether mass flow or funnel flow will occur.

2.2.1.3 Other Types of Flow

Expanded flow is an intermediate type of flow besides the main two above. Expanded flow is a combination of mass flow and funnel flow. In this kind of flow, the lower part of the hopper operates in mass flow and the upper portion (nearer the cylindrical walls) operates in mass flow.

Eccentricity in filling and discharge cause unsymmetrical loading and hence provided added problems to bin design. Jenike (58) has discussed harmful flow irregularities such as arching, pulsation and shock. Pulsation occurs when the slope of the hopper wall (or of a part of the hopper wall) is in the "uncertain" region (see Figure 2.8). Pulsation results from repetitive formation and collapse of an obstruction to flow. The frequency of pulsation is directly proportional to rate of outflow, while the amplitude tends to be higher at low flow rates than at higher rates. Pulsation ceases with low enough heads of material. Pulsation occurs only when coarse materials are present; fine materials tend to inhibit pulsation. According to Jenike, pulsation is generated at
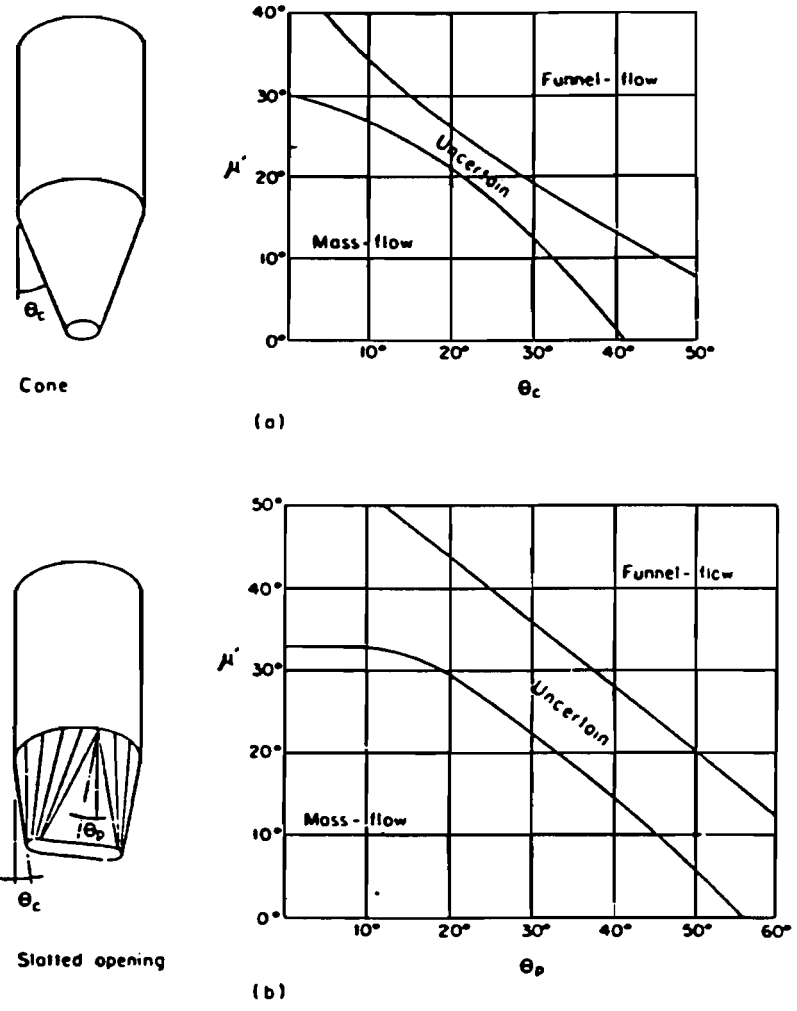
Figure 2.8. Mass flow funnel flow bounds (Safarian and Harris, 1985)
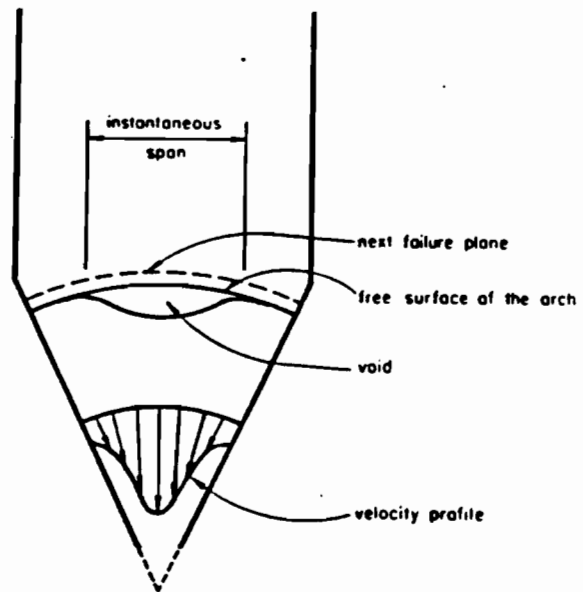
Figure 2.9. Suggested mechanism of pulsation by Jenike
(Safarian and Harris, 1985)

a transition or an effective transition in cylinder
diameter. High pressures, due to head h_c, compact the
solid flowing down the cylinder into a firm plug. A large
part of pressure due to the head is transferred to the
abuttments during transition. The highly consolidated
material there is capable of forming a stable arch of some
span. The arch does not break up and flow until that span
has been exposed through outflow of material from beneath
the arch. Figure 2.9 shows the velocity profile of a solid
flowing in the converging part of a channel. Material
flows fastest at the center where it forms a void and
exposes a stable arch. The void and the span of the arch
increase, gradually increasing the stresses in the arch.
When the strength of the material is exceeded, the arch
collapses, and the plug slips and fills the void. The
process is then repeated. Pulsation can be reduced by
reducing h_c. This may be accomplished by a low H/D (height
to diameter) ratio, rough cylinder walls, convergent
cylinder, silo construction containing a variety of
convergent, divergent and rough ledges, and the use of a
circumferential shelf. According to Jenike (58), periodic
shocks are experienced in funnel flow bins containing
solids with less fines. These shocks can be destructive in
large silos. Shocks appear to be caused by recurring
instability of stagnant material around the flow channel.

The stagnant material slides inward into the channel,
forming a secondary channel. This consolidates the
material in the flow channel, which re-forms with higher
wall pressures, capable of stabilizing the material around
it. As material discharges, it dilates, wall pressures
decrease, and a new collapse occurs. Shocks can be
eliminated or at least minimized by expanding the flow
channel to a base diameter of some eight feet.

2.3 Methods of Computing Total Pressures

Generally, there are two approaches to determining
total pressures -- static plus overpressures. One is to
modify the computed static pressure using overpressure
factors; the second is to compute total pressures directly.
A review of some of these methods follows.

2.3.1 Jenike's Method

For computing pressures, Jenike divides the silos into
the following three zones (see Figure 2.10):

1. Top zone -- from top to distance D (diameter) below
   the top.
2. Lower zone -- balance of the cylindrical silo below
   the top zone.
3. Hopper

In the top zone he suggests lateral pressure be com-
puted as 1.5 times the Janssen static pressure, but using
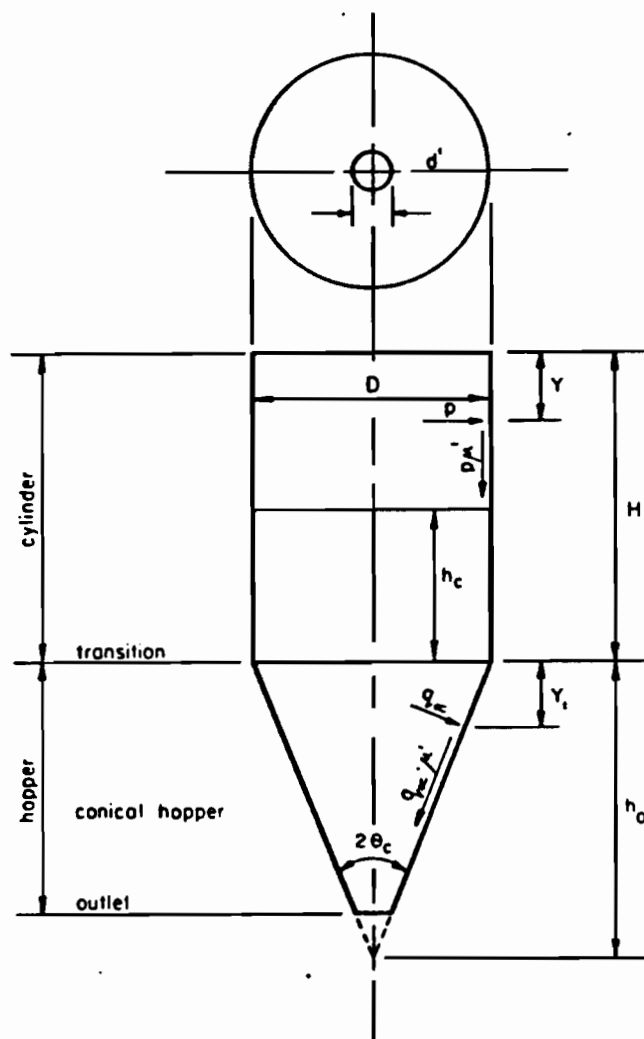
Figure 2.10. Axi-symmetric mass-flow by Jenike
(Safarian and Harris, 1985)
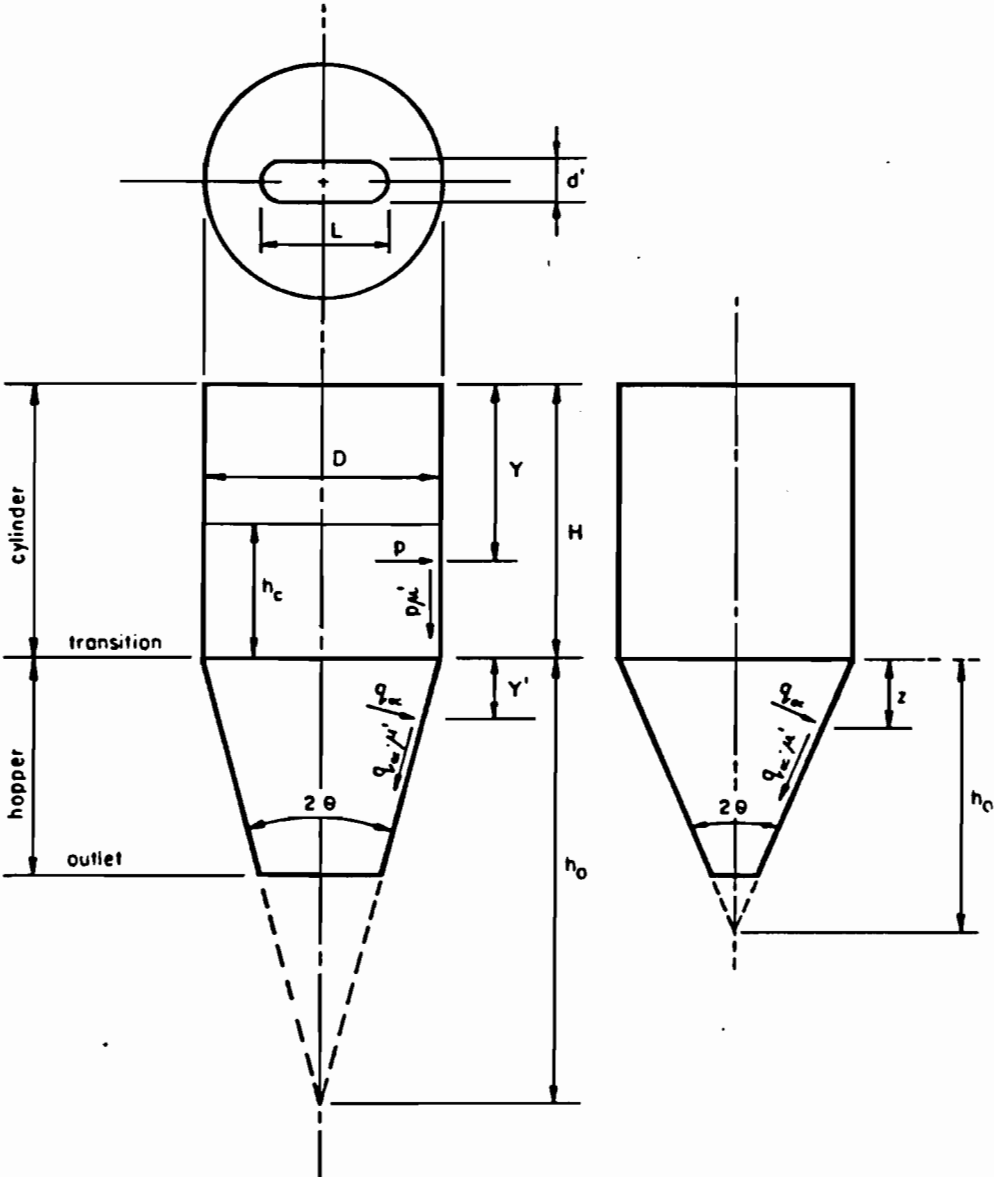
Figure 2.11.   Transition mass flow by Jenike (Safarian
and Harris, 1985)

$$k = (1 - \sin\phi)/(1 + \sin\phi)$$

or

$$k = 0.4$$

whichever is larger. For the lower portion of the silo cylinder, the pressure is computed using the principle of minimum energy. Jenike presented figures for the values of H/D, μ'k and PγD.

For the mass-flow hopper itself, pressure normal to the hopper wall depends on "effective head," h_c, of stored material acting at the transition from cylinder to cone. This effective head is computed

$$hc = \frac{R}{\mu'k} \left(1 - e^{-\mu'ky/R}\right) \tag{2.24}$$

Total pressure normal to the walls of the hopper qα,des, which is solved by Jenike through adapting Janssen equation to a converging channel. The resulting equation is:

$$q\alpha,\ des = \gamma k \left[\frac{h_o - Y_1}{n-1} + \left(h_c - \frac{h_o}{n-1}\right) \left(\frac{h_o - Y_1}{h_o}\right)^n \right] \tag{2.25}$$

in which n = (1 + m)[k(1 + μ'/tanθ_c) - 1]; m is a constant and is 1.0 for axi-symmetric flow (as in a conical hopper), and 0.0 for "plane flow" (as in a wedge-shaped hopper); and

h_o = height of hopper from vertex to base (different values for the main hopper and the transition ring).

2.3.2 Reimbert Method for Operational Pressures in Silos

Marcel and André Reimbert (1980) introduced a method for calculating design or operational pressures. This method, which includes the effect of eccentric withdrawal, was developed by using experimentally determined numerical factors as multipliers to either Reimbert or the Janssen static pressures. In this method, dynamic factor K_d is used for emptying conditions only (see Figure 2.12).

Overpressure factor K_b is multiplied by factor K_d for simultaneous filling and emptying. The forces were determined using fine sand as the stored material. To determine proper values of K_d and K_b for materials other than fine sand, these factors are multiplied by Ka_1 for emptying and Ka_2 for simultaneous filling and emptying. These factors are based on the arrangement of discharge points and on silo slenderness, e_1 where e_1 = H/a for square and polygonal silos and

a = length of side

e_1 = H/1·12D for circular silos.

The Reimbert method is limited because values of Ka are
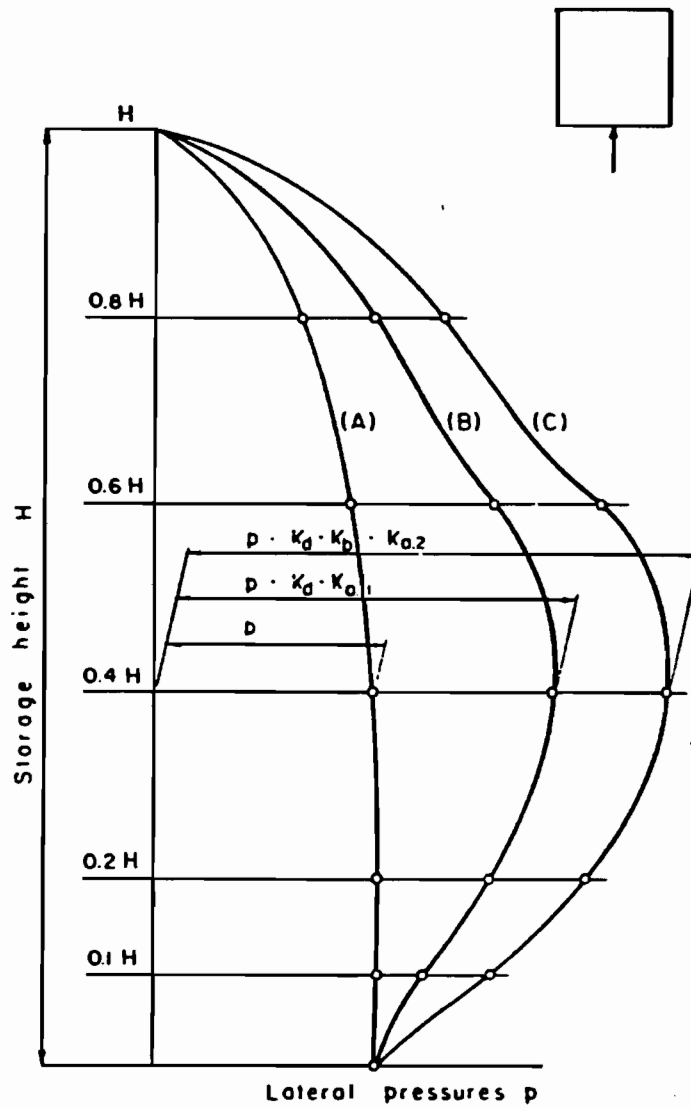
Figure 2.12. Design lateral curves pressure by
M. and A. Reimbert (Safarian and Harris,
1985)

provided for only a limited variety of materials; use of these factors is further limited because they are valid for noncohesive materials only.

2.3.3 Walker's Method for Total Pressure

This method considers equilibrium of a thin lamina of powdery material, shear strength of material under its actual history of compression in the bin, and a Mohr's circle representation of stresses in the flowing material (28). The Walker's equation for horizontal pressure on the wall of a vertical cylinder is:

$$P_y = \frac{\gamma D}{4BF}\left[1 - \exp(-4BF_y/D)\right] \tag{2.26}$$

Average vertical pressure at depth Y is:

$$q_y = \frac{\gamma D}{4BF}\left[1 - \exp(-4BF_y/D)\right] \tag{2.27}$$

where,

F = distribution factor for vertical pressure, equal to 1.0 when the vertical pressure is uniform over the entire horizontal cross section

B = a function of the "effective internal friction, ϕ," and wall coefficient of friction μ'

ϕ = the slope of the effective yield locus, it is determined from the Mohr's circle plot of a series of direct shear tests of the material to be stored

(see Figure 2.13).

$$B = \sin\varepsilon \sin\phi/(1 - (\cos\varepsilon/\sin\phi))$$

in which

$$\varepsilon = m + \sin^{-1}(\sin\mu'/\sin\phi)$$

the term $\sin^{-1}$ being for an angle larger than 90°.

According to Walker (28), for all but rougher walls the

product BF is practically equal to $\mu'k$, and the

distribution factor is approximately 1.0. For rougher

walls, BF is slightly larger than $\mu'k$; thus this equation

shows lower average vertical pressures and higher wall

pressures when rough walls are used. In Walker's method

the normal static pressure on an inclined wall of a hopper

is:

$$V_y = q_y \frac{\sin2\theta \cos\mu}{\sin(\mu + 2\theta) + \sin\mu} \tag{2.28}$$

when

$$\sin\mu < \sin(\mu + 2\theta)\sin\phi, \quad \text{otherwise}$$

Design emptying pressures are:

$$q_{\alpha'} \text{ des} = \frac{(1 + \sin\phi \cos\varepsilon)\, q_{es}}{1 - \sin\phi \cos(2\theta + \varepsilon)} \tag{2.29}$$

and
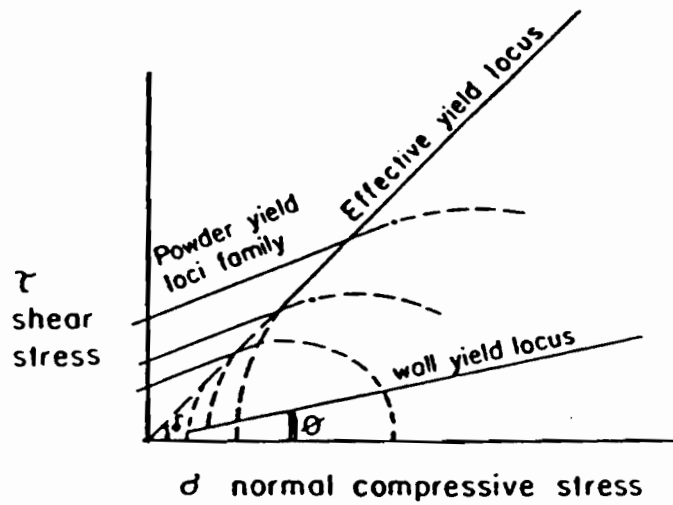
Figure 2.13. Effective yield locus by Walker (Safarian and Harris, 1985)
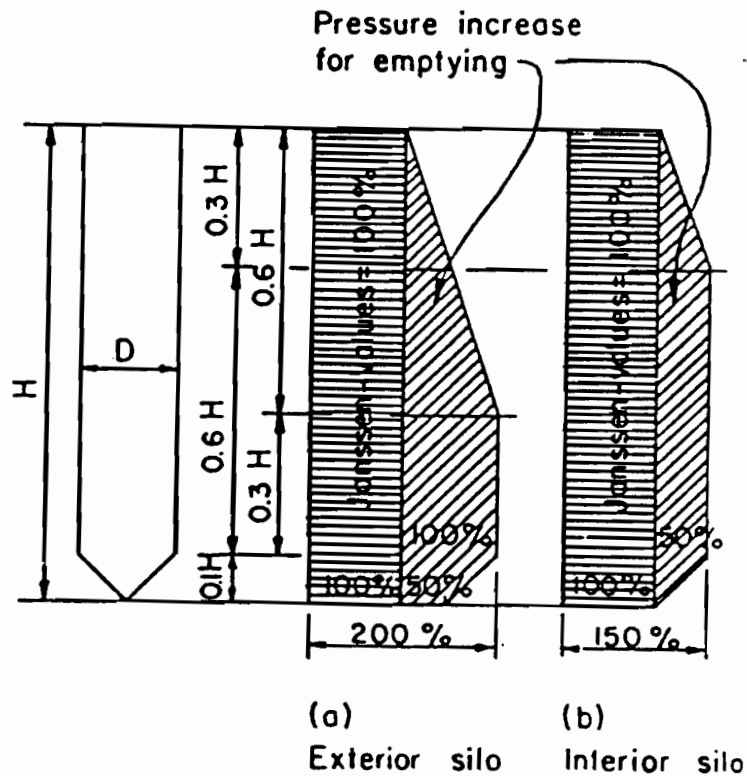
Figure 2.14. Lateral pressure scheme for grain and wheat flour by Theimer (Safarian and Harris, 1985)

$$q \text{ des} = \frac{\gamma h_h Y_h}{(K_h - 1)h_h} + \left(q_H - \frac{\gamma h_h}{K_h - 1}^s \right) \left(\frac{Y_h}{h_h} \right)^{K_h} \qquad (2.30)$$

θ = hopper half apex angle

C_h = 0 for conical or pyramidal hopper

C_h = 1 for conical or pyramidal hopper

Y_h = distance above apex

des = design

α = subscript for pressure on sloping surface

h_h = hopper height, apex to top

$$K_h = \frac{(1+C_h) \ \sin\theta \ \sin(2\theta + \varepsilon)}{+ \text{ on } \theta \ (1 - \sin\theta \ \cos(2\theta + \varepsilon)}$$

q_H = vertical pressure at top of hopper.

2.3.4   Theimer's Approach

This method proposes a solution for determining pressures on walls of grain and wheat flour silos (58). Lateral pressure on silo walls are calculated with allowances for withdrawal overpressures, temperature stesses, material bridging and so on; the pressures are calculated thus (see Figure 2.14):

For exterior silos:

$$P_{des} = \frac{\gamma DY(4D + Y)}{2\mu'(2D + Y)^2} \qquad (2.31)$$

For interior silos

$$P_{des} = \frac{3\gamma DY(4D + Y)}{8\mu'(2D + Y)^2} \qquad (2.32)$$

where

D = inside diameter of circular silos or clear span, a,

of a square or polygonal silo

For rectangular silos with sides b and c an imaginary

span is computed as:

$$a = \frac{bc}{2(b+c)}$$

Theimer recommends using the following properties in the

above equations:

For grain γ = 0.8 MPa/m^3

ϕ = 30% angle of repose

μ'= tan 0.75ϕ

= 0.414

Coefficient of friction against concrete wall

α = 0.6 MPa/m^3

ϕ = 25°

$\mu' = \tan (2/3\phi)$

$= 0.299$

Figure (2.14) shows variation due to emptying based on Theimer's approach.

2.3.5 Safarian's Approach (58)

This procedure involves the determination of either Janssen's or Reimbert's method, and then multiplying them by an overpressure factor, c_d, to obtain design pressures. Safarian recommends that the effect of eccentric discharge be considered by adding a correction, P_{ecc}, to the lateral design pressure, P_{des}

2.4 Discussion

Of the methods described in the preceeding sections, the ones most frequently used for determination of static pressure in silos are the methods of Janssen (1895) and Reimbert (1976). However the application of these methods in design has resulted in failure of numerous grain storage facilities (Tyson 1980).

Sundaram and Cowin (1979) questioned Janssen's assumption that the full frictional force at the walls is mobilized for if not, Janssen's solution would be a lower bound to the actual material pressures. They suggest that

Janssen's formula be modified to an inequality, which obviously is not suitable for design purposes. Walker (1966), on the other hand, describes how full mobilization of wall friction is accomplished by the compression of loaded material below charging material. The greatest controversy about the use of Janssen's equation stems from his assumption that vertical and horizontal pressures are uniform throughout a horizontal cross-section. This leads to a constant ratio of lateral to vertical pressure, k, commonly called the pressure ratio. If k is to be considered a material property, then it should be unaffected by external factors. If it is not a constant then it should only vary with the material. There are conflicting reports from researchers on this factor. Clower et al. (1973) and Moysey and Brown (1979) concluded that the pressure ratio was constant with depth. Ketchum and Lenczner (1963), and Kramer (1944) as quoted by Britton (11), all found that k increased with the depth. Jaky (1948) and Reimbert and Reimbert (1976) found k to be variable but following no simple pattern with increasing depth.

If k varies randomly within the material then this implies that k is not a material property. Alternatively the researchers may not have been measuring the pressure ratio but rather, a value which is influenced by external factors. There is therefore urgent need to verify the

validity of k. If it exists then a method for determining it accurately is needed. Otherwise its use in load calculations should be avoided.

It is generally accepted that the maximum lateral pressures occur in silos during emptying, but there is disagreement as to the location and magnitude of these maximum pressures. This is reflected by the wide range of design pressures suggested by various codes such as the American Concrete Standard ACI 313-77 (1977), the German code DIN 1055 (1964), and the Soviet code CH-302-65 (1965). Suggested dynamic overpressures range from 1.3 to 4.0 times the lateral pressure predicted from the static condition. The various theories and equations, discussed in previous sections, developed for the prediction of both static and dynamic pressures have yet to be adequately defined.

There is need for the development of prediction equations which take into account the physical properties of granular materials and bins which influence pressures. These properties include fill particle size, discharge rate, height to diameter ratio, bin wall mechanical properties, hopper design, discharge eccentricity, and material characterization. The next two sections are devoted to discussing material characterization and experimental design.

3. MATERIAL CHARACTERIZATION

The solution to grain storage structure design problems, such as the evaluation of the interaction between the loads imposed on thin walled storage structures by grains and deformation of the storage structure wall or the evaluation of loads imposed on confining structures by particulate media during flow, would be enhanced by description of the load-deformation behaviour of biological particulate media en-masse (34). However there is controversy as to whether such materials are elastic, viscoelastic, elastoplastic or elastoviscoplastic.

The two modes of deformation which control the mechanical behaviour of particular media en-masse are (34):

(i)   reorientation of individual particles from one more or less dense configuration to another, and

(ii) deformation of individual particles due to contact type loads.

The actual mode of deformation is a complex combination of the aforementioned mechanisms. Narayan and Bilanski (34) suggested, however, that for wheat en-masse particle reorientation is the predominant deformation at low loads, whereas at high loads particle deformation is the

44

predominant mechanism. Analytical evaluation of the deformation of biological media en-masse is complicated by irregular shape, non-uniform size, and inelastic nature of individual particles (34). According to Manbeck and Nelson (35) the problem of predicting pressures in biological particulate media en-masse is very similar to the problems encountered with granular non-cohesive soils, the major differences being particle sizes, shapes and deformation properties. Some soil mechanicians have taken the stand that the study of the load-deformation behavior of granular materials might better be approached experimentally rather than theoretically. For example Ko and Scott (34), commenting upon the direction taken by soil mechanists with regard to establishment of valid earth presure theory, have noted:

> …The analytical solutions which have been employed represent situations which are extremely idealized versions of real life counterparts. The solutions referred to are those for various simple stress distributions of linearly elastic isotropic homogeneous media on the one hand, and certain results derived from the upper bound methods of ideally plastic analysis on the other hand. It seems to the authors [Ko and Scott] that this situation has inhibited the study of the real stress-strain behavior, or constitutive relations of soils, and that work has consequently tended to concentrate on the stress conditions at failure.

Studies of the responses of cereal grains to mechanical stresses have progressed from analyses based on simple Hookian models to viscoelastic models using generalized Kelvin and Maxwell models, used singly or jointly (20).

More recently elastoplastic models have been used (78).
Upon repeated uniaxial loading, Shapolyanskaya (1952) found
that the load-deformation behavior of wheat kernels
approached that of an elastic body. Thus, applying the
Hertz theory of contact stresses, he evaluated a modulus of
elasticity for wheat kernels. In his study of core samples
of wheat kernels, Zoerb (1960) noted the same strain
hardening tendencies but concluded that plastic rather than
elastic behavior characterized the mechanical properties of
wheat. Shelef and Mohsenin (1967) supported Zoerb's
observations, as did Arnold and Roberts (1969) by means of
a variety of parallel-plate and indenter uniaxial
compression tests.

Manbeck and Nelson (34, 35), Schott and Britton (60),
Mohsenin (38) and Herum (20) are among the researchers who
categorized various grains as being viscoelastic. Zhang et
al. (79, 80) categorize wheat as being elastoplastic.
Bishara (8) categorizes grains as being non-time dependent
in behavior. While some earlier researchers treated the
materials as elastic, the author believes that the
materials are very complex and may be defined as being
elastic-viscoplastic. The various models of material
characterization are discussed below.

3.1 <u>Viscoelasticity</u>

Mechanical behavior of agricultural products, being time dependent, must logically be studied applying the principles of rheology and viscoelasticity in which both viscous and elastic responses are taken into consideration (39). Viscoelasticity is the behavior of materials in which the materials behave both as an elastic solid and a viscous fluid. The time-dependent behavior of viscoelastic materials must be expressed by constitutive equations which include time as a variable in addition to the stress and strain variables.

There are some basic phenomena which are common to many viscoelastic materials (16). These are (see Figure 3.1):

  (i)   Instantaneous elasticity

 (ii)   Creep under constant stress

(iii)   Stress relaxation under constaint strain

 (iv)   Instantaneous recovery

  (v)   Delayed recovery

 (vi)   Permanent set

In general there are two alternative forms used to represent stress-strain-time relations of viscoelastic materials. They are called the differential operator method and the integral representation (16). The differential operator method requires fairly simple mathematical processes of analysis and has therefore been
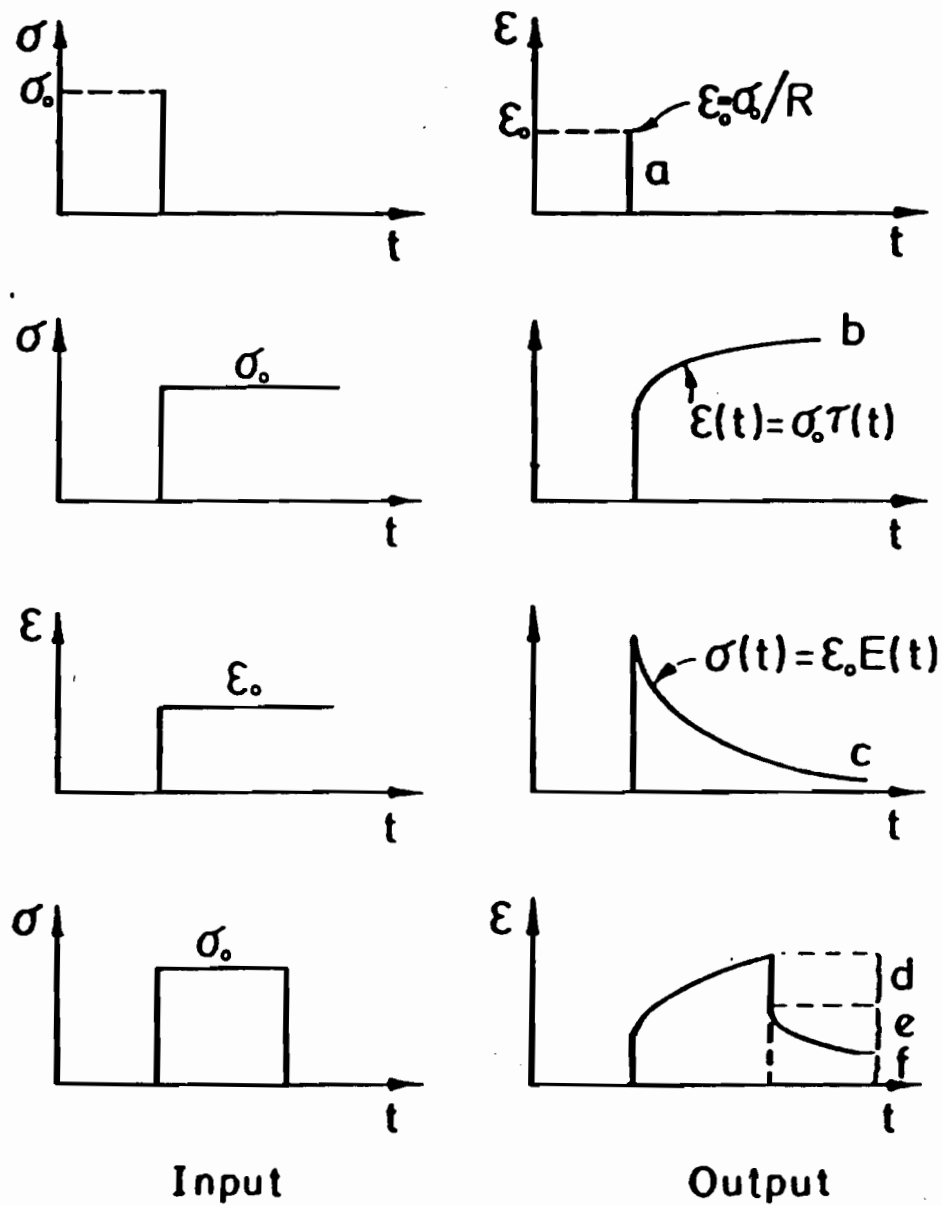
Figure 3.1. Phenomena common to many viscoelastic
materials: a. Instantaneous elasticity
b. Creep
c. Stress relaxation
d. Instantaneous recovery
e. Delayed recovery
f. Permanent set

widely used. The integral representation is able to describe the time dependence more generally, but sometimes leads to difficult mathematics in stress analysis (16).

3.1.1 Creep

Creep is a slow continuous deformation of a material under constant stress (16). Generally creep can be described in terms of three different stages (see Figure 3.2):

(i) Primary creep -- the first stage at which creep occurs at a decreasing rate

(ii) Secondary stage -- proceeds at a nearly constant rate

(iii) Third or tertiary stage occurs at an increasing rate and may terminate in failure.

Total strain ε at any instant of time t in creep of a linear material (see 3.2) is represented as the sum of the instantaneous elastic strain ε^e and the creep strain ε^c

$$\varepsilon = \varepsilon^e + \varepsilon^c \tag{3.1}$$

The strain rate ε is found by differentiating (3.1), noting that ε^e is a constant:

$$\varepsilon = \frac{d\varepsilon}{dt} = \frac{d\varepsilon^c}{dt} \tag{3.2}$$
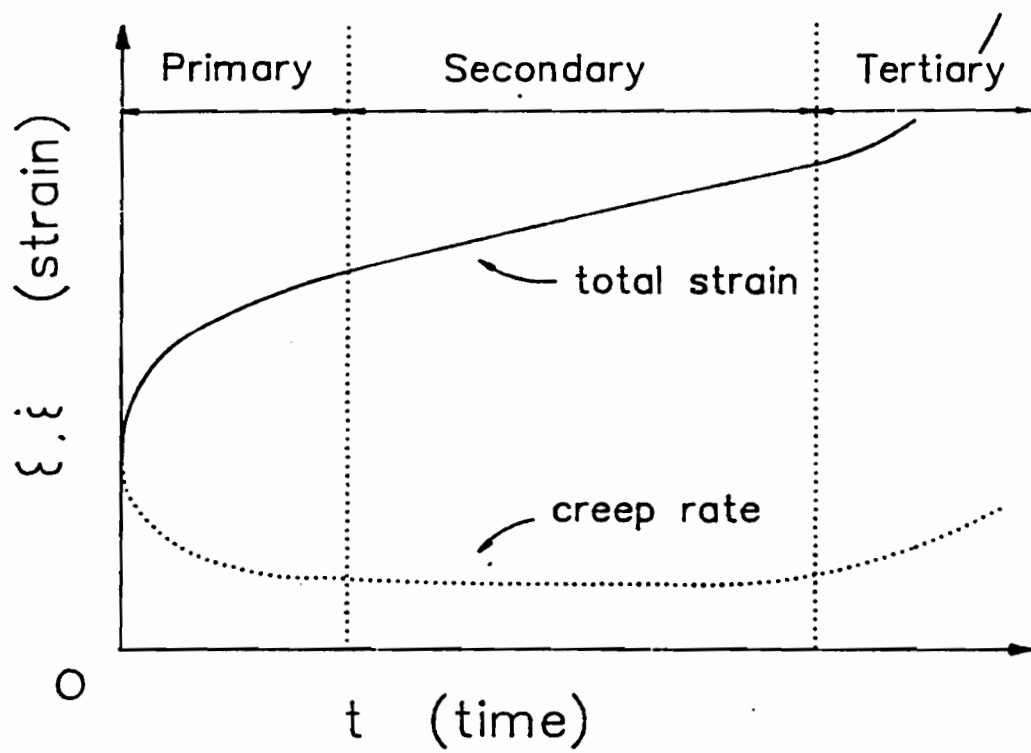
Figure 3.2. Three stages of creep (Findley, 1976)

3.1.2 Recovery

If the load is removed, a reverse elastic strain followed by recovery of a portion of the creep will occur at a continuously decreasing rate.

3.1.3 Relaxation

Viscoelastic materials subjected to a constant strain will relax under constant strain so that stress gradually decreases (16) (see Figure 3.3).

3.1.4 Linearity

The material is said to be linearly viscoelastic if stress is proportional to strain at a given time, and the linear superposition principle holds. These linear requirements can be stated mathematically in two equations (16):

$$\varepsilon[c\sigma(t)] = c\varepsilon[\sigma(t)] \tag{3.3}$$

$$\varepsilon[\sigma_1(t) + \sigma_2(t-t_1)] = \varepsilon[\sigma_1(t)] + \varepsilon[\sigma_1(t-t_1)] \tag{3.4}$$

in which

ε = strain output

σ = stress input

c = constant

Equation (3.3) states that the strain-time output due
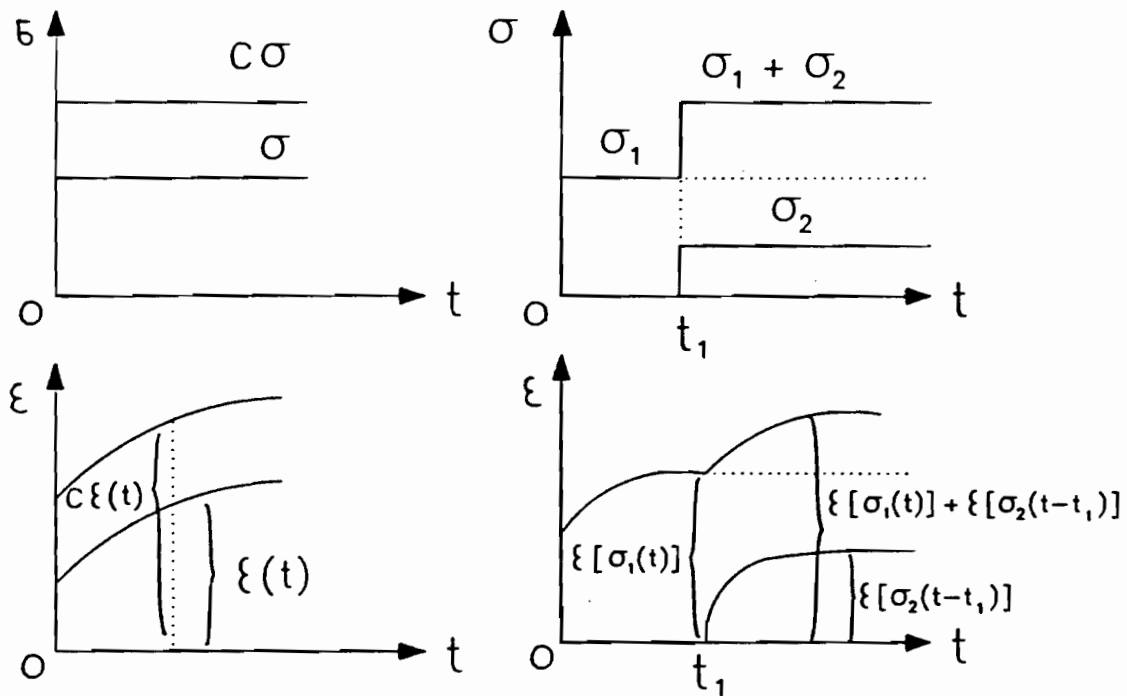
Figure 3.3. Illustration of behavior of a linear model
(Findley, 1976)

to a stress input $c\sigma(t)$ equals the scalar c times the

strain output due to a stress input $\sigma(t)$. The second

requirement is the Boltzmann superposition principle which

states that strain output due to two arbitrary but

different stress inputs applied at different times, $\varepsilon[\sigma_1(t)$

$+ \sigma_2(t-t_1)]$ equals the sum of the strain outputs from $\sigma_1(t)$

and $\sigma_2(t-t_1)$ each acting separately.

3.1.5 Viscoelastic Models

All linear viscoelastic models are made up of linear

elastic springs and linear viscous dashpots (16). Inertia

effects are neglected in such models.

In the linear spring shown in Figure 3.4(a)

$$\sigma = R\varepsilon \tag{3.5}$$

where

R = linear spring constant or Young's modulus.

The spring element exhibits instantaneous elasticity

and instantaneous recovery as shown in Figure 3.4(b).

Figure 3.4(c) shows a linear dashpot, where

$$\sigma = \eta\frac{d\varepsilon}{dt} = \eta\dot{\varepsilon} \tag{3.6}$$

where
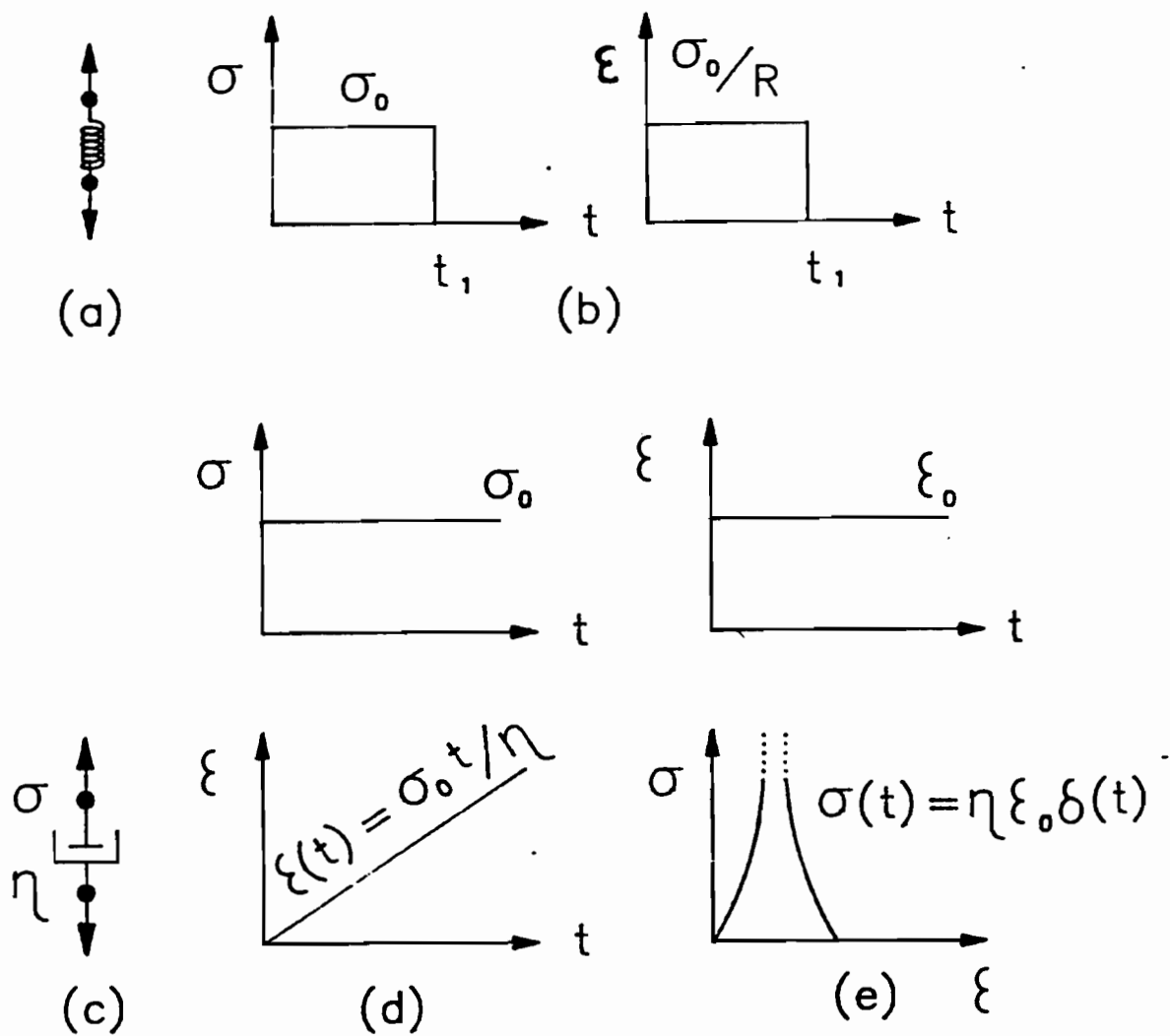
Figure 3.4. Behavior of linear spring and linear dashpot (Findley, 1976)

η = coefficient of viscosity.

Equation 3.6 states that the strain rate ε is proportional to the stress, i.e., the dashpot will deform continuously at a constant rate when it is subjected to a step constant stress as in Figure 3.4(d). However, when a step input of constant strain is applied to the dashpot the stress will have an infinite value at the instant of strain application and will then diminish rapidly with time at t = o+ and will remain zero as shown in Figure 3.4(e). This behavior is expressed mathematically using the Dirac delta function $\sigma(t)$, where

$$\delta(t) = 0 \quad \text{for } t \neq 0$$

$$\delta(t) = \infty \quad \text{for } t = 0$$

Thus the stress resulting from applying a step charge in strain ε_0 is

$$\sigma(t) = \eta\varepsilon_0 \tag{3.7}$$

An infinite stress is impossible in reality. It is therefore impossible to impose instantaneously any finite deformation on the dashpot.

3.1.5.1 Maxwell Model

The Maxwell model is a two-element model consisting of
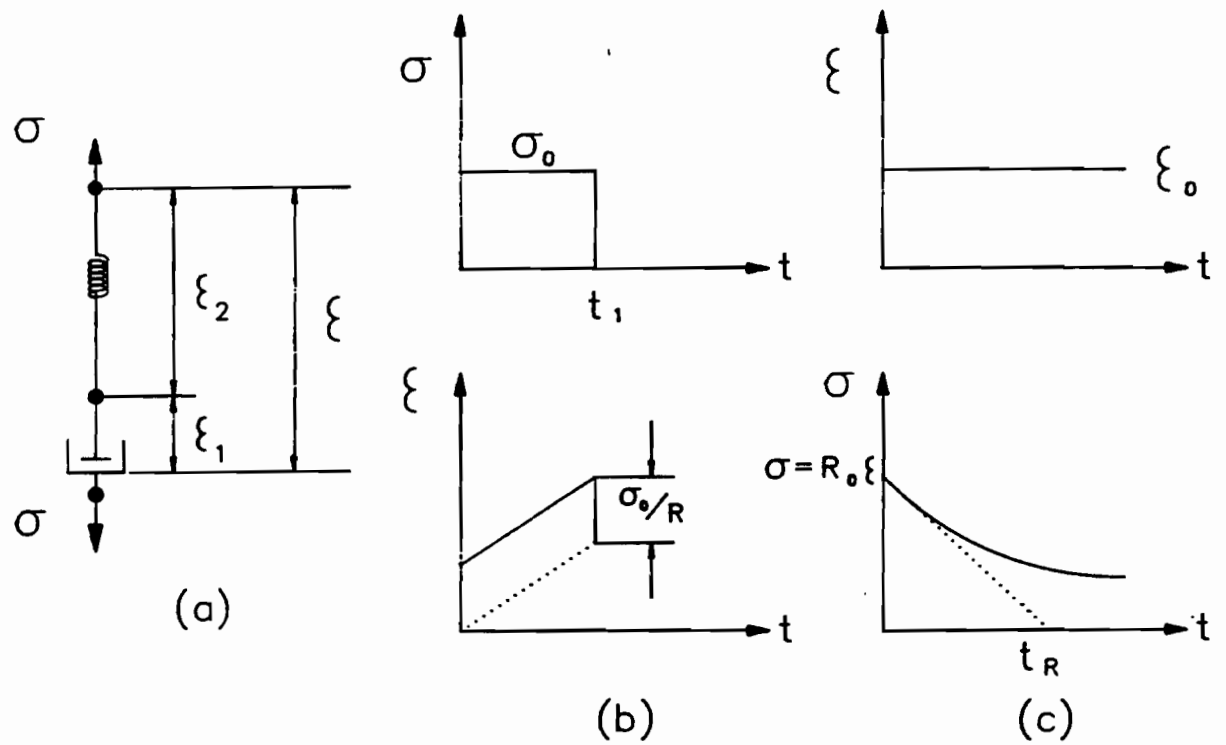
Figure 3.5.   Behavior of Maxwell model (Findley, 1976)

a linear spring element and linear viscous dashpot element connected in series as shown in Figure 3.5. Since both elements are in series

$$\varepsilon = \varepsilon_1 + \varepsilon_2$$

therefore

$$\dot{\varepsilon} = \dot{\varepsilon}_1 + \dot{\varepsilon}_2 \tag{3.8}$$

and using (3.5) and (3.6)

$$\dot{\varepsilon} = \frac{\dot{\sigma}}{R} + \frac{\sigma}{\eta} \tag{3.9}$$

For a constant stress σ_0 at time $t = 0$, integrating 3.9 and applying these initial conditions

$$\varepsilon(t) = \frac{\sigma_0}{R} + \frac{\sigma_0}{\eta}t \tag{3.10}$$

From (3.9); if the stress is removed from the Maxwell model at time t_1, the elastic strain σ_0/R in the spring returns to zero instantaneously, while $(\sigma_0/\eta)t_1$ represents a permanent strain which does not disappear.

For a constant strain ε_0 at $t = 0$ Equation (3.9) yields

$$\sigma(t) = \sigma_0 e^{\frac{Rt}{\eta}} = R\varepsilon_0 e^{-Rt/\eta} \tag{3.11}$$

where ε_0 is the initial strain at t = 0+, 0+ being the time

just after application of the strain. Equation (3.11)

describes the stress relaxation phenomenon for a Maxwell

model under constant strain. Figure 3.6(c) refers to this

phenomenon. The rate of change of stress is,

$$\dot{\sigma} = (\sigma_0 R/\eta)^{-Rt/\eta} \qquad (3.12)$$

Thus the initial rate of change of stress at t = 0+ is

$\dot{\sigma} = \sigma_0 R/\eta$. If the stress were to decrease continously at

this initial rate, the relaxation equation would have the

following form

$$\sigma = -(\sigma_0 Rt/\eta) + \sigma_0 \qquad (3.13)$$

From (3.13), the stress would reach zero at t = t_R which is

called the relaxation time of the Maxwell model. The

relaxation time characterizes one of the viscoelastic

properties of the material.

Most of the relaxation stress occurs before time t_R

(10), since the variable factor

$$e^{-t/t_R}$$

in (3.11) converges towards zero very rapidly for t < t_R.

For t = t_R, $\sigma(t)$ = 0.37 σ_0. Thus only 37% of the initial

stress remains at $t = t_R$.

The constitutive equation for the generalized Maxwell model, see Figure (3.6), is

$$\varepsilon = \sigma \sum_{i=1}^{N} \frac{1}{R_i} + \sigma \sum_{i=1}^{N} \frac{1}{\eta_i} \qquad (3.14)$$

Equation (3.14) is equivalent to Equation (3.9), consequently a chain of elements of springs and dashpot is equivalent to a Maxwell model as in Figure (3.6). Maxwell models in parallel represent instantaneous elasticity, delayed elasticity with various retardation times, stress relaxation with various relaxation times and also viscous flow.

From Figure (3.7), the strain contribution of the first element is

$$D\varepsilon = \frac{D\sigma_1}{R_1} + \frac{\sigma_1}{\eta_1} \qquad (3.15)$$

where D is the differential operator with respect to time,

$$D = \frac{d}{dt} .$$

Therefore,

$$\sigma_1 = \frac{D}{\dfrac{D}{R_1} + \dfrac{1}{\eta_1}} \varepsilon$$

The i-th element yields
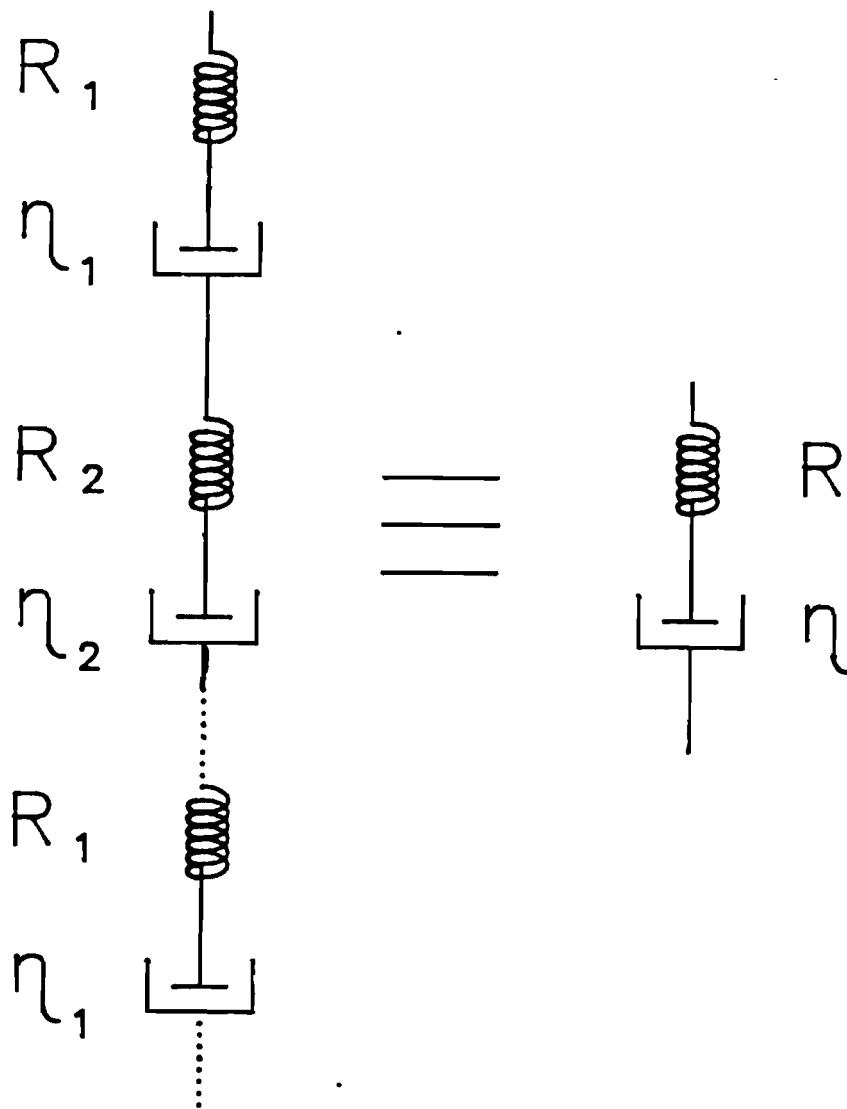
Figure 3.6 Generalized Maxwell model in series
(Findley, 1976)

$$\sigma_i = \frac{D}{\dfrac{D}{R_i} + \dfrac{1}{\eta_i}} \varepsilon \qquad (3.16)$$

The sum of both sides of (3.16) is

$$\sigma = \sum_{i=1}^{a} \sigma_i = \left(\sum_{i=1}^{a} \frac{D}{\dfrac{D}{R_i} + \dfrac{1}{\eta_i}} \right) \varepsilon \qquad (3.17)$$

By multiplying both sides by

$$\prod_{i=1}^{a} \left(\frac{D}{R_i} + \frac{1}{\eta_i} \right) , \text{ where } \prod_{i=1}^{a}$$

denotes the product of a-terms, the time operator D can be removed from the denominator of the equation. The open form of this process is

$$\left[\left(\frac{D}{R_1} + \frac{1}{\eta_1} \right) \left(\frac{D}{R_2} + \frac{1}{\eta_2} \right) \cdots \right] \sigma$$

$$= \left[\left(\frac{D}{R_1} + \frac{1}{\eta_1} \right) \left(\frac{D}{R_2} + \frac{1}{\eta_2} \right) \cdots \right] \left[\frac{D}{\dfrac{D}{R_1} + \dfrac{1}{\eta_1}} + \frac{D}{\dfrac{D}{R_2} + \dfrac{1}{\eta_2}} + \cdots \right] \varepsilon$$

$$(3.18)$$

3.1.6 Creep compliance

For a creep test a step of constant stress $\sigma = \sigma_0 H(t)$ is applied and the time-dependent strain $\varepsilon(t)$ is measured. For linear material,
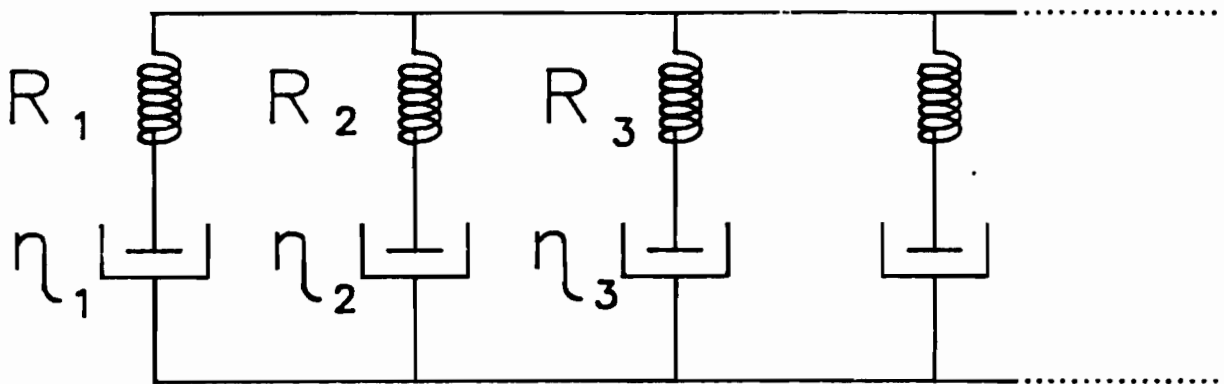
Figure 3.7. Generalized Maxwell model in parallel
(Findley, 1976)

$$\epsilon(t) = \sigma_0 J(t) \tag{3.19}$$

or, $\quad J(t) = \epsilon(t)/\sigma_0 \tag{3.20}$

where

    $J(t)$ = creep compliance which is the creep strain

        per unit of applied stress

    $H(t)$ = Heaviside unit function

$J(t)$ is a material property, for example, for a Maxwell model,

$$J(t) = \left(\frac{1}{R} + \frac{1}{\eta}t \right)$$

3.1.7   Relaxation Modulus

In a relaxation test a step of constant strain

$\epsilon = \epsilon_0 H(t)$ is applied and stress $\sigma(t)$ is measured. The material behavior is represented by

$$\sigma(t) = \epsilon_0 E(t) \tag{3.21}$$

or

$$E(t) = \frac{\sigma(t)}{\epsilon_0}$$

where

    $E(t)$ = relaxation modulus, which is the stress per unit

        applied strain

$E(t)$ is a material property and $E(t) = Re^{-RT/\eta}$, for example, for a Maxwell material.

Creep and stress relaxation phenomena are two aspects of the same viscoelastic behavior of materials, therefore they should be related.

Applying Laplace transform to (3.19) and (3.21),

$$\hat{\varepsilon}(S) = SJ(S)\hat{\sigma}(S) \tag{3.22}$$

$$\hat{\sigma}(S) = s\hat{E}(s)\varepsilon(S) \tag{3.23}$$

Therefore

$$\frac{\hat{\sigma}(s)}{\hat{\varepsilon}(s)} = s\hat{E}(s) = \frac{1}{s\hat{J}(s)} \tag{3.24}$$

or $\quad \hat{J}(s)\hat{E}(S) = 1/S^2 \tag{3.25}$

Applying the inverse Laplace transform,

$$\int_0^t J(t - \tau)E(\tau)\,d\tau = t \tag{3.26}$$

or

$$\int_0^t E(t - \tau)J(\tau)\,d\tau = t \tag{3.27}$$

By using the initial and the final value theorems, we get,

$$E(0)J(0) = 1 \tag{3.28}$$

or, $\quad E(\infty)J(\infty) = 1 \tag{3.29}$

where

$E(0)$, $J(0)$ = initial (time-dependent or glassy) relaxation modulus and creep compliance respectively

$E(\infty)$, $J(\infty)$ = long-time (or rubbery) relaxation

modulus and creep compliance

respectively.

3.1.8 Three dimensional representation of viscoelastic behavior

In the most general case the integral representation may take the form (16),

$$\varepsilon_{ij}(t) = \int C_{ijkl}(t-\tau)\,\sigma_{kl}(\tau)\,d\tau \qquad (3.30)$$

where,

C_{ijkl} = creep functions which in general have 21 constants for anisotropic linear viscoelastic materials, for isotropic material the number is reduced to 2.

It may be more convenient to separate the stress and strain tensors into deviatoric and dilatational components (16), therefore

$$S_{ij}(t) = 2\int_0^t G(t - \tau)\frac{\partial d_{ij}}{\partial \tau}d\tau \qquad (3.31)$$

$$\sigma_{ii}(t) = 2\int_0^t K(t - \tau)\frac{\partial e_{ij}(\tau)}{\partial \tau}\partial\tau \qquad (3.32)$$

where

$G(t)$ = stress relaxation modulus in shear, which is time-dependent

$K(t)$ = hydrostatic or bulk stress relaxation modulus.

3.2 Elastoplasticity

Elastoplastic behavior of materials is characterized by the presence of both elastic (recoverable) and plastic (permanent) strains when the material is stressed. Figure 3.8 is an illustration of elastoplastic behavior in a triaxial test. Both elastic and plastic strains occur from the beginning of loading. The plastic strains are initially smaller than the elastic strains, but at higher stress levels the plastic strains dominate the elastic strains. If,

$\{d\varepsilon_{ij}\}$ = total strain increment

$\{d\varepsilon^P_{ij}\}$ = plastic component of $d\varepsilon_{ij}$

$\{d\varepsilon_{ij}^e\}$ = elastic component of $d\varepsilon_{ij}$

Then,

$$\{d\varepsilon_{ij}\} = \{d\varepsilon^e_{ij}\} + \{d\varepsilon^P_{ij}\} \tag{3.33}$$

Lade (30) proposed a modification to (3.33), which has been experimentally verified for wheat by Zhang et al (78), the form of which is

$$\{d\varepsilon_{ij}\} = \{d\varepsilon^e_{ij}\} + \{d\varepsilon^c_{ij}\} + \{d\varepsilon^P_{ij}\} \tag{3.34}$$

where

$\{d\varepsilon^c_{ij}\}$ = plastic collapse component of $\{d\varepsilon_{ij}\}$

$\{d\varepsilon^P_{ij}\}$ = plastic expansive component of $\{d\varepsilon_{ij}\}$
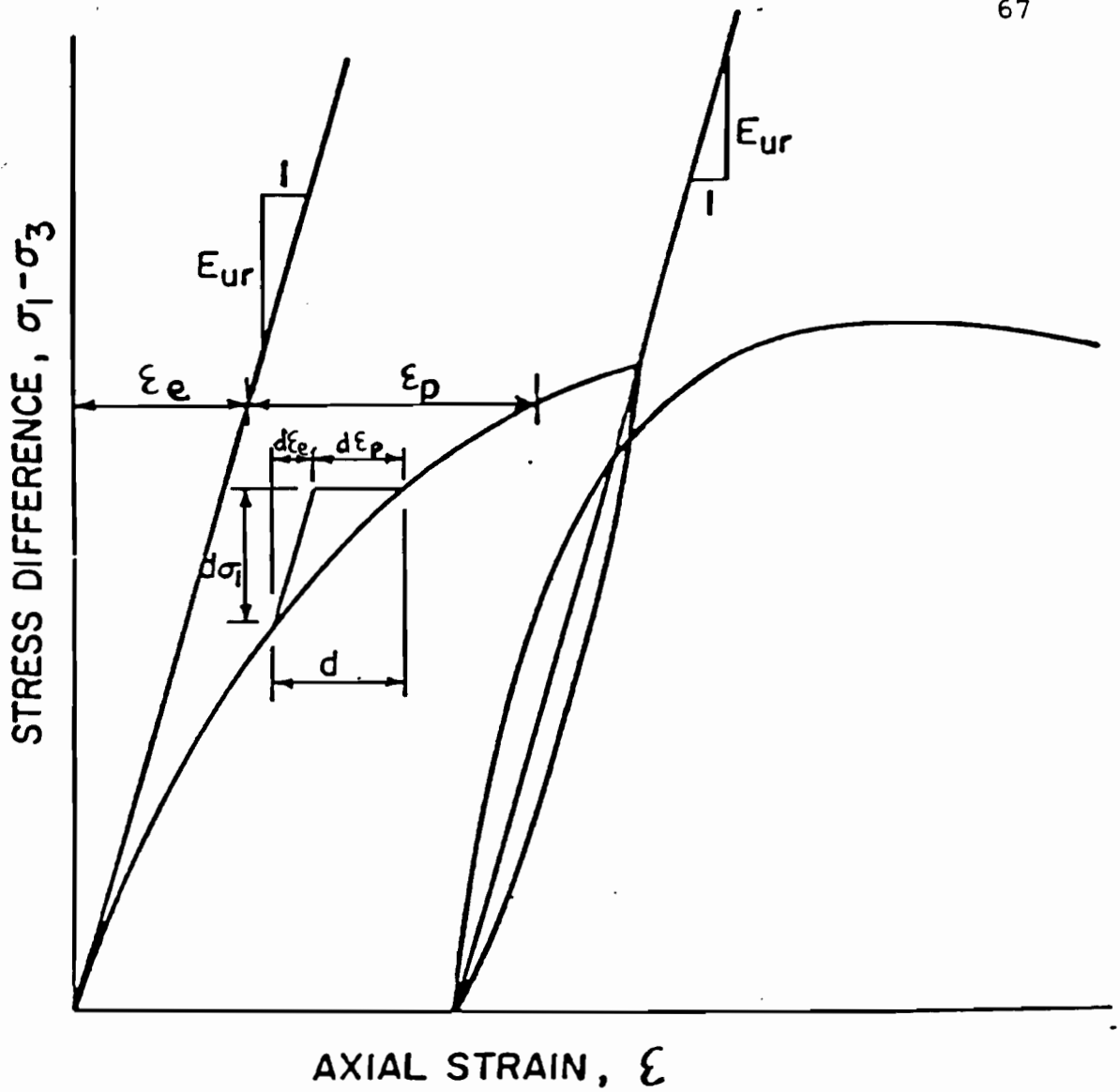
Figure 3.8.   Illustration of elastic and plastic strain
              components in triaxial compression test
              (Coon, 1971)

The nature of the strains described in Figure 3.9 are discussed below.

3.2.1 Elastic Strains

The elastic strain increments, which are recoverable upon loading, are calculated by Hooke's Law, using the unloading-reloading modulus defined by Duncan and Chang (30).

$$E_{ur} = K_{ur} \cdot P_a \left(\frac{\sigma_3}{P_a} \right)^n \qquad (3.35)$$

where

K_{ur} = modulus number (dimensionless)

n = dimensionless exponent

σ_3 = confining pressure

P_a = atmospheric pressure.

K_{ur}, n, σ_3 and P_a are determined using triaxial compression tests.

3.2.2 Plastic strains

In most plasticity theories, the constitutive equations consist of some form of (62):

1) Yield criterion which determines the onset of permanent deformation.
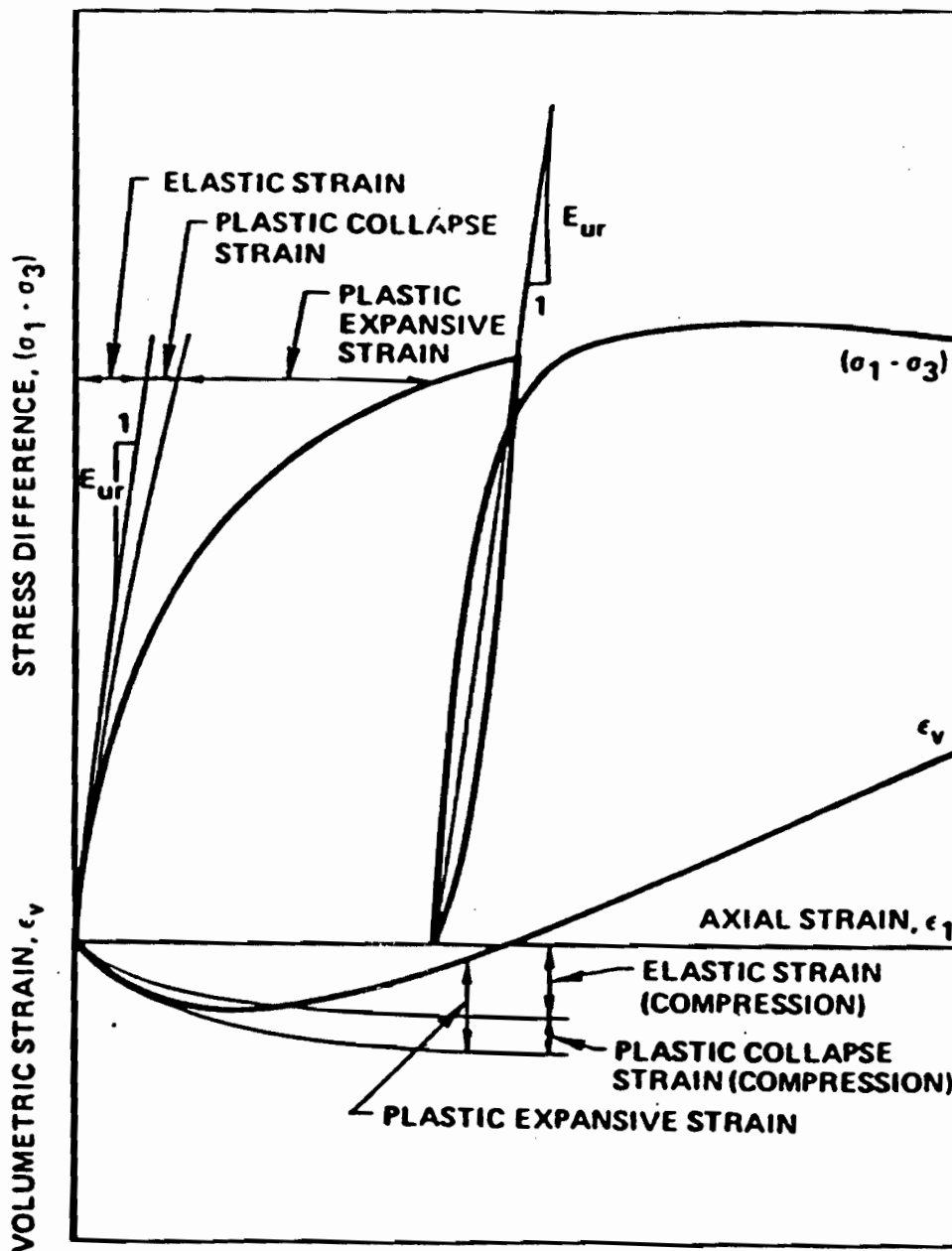
Figure 3.9. Schematic representation of elastic, plastic collapse and plastic expansive strain components (Lade, 1977)

2) A rule which relates the rate of plastic
   deformation to stress and other variables.

3) Hardening or softening law which describes rate at
   which the material hardens or softens while
   undergoing plastic deformation.

3.2.2.1 Yield criteria

Yield criteria define the limit of elasticity under
given stressing situations. The yield surface is a law
defining the limit of elasticity under any combination of
stresses. It has been determined experimentally that
hydrostatic pressure does not affect yielding, except for
very high pressures (37).

The Coulomb-Mohr failure criterion is the ideally plas-
tic yield conditions and can be represented in the form
proposed by Drucker and Prager (1952) as (see Figure 3.10),

$$f = \sqrt{J_2} - k + \alpha J_1 = 0 \qquad (3.36)$$

where

J_1 = the first invariant of stress deviator tensor

J_2 = the second invariant of stress deviator tensor

α = a coefficient which depends on angle of internal
friction

k = a constant proportional to the cohesion

f = plastic potential

The above model has the following shortcomings:

1) The amount of dilatancy (plastic rate increase under shear loading) predicted is much greater than observed experimentally.

2) Tests indicate a considerable hysteris in a hydrostatic loading-unloading path which cannot be predicted using the same elastic bulk modulus of loading and uinloading and a yield surface which does not cross the hydrostatic (J_1) axis.

3) At high pressure levels, as the material passes to a fluid state, shear strength should not vary with hydrostatic pressure, i.e., the yield condition should be essentially independent of J_1 for large J_1.

Roscoe and his co-workers at Cambridge University (1969) formulated a cohesionless two-dimensional yield model for soils (granular material) which, when generalized as shown in Figure 3.11. The discontinuous slope at the intersection with the J_1 axis predicts behavior that does not seem to be supported by experiments. There are also mathematical doubts about uniqueness of the model.

A group at the Massachusetts Institute of Technology (Christian, 1966, Tang and Hoeg, 1968) has suggested a
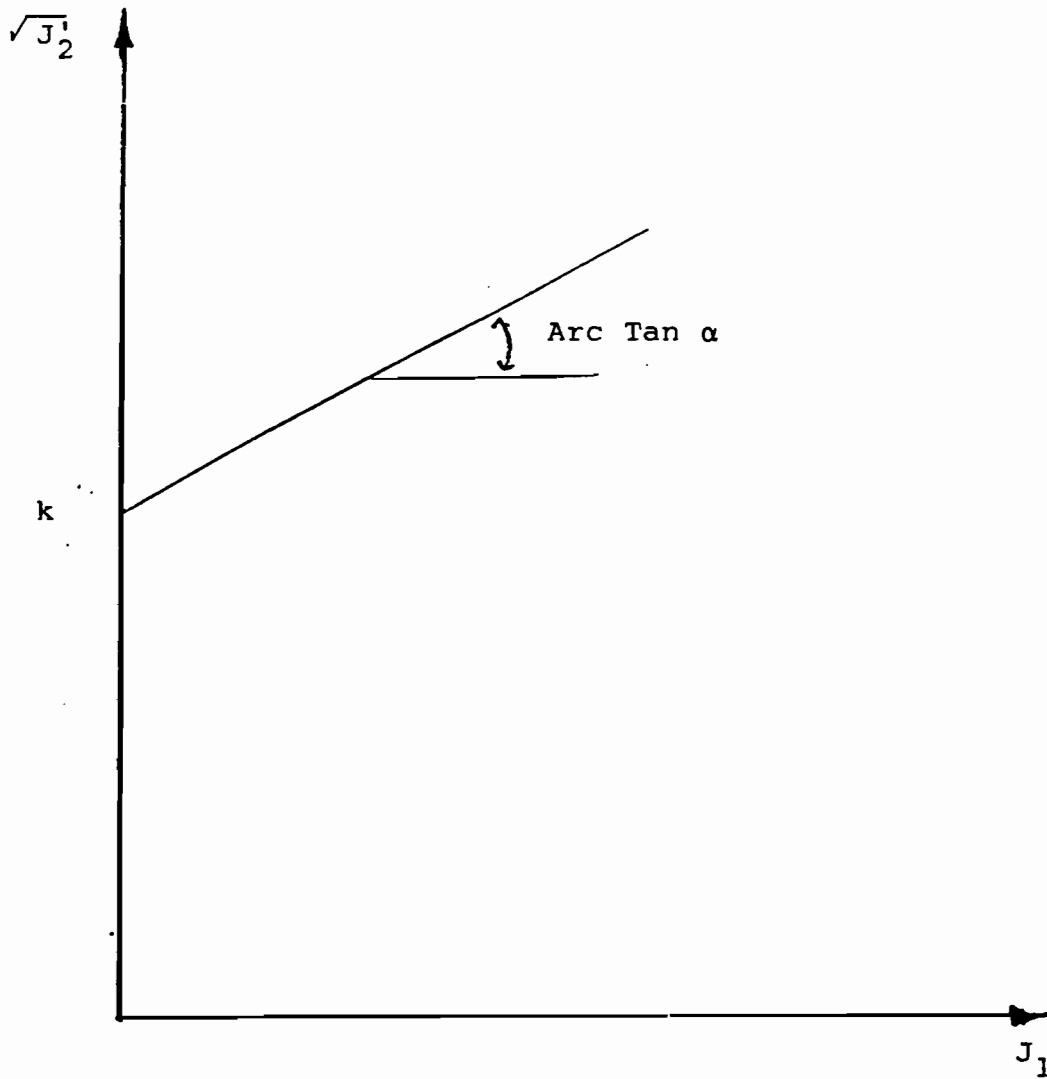
Figure 3.10. Drucker-Prager yield model (Coon, 1971)
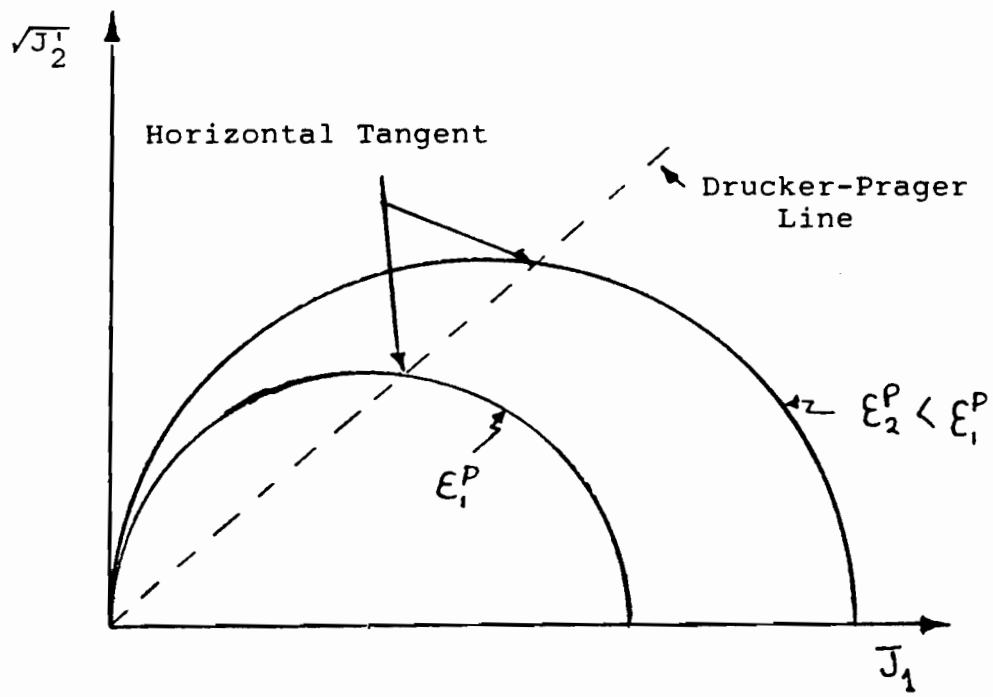
Figure 3.11. Model proposed by Roscoe et al. (Coon, 1971)
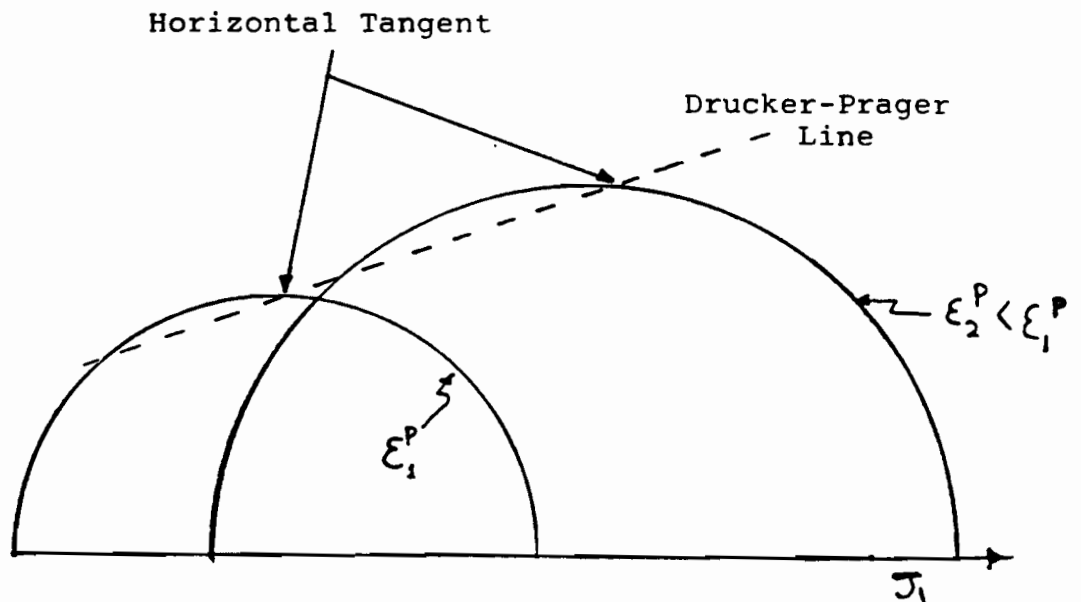
Figure 3.12. MIT model (Coon, 1971)

related model, shown in Figure 3.12 where the yield curves are ellipses of constant eccentricity, and used it in a diagram to study a step footing.

3.2.2.2 Work Hardening

The work done per unit volume on an element during straining is

$$dW = \sigma_{ij}d\varepsilon_{ij} = \sigma_{ij}(d\varepsilon_{ij}^e + d\varepsilon_{ij}^p)$$

$$= dW^e + dW^p \qquad \qquad (3.37)$$

where

    dW = work done per unit volume

    e = refers to elastic component

    p = refer to plastic component

Now,

$$dW^e \equiv \sigma_{ij}d\varepsilon_{ij}^e \quad \text{is recoverable elastic energy.}$$

$$dW^p \equiv \sigma_{ij}d\varepsilon_{ij}^p \quad \text{is unrecoverable due to the irreversible}$$

plastic straining. This is the plastic work per unit volume.

Now

$$dW^p = \sigma_{ij}d\varepsilon_{ij}^p = S_{ij}d\varepsilon_{ij}^p \qquad \qquad (3.38)$$

where

$$S_{ij} = \text{deviatoric stress tensor}$$

In terms of principal stresses,

$$dW^P = S_1 d\varepsilon_1^P + S_2 d\varepsilon_2^P + S_3 d\varepsilon_3^P \qquad (3.39)$$

Generally, there are two hypotheses used to measure work hardening (37). The first one is the "equivalence of plastic work" hypothesis, where the amount of work-hardening is thought to depend only on the total plastic work and to be independent of strain path. The implication is that resistance to further yielding de- pends only on the amount of work done on the material. This amount of work is measured by the yield criterion. Therefore,

$$F(\sigma_{ij}) = K \qquad (3.40)$$

where

   F = yield criterion

   K = is a function of plastic work done per unit volume;

   it changes as the material work hardens assuming

   isotropic hardening, i.e., $F(\sigma_{ij})$ remains the same.

We can write,

$$F(\sigma_{ij}) = f(W^P) \qquad (3.41)$$

where,

$$W^P = \int \sigma_{ij} d\varepsilon_{ij}^P \qquad (3.42)$$

In the second hypothesis, the equivalent plastic strain, $d\varepsilon_p$, is used as a measure of work hardening. If

   $d\varepsilon_p$ = equivalent plastic strain

$$= \frac{\sqrt{2}}{3} \left[\begin{array}{c} (d\varepsilon_x^p - d\varepsilon_y^p)^2 + (d\varepsilon_y^p - d\varepsilon_z^p) + d\varepsilon_z^p - d\varepsilon_x^p)^2 \\ + 6(d\varepsilon_{xy}^p)^2 + 6(d\varepsilon_{xy}^p)^2 + (d\varepsilon_{zx}^p)^2 \end{array} \right]^{1/2} \tag{3.43}$$

then,

$$\varepsilon_p = \int d\varepsilon_p \tag{3.44}$$

$$= \text{plastic strain}$$

The yield function is assumed to be a function of the equivalent plastic strain, and,

$$F(\sigma_{ij}) = H(\varepsilon_p) \tag{3.45}$$

If,

$$\sigma_e = \frac{1}{\sqrt{2}} \left[(\sigma_x - \sigma_y)^2 + (\sigma_y - \sigma_z)^2 + (\sigma_z - \sigma_x)^2 + 6(\tau_{xy}^2 + \tau_{yz}^2 + \tau_{zx}^2) \right]^{1/2}$$

$$= \text{equivalent stress} \tag{3.46}$$

then

$$\sigma_e = H(\varepsilon_p) \tag{3.47}$$

Assuming von Mises yield criterion (see Appendix A) and isotropic hardening, the above hypotheses are equivalent,

$$W^p = \int \sigma_{ij} d\varepsilon_{ij}^p = \int \sigma_e d\varepsilon_p \tag{3.48}$$

Hence

$$\sigma_e = f \left(\int \sigma_e d\varepsilon_p \right)$$

$$= H(\varepsilon_p) \tag{3.49}$$

Generally, (3.46) and (3.47) need not be the same because

of anisotropy and Baushinger effect.

Generally, there are three modes of hardening:

(i) Isotropic Hardening -- in this case the yield
surface is allowed to expand concentrally from the initial
yield surface without a change in shape, the yield
condition is expressed mathematically as:

$$f(S_{ij}) - q_i = 0 \qquad (3.51)$$

where,

S_{ij} = stress tensor

q_i = history of deformation parameters

f = history dependent function.

(ii) Kinematic Hardening -- here Baushinger effect is
allowed for by letting the yield surface move in space
without changing its shape or size therefore,

$$f(S_{ij} - \alpha_{ij}) - q_1 = 0 \qquad (3.52)$$

where

q_1 = a constant

and for Prager Linear Kinematic Hardening (62)

$$\alpha_{ij} = c\varepsilon_{ij} \qquad (3.53)$$

Eisenberg (1968,62) proved that for nonlinear kinematic
hardening,

$$\alpha_{ij} = q_2\varepsilon_{ij} \qquad (3.54)$$

where

$$q_2 = \text{constant} \tag{3.55}$$

Behavior incorporating isotropic and kinematic hardening can be made by letting q_1 above be a variable

(iii) Anisotropic Hardening -- Here the yield surface expands, rotates, distorts and is translated in space.

3.2.2.3 Plastic Stress Strain Relations

Drucker (1950,1952,37) has presented a general derivation of plastic stress strain relations for a given state of stress, if an external agency applies an additional set of stresses and then slowly removes them. Work hardening implies that for all such added sets of stresses the material will remain in equilibrium, and

1) Positive work is done by the external agency during the application of the set of stresses

2) The net work performed by it over the cycle of application and removal is zero or positive

Mathematically, suppose that to a state of stress $\sigma_{ij}*$ and strain ε_{ij} some external agency applies small surface forces so that the stress at each point is changed by an amount $d\sigma_{ij}$ and strain by an amount $d\varepsilon_{ij}$ (see Figure 3.13). Part of
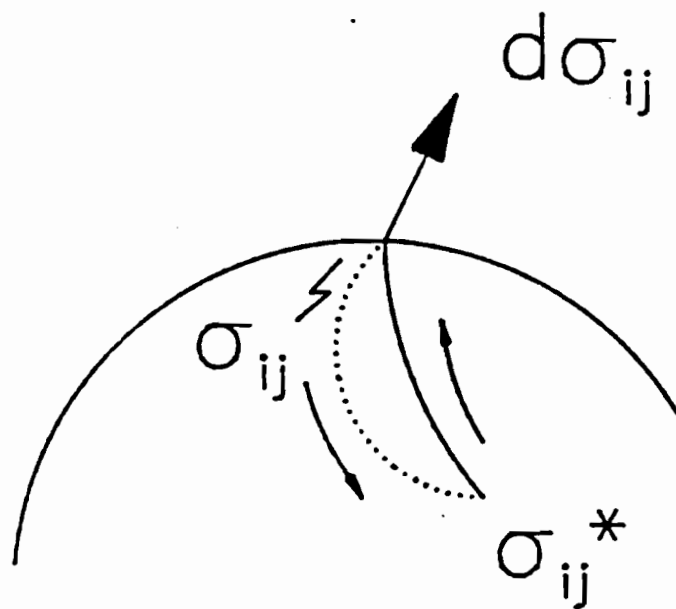
Figure 3.13. Stress path produced by external agency
(Mendelson, 1968)

$d\sigma_{ij}$ is elastic and part may be plastic, i.e.,

$$d\varepsilon_{ij} = d\varepsilon_{ij}^e + d\varepsilon_{ij}^p$$

Now suppose these added forces are removed, thus releasing the elastic strain increments, $d\varepsilon_{ij}^e$. It then follows from implication (1) above that for work hardening

$$d\sigma_{ij}\, d\varepsilon_{ij} > 0 \tag{3.56}$$

and, from (2),

$$d\sigma_{ij}(d\varepsilon_{ij} - d\varepsilon_{ij}^e) \geq 0$$

or

$$d\sigma_{ij}(d\varepsilon_{ij}^e + d\varepsilon_{ij}^p) > 0$$

$$d\sigma_{ij}d\varepsilon_{ij}^p \geq 0 \tag{3.57}$$

Equation (3.57) is the mathematical definition of work hardening.

In the derivation of a relation for plastic stress and strain, two further assumptions are made:

1) A loading function exists. At each stage of the plastic deformation there exists a function $f(\sigma_{ij})$ so that further deformation takes place only for $f(\sigma_{ij}) > k$. Both f and k may depend on the existing state of stress and on the history of strain.

2) The relation between infinitesimals of stress and plastic strain is linear, i.e.,

plastic strain is linear, i.e.,

$$de^p_{ij} = C_{ijkl}d\sigma_{kl} \qquad (3.58)$$

Equation (3.58) seems reasonable but has no theoretical justification, it is merely an assumption (37)

c_{ijkl} = tensors which may be a function of stress, strain and history of loading; (3.58) implies that they are independent of $d\sigma_{kl}$.

From (1) above, it follows that,

$$df(\sigma_{ij}) > 0 \qquad (3.59)$$

or

$$\frac{\partial f}{\partial \sigma_{ij}}d\sigma_{ij} > 0 \qquad (3.60)$$

From (2) above, it follows that superposition principle may be applied to stress and strain increments, i.e., if

$d\sigma'_{ij}$ and $d\sigma''_{ij}$ are two stress increments producing strain

increments, $de^{p'}_{ij}$ and $de^{p''}_{ij}$, then an increment $d\sigma_{ij} = d\sigma^{p'}_{ij}$

$+ d\sigma^{p''}_{ij}$, will produce an increment, $de^{p'}_{ij} + de^{p''}_{ij}$.

Now assume that for a state of stress σ_{kl}, an increment

of stress $d\sigma_{kl}$ producing plastic flow is imposed. The
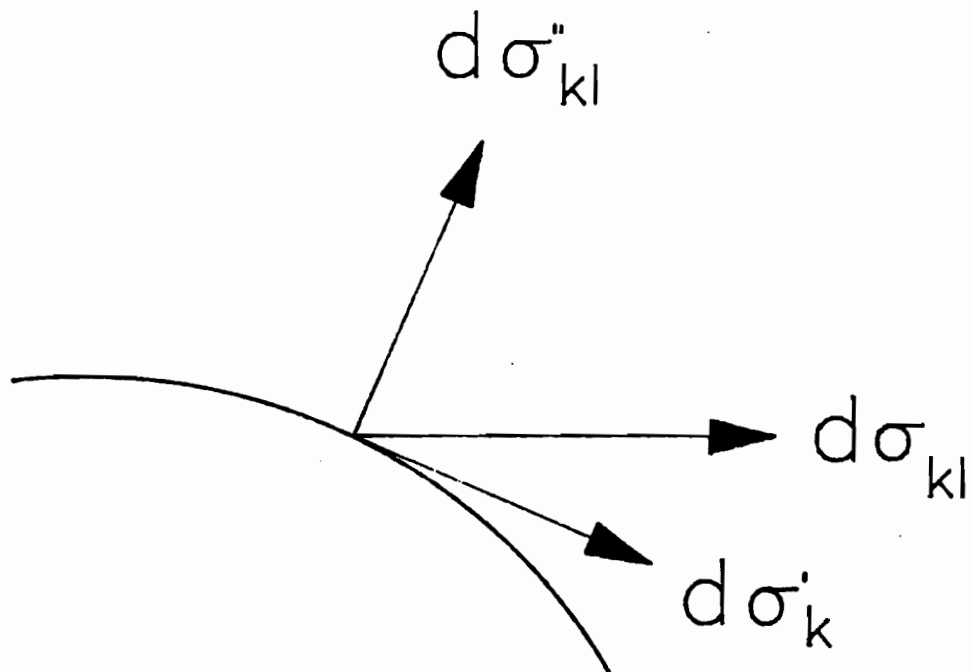
Figure 3.14.   Decomposition of stress increment vector
               (Mendelson, 1968)

increment $d\sigma_{kl}$ can be decomposed into two parts $d\sigma'_{kl}$ and

$d\sigma''_{kl}$ such that $d\sigma'_{kl}$ produces flow and $d\sigma''_{kl}$ is proportional

to the gradient of $f(\sigma_{ij})$, see Figure 3.23.

Since $d\sigma_{kl}$ produces flow,

$$\frac{\partial f}{\partial \sigma_{kl}} d\sigma_{kl} = \frac{\partial f}{\partial \sigma_{kl}} \left(d\sigma'_{kl} + d\sigma''_{kl} \right) > 0 \tag{3.61}$$

But $d\sigma'_{kl}$ produces no plastic flow, therefore

$$\frac{\partial f}{\partial \sigma_{kl}} d\sigma'_{kl} = 0 \tag{3.62}$$

Also, $d\sigma''_{kl}$ has been taken proportional to the

gradient of f; therefore

$$d\sigma''_{kl} = a\frac{\partial f}{\partial_{kl}} \tag{3.63}$$

where a = scalar > 0

from (3.61), (3.62) and (3.63)

$$\frac{\partial f}{\partial \sigma_{kl}} d\sigma_{kl} = \frac{\partial f}{\partial \sigma_{kl}} d\sigma''_{kl} = \frac{\partial f}{\partial \sigma_{kl}} a\partial_{kl}\partial F > 0 \tag{3.64}$$

Hence,

$$a = \frac{\partial f/\partial \sigma_{kl}}{(\partial F/\partial \sigma_{mn})(\partial F/\partial \sigma_{mn})} \tag{3.65}$$

Equation (3.65) proves the proposed decomposition. From the above

$$d\varepsilon_{ij}^{p} = h_{ij}a \tag{3.66}$$

or

$$d\varepsilon_{ij}^{p} = g_{ij}\frac{\partial f}{\partial \sigma_{kl}}d\sigma_{kl} \tag{3.67}$$

where g_{ij} = stress, strain, and history of loading

dependent.

From the second of conditions of (3.113),

$$d\sigma_{ij}d\varepsilon_{ij}^{p} = (d\sigma_{ij}' + d\sigma_{ij}'')d\varepsilon_{ij}^{p} \geq 0 \tag{3.68}$$

But $d\sigma_{ij}'$ produces no flow, hence

$$d\sigma_{kl}'d\varepsilon_{ij}^{p} = d\sigma_{kl}'g_{ij}\frac{\partial f}{\partial \sigma_{kl}}d\sigma_{kl} = 0 \tag{3.69}$$

But

$$\frac{\partial f}{\partial \sigma_{kl}}d\sigma_{kl} > 0$$

Hence

$$d\sigma_{ij}'g_{ij} = 0$$

Hence, comparing with (3.66)

$$g_{ij} = G\frac{\partial f}{\partial \sigma_{ij}} \tag{3.70}$$

where,

G = scalar which may depend on stress, strain

and history.

Therefore,

$$d\varepsilon_{ij}^{p} = G\frac{\partial f}{\partial \sigma_{ij}} \frac{\partial f}{\partial \sigma_{kl}} d\sigma_{kl} \qquad (3.71)$$

or

$$d\varepsilon_{ij}^{p} = G\frac{\partial f}{\partial \sigma_{ij}}df \qquad (3.72)$$

(3.72) is the general stress-strain relation consistent with the above assumptions.

For the specific case of the von Mises yield function (describ3ed in Appendix A), let

$$f = J_2 = \frac{1}{6}[(\sigma_1 - \sigma_2)^2 + (\sigma_2 - \sigma_3)^2 + (\sigma_3 - \sigma_1)^2]$$

$$\frac{\partial f}{\partial \sigma_1} = \frac{2}{3}[\sigma_1 - \frac{1}{2}(\sigma_2 + \sigma_3)]$$

therefore,

$$d\varepsilon_1^{p} = \frac{2}{3}d\lambda[\sigma_1 - \frac{1}{2}(\sigma_2 + \sigma_3)] \qquad (3.73)$$

where

$$d\lambda = Gdf \qquad (3.74)$$

(3.74) is called the Prandtl-Reuss equations.

For the Tresca yield condition (see Appendix A),

$$f = \frac{1}{2}(\sigma_1 - \sigma_3)$$

$$\frac{\partial f}{\partial \sigma_1} = \frac{1}{2}, \quad \frac{\partial f}{\partial \sigma_2} = 0, \quad \frac{\partial f}{\partial \sigma_3} = \frac{1}{2}$$

Then

$$d\varepsilon_1^P = \frac{1}{2}d\lambda$$

$$d\varepsilon_2^P = 0$$

$$d\varepsilon_3^P = \frac{1}{2}d\lambda \qquad (3.75)$$

From the above, it is noted that Tresca and von Mises yield criteria have different associated flow rules, i.e., stress-strain relations associated with each criterion.

3.3 Discussion

As discussed earlier in this section, the mechanical behaviors of biological grains are complex. They exhibit elastic, plastic and time dependent properties. It may therefore seem that some of them at least are elastoviscoplastic in behavior. Any constitutive relations developed for such materials must therefore incorporate parameters which account for the totality of mechanical behavior, otherwise the constitutive equation may have limitations in predicting loads in silos.

4. MATERIAL PROPERTIES AND EXPERIMENTAL DESIGN

As already discussed the complex nature of grain-bin interaction especially during dynamic conditions makes governing equations and their theoretical solutions too complex. Even if an adequate quantitative theory could be worked out, experiments are still necessary to verify it because theories are invariably based on certain assumptions which may or may not be precisely satisfied in practice. Dimensional analysis combined with experiments is therefore a powerful tool in development of governing* equations.

4.1. Similitude Concepts

Murphy (43) has defined a scale model as a device which is so related to a physical system that observations on the model may be used to predict accurately the performance of the physical system in the desired respect. The physical system for which the predictions are made is called the

---

*A glossary of similitude theory terms is included in the Appendix.

prototype. The experimenter uses similitude principles in the selection of experiments capable of yielding information significant to the study, and to avoid redundant experiments. The results of tests performed under one set of conditions can be applied to another set of conditions. This procedure is made possible and justifiable by the laws of similarity.

The principles of similitude can also be used to get a prediction equation for a particular system. According to Murphy (43) all physical systems can be described by a dimensionally homogeneous relationship among physical quantities of the form*

$$C_0 = Q_1^{q_1} \cdot Q_2^{q_2} \cdot Q_3^{q_3} \ldots\ldots Q_i^{q_i} \qquad (4.1)$$

where

C_0 = dimensionless coefficient

Q_i's are governing quantities for the system, and

q_i's are dimensionless exponents.

According to the Buckingham-Pi theorem,* for relationships of the form in Equation (4.1), "The number of dimensionless and independent groups that can be formed from the Q's is (i-r) where i is the number of governing

---

*Proof is included in the Appendix.

quantities, and r is the rank of the dimensional matrix of the Q's."

4.1.1 The Prediction Equation

The concept of component equations is used to obtain a prediction equation. A component equation is one obtained by finding a mathematical expression that fits the data from a set of experiments in which all but one of the independent Π-terms is held constant.

For example, if

$$\Pi_1 = f(\Pi_2, \Pi_3)$$

one can obtain a component equation relating Π_1 and Π_2 by varying Π_2 through some selected range of values. Π_1 is measured for each value of Π_2, while controlling Π_3 so that its value does not change. From this experiment one can obtain

$$\Pi_{12} = f_2(\Pi_2, \overline{\Pi}_3)$$

where $\overline{\Pi}_3$ means Π_3 is held constant.

Similarly, a component equation relating Π_1 and Π_3 can be found:

$$\Pi_{13} = f_3(\overline{\Pi}_2, \Pi_3)$$

If the data for $\Pi_{13} = f(\Pi_3)$, from each component experiment plot as a straight line on log-log coordinates, then each component equation has the form

$$\Pi_1 = A\Pi_i^{n_i} \qquad (4.2a)$$

and the prediction equation for the system is

$$\Pi_1 = \phi \cdot \Pi_2^{m_2} \cdot \Pi_3^{m_3} \ldots\ldots\ldots \Pi_{i-r}^{m_i-r} \qquad (4.2)$$

where all the Π's are dimensionless and independent products that can be formed from the given Q's and ϕ can be a function of the independent Π terms.

There may be experiments for which the data does not plot as straight line on log-log coordinates. For these experiments one can use other proposed chosen mathematical functions for the data.

Equation (4.2) above can be rewritten in the more general form

$$\Pi_1 = \phi\Pi_2' \cdot \Pi_3' \ldots\ldots \Pi_i' \ldots\ldots \Pi_n' \qquad (4.3)$$

where

$$\Pi_1 = f(\Pi_i)$$

Here, $f(\Pi_i)$ is an appropriate function which may be

non-linear when Π_1 is plotted as a function of Π_i on

log-log coordinates. For each observation of Π_i as a

function of one independent Π-term, ϕ can be evaluated from

$$\phi = \frac{\Pi_1}{\Pi_2^{'}\ \Pi_3^{'}\ \ldots\ldots\Pi_n^{'}}$$

and the mean value of ϕ calculated.

The precision of the prediction equation can be

evaluated by first plotting Π_i observed (Π_{io}) versus Π_i

calculated (Π_{ic}), where Π_i i.e., Π_{io} observed is

experimentally measured Π_i for each experiment, and Π_{ic} is

the value computed by applying the prediction equation and

then calculating the correlation coefficient, Π_{io} versus

Π_{ic}.

4.2 Selection of Fundamental Physical Quantities

The initial step in the development of a prediction

equation is to identify the nonredundant independent and

complete set of physical quantities pertinent to the
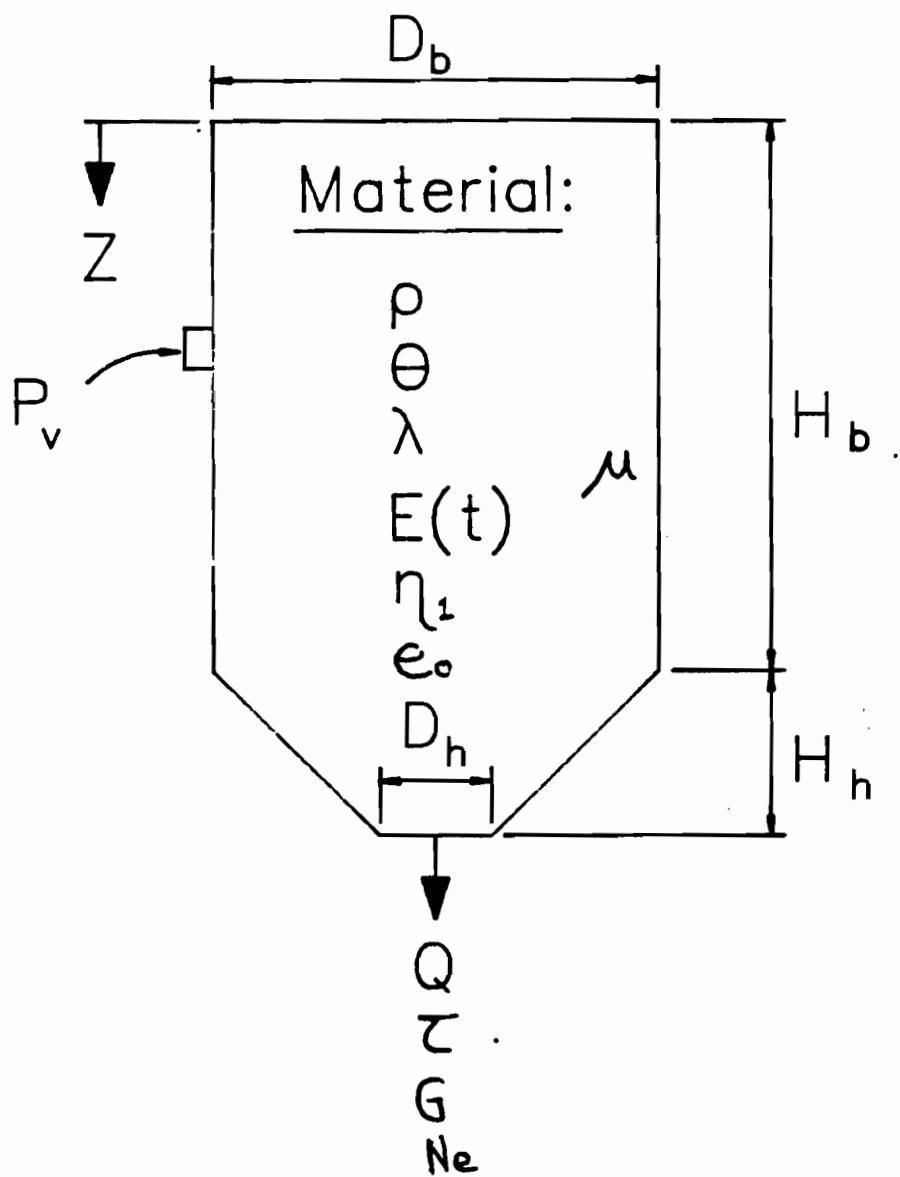
Figure 4.1. Identification of quantities in grain-bin system

desired system. Figure 4.1 is a representation of the physical quantities in a grain bin.

4.2.1 Static System

4.2.1.1 Gravity (G)

Gravity field forces are responsible for weight of the grain on the bin floor or hopper. If there were no gravity the material would not exert any force on the bin wall or bottom and would not flow when the outlet is opened. Hence gravity is a pertinent physical quantity to the system.

4.2.1.2 Bin diameter (D), wall height (H), and place of occurrence (Z)

Reimbert and Reimbert (54), Safarian (28) and many other authors discuss the variations in wall pressure due to different grain heights and silo diameters. The author assumes that critical values of the bin loads will occur for the case of the bin being filled to the top. Z is the distance from the top to where the wall pressure is measured.

4.2.1.3 Grain Particle Density (ρ)

Versavel (77) as well as many researchers have written

on the importance of grain density to (ρ) grain pressures in silos. Grain particle density is therefore considered as a pertinent physical quantity.

4.2.1.4 Characteristic length of fill particles (λ)

Singh (63) has discussed the importance of the

characteristic particle length (λ). This quantity is

considered to be pertinent.

4.2.1.5 Angle of internal friction of the fill

   particle under static conditions (ϕ)

Gaylord and Gaylord (10), Reimbert and Reimbert (25),

Moysey (20), and Schwedes (30) as well as many others have

documented the influence of the angle of internal friction

of the ensiled material on silo loads. The above quantity,

ϕ, is therefore considered to be pertinent.

4.2.1.6 Wall friction between fill and the inside

   surface of the silo

Schwedes (61), Briassou (7), and Mohsehin (39) have all

contributed to the vast pool of literature on the effect of

the material-wall friction (μ) and silo loads. It seems

obvious that some of the weight of the ensiled material is

carried by the wall due to friction.

4.2.1.7 Bin wall modulus of elasticity (E_w)

Tyson and Manbeck (74) have discussed the interaction

between bin wall stiffness and emptying pressures. Singh

(63) has also discussed the same factor in similar

circumstances. The author believes that even in the static

conditions this factor affects silo loads, as it relates wall deformations to grain loads.

4.2.1.8 Silo wall thickness (t_w) and Poisson's ratio (v_w)

Silo wall thickness is obviously important to the ability of the silo wall to withstand loads. The thicker the wall the more load it can withstand and vice versa.

Poisson's ratio v is obviously important because of the multi-dimensionality of the applied load.

4.2.1.9 Horizontal (P_h) and Vertical Pressures (P_v)

The horizontal (P_h) and vertical (P_v) wall pressure are the quantities to be predicted.

4.2.1.10 The Ratio of the Horizontal to the Vertical Pressure (k)

The lateral to vertical grain pressure ratio, or pressure ratio as it is commonly termed, is an assumed coefficient relating lateral and vertical pressures at any point in a grain mass (9). Janssen (1895) first proposed the use of this coefficient (which he assumed to be constant) in silo pressure calculations. Koenen improved Janssen's method by introducing the term $k = (1 - \sin\phi)/(1 + \sin\phi)$, or simply $k = \tan^2 (45° - \phi/2)$. If the pressure

ratio is to be considered an independent material property then it should be unaffected by external factors. If it is not a constant then it should only vary within the material. Clower et al. (1973) and Moysey and Brown (1979) concluded that the pressure ratio was constant with depth (i.e., pressure) (90). However several investigations found that k was not constant but varied with depth. Ketchum and Williams (1919), Lenczner (1963), and Kramer (1944) all found that k increased with depth of grain. Pleissner (Ketchum 1919) and Caughey et al. (1951) found that k decreased with depth. Jaky (1948) and Reimbert and Reimbert (1976) found k to be variable but following no simple pattern with increasing depth.

The work of the last group of investigators would indicate that k may not be a valid property. Alternatively investigators may not be measuring the pressure ratio but a value which has been influenced by external factors.

The different methods of determining k by various investigators may also influence the values they obtained. Loewer et al (31) used a method described by Clower et al (1973); this method involved measuring frictional resistance caused by drawing two blades, one oriented horizontally and the other vertically, through the confined granular mass. The enclosure for the granular material was 0.457 m by 0.457 m by 0.076 m high. Britton and Versavel

(11) used the method developed by Jofriet and Negi (1983), which involved the use of a 0.203 m diameter by 0.40 m high model silo. They then used the differential form of the Janssen's formula to evaluate the product of k and the

grain-wall coefficient of static friction, μk, from data obtained by applying different vertical loads to the grain-filled model. Load measurements were made with a load cell. This method presupposes the validity of the Janssen's formula and the existence of an independent k, both of which are still subject to controversy. Thompson (68) used a 0.15 m by 0.3 m by 0.3 m high grain container, with flexible diaphragms on two walls to evaluate k. Other researchers have used split models mounted with strain gages or load cells to evaluate k. The size of the model used for evaluating k is obviously important. Safarian and Harris (68) have discussed pressure variations due to depth and width of silos. To diminish these effects it is, obviously, necessary to diminish the size of the experimental specimen holder (model bin). The property k is thought to be a material property occurring at specific points within the grain mass. It is therefore necessary to simulate conditions at a point by using models which are as small as possible in the evaluation; otherwise some average property would be evaluated.

A method of experimentally investigating the validity

of k is described in Section 4.3.

4.2.1.11 Relaxation Modulus (E(t))

The relaxation modulus of the material is thought to be an adequate index of the viscoelastic properties of the material. Although it applies to linearly viscoelastic material, it may also provide an approximation of the behavior of non-linearly viscoelastic materials. It was therefore included in the study.

4.2.1.12 Yield Constant (η_1)

As discussed in Section 3, plasticity is also an important characteristic in the behavior of the biological grains. Manbeck and Nelson (35) included an index stress

level σ_c to account for the yielding and subsequent plastic behavior of wheat en masse. Zhang et al. (78) have

evaluated the yield constant (η_1) for wheat en masse using

criteria developed by Lade (29). The yield constant η_1 is

dimensionless and can be evaluated by plotting (I_1^3/I_3 - 27)

versus I_1/P_a on log-log space.

I_1, I_3 = the first and third invariants of stress

P_a = atmospheric pressure

at failure

$$f_p = \eta_1$$

where f_p = plastic expansive loading function,
dimensionless.

The yield constant is considered to be an index of the plasticity of the material as it is derived in terms of the stress invariants which are important to plasticity as discussed in Section 3. The plastic strains involved are small, just above yielding, hence η_1 represents yield and subsequent immediate plastic deformation.

4.2.1.13 Initial Voidage of Fill Material (e_0)

Manbeck and Nelson (35) described (e_0) as a pertinent quantity to the development of pressure in wheat.

4.2.1.14 Poisson's Ratio of Fill Material (v_g)

The Poisson's ratio of a material is an important property of the material load deformation characteristics during elastic loading. As most fill materials exhibit, in part, elasticity v_g is a pertinent quantity to the development of loads.

4.2.2 Dynamic Conditions (During Emptying)

In addition to the above physical quantities, others

are pertinent to the system under dynamic conditions.

4.2.2.1 Newton's Second Law Inertial Coefficient (Ne)

Due to material aceleration inertial forces may be

developed in the system. Hence Ne (Newton's Second Law

Inertial Coefficient) is thought to be a pertinent

quantity.

4.2.2.2 Elapsed Time of Discharge (τ)

The process of emptying is a time dependent phenomenon

(31). Hence τ is considered a pertinent quantity. This

factor is also important to the viscoelasticity of the

material.

4.3 Investigation of the Validity of Janssen's
Constant "k"

The objective of the experimental procedure described below is to ascertain whether or not the proposed quantity "k", the ratio of the horizontal to the vertical pressure at a specified point in the grain mass, is pertinent to the development of grain pressures, is independent, and can be evaluated as a property of a system of a grain filled bin. An experimental procedure for measuring both the vertical and horizontal pressure was devised. Figure 4.2 is a schematic representation of the experimental apparatus. A lucite cylinder 5.08 cm in diameter by 5.08 cm high with a wall thickness of 0.158 cm was filled with various granular materials. The cylinder was made as small as possible in order to eliminate variations due to location within the grain mass, as "k" is thought to exist at all specific points within the grain mass. An Instron testing machine was used to apply surcharge pressure to the granular material at increasing intensities as to model increases in pressure with depth in a granular mass.

A Hewlett Packard data acquisition unit 3497A and a micro-computer HP9836A were used for control, measurement and storage of data. The vertical pressures, P_v, were measured directly from the Instron machine by the data
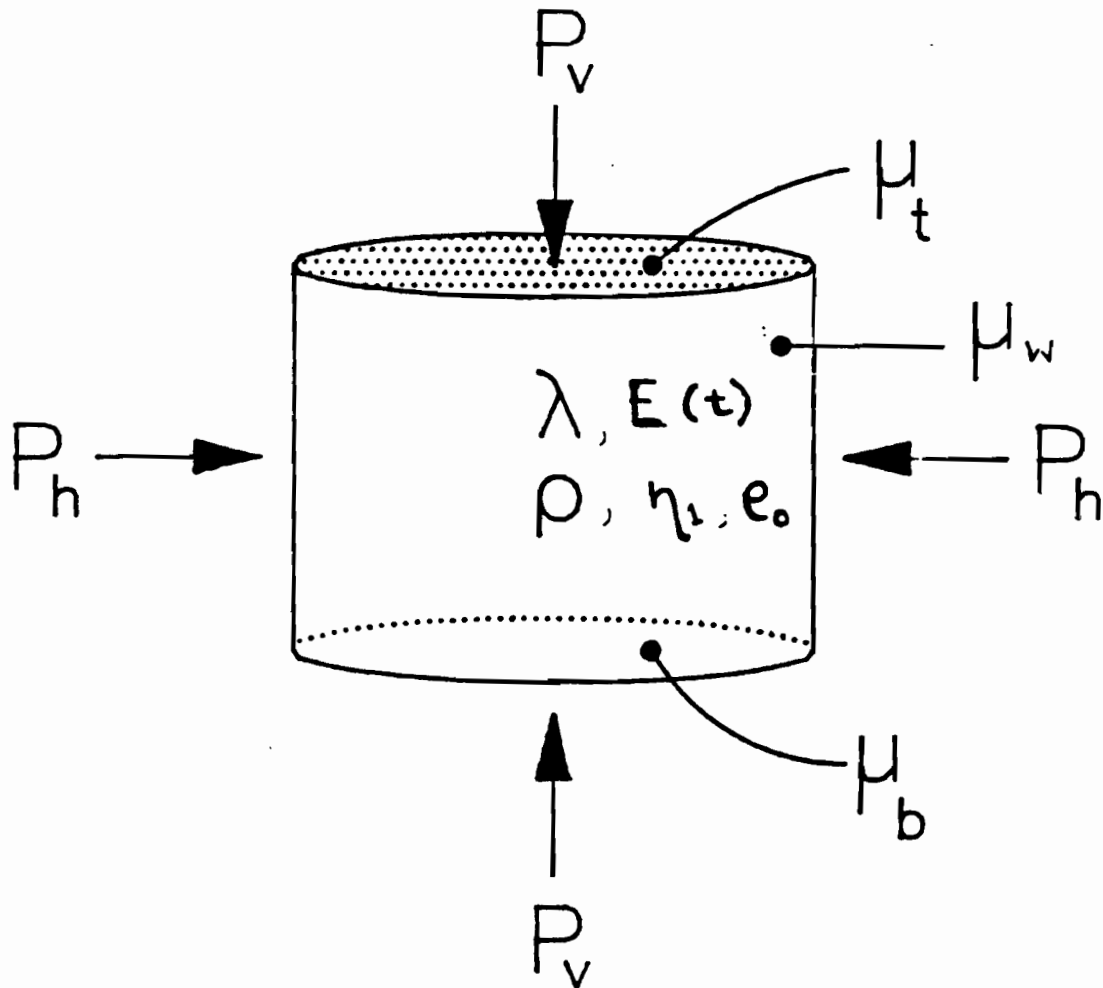
Figure 4.2. Cell used for verifying the validity of 'K'
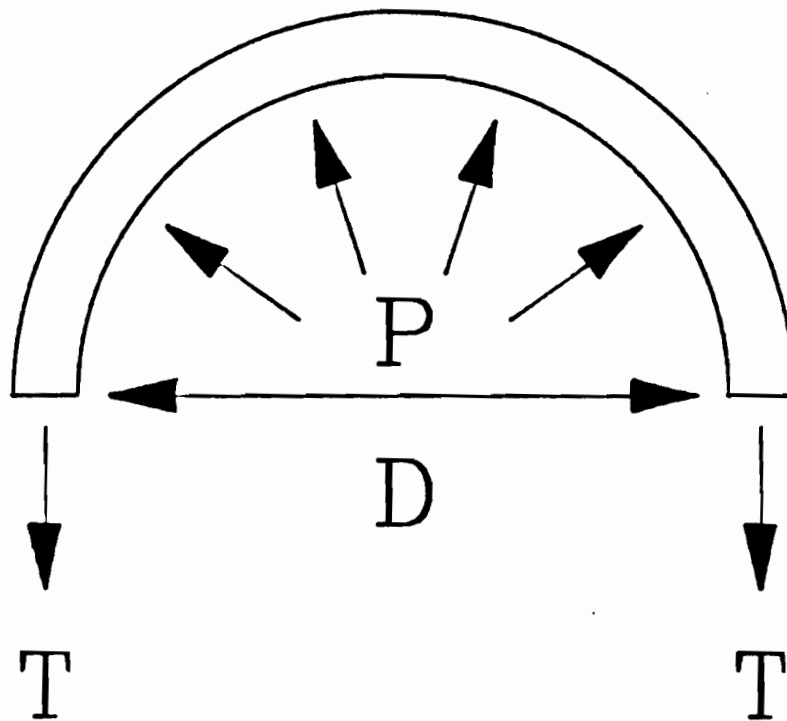
Figure 4.3. Forces in a thin cylinder

acquisition unit. The horizontal pressures, P_h, were calculated from strain gage measurements. Two SR-4 electrical strain gages were bonded to the outside surface of the lucite cylinder for measuring strains. The lucite cylinder acted as a thin shell, hence the horizontal pressures were evaluated as follows (52),

$$\sigma_x = \frac{E}{(1-v^2)} (\varepsilon_x - v\varepsilon_\theta) \tag{4.4}$$

$$\sigma_\theta = \frac{E}{(1-v^2)} (\varepsilon_\theta + v\varepsilon) \tag{4.5}$$

where

σ_x = vertical (axial) stress in the cylinder wall

σ_θ = circumferential stress in the wall

ε_x = vertical (axial) stress in the cylinder wall

E = modulus of elasticity of the wall material

v = Poisson's ratio of the wall material

Figure 4.3 is a representation of the forces in a thin cylinder with internal pressure. The hoop tensile stress:

$$T = \frac{P_h D}{2} \tag{4.6}$$

where

P_h = normal pressure in the cylinder

D = internal diameter of cylinder

T = hoop tensile stress

Hence

$$\sigma_\theta = \frac{P_h D}{2} \cdot \frac{1}{h} \qquad (4.7)$$

where

h = thickness of the cylinder

Using (4.6) and (4.7) jointly we get,

$$P_h = \frac{2Eh}{D(1-v^2)} \, (\varepsilon_\theta - v\varepsilon_x) \qquad (4.8)$$

Having calculated the horizontal pressure, then Janssen's constant

$$k = \frac{P_h}{P_v} \qquad (4.9)$$

P_v was measured directly by the data acquisition system described above.

For the system shown in Figure 4.2, a list of pertinent physical quantities can be drawn (Table 4.1).

The rank of the dimensional matrix, Table 4.2, is 5.

Hence 19 independent Π terms are needed to completely describe the system. Table 4.3 is a list of such a set.

The prediction equation is therefore

$$k = f(\frac{P_v}{\rho G \lambda}, \, \frac{H}{D}, \, \mu_w, \, \phi, \, \eta_1, \, \mu_t, \, \mu_b, \, \frac{\lambda}{D}, \, n, \, e_0, \, v, \, v_g, \, \frac{h}{D},$$

$$\frac{E_w}{\rho G D}, \, \alpha \Delta T, \, \frac{h}{H}, \, \frac{E(t)}{\beta \tau} \qquad (4.10a)$$

or

Table 4.1 Pertinent Physical Quantities for Evaluating "k"

No.	Symbol	Description	Units	Dimensions

Independent
Quantities:

No.	Symbol	Description	Units	Dimensions
(1)	P_v	Applied vertical (surcharge) pressure	N/m^2	FL^{-2}
(2)	H	Cell height	m	L
(3)	D	Cell diameter	m	L
(4)	τ	Elapsed time	s	T
(5)	β	Loading rate of P_v	$N/(m^2 s)$	$FL^{-2}T^{-1}$
(6)	ρ	Particle mass density of fill material	Kg/m^3	ML^{-3}
(7)	μ_w	Wall-grain static coefficient of friction	--	--
(8)	ϕ	Granular material angle of internal friction	--	--
(9)	G	Gravity field strength	N/Kg	FM^{-1}
(10)	E_w	Elastic modulus of wall material	N/m^2	FL^{-2}
(11)	E(t)	Relaxation modulus of fill material	N/m^2	FL^{-2}
(12)	λ	Geometric mean diameter of fill material (characteristic length)	m	L
(13)	η_1	Yield constant	--	--

Table 4.1, cont.

No.	Symbol	Description	Units	Dimensions
(14)	μ_t	Granular materials-top shaft coefficient of static friction	--	--
(15)	μ_b	Granular material-bottom shaft coefficient of static friction	--	--
(16)	h	Cell wall thickness	m	L
(17)	n	Number of loading cycles	--	--
(18)	e_0	Initial void ratio	--	--
(19)	ν	Poisson's ratio for bin wall material	--	--
(20)	ν_g	Poisson's ratio of granular material	--	--
(21)	Δm	Change in moisture content	--	--
(22)	ΔT	Change in temperature	K	θ
(23)	α	Temperature coefficients of fill material	m/(mK)	θ^{-1}
Dependent Quantity:				
(24)	P_h	Horizontal pressure	N/m^2	FL^{-2}

Table 4.2   Dimensional Matrix for Verifying
             Janssen's Constant

		F	M	L	T	θ
1.	P_v	1	0	-2	0	0
2.	H	0	0	1	0	0
3.	D	0	0	1	0	0
4.	τ	0	0	0	1	0
5.	β	1	-2	0	-1	0
6.	ρ	0	1	-3	0	0
7.	μ_w	0	0	0	0	0
8.	ϕ	0	0	0	0	0
9.	G	1	-1	0	0	0
10.	E_w	1	-2	0	0	0
11.	$E(t)$	1	-2	0	0	0
12.	λ	0	0	1	0	0
13.	η_1	0	0	1	0	0
14.	μ_t	0	0	0	0	0
15.	μ_b	0	0	0	0	0
16.	h	0	0	1	0	0
17.	n	0	0	0	0	0
18.	e_0	0	0	0	0	0
19.	ν	0	0	0	0	0
20.	ν_g	0	0	0	0	0
21.	Δ_m	0	0	0	0	0
22.	Δ_T	0	0	0	0	1
23.	α	0	0	0	0	-1
24.	P_h	1	0	-2	0	0

Table 4.3 Π Terms for Evaluating "k"

No.	Dimensionless Π term	Physical Significance

Dependent term:

Π_1 k   Janssen's Constant ratio of P_h to P_v

Independent terms:

Π_2 $P_v/\rho G\lambda$ Index of the ratio of applied surcharge pressure to gravity forces

Π_3 H/D   Height to diameter ratio of cylindrical container

Π_4 μ_w Fill particle to cell wall friction

Π_5 ϕ Measure of the stability of fill material

Π_6 η_1 Index of yield of fill material and subsequent plastic behavior

Π_7 μ_t Grain-plunger coefficient of friction

Π_8 μ_b Grain-bottom platform coefficient of friction

Π_9 λ/D Ratio of the fill particle mean diameter to cylinder diameter

Π_{10} n   Number of loading cycles

Π_{11} e_0 Initial voidage

Table 4.3, cont.

No.	Dimensionless Π term	Physical Significance
Π_{12}	ν	Poisson's ratio of wall material
Π_{13}	ν_g	Poisson's ratio of fill material
Π_{14}	ΔM	Change in grain moisture content
Π_{15}	h/D	Ratio of cell wall thickness to diameter
Π_{16}	$E_w/\rho GD$	Index of the ratio of elastic to gravity forces
Π_{17}	$\alpha \Delta T$	Index of thermo-mechanical properties of fill material
Π_{18}	h/H	Determines structural stability of the cell
Π_{19}	$E(t)/\beta \tau$	Defines loading rate and time dependent properties

Thesis missing

Pg. 111

Table 4.4 Values of Physical Properties of Material used
in Evaluating 'k'

Physical Property	Sand	Wheat	Corn	Soy
1. P_v	varied	varied	varied	varied
2. H	5.08×10^{-2}m	5.08×10^{-2}m	5.08×10^{-2}m	5.08×10^{-2}m
3. D	5.08×10^{-2}m	5.08×10^{-2}m	5.08×10^{-2}m	5.08×10^{-2}m
4. τ	0-90s	0-90s	0-90s	0-90s
5. β	353 N/(m^{2}s)	353 N/(m^{2}s)	353 N/(m^{2}s)	353 N/(m^{2}s)
6. ρ	1.6×10^3 kg/m^3	1.29×10^3 kg/m^3	1.19×10^3 kg/m^3	1.18×10^3 kg/m^3
7. ϕ	34 deg	31 deg	33 deg	36 deg
8. G	9.81 N/kg	9.81 N/kg	9.81 N/kg	9.81 N/kg
9. E_w	3.1×10^9 N/m^2	3.1×10^9 N/m^2	3.1×10^9 N/m^2	3.1×10^9 N/m^2
10. λ	4.9×10^{-4}m	3.1×10^{-3}m	1.6×10^{-2}m	5.8×10^{-2}m
11. η_1	28	9.91	9.91	9.91
12. μ_w	0.50	0.36	0.33	0.31
13. μ_t	0.30	0.52	0.68	0.47
14. μ_b	0.30	0.52	0.68	0.47
15. h	1.6×10^{-3}m	1.6×10^{-3}m	1.6×10^{-3}m	1.6×10^{-3}m
16. n	1 - 5	1 - 5	1 - 5	1 - 5

Table 4.4, cont.

Physical Property	Sand	Wheat	Corn	Soy
17. e_0	0.358	0.401	0.400	0.361
18. v	0.35 0.35	0.35	0.35	
19. v_g	0.25	0.32	0.32	0.33
20. Δ_m	0	0	0	0
21. Δ_t	0	0	0	0
22. α	1.7×10^{-6}	2.4×10^{-6}	2.3×10^{-6}	2.3×10^{-6}
23. P_h	varied	varied	varied	varied

Table 4.5 Values of Non-Varied Π* Terms for Evaluating "k"

No.	P-term	Values			
		Sand	Wheat	Corn	Soy
Π_3	H/D	1	1	1	1
Π_4	μ_w	0.5	0.36	0.33	0.31
Π_5	ϕ	34 deg	31 deg	33 deg	36 deg
Π_6	η_1	28	9.91	9.91	9.91
Π_7	μ_t	0.30	0.52	0.68	0.47
Π_8	μ_b	0.30	0.52	0.68	0.47
Π_9	λ/D	9.6×10^{-3}	6.1×10^{-2}	3.1×10^{-1}	1.1×10^{0}
Π_{11}	e_0	0.358	0.401	0.400	0.361
Π_{12}	ν	0.35	0.35	0.35	0.35
Π_{13}	ν_g	0.25	0.32	0.32	0.33
Π_{14}	Δ_m	0	0	0	0
Π_{15}	h/D	0.031	0.031	0.031	0.031
Π_{16}	$E_w/\rho GD$	3.9×10^6	4.8×10^6	5.2×10^6	5.3×10^3
Π_{17}	$\alpha \Delta T$	0	0	0	0
Π_{18}	h/H	0.031	0.031	0.031	0.031

*along columns

$$\Pi_1 = f(\Pi_2, \Pi_3, \Pi_4, \Pi_5, \Pi_6, \Pi_7, \Pi_8,$$

$$\Pi_9, \Pi_{10}, \Pi_{11}, \Pi_{12}, \Pi_{13}, \Pi_{14}, \Pi_{15},$$

$$\Pi_{16}, \Pi_{17}, \Pi_{18}, \Pi_{19}) \tag{4.10b}$$

The objective of the study was to verify whether the ratio of the horizontal to the vertical pressure, k, is a pertinent quantity to the development of pressures in ensiled granular materials. Component experimental procedures relating Π_1 (k) and Π_2 ($P_v/\rho G\lambda$) the term containing the secondary quantity (P_v) the vertical pressure were performed since the influence of k on vertical pressure was being investigated, i.e., Π_2 was varied and corresponding variations of Π_1 recorded as the rest of the Π terms were held constant, that is:

$$\Pi_1 = f(\Pi_2, \Pi_3, \overline{\Pi_4, \Pi_5, \Pi_6, \Pi_7, \Pi_8},$$

$$\overline{\Pi_9, \Pi_{10}, \Pi_{11}, \Pi_{12}, \Pi_{13}, \Pi_{14}, \Pi_{15}}$$

$$\overline{\Pi_{16}, \Pi_{17}, \Pi_{18}})$$

or

$$\Pi_1 = \phi \Pi_2^n \tag{4.11b}$$

The bar denotes the Π terms which were held constant, see Table 4.6. The value of Π_{18} could not be held precisely constant as the value of $E(t)$ (see Table 4.5.1) varied during the test. The distortions due to this were held to a minimum by conducting the tests for relatively short periods of time (Table 4.5). The influence of the loading rate was also minimized by carrying out the experiment at loading rates of below 645 kPa/s which according to Manbeck and Nelson (35) results in quasi-static loading.

The values of e_0 and ρ used for the experiments were obtained from the "Agricultural Engineering Standards" (1986). The values of μ_w, vg, ϕ, μ_w, μ_t and μ_b were obtained from "Physical Properties of plant and Animal Materials" by Mohsenin (1986). ε_0 of sand was obtained from "Flow through Porous Media" by R. DeWeist. The values of η_1 were obtained from Zhang et al (79); this constant has not been evaluated for corn and soybeans, hence the values used were assumed to be the same as for

wheat. The experiments were held in a room maintained at 24°C and 50% RH. The moisture contents for wheat, corn, soybeans and sand were 12.5, 12.5, 10.0, 2.0 wet basis

respectively. The values of μ_t and μ_b for sand were obtained from "Principles of Farm Machinery" by Kepner et al.

The relaxation moduli (E(t)'s) for the material were evaluated by applying sudden strains to the granular materials confined in a rigid cylindrical aluminum cell of 5.08 cm diameter by 5.08 cm high. The values of time and stress were obtained by the data acquisition system and the load cell as described above (see Figures 4.7*** and Tables 4.5.1 and 4.7).

The vertical pressure, P_v, was applied over a period of 90 seconds in ten increasing steps to a maximum value. The loads were then removed (i.e., the pressure, P_v, was reduced to zero) and the loading process repeated. The cyclic loading pattern, cycle, was repeated five times for each material.

The equations of the fitted curves of the results (Tables 4.6 and Figure 4.3* to 4.6 and 8-4.3 to 8-4.6**)

---

*For all the plots the term "Linear-plot" means that the axes are linear, i.e., arithmetic.

**Figures prefixed "8" are in Appendix C.

***This shorthand means Figures 4.7.1, 4.7.2, etc., throughout the text.

Plate 1:   The Lucite cylinder used for the evaluation
            of "k"
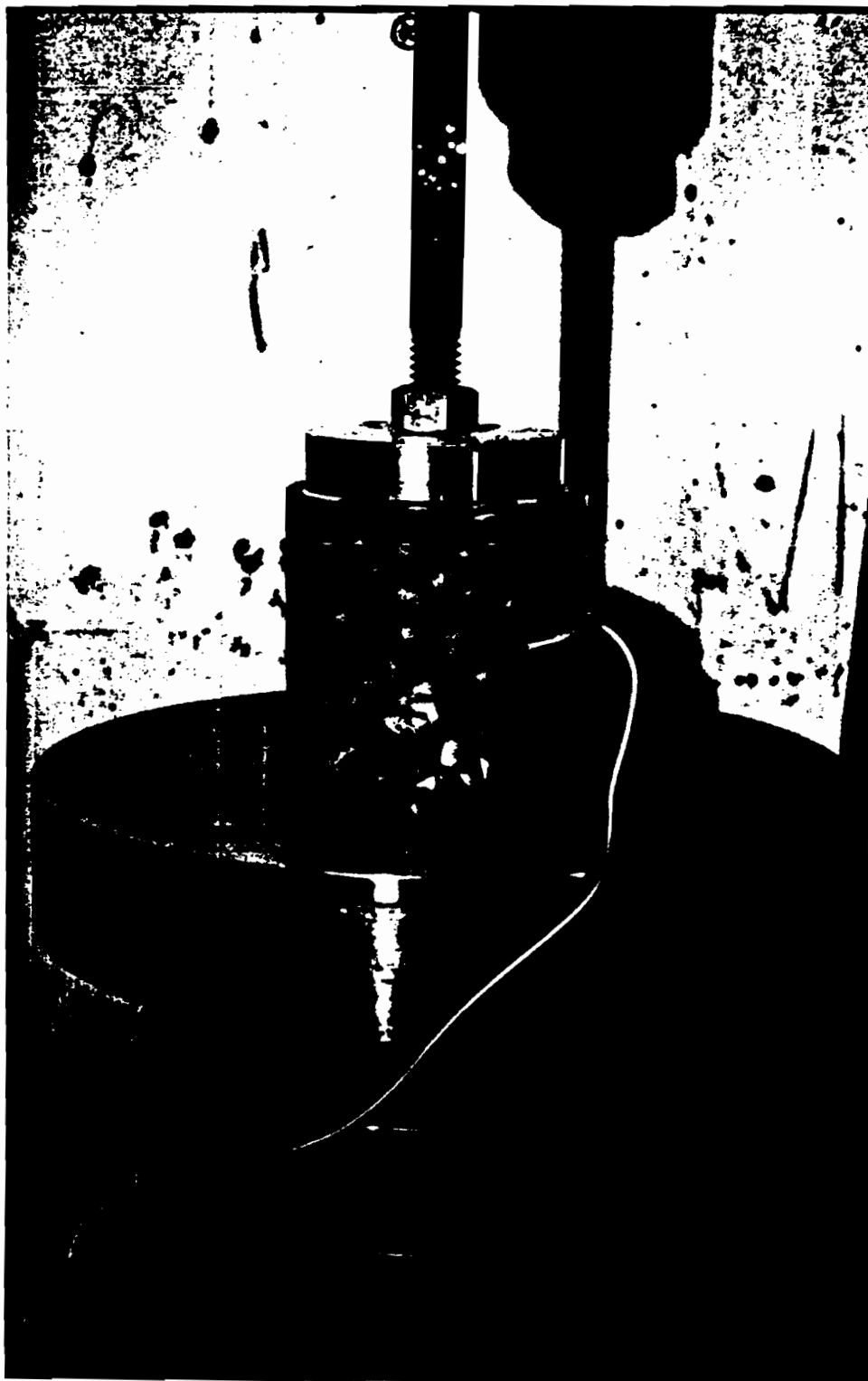
were fitted using the model in equation (4.116 for the log-log model, and using the model in equation (4.12) below for the semi-log model.

$$\Pi_1 = a_0 + a_1 \log \Pi_2'' + a_2 (\log \Pi_2)^2 + \ldots + a_n (\log \Pi_2)^n$$

(4.12)

The properties of the materials used are described in Table 4.4.

Table 4.5.1   Relaxation Moduli of the Materials

Material	Relaxation Modulus
Sand	$E(t) = (1.271 \times 10^7) e^{(-t/1600)} + (3.930 \times 10^5) e^{(-t/36.1)}$ $+ (2.961 \times 10^5) e^{(-t/2.94)}$
Wheat	$E(t) = (1.953 \times 10^6) e^{(-t/3446)}$ $+ (3.825 \times 10^5) e^{(-t/16.74)}$
Soybeans	$E(t) = (4.815 \times 10^6) e^{(-t/4677)} + (3.920 \times 10^5) e^{(-t/28.8)}$ $+ (6.352 \times 10^5) e^{(-t/2.453)}$
Corn	$E(t) = (4.742 \times 10^6) e^{(-t/3092)} + (2.976 \times 10^5) e^{(-t/71.25)}$ $+ (6.292 \times 10^5) e^{(-t/6.98)}$

Table 4.6.1 Component Experiment Results for Sand for
Evaluation of "k"

Cycle	Experiment 1 Π_1	Experiment 1 Π_2 x10^4	Experiment 2 Π_1	Experiment 2 Π_2 x10^4	Experiment 3 Π_1	Experiment 3 Π_2 x10^4
1	0.389	0.307*	0.414	0.301	0.399	0.312
	0.396	0.313	0.447	0.495	0.393	0.326
	0.526	0.642	0.458	0.699	0.461	0.600
	0.514	1.023	0.486	0.910	0.500	1.100
	0.541	1.312	0.533	1.700	0.543	1.418
	0.544	1.695	0.541	1.980	0.547	1.770
	0.552	2.001	0.550	2.228	0.551	1.896
	0.547	2.384	0.564	2.316	0.559	2.434
	0.552	2.675	0.569	2.861	0.565	2.745
	0.542	2.970	0.578	3.100	0.581	2.900
2	0.344	0.700	0.360	0.698*	0.341	0.691
	0.362	0.812	0.376	0.087	0.378	0.989
	0.377	1.100	0.406	1.053	0.408	1.300
	0.401	1.300	0.421	1.346	0.433	1.587
	0.428	1.479	0.436	1.723	0.455	1.923
	0.435	2.016	0.453	2.246	0.475	2.246
	0.444	2.500	0.461	2.690	0.483	2.519
	0.454	2.916	0.472	3.038	0.484	3.100
	0.461	2.999	0.472	3.129	0.488	2.134
	0.466	3.100	0.473	3.177	0.489	3.233
3	0.291	0.370*	0.300	0.380	0.289	0.368
	0.361	0.781	0.321	0.700	0.348	0.802
	0.385	1.022	0.343	1.300	0.386	1.111
	0.396	1.321	0.371	1.636	0.394	1.299
	0.414	1.677	0.420	1.977	0.400	1.678
	0.424	2.013	0.431	2.344	0.411	2.133
	0.432	2.367	0.445	2.516	0.431	2.467
	0.444	2.665	0.452	2.756	0.438	2.721
			0.460	2.900	0.452	2.889
					0.465	2.954

Table 4.6.1, cont.

Cycle	Experiment 1 Π_1	Experiment 1 Π_2 x10^4	Experiment 2 Π_1	Experiment 2 Π_2 x10^4	Experiment 3 Π_1	Experiment 3 Π_2 x10^4
4	0.398	0.399*	0.409	0.400	0.406	0.438*
	0.409	0.607	0.414	0.512	0.417	0.427
	0.419	0.889	0.429	0.696	0.420	0.766
	0.431	1.113	0.440	0.998	0.433	1.416
	0.441	1.721	0.451	1.614	0.442	1.995
	0.443	2.001	0.463	2.133	0.455	2.326
	0.443	2.714	0.471	2.666	0.462	2.663
	0.458	2.971	0.472	2.914	0.470	3.103
	0.470	3.104	0.479	3.103	0.474	3.326
	0.488	3.331	0.481	3.200	0.476	3.297
5	0.310	0.332	0.352	0.372*	0.300	0.301
	0.333	0.412	0.340	0.385	0.377	0.367
	0.351	0.593	0.328	0.663	0.343	0.488
	0.368	0.919	0.361	1.070	0.359	1.012
	0.380	1.299	0.372	1.350	0.376	1.333
	0.391	1.714	0.388	1.631	0.393	1.858
	0.395	1.967	0.399	2.038	0.401	1.983
	0.400	2.421	0.407	2.331	0.401	2.208
	0.409	2.816	0.415	2.700	0.421	2.699
	0.413	3.095	0.422	2.982	0.431	2.964

*experiment used for analysis

Table 4.6.2   Component Experiment Results for Wheat,
for Evaluation of "k"

Cycle	Experiment 1		Experiment 2		Experiment 3	
	Π_1	Π_2 $\times 10^3$	Π_1	Π_2 $\times 10^3$	Π_1	Π_3 $\times 10^4$
1	0.224	0.403*	0.224	0.419	0.241	0.463
	0.221	0.429	0.289	0.416	0.268	0.707
	0.317	1.121	0.3100	1.213	0.3035	1.010
	0.347	1.757	0.361	1.689	0.357	1.609
	0.386	2.318	0.406	2.471	0.416	2.514
	0.425	2.911	0.444	2.999	0.448	3.111
	0.459	3.482	0.479	3.571	0.477	3.721
	0.4995	4.114	0.496	4.300	0.490	4.001
	0.524	4.704	0.6528	4.912	0.514	4.680
	0.538	5.252	0.545	5.517	0.557	5.800
2	0.346	0.674*	0.341	0.699	0.339	0.700
	0.33	0.640	0.378	1.014	0.387	1.101
	0.398	1.157	0.408	1.366	0.411	1.320
	0.426	1.707	0.455	1.919	0.465	1.922
	0.490	2.298	0.75	2.264	0.481	2.198
	0.527	2.820	0.525	3.111	0.500	2.814
	0.537	3.607	0.565	0.409	0.539	3.455
	0.570	4.133	0.577	4.331	0.589	4.616
	0.593	4.781	0.589	4.612	0.608	5.203
	0.605	5.367	0.610	5.213	0.620	5.501
3	0.415	0.700	0.411	0.699	0.384	0.559*
	0.449	1.001	0.445	1.111	0.389	0.557
	0.476	1.310	0.477	1.321	0.474	1.127
	0.499	1.601	0.499	1.644	0.518	1.647
	0.551	2.714	0.577	2.517	0.562	2.230
	0.565	2.816	0.590	3.100	0.579	2.861
	0.600	3.457	0.596	3.717	0.596	3.447
	0.611	4.113	0.632	3.604	0.593	4.103
	0.630	4.719	0.648	5.212	0.627	4.728
	0.642	5.300	0.656	5.500	0.638	5.106

Table 4.6.2, cont.

Cycle	Experiment 1 Π_1	Experiment 1 Π_2 $\times 10^3$	Experiment 2 Π_1	Experiment 2 Π_2 $\times 10^3$	Experiment 3 Π_1	Experiment 3 Π_2 $\times 10^3$
4	0.500	0.707*	0.253	0.388*	0.503	0.681
	0.520	1.090	0.526	0.707	0.513	0.991
	0.546	1.311	0.432	1.125	0.529	1.121
	0.555	1.688	0.532	1.696	0.544	1.599
	0.570	2.512	0.577	2.348	0.572	2.361
	0.574	2.888	0.579	2.968	0.582	2.971
	0.578	3.122	0.598	3.497	0.600	3.512
	0.599	4.000	0.606	4.061	0.600	4.000
	0.609	4.777	0.612	4.714	0.604	4.721
	0.612	5.840	0.615	5.354	0.605	5.400
5	0.384	0.655	0.391	0.700	0.383	0.636*
	0.516	1.212	0.517	1.301	0.512	1.267
	0.518	1.313	0.519	1.642	0.571	2.194
	0.587	2.800	0.525	1.919	0.593	2.820
	0.592	3.106	0.575	2.507	0.593	3.507
	0.599	4.346	0.601	2.444	0.603	4.342
	0.610	5.240	0.611	4.914	0.606	5.233
	0.611	5.311	0.613	5.406	0.615	5.854
	0.615	5.500	0.616	5.800	0.621	5.847
	0.624	5.889	0.622	6.119	0.618	5.939

*experiment used for analysis

Table 4.6.3   Component Experiment Results for Soybeans, for Evaluation of "k"

Cycle	Experiment 1 Π_1	Experiment 1 Π_2 x10^2	Experiment 2 Π_1	Experiment 2 Π_2 x10^2	Experiment 3 Π_1	Experiment 3 Π_2 x10^2
1	0.254	1.104*	0.241	1.004	0.240	1.100
	0.234	1.125	0.296	1.113	0.293	2.231
	0.290	2.348	0.331	2.216	0.329	3.299
	0.286	3.558	0.361	3.333	0.358	4.389
	0.432	4.789	0.379	4.445	0.382	4.577
	0.422	6.346	0.407	6.496	0.402	6.444
	0.413	7.460	0.427	7.321	0.221	7.621
	0.431	8.972	0.445	8.800	0.437	8.811
	0.435	9.958	0.453	9.900	0.452	9.901
	0.464	11.118	0.466	12.100	0.465	11.119
2	0.184	1.100	0.203	1.042*	0.191	1.052
	0.186	1.103	0.206	1.027	0.196	1.139
	0.248	2.300	0.193	2.380	0.252	2.229
	0.335	4.399	0.309	4.421	0.336	4.379
	0.369	5.514	0.370	5.878	0.370	5.601
	0.436	7.673	0.428	7.303	0.439	7.711
	0.452	8.808	0.472	8.613	0.454	8.514
	0.475	9.919	0.519	9.993	0.481	9.621
	0.497	11.032	0.533	10.960	0.499	10.55
	0.516	12.222	0.541	12.000	0.521	12.21
3	0.260	1.100	0.308	2.201	0.291	1.810*
	0.343	3.333	0.334	2.817	0.307	1.821
	0.354	4.441	0.343	3.310	0.348	3.693
	0.384	6.061	0.354	4.561	0.391	4.923
	0.397	0.777	0.371	5.755	0.405	6.503
	0.408	0.871	0.408	8.880	0.417	8.257
	0.411	9.901	0.410	9.000	0.421	9.245
	0.417	10.56	0.418	9.861	0.430	11.10
	0.430	11.01	0.426	11.01	0.438	12.21
	0.435	12.00	0.435	12.11	0.432	12.24

Table 4.6.3, cont.

Cycle	Experiment 1 Π_1	Experiment 1 Π_2 $\times 10^2$	Experiment 2 Π_1	Experiment 2 Π_2 $\times 10^2$	Experiment 3 Π_1	Experiment 3 Π_2 $\times 10^2$
4	0.471	1.414*	0.470	1.390*	0.474	1.390
	0.461	1.612	0.447	1.436	0.474	1.426
	0.455	2.500	0.454	2.460	0.461	2.396
	0.458	3.667	0.457	3.150	0.455	3.013
	0.453	5.218	0.445	5.046	0.459	5.406
	0.445	6.497	0.438	6.391	0.455	6.931
	0.439	7.555	0.433	7.586	0.449	7.856
	0.433	9.139	0.436	8.865	0.450	8.719
	0.445	10.050	0.430	10.150	0.444	11.001
	0.445	11.111	0.440	11.220	0.442	11.414
5	0.437	1.569*	0.429	1.616	0.438	1.579
	0.424	1.591	0.429	1.728	0.436	1.622
	0.425	2.509	0.400	2.109	0.433	2.613
	0.375	3.829	0.399	4.999	0.409	3.998
	0.365	4.958	0.379	5.873	0.409	5.001
	0.373	6.144	0.392	6.244	0.401	6.061
	0.387	7.621	0.392	7.591	0.399	7.497
	0.404	8.777	0.407	8.849	0.400	8.719
	0.413	9.956	0.412	9.538	0.400	10.666
	0.426	11.150	0.426	12.000	0.441	11.213

*experiment used for analysis

Table 4.6.4 Component Experiment Results for Corn,
for Evaluation of "k"

Cycle	Experiment 1 Π_1	Π_2 $\times 10^2$	Experiment 2 Π_1	Π_2 $\times 10^2$	Experiment 3 Π_1	Π_2 $\times 10^2$
1	0.779	2.389*	0.786	2.516*	0.783	2.490
	0.607	3.757	0.609	3.710	0.614	3.671
	0.478	4.846	0.511	4.907	0.515	4.921
	0.436	6.492	0.431	0.102	0.427	6.553
	0.431	7.534	0.429	7.321	0.432	7.543
	0.382	8.835	0.371	8.511	0.377	8.794
	0.349	9.876	0.341	9.781	0.343	9.621
	0.319	11.47	0.325	11.00	0.313	11.473
2	0.799	2.431	0.819	2.444	0.808	2.429*
	0.598	3.661	0.674	3.409	0.618	3.561
	0.567	4.898	0.533	4.714	0.512	4.954
	0.453	6.384	0.482	6.412	0.461	6.371
	0.401	7.888	0.417	7.534	0.415	7.530
	0.361	9.127	0.358	9.211	0.369	9.024
	0.352	9.833	0.333	10.001	0.340	9.946
	0.326	11.009	0.298	11.31	0.315	10.94
3	0.593	2.500	0.637	2.449*	0.601	2.510
	0.437	3.701	0.439	3.833	0.433	3.722
	0.351	4.991	0.326	5.027	0.347	5.006
	0.296	6.111	0.270	6.265	0.293	6.127
	0.257	7.314	0.240	7.449	0.241	7.366
	0.229	8.503	0.223	8.528	0.225	8.517
	0.206	9.786	0.208	9.813	0.210	9.711
	0.188	10.900	0.194	10.890	0.185	10.908
	0.174	12.13	0.188	12.03	0.169	12.21
4	0.471	2.490	0.378	3.473*	0.462	2.530
	0.343	3.712	0.384	3.392	0.348	3.723
	0.350	5.107	0.306	4.310	0.351	5.107
	0.291	6.119	0.233	5.837	0.296	6.139
	0.237	7.349	0.195	7.684	0.229	7.381
	0.200	8.533	0.177	9.342	0.206	8.524
	0.193	9.726	0.171	10.63	0.188	9.712
	0.178	10.95	0.149	11.91	0.188	9.712
	0.167	12.03	0.149	12.20	0.174	10.95
	0.164	12.31	0.151	12.46	0.164	12.31

Table 4.6.4, cont.

Cycle	Experiment 1 Π_1	Experiment 1 Π_2 x10^2	Experiment 2 Π_1	Experiment 2 Π_2 x10^2	Experiment 3 Π_1	Experiment 3 Π_2 x10^2
5	0.868	1.478*	0.487	1.300	0.483	1.333
	0.779	1.947	0.607	2.516	0.597	2.569
	0.459	3.520	0.439	3.718	0.441	3.724
	0.364	4.848	0.383	4.923	0.392	4.908
	0.318	6.001	0.329	6.144	0.318	6.199
	0.279	7.526	0.292	7.309	0.288	7.339
	0.264	8.566	0.263	8.511	0.255	8.523
	0.247	9.674	0.240	9.742	0.241	9.742
	0.232	10.78	0.221	10.91	0.229	10.91
	0.214	11.94	0.206	12.11	0.201	12.18

*experiment used for analysis

Table 4.7.1 Experimental Results for Relaxation
Tests for Sand $\varepsilon_0 = 0.019$

Experiment 1*		Experiment 2		Experiment 3	
Time (Sec)	Stress (N/m^2) $\times 10^5$	Time (Sec)	Stress (N/m^2) $\times 10^5$	Time (Sec)	Stress (N/m^2) $\times 10^5$
0	2.523	0	2.546	0	2.543
1	2.497	1	2.488	1	2.515
2	2.480	2	2.466	2	2.506
3	2.477	3	2.461	3	2.503
4	2.476	4	2.448	4	2.498
5	2.467	5	2.447	5	2.495
6	2.468	6	2.437	6	2.493
7	2.460	7	2.438	7	2.490
8	2.461	8	2.430	12	2.490
13	2.449	9	2.431	22	2.475
23	2.423	14	2.428	32	2.477
33	2.423	24	2.405	42	2.477
43	2.407	34	2.398	52	2.463
53	2.403	44	2.391	62	2.466
63	2.411	54	2.398	72	2.459
73	2.402	64	2.393	82	2.467
83	2.403	74	2.388	92	2.464
113	2.400	84	2.375	112	2.456
133	2.385	94	2.369	132	2.459
153	2.384	114	2.371	152	2.447
173	2.376	134	2.367	172	2.447
193	2.373	154	2.368	192	2.444
233	2.370	174	2.356	232	2.442
273	2.364	194	2.353	272	2.449
313	2.370	234	2.349	312	2.440
		214	2.349		
		314	2.348		

*experiment used for analysis

Table 4.7.2 Experimental Results for Relaxation
Tests for Wheat $\varepsilon_0 = 0.134$

Experiment 1		Experiment 2		Experiment 3	
Time (Sec)	Stress* (N/m^2) $x10^5$	Time (Sec)	Stress (N/m^2) $x10^5$	Time (Sec)	Stress (N/m^2) $x10^5$
0	2.564*	0	2.305	0	2.564
1	7.452	1	2.374	1	2.452
2	2.412	2	2.237	2	2.412
3	2.374	3	2.177	3	2.374
4	2.352	4	2.131	4	2.352
5	2.325	5	2.105	5	2.725
6	2.311	6	2.075	6	2.311
7	2.290	7	2.061	7	2.290
8	2.281	8	2.038	8	2.281
13	2.223	9	2.028	13	2.223
23	2.126	14	1.982	23	2.126
33	2.103	24	1.911	33	2.103
43	2.076	34	1.883	43	2.076
53	2.069	44	1.853	53	2.069
63	2.045	54	1.834	63	2.045
73	2.034	64	1.825	73	2.034
83	2.024	74	1.801	83	2.024
103	2.005	84	1.800	103	2.005
123	2.000	94	1.779	123	2.000
143	1.984	114	1.762	143	1.984
163	1.965	134	1.752	163	1.965
183	1.963	154	1.747	183	1.963
223	1.947	174	1.727	223	1.947
263	1.935	194	1.728	263	1.935
303	1.912	234	1.711	303	1.912
		314	1.689		

*experiment used for analysis

Table 4.7.3   Experimental Results for Relaxation
Tests for Soybeans $\varepsilon_0 = 0.035$

Experiment 1		Experiment 2		Experiment 3	
Time (Sec)	Stress (N/m) $x10^5$	Time (Sec)	Stress (N/m^2) $x10^5$	Time (Sec)	Stress (N/m^2) $x10^5$
0	2.344*	0	2.571	0	2.532
1	2.462	1	2.437	1	2.484
2	2.416	2	2.388	2	2.459
3	2.383	3	2.366	3	2.436
4	2.368	4	2.342	4	2.423
5	2.348	5	2.332	5	2.406
6	2.341	6	2.314	6	2.399
7	2.325	7	2.308	7	2.385
8	2.322	8	2.295	8	2.380
9	2.309	9	2.291	13	2.345
14	2.287	14	2.263	23	2.327
24	2.243	24	2.231	33	2.298
34	2.224	34	2.195	43	2.275
44	2.203	44	2.177	53	2.254
54	2.202	54	2.171	63	2.251
64	2.178	64	2.153	73	2.233
74	2.176	74	2.153	83	2.226
84	2.163	84	2.137	93	2.214
94	2.164	94	2.125	113	2.212
114	2.145	114	2.117	133	2.186
134	2.141	134	2.104	153	2.174
154	2.133	154	2.103	173	2.175
174	2.112	174	2.081	193	2.156
194	2.117	194	2.073	233	2.146
234	2.085	234	2.061	273	2.138
274	2.071	274	2.049	313	2.122
314		314	2.038		

*experiment used for analysis

Table 4.7.4   Experimental Results for Relaxation
Tests for Corn $\varepsilon_0 = 0.65$

Experiment 1		Experiment 2*		Experiment 3	
Time (Sec)	Stress (N/m) $x10^5$	Time (Sec)	Stress (N/m^2) $x10^5$	Time (Sec)	Stress (N/m^2) $x10^5$
0	2.463	0	2.540	0	2.412
1	2.412	1	2.496	1	2.458
2	2.374	2	2.424	2	2.387
3	2.343	3	2.389	3	2.346
4	2.326	4	2.360	4	2.363
5	2.314	5	2.344	5	2.302
6	2.297	6	2.324	6	2.288
7	2.290	7	2.315	7	2.274
8	2.277	8	2.299	8	2.263
13	2.242	9	2.293	9	2.209
33	2.210	14	2.249	14	2.177
43	2.171	24	2.203	24	2.137
53	2.162	34	2.180	34	2.127
63	2.143	44	2.156	44	2.112
73	2.126	54	2.146	54	2.099
83	2.114	64	2.136	64	2.082
93	2.100	74	2.127	74	2.076
113	2.099	84	2.110	84	2.068
133	2.075	94	2.108	94	2.043
153	2.073	114	2.080	114	2.032
173	2.062	134	2.068	134	2.025
193	2.042	154	2.068	154	2.020
233	2.041	174	2.049	174	2.012
273	2.034	194	2.047	194	2.012
313	2.030	234	2.025	234	1.988
		274	2.018	274	1.987
		314	2.006	314	1.965

*experiment used for analysis

Table 4.8.1   Component Equations for Π_1 versus Π_2, Log-Log Model

Material	Cycle	Component Equation	Coefficient of Determination (r^2)
Sand	1	$\Pi_1 = 0.131\ \Pi_2^{0.144}$	0.799
	2	$\Pi_1 = 0.090\ \Pi_2^{0.161}$	0.974
	3	$\Pi_1 = 0.057\ \Pi_2^{0.203}$	0.966
	4	$\Pi_1 = 0.069\ \Pi_2^{0.964}$	0.929
	5	$\Pi_1 = 0.142\ \Pi_2^{0.104}$	0.837
Wheat	1	$\Pi_1 = 0.028\ \Pi_2^{0.345}$	0.994
	2	$\Pi_1 = 0.051\ \Pi_2^{0.290}$	0.998
	3	$\Pi_1 = 0.097\ \Pi_2^{0.222}$	0.978
	4	$\Pi_1 = 0.019\ \Pi_2^{0.267}$	0.722
	5	$\Pi_1 = 0.929\ \Pi_2^{0.184}$	0.863
Corn	1	$\Pi_1 = 15.35\ \Pi_2^{-0.548}$	0.980
	2	$\Pi_1 = 21.58\ \Pi_2^{-0.60}$	0.994
	3	$\Pi_1 = 43.75\ \Pi_2^{-0.779}$	0.984
	4	$\Pi_1 = 24.32\ \Pi_2^{-0.718}$	0.988
	5	$\Pi_1 = 26.49\ \Pi_2^{-0.684}$	0.992
Soybean	1	$\Pi_1 = 0.062\ \Pi_2^{0.288}$	0.896
	2	$\Pi_1 = 0.024\ \Pi_2^{0.433}$	0.913
	3	$\Pi_1 = 0.103\ \Pi_2^{0.200}$	0.962
	4	$\Pi_1 = 0.527\ \Pi_2^{-0.028}$	0.711

Table 4.8.2   Component Equations for Π_1 versus Π_2, Semi-Log Model

Material	Cycle	Component Equation	Coefficient of Multiple Determination (R^2)
Sand	1	$\Pi_1 = -27.209 + 19.74 \log\Pi_2$ $- 4.683(\log\Pi_2)^2 + 0.371(\log\Pi_2)^3$	0.976
	2	$\Pi_1 = -1.305 + 0.674 \log\Pi_2$ $- 0.068(\log\Pi_2)^2$	0.988
	3	$\Pi_1 = -0.310 + 0.171 \log\Pi_2$	0.984
	4	$\Pi_1 = 1.546 - 0.619 \log\Pi_2$ $+ 0.085(\log\Pi_2)^2$	0.984
	5	$\Pi_1 = 26.560 - 19.294 \log\Pi_2$ $+ 4.683(\log\Pi_2)^2 - 0.377(\log\Pi_2)^3$	0.988
Wheat	1	$\Pi_1 = 1.092 - 0.765 \log\Pi_2$ $- 0.765(\log\Pi_2)^2 + 0.166(\log\Pi_2)^3$	0.996
	2	$\Pi_1 = 0.196 + 0.068 \log\Pi_2$	0.990
	3	$\Pi_1 = -0.0952 + 0.660 \log\Pi_2$ $- 0.063(\log\Pi_2)^2$	0.994
	4	$\Pi_1 = 2.693 + 1.762 \log\Pi_2$ $- 0.235(\log\Pi_2)^2$	0.984
	5	$\Pi_1 = -2.849 - 1.838 \log\Pi_2$ $- 0.244(\log\Pi_2)^2$	0.994

Table 4.8.2, cont.

Soybeans	1	$\Pi_1 = 9.079 - 10.864 \log\Pi_2$ $+4.352(\log\Pi_2)^2 + 0.563 (\log\Pi_2)^3$	0.908
Soybeans	2	$\Pi_1 = 10.106 - 11.452 \log\Pi_2$ $+ 4.255(\log\Pi_2)^2 - 0.563(\log\Pi_2)^3$	0.998
	3	$\Pi_1 = -0.600 + 0.566 \log\Pi_2$ $- 0.075(\log\Pi_2)^2$	0.984
	4	$\Pi_1 = 1.719 - 0.685 \log\Pi_2$ $+ 0.089(\log\Pi_2)^2$	0.726
	5	$\Pi_1 = 2.452 + 1.562 \log\Pi_2$ $+ 0.294(\log\Pi_2)^2$	0.785
Corn	1	$\Pi_1 = -2.849 + 1.838 \log\Pi_2$ $-0.244(\log\Pi_2)^2$	0.994
	2	$\Pi_1 = 6.114 - 3.412 \log\Pi_2$ $+ 0.496(\log\Pi_2)^2$	0.994
	3	$\Pi_1 = 8.531 - 5.364 \log\Pi_2$ $+ 0.862(\log\Pi_2)^2$	0.998
	4	$\Pi_1 = 6.095 - 3.771 \log\Pi_2$ $- 3.771(\log\Pi_2)^2$	0.996
	5	$\Pi_1 = - 4.305 + 0.680(\log\Pi_2)^2$	0.994
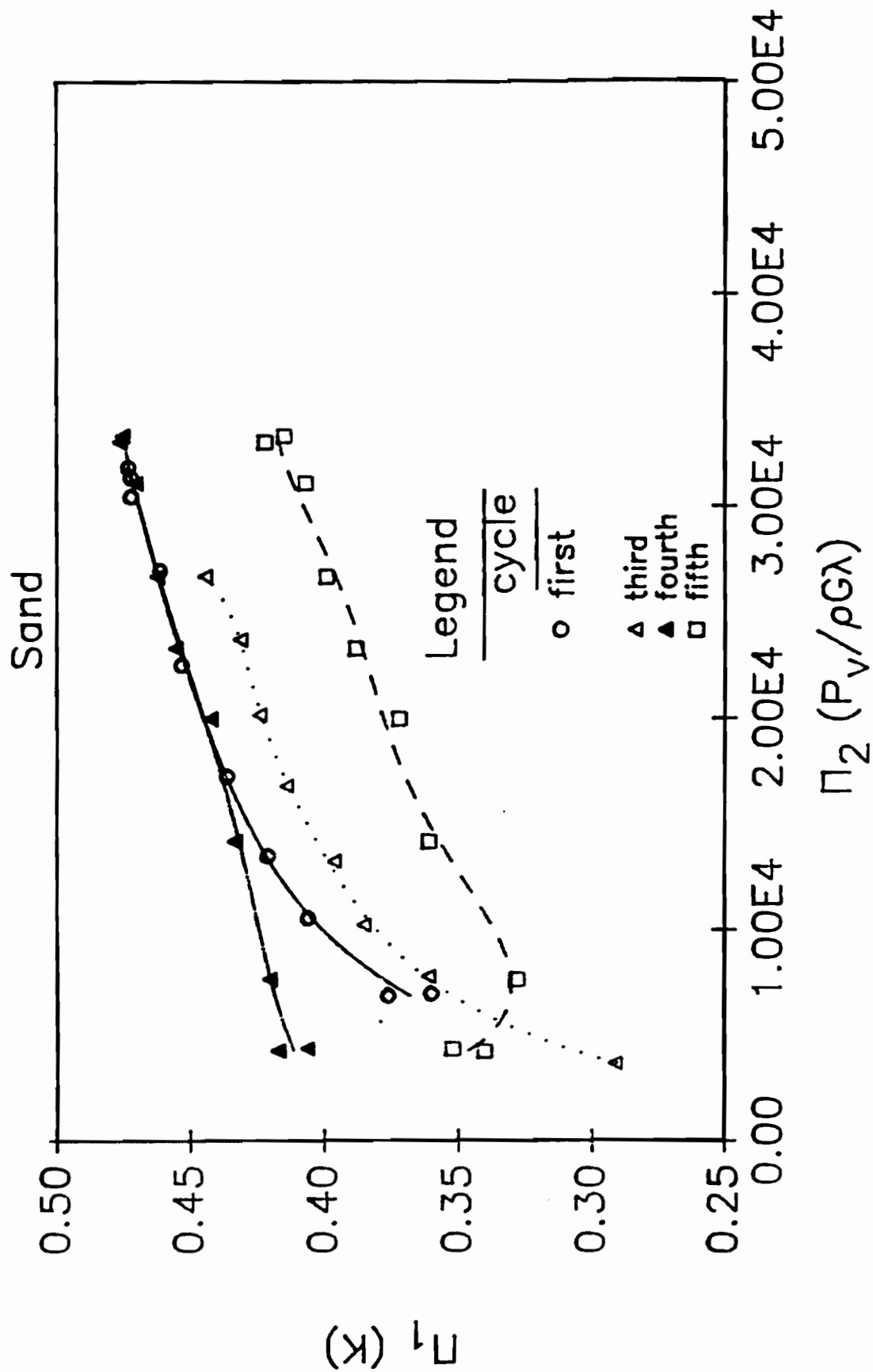
Figure 4.3.1.1. Linear plot of Π_1 versus Π_2 for five loading cycles of sand
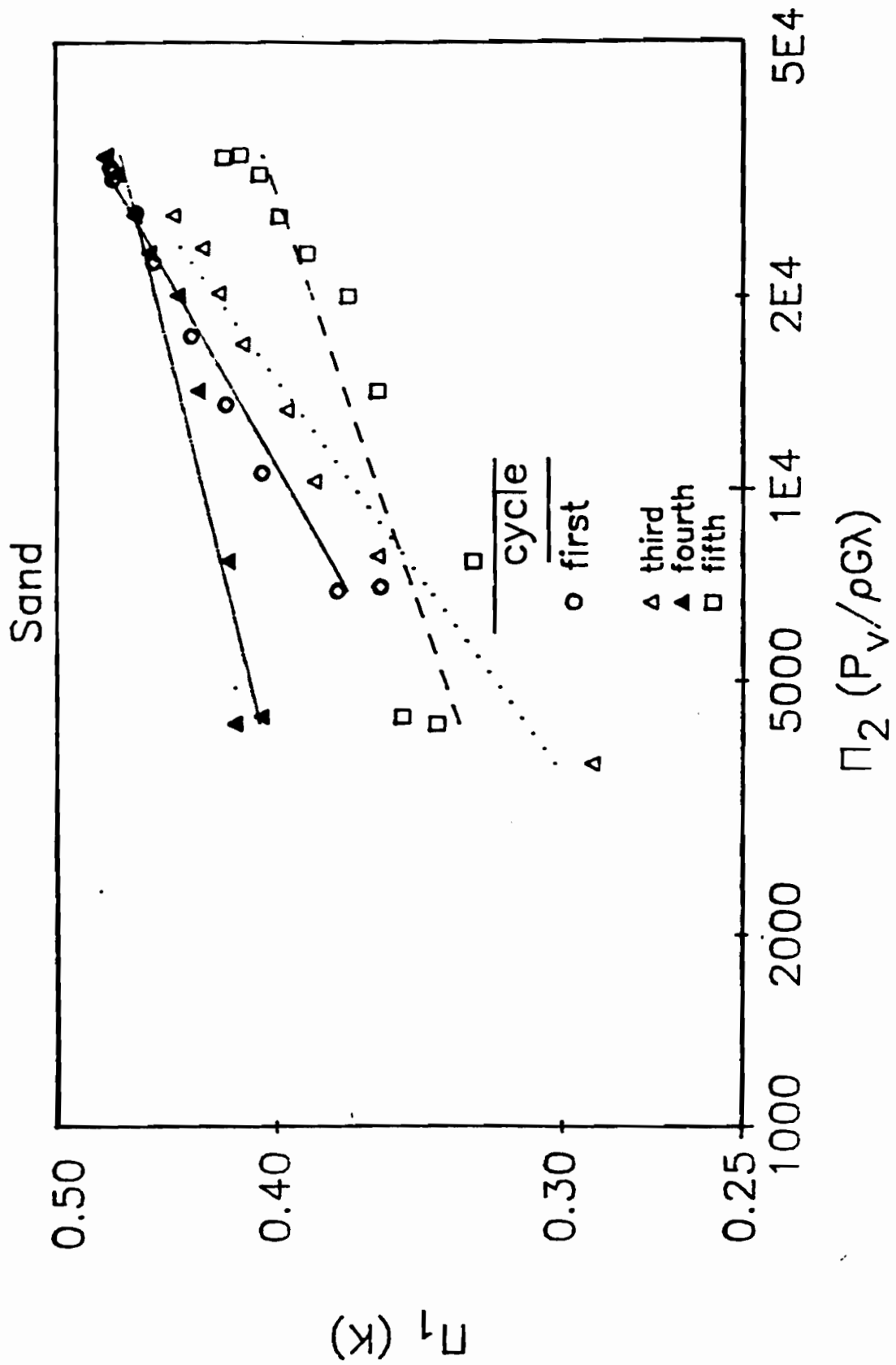
Figure 4.3.1.2. Log-log plot for five loading cycles of sand
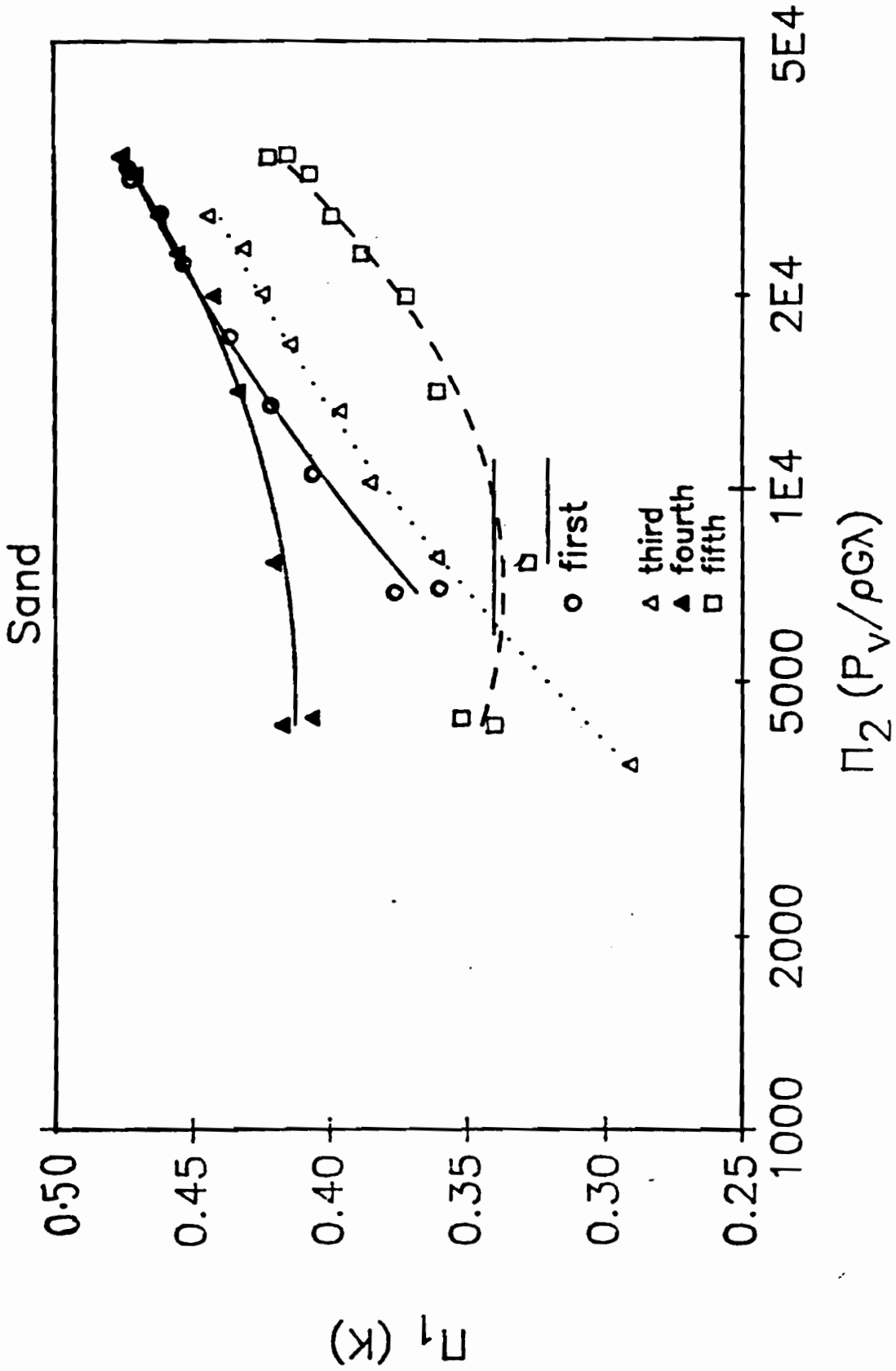
Figure 4.3.1.3. Semi-log plot of Π_1 versus Π_2 for five loading cycles of sand
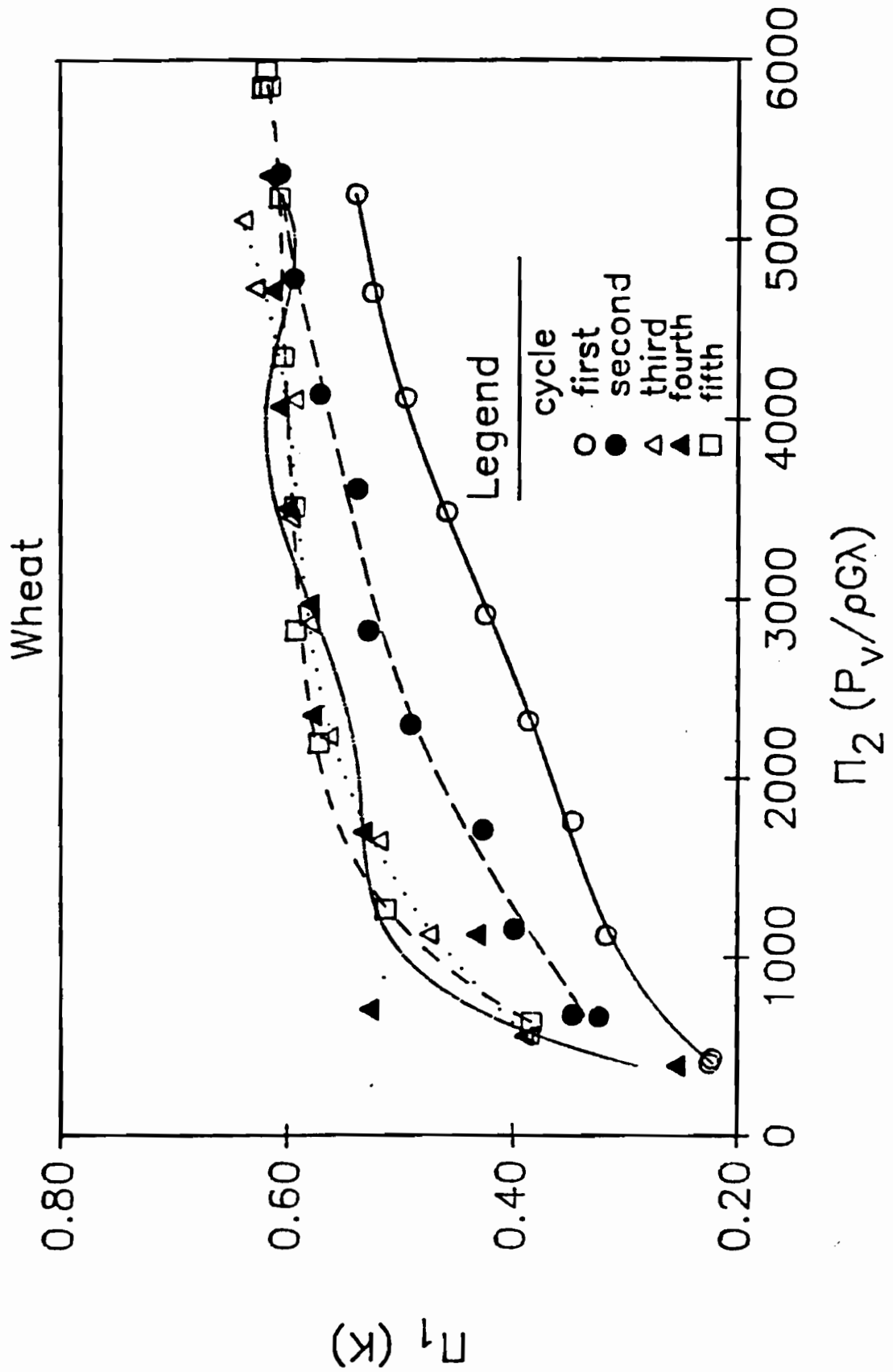
Wheat

Figure 4.4.1.1. Linear plot of Π_1 versus Π_2 for five loading cycles of wheat
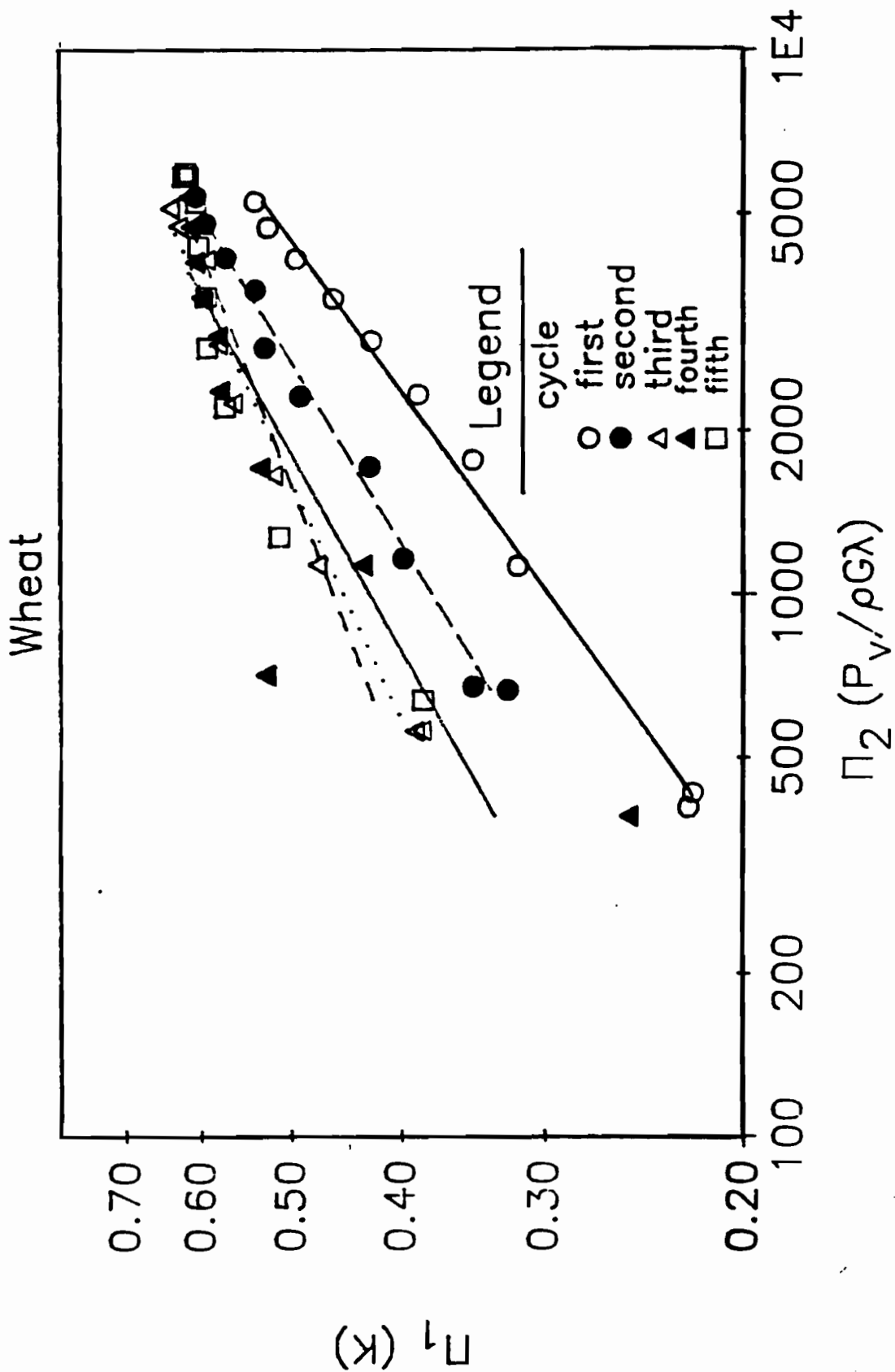
Figure 4.4.1.2. Log-log plot of Π_1 versus Π_2 for five loading cycles of wheat
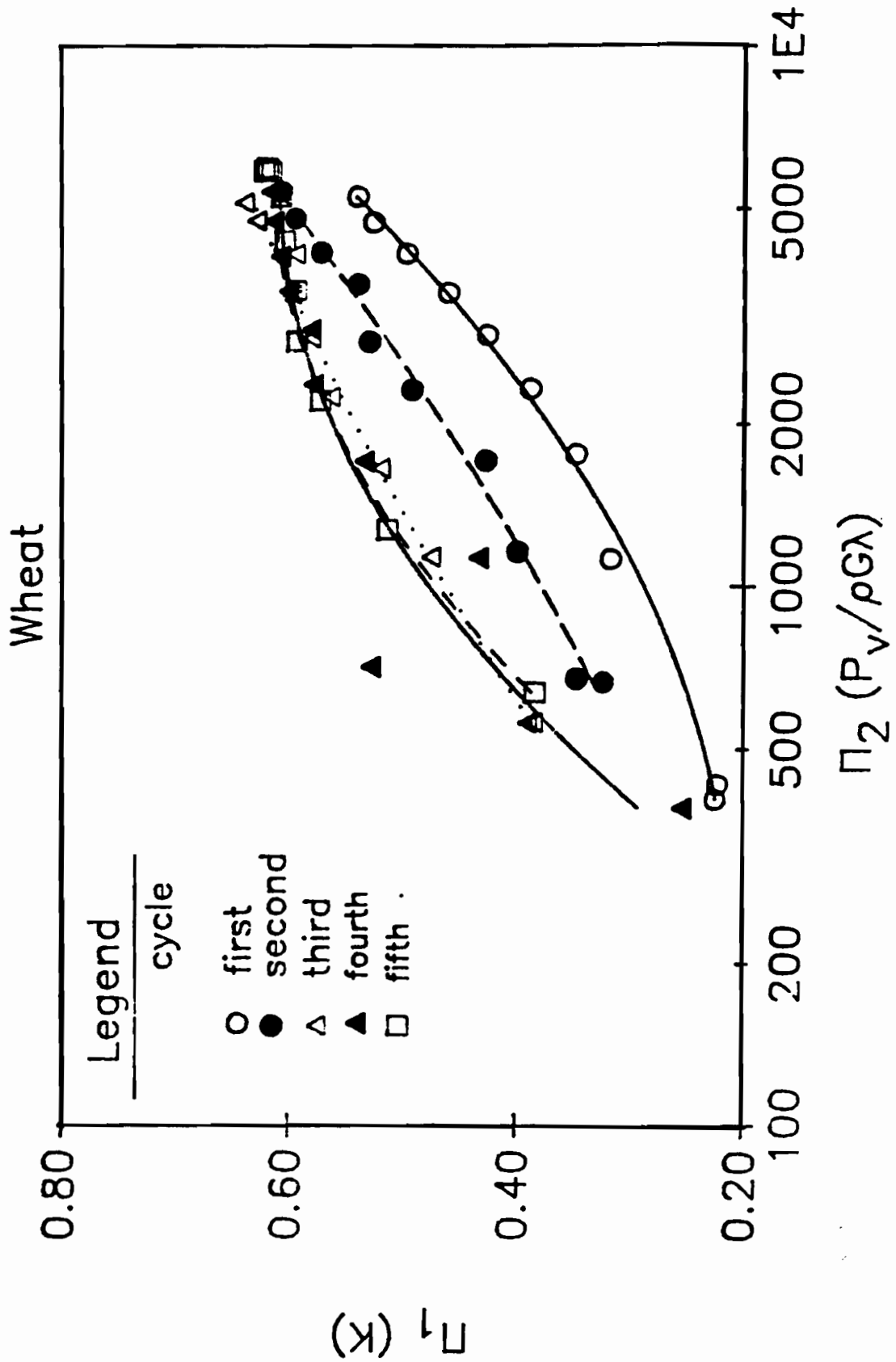
Figure 4.4.1.3. Semi-log plot of Π_1 versus Π_2 for five loading cycles of wheat
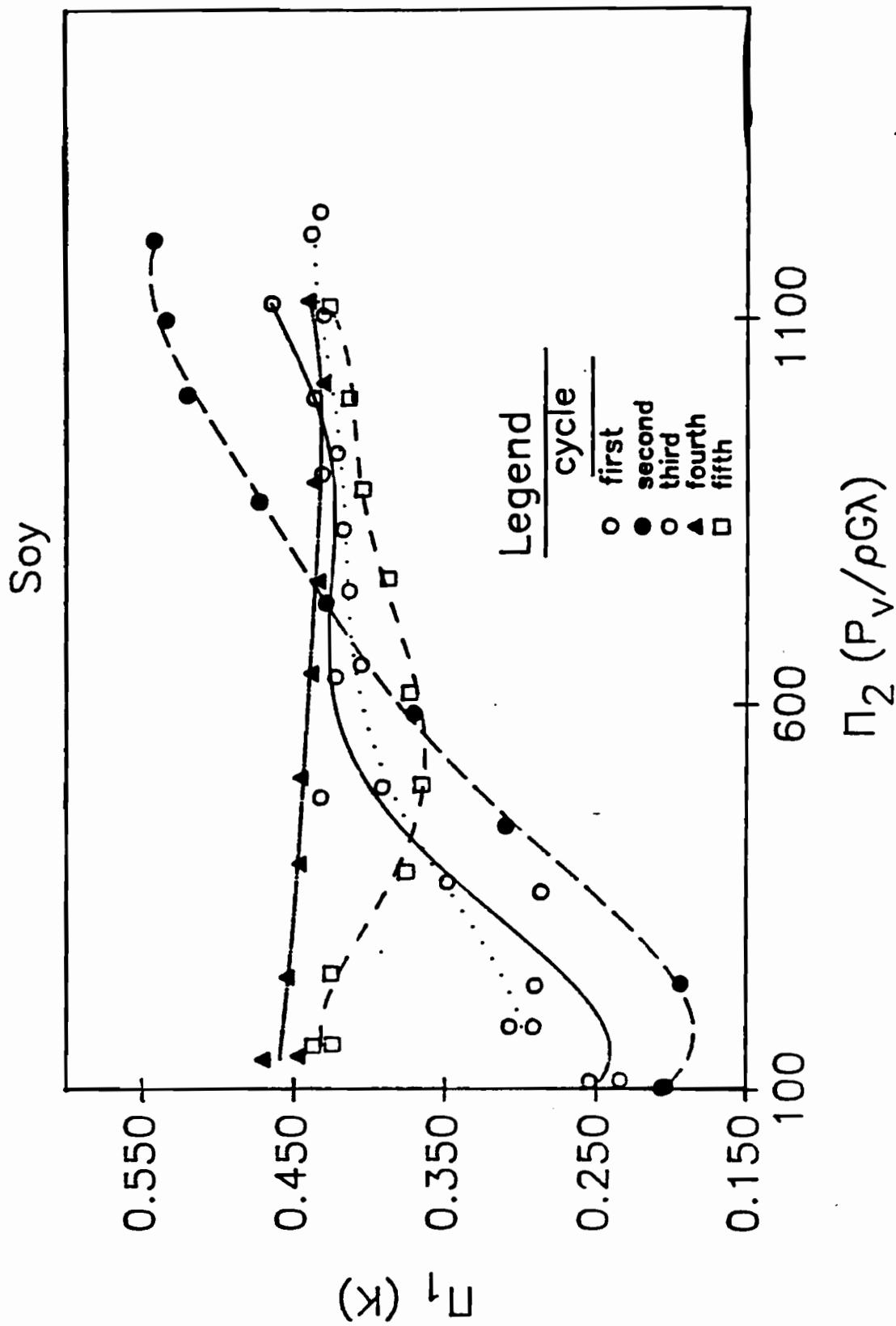
Figure 4.5.1.1. Linear plot of Π_1 versus Π_2 for five loading cycles of soybeans
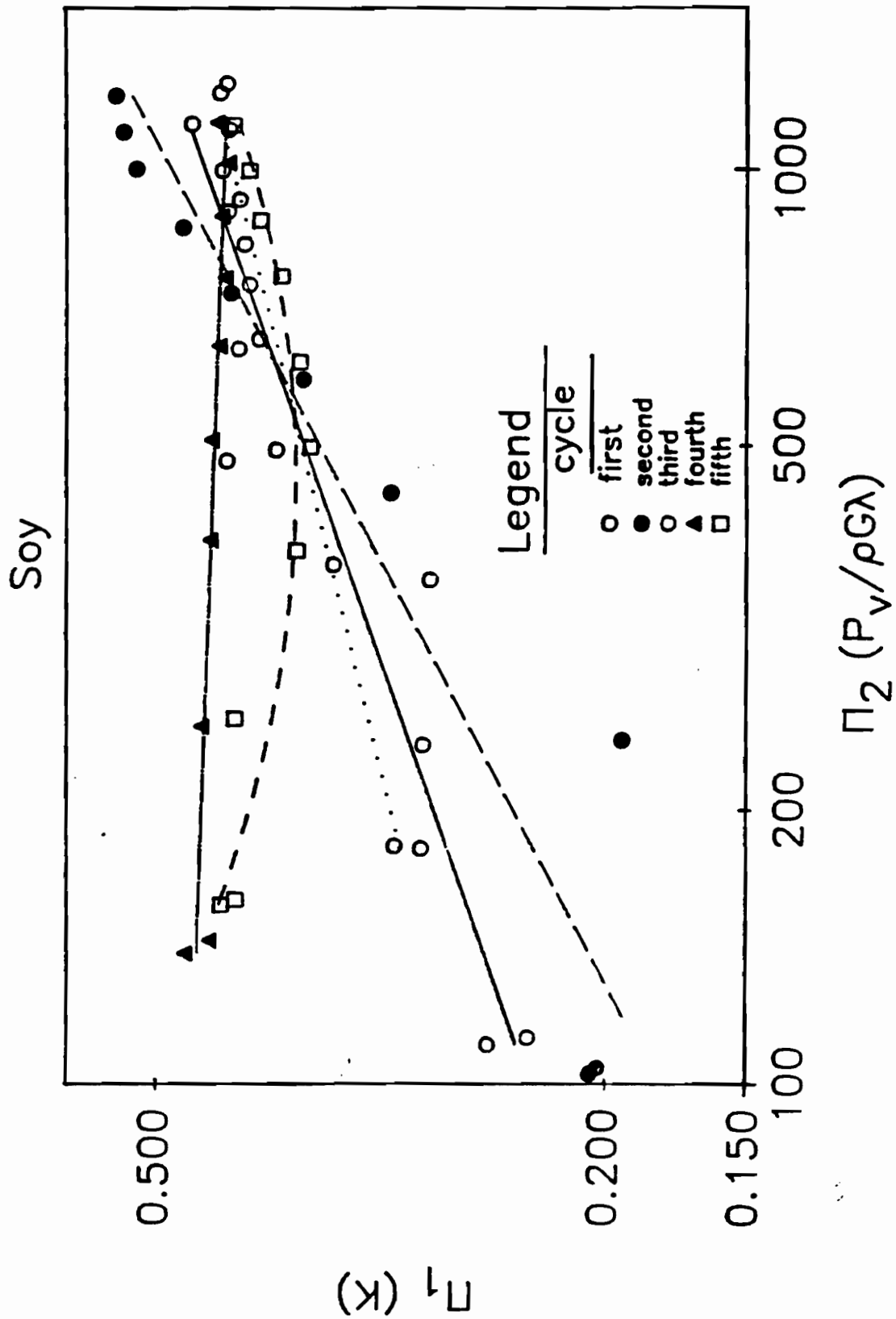
Figure 4.5.1.2. Log-log plot of Π_1 versus Π_2 for five loading cycles of soybeans
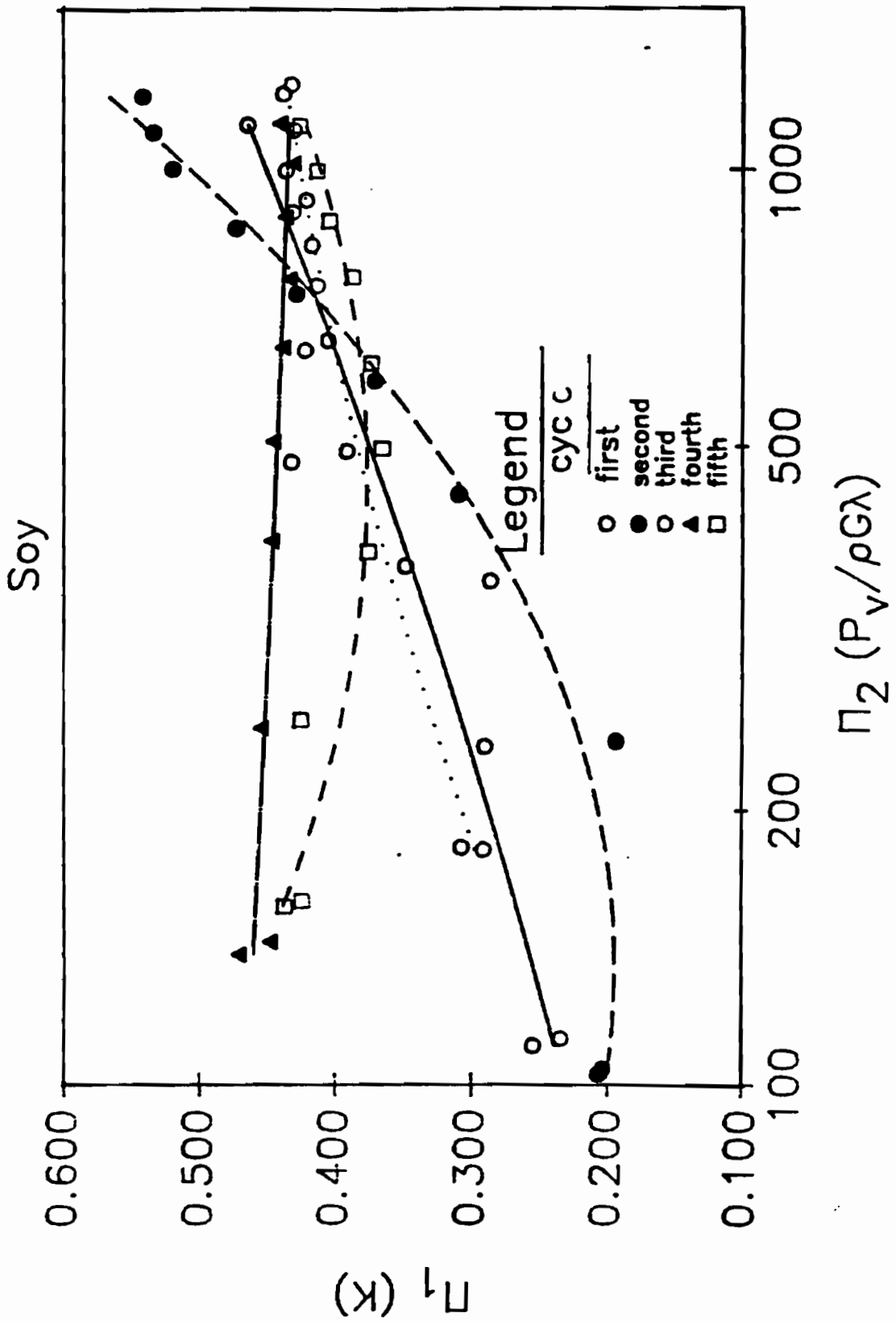
Figure 4.5.1.3. Semi-log plot for five loading cycles of soybeans
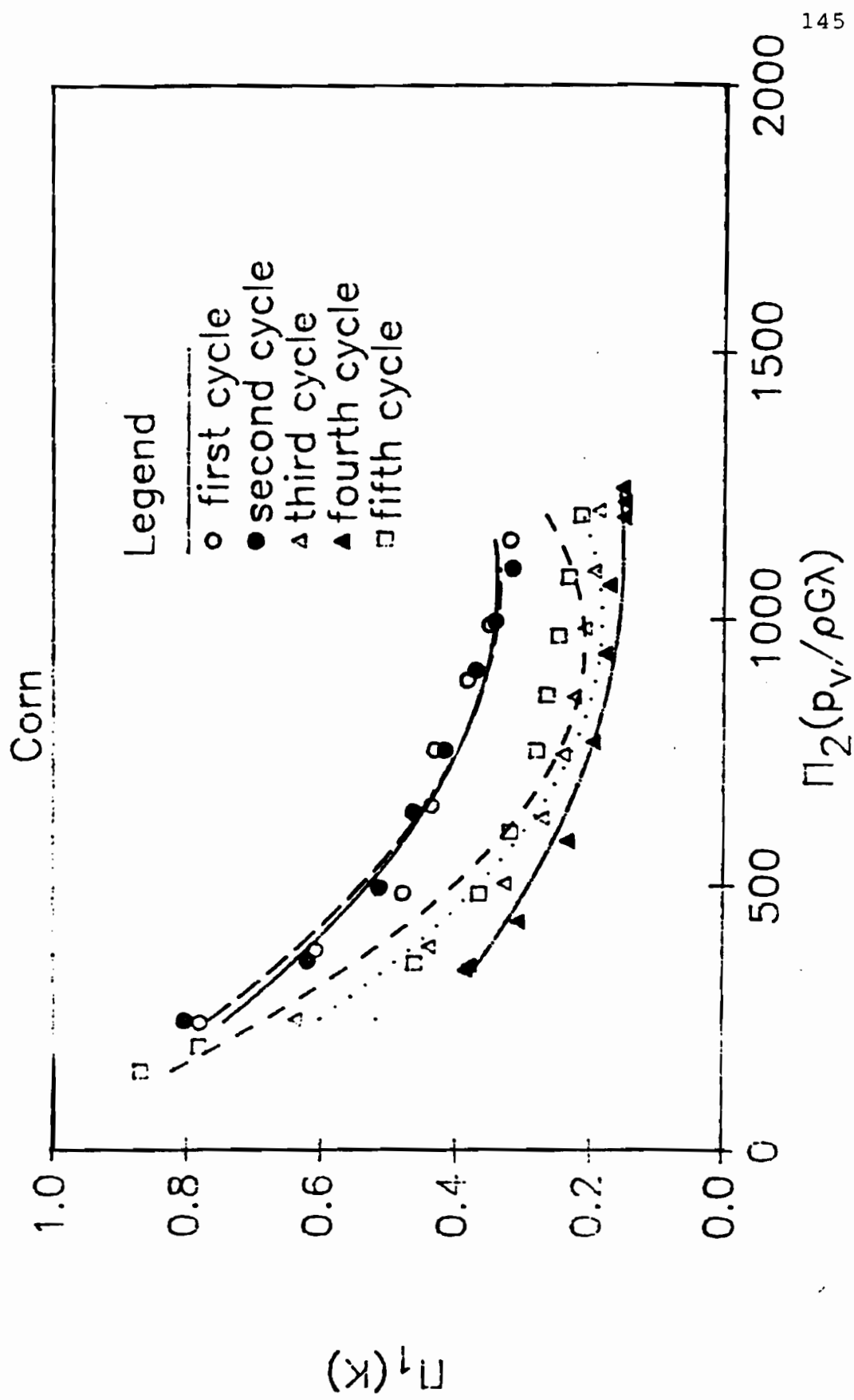
Figure 4.6.1.1. Linear plot of Π_1 versus Π_2 for five loading cycles of corn
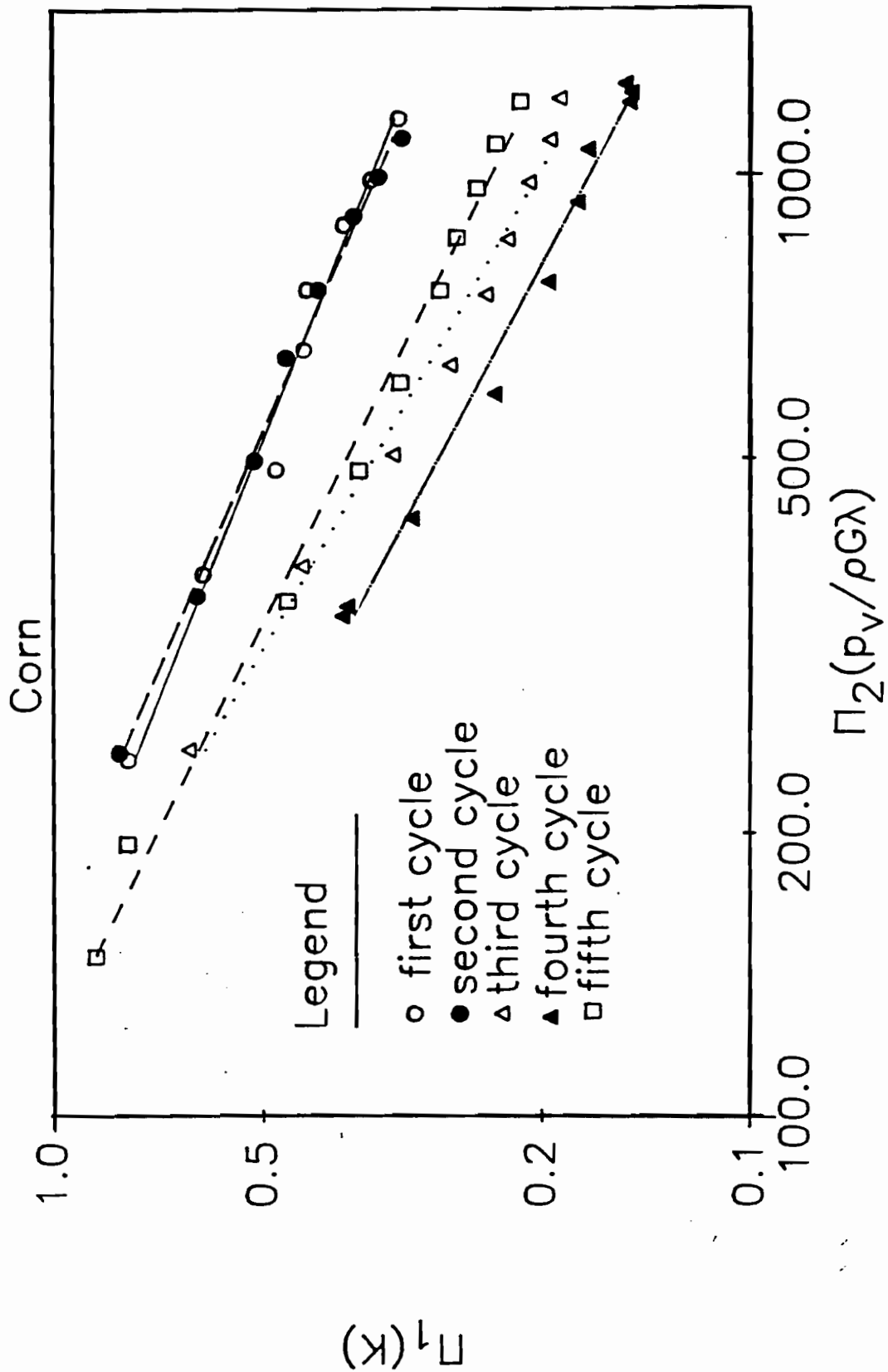
Figure .4.6.1.2. Log-log plot of Π_1 versus Π_2 for five loading cycles of corn
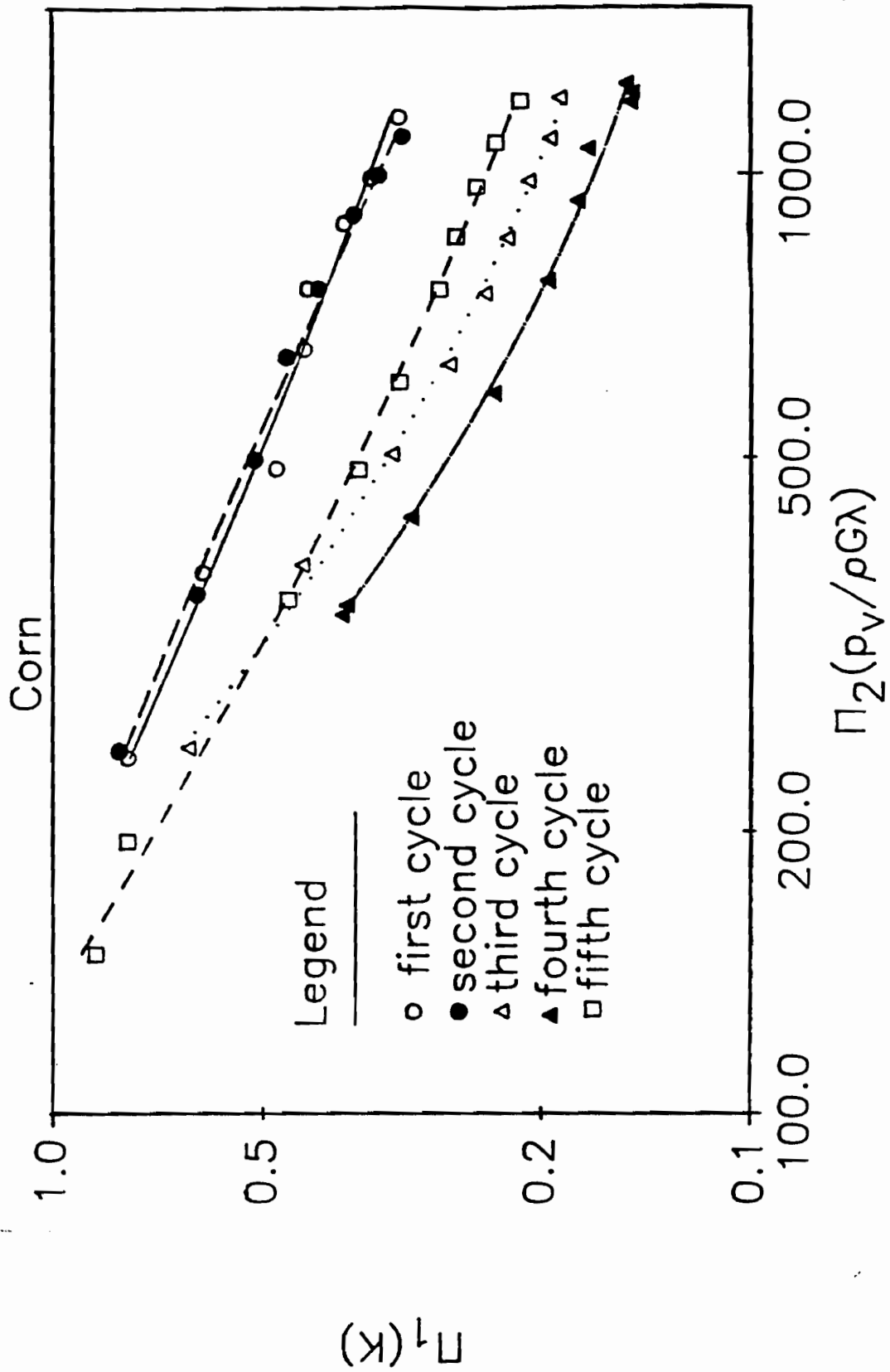
Figure 4.6.1.3. Semi-log plot of Π_1 versus Π_2 for five loading cycles of corn
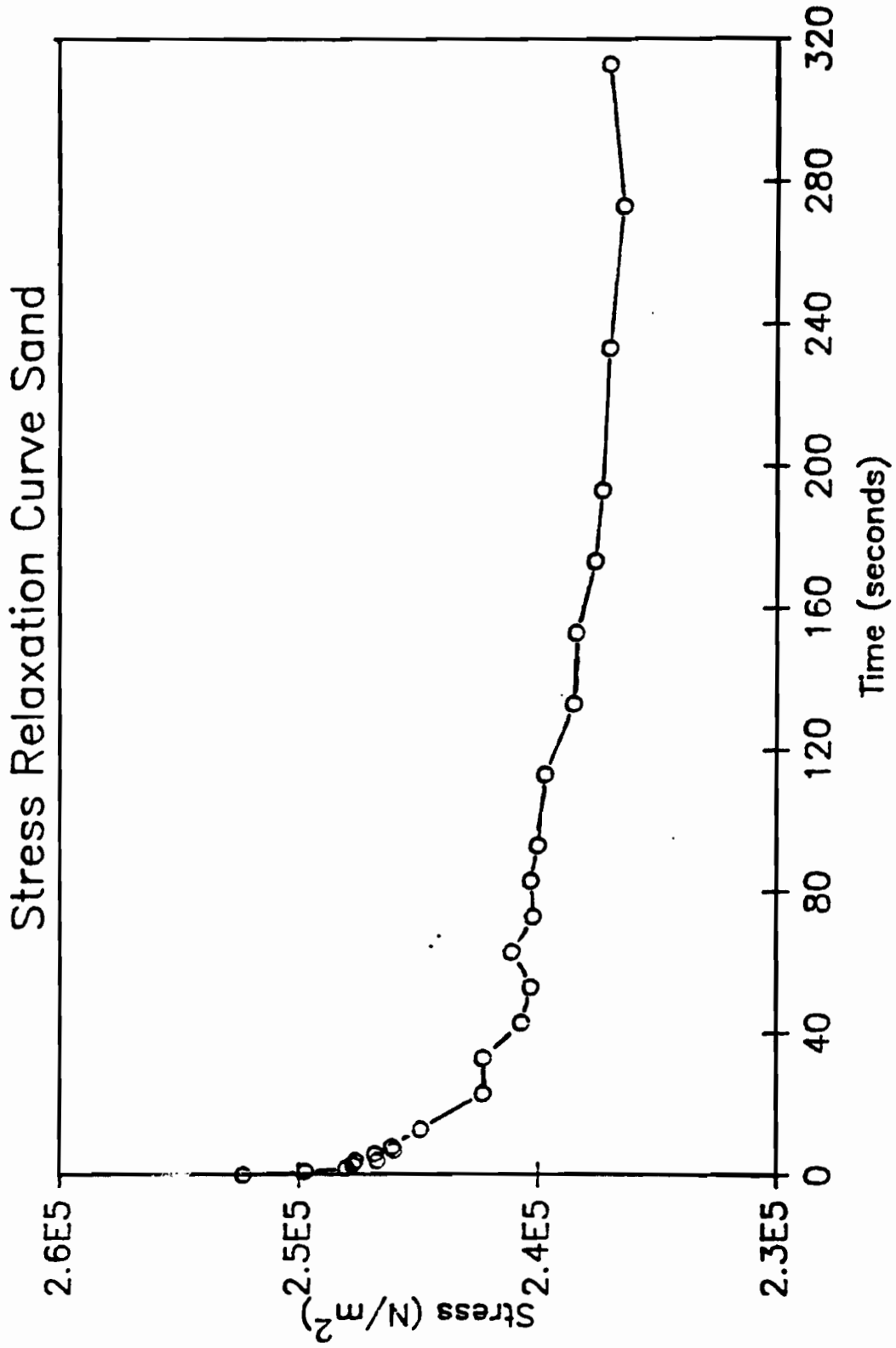
Figure 4.7.1.   Stress relaxation curve for sand
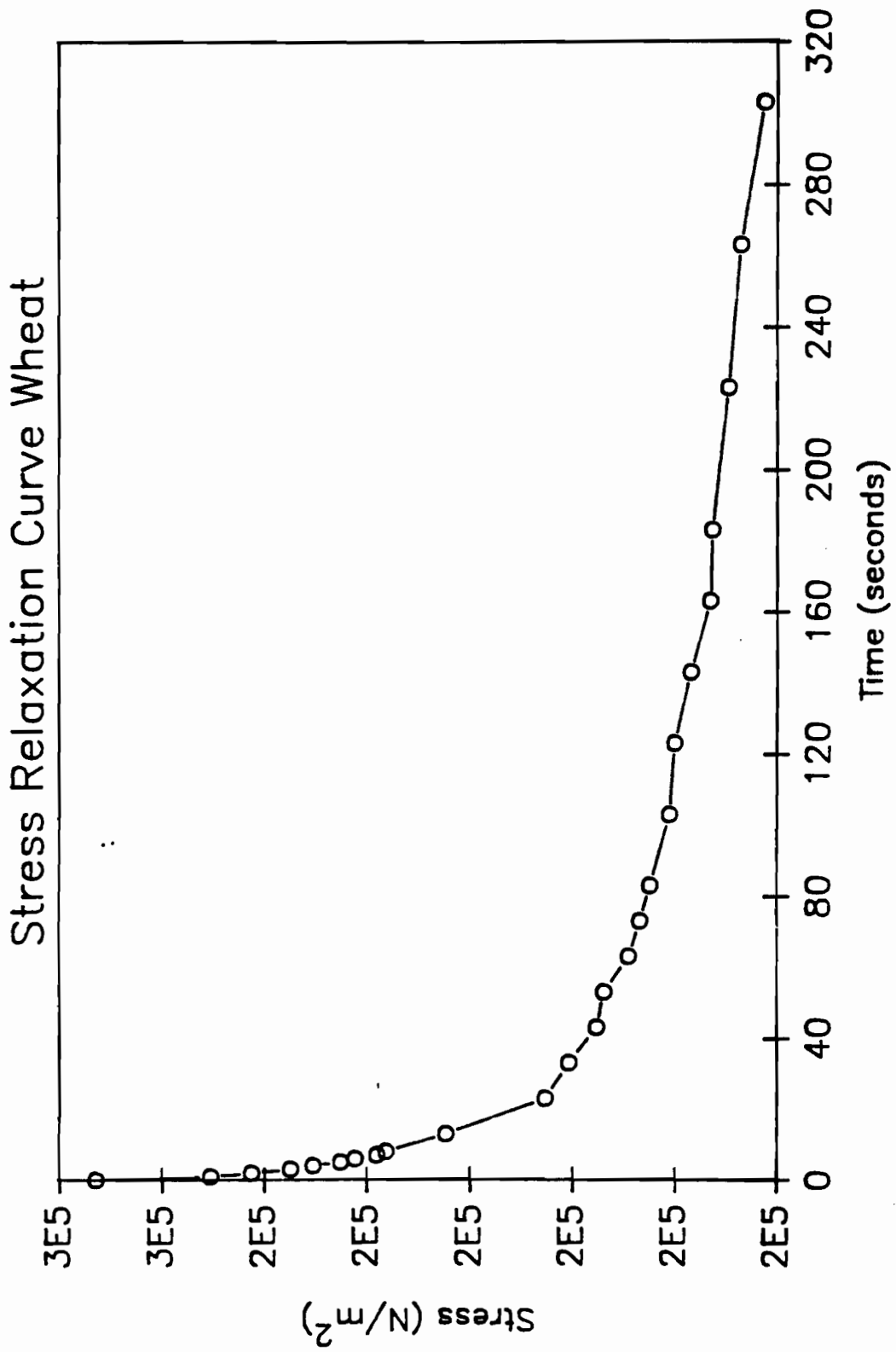
Figure 4.7.2.   Stress relaxation curve for wheat
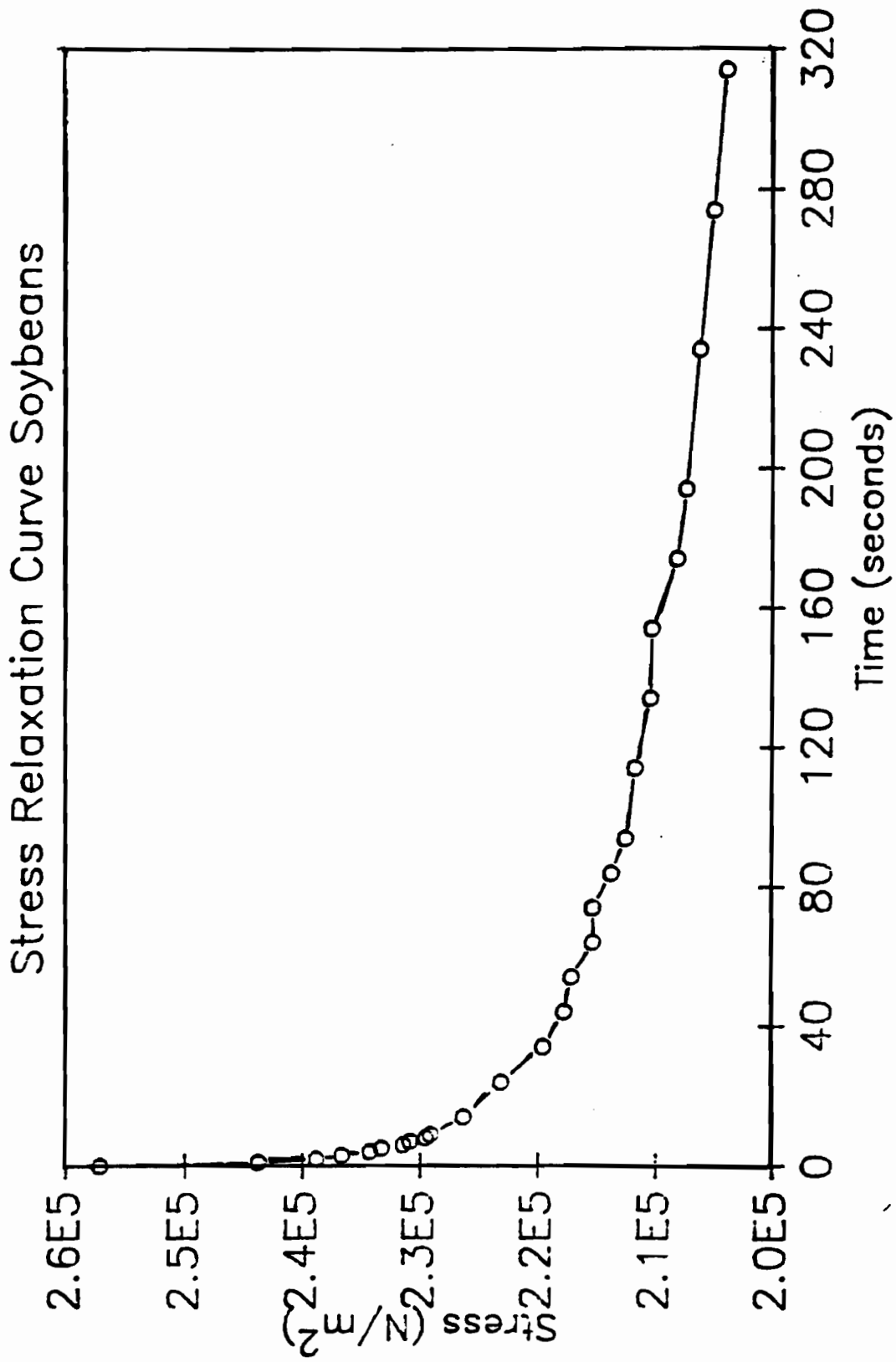
Figure 4.7.3. Stress relaxation curve for soybeans
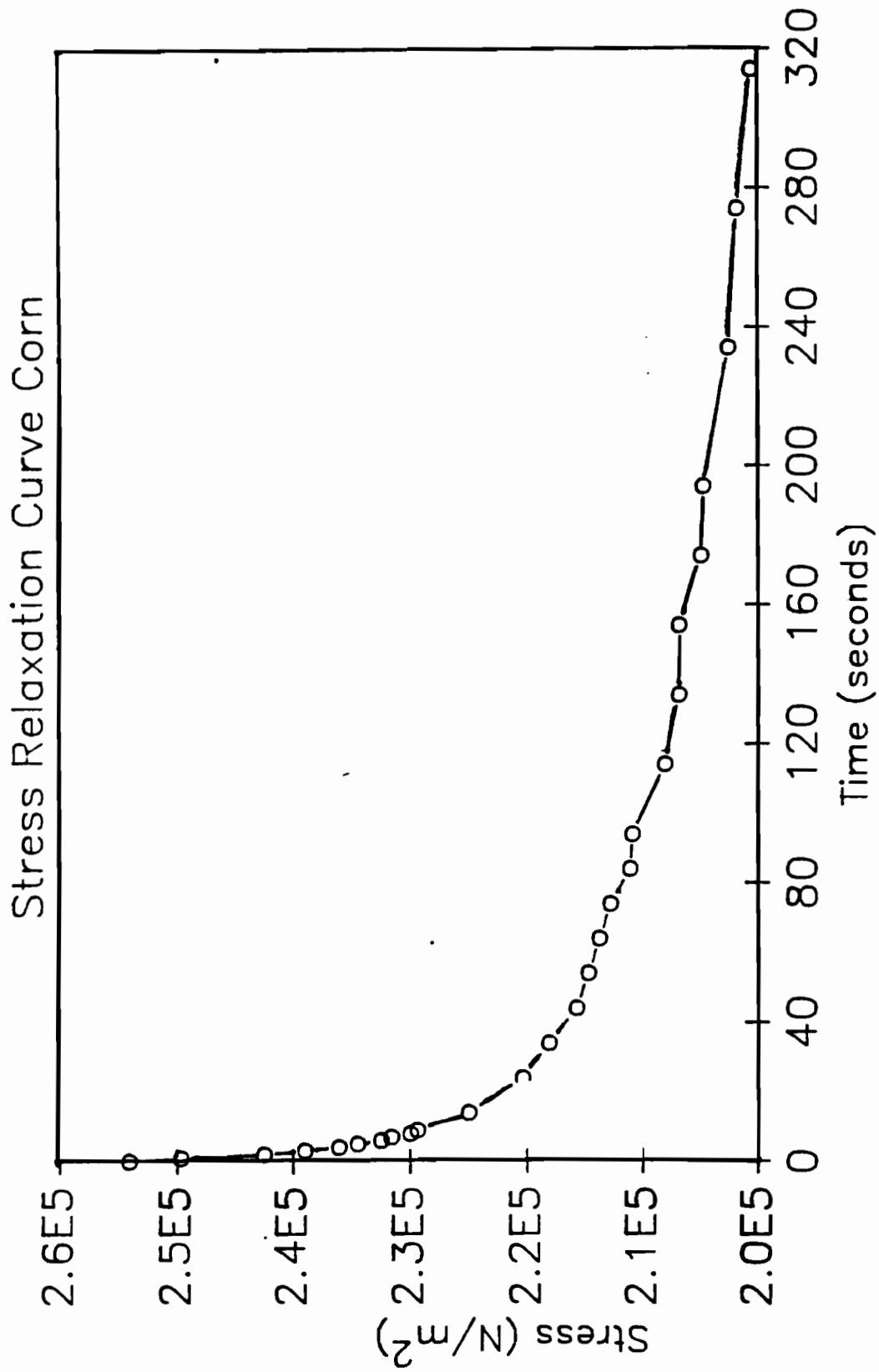
Figure 4.7.4. Stress relaxation curve for corn

4.4 Experimental Procedures for Developing a Prediction Equation for Pressures in Bins

The first objective of the study was met by identifying the physical quantities pertinent to pressures in cylindrical grain silos, as outlined in Section 4.2. Table 4.9 is a summary of the pertinent quantities. The second objective was met by writing equations (4.10) and (4.11). This section deals with the third objective, i.e., to arrive at the quantitative form of the prediction equation.

The rank of the dimensional matrix, Table 4.10, is 4, hence 16 independent terms are required to uniquely define the system. Possible form of the prediction equation for a model bin is therefore

$$\frac{P_h}{G\rho\lambda} = f(\frac{H_b}{D}, \ \mu_w, \ \phi, \eta_1, \ e_0, \ v_g, \ \frac{z}{H_b}, \ \frac{H_h}{D}, \ \frac{e}{D}, \ \frac{\lambda}{D}, \ \frac{Q^2 Ne}{GD_5},$$

$$\frac{\tau Q}{D^2 H_b}, \ \frac{D_h}{D}, \ \frac{E(t)}{\rho G\lambda})$$

or

$$\frac{P_h}{G\rho\lambda} = \phi \cdot (\frac{H_b}{D})^{n_1} \cdot (\mu_w)^{n_2} \cdot (\phi)^{n_3} \cdot (\eta_1)^{n_4} \cdot (e_0)^{n_5} \cdot (v_g)^{n_6} \cdot (\frac{z}{H_b})^{n_7}$$

$$(\frac{e}{D})^{n_8} \cdot (\frac{\lambda}{D})^{n_9} \cdot (\frac{Q^2 Ne}{GD^5})^{n_{10}} \cdot (\frac{\tau Q}{D^2 H_b})^{n_{11}} \cdot (\frac{D_h}{D})^{n_{12}} \cdot (\frac{E(t)}{\rho G\lambda})^{n_{13}} \cdot (\frac{e}{D_h})^{n_{14}}$$

Due to ease of fabrication, the model bins were constructed of steel. The maximum physical dimension (height, H_b) that

Table 4.9 Pertinent physical quantities for model bins

No.	Symbol	Description	Units	Dimensions
Dependent Quantity:				
1	P_h	Horizontal pressure at bin wall	N/m^2	FL^{-2}
Independent Quantities:				
2	D	Inside diameter of bin	m	L
3	H_b	Bin height	m	L
4	H_f	Bin fill height	m	L
5	e	Eccentricity of discharge	m	L
6	z	Depth at which P_h occurs	m	L
7	Q*	Emptying rate of fill material	m^3/s	L^3T^{-1}
8	ρ	Density of fill material	Kg/m^3	ML^{-3}
9	λ	Geometric mean diameter of particles	m	L
10	μ_w	Wall-grain coefficient of static friction	--	--
11	ϕ	Angle of internal friction of material	--	--
12	τ	Elapsed time	S	T
13	E(t)	Relaxation modulus of fill material	N/m^2	FL^{-2}
14	G	Gravity field strength	N/Kg	FM^{-1}

Table 4.9, cont.

No.	Symbol	Description	Units	Dimensions
15	η_1	Yield constant of fill material	--	--
16	Ne*	Newton's second law inertial coefficient	N-sec^2/ Kg-m	$FM^{-1}L^{-1}T^2$
17	H_h	Hopper height	m	L
18	D_h	Hopper discharge diameter	m	L
19	e_0	Initial voidage of fill	--	--
20	v_g	Poisson's ratio of fill material	--	--

*important during dynamic conditions

Table 4.10   Dimensional Matrix for Model Bins   155

		F	M	L	T
1	P_h	1	0	-2	0
2	D	0	0	1	0
3	H_b	0	0	1	0
4	H_f	0	0	1	0
5	e	0	0	1	0
6	z	0	0	1	0
7	Q	0	3	0	-1
8	ρ	0	1	-3	0
9	λ	0	0	1	0
10	μ_w	0	0	0	0
11	ϕ	0	0	0	0
12	τ	0	0	0	1
13	E(t)	1	0	-2	0
14	G	1	-1	0	0
15	η_1	0	0	0	0
16	Ne	1	-1	-1	2
17	D_h	0	0	1	0
18	H_h	0	0	1	0
19	e_0	0	0	0	0
20	v_g	0	0	0	0

Table 4.11   Π Terms for the Model Bins

No.	Dimensionless Π term	Physical Significance
Dependent term:		
Π_1	$P_h/G\rho\lambda$	Index of the ratio of horizontal pressure to gravity forces
Independent term:		
Π_2	H_b/D	Height to diameter ratio of cylindrical bin, significant property of a thin shell
Π_3	μ_w	Fill particle to bin wall friction
Π_4	ϕ	Measure of stability of fill material
Π_5	η_1	Index of yield of fill material and subsequent plastic behavior
Π_6	e_0	Initial voidage
Π_7	v_g	Poisson's ratio of fill material
Π_8	Z/H_b	Defines where P_h occurs
Π_9	H_h/D_b	Hopper geometry index
Π_{10}	e/D	Eccentricity of discharge
Π_{11}	λ/D	Ratio of particle geometric mean diameter to bin diameter

No.	Dimensionless Π term	Physical Significance
Π_{12}	$Q^2 Ne/GD^s$	Index of the ratio of inertial to gravity forces
Π_{13}	$\tau Q/D^2 H_b$	Index of the quantity of fill discharged to total bin content
Π_{14}	D_h/D	Hopper opening diameter to bin diameter
Π_{15}	$E(t)/\rho G\lambda$	Index of the ratio of viscoelastic to gravity forces
Π_{16}	e/D_h	Ratio of the hopper eccentricity to the opening diameter

could be fabricated in the laboratory was 1.219 m. A bin thickness of 1.588×10^{-3} m was used as this was both rigid and easy to form. The physical dimensions of the bins used in the study are outlined in Table 4.9. The effect of dynamic overpressures were studied with bin 4 of Table 4.12.1. Centric discharge was used for all the bins. Hence the ratio e/D was zero for all the tests.

The bin hoppers were designed so as to accomplish mass flow, since dynamic overpressures are observed for this kind of flow (63). The value of the hopper half angle θ_c was obtained from Figure 2.8 for a value of material wall friction, μ', of 0.5 (see Table 4.5),

$$Tan^{-1} \; 0.5 = 26.565°$$

Hence from Table 4.5,

$$\theta_c = 12.5°$$

and,

$$2 \; \theta_c = 25°$$

The hopper opening diameter (D_h) was then 0.559m, the hopper height H_h) was 0.457m.

Table 4.12.2 is an outline of the physical dimensions of the model bins (see Plate 3) used to study the effects

of Π_{11} (λ/D) and Π_{15} ($E(t)/\rho G\lambda$) versus Π_1 ($P_h/\rho G\lambda$). The bins were filled with sand of average particle diameter 6.3 x 10^{-4}m and mass density 1601.4 kg/m^3. The values of Π_9 (H_h/D_b), Π_{10} (e/D), Π_{12} (Q^2Ne/GD^5), Π_{13} ($\tau Q/D^2H_b$), Π_{14} (D_h/D), and Π_{16} (e/D_h) were all set to zero by having no hopper, eccentricity of discharge or discharge. For the component experiment of Π_1 ($P_h/\rho G\lambda$) versus Π_{11} (λ/D) the value of Π_{15} ($E(t)/\rho G\lambda$) was set at 1.353 x 10^{-1}. For the component experiment of Π_1 ($P_h/\rho G\lambda$) versus Π_{15} ($E(t)/\rho G\lambda$) the value of λ/D was set at 1.6 x 10^{-3}. The rest of the non-varied Π-terms were held constant as per Table 4.5. Π_2 (H_b/D) and Π_8 (Z/H_b) were set at 1.57 and 6.49 x 10^{-1} respectively.

The component experiments for relating Π_1 ($P_h/\rho G\lambda$) to Π_{11} (λ/D) were carried out using four bins with the dimensions outlined in Table 4.12.2 (see Plates 4 and 5). The bins were filled with dried sand, as outlined in Section 4.3, to the top, i.e., completely filled. Pressures were measured using load cells illustrated in

Figure 4.8 (see Plates 2 and 6). The pressures were measured 24 hours after the bins were filled. Three runs of the experiments were carried out (see Table 4.13).

Bin 1 described in Table 4.12.2 (see Plate 5) was used for component experiments relating Π_1 ($P_h/\rho G\lambda$) to

Π_{15} ($E(t)/\rho G\lambda$). The value of $E(t)$ used for the experiments is as per Table 4.5.1. The bin was filled with sand and values of P_h measured with the load cells every 20 seconds, the values of Π_{15} were calculated using the micro-computer described in Section 4.3 for each time interval. Three runs of the experiments were carried out (see Table 4.14). The data acquisition, manipulation and storage for the above two series of experiments were carried out using the Hewlett Packard equipment described in Section 4.3.

Tables 4.13 and 4.14 are results of component experiments for Π_1 versus Π_{11} and Π_{15} respectively.

Figures 4.9 and 4.10 are plots of Π_1 versus Π_{11} and Π_{15} respectively. The equations of the log-log plots for Figures 4.9 and 4.10 are:

$$\Pi_1 = 0.00\ 168\ \Pi_{11}^{1.227} \tag{4.15}$$

and

0.196 IN^2 LOADING SURFACE AREA

.50" DIA.

.38"

.38"

10-32 UNF

4 CONDUCTOR, COLOR CODED, CABLE, 5 FEET IN LENGTH
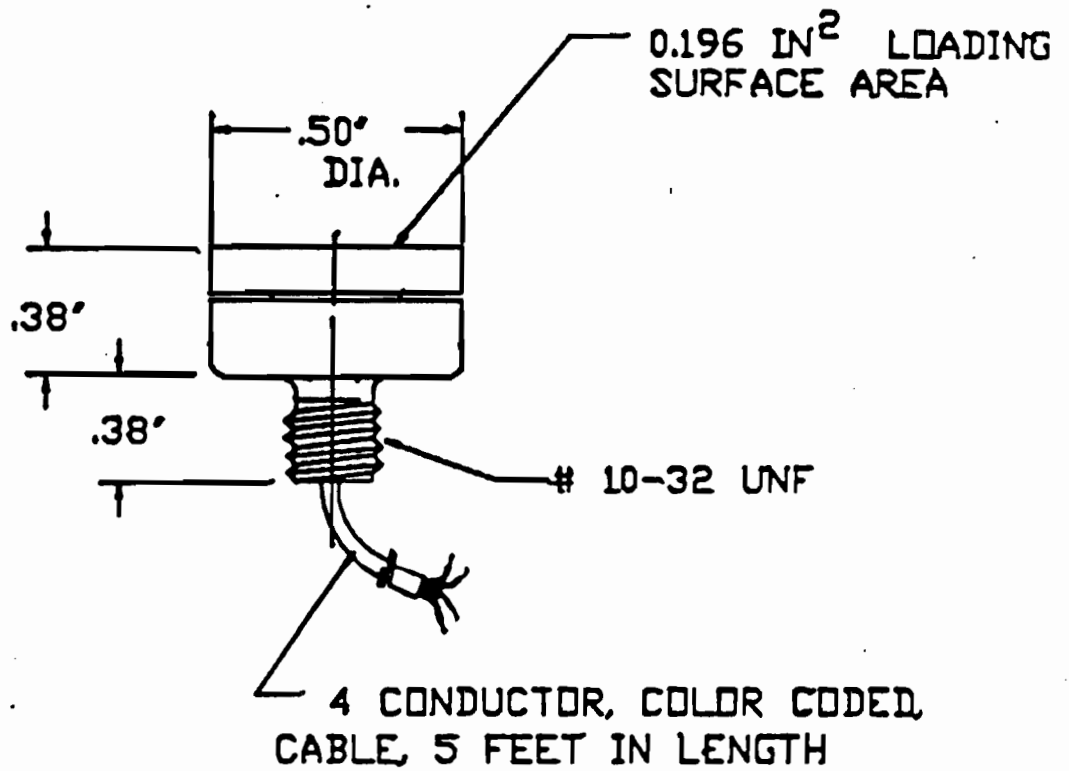
Figure 4.8. Dimensions of the load cells

Table 4.12.1   Physical Dimensions of Model Bins

Bin	Height (H_b) m	Diameter (D) m	Hopper Height (H_h) m	Hopper Diameter (D_h) m	H_b/D
1	1.22	0.76	0.46	0.76	1·6
2	1.07	0.76	0.46	0.76	1·4
3	0.91	0.76	0.46	0.76	1·2
4	0.76	0.76	0.46	0.70	1

Table 4.12.2   Physical Dimensions of Model Bins Without Hoppers

Bin	Height (H_b) M	Diameter (D) M	H_b/D	Z/H
1	0.610	0.389	1.57	0.649
2	0.503	0.320	1.57	0.649
3	0.396	0.251	1.57	0.649
4	0.290	0.184	1.57	0.649

164

Plate 2: View of a load cell
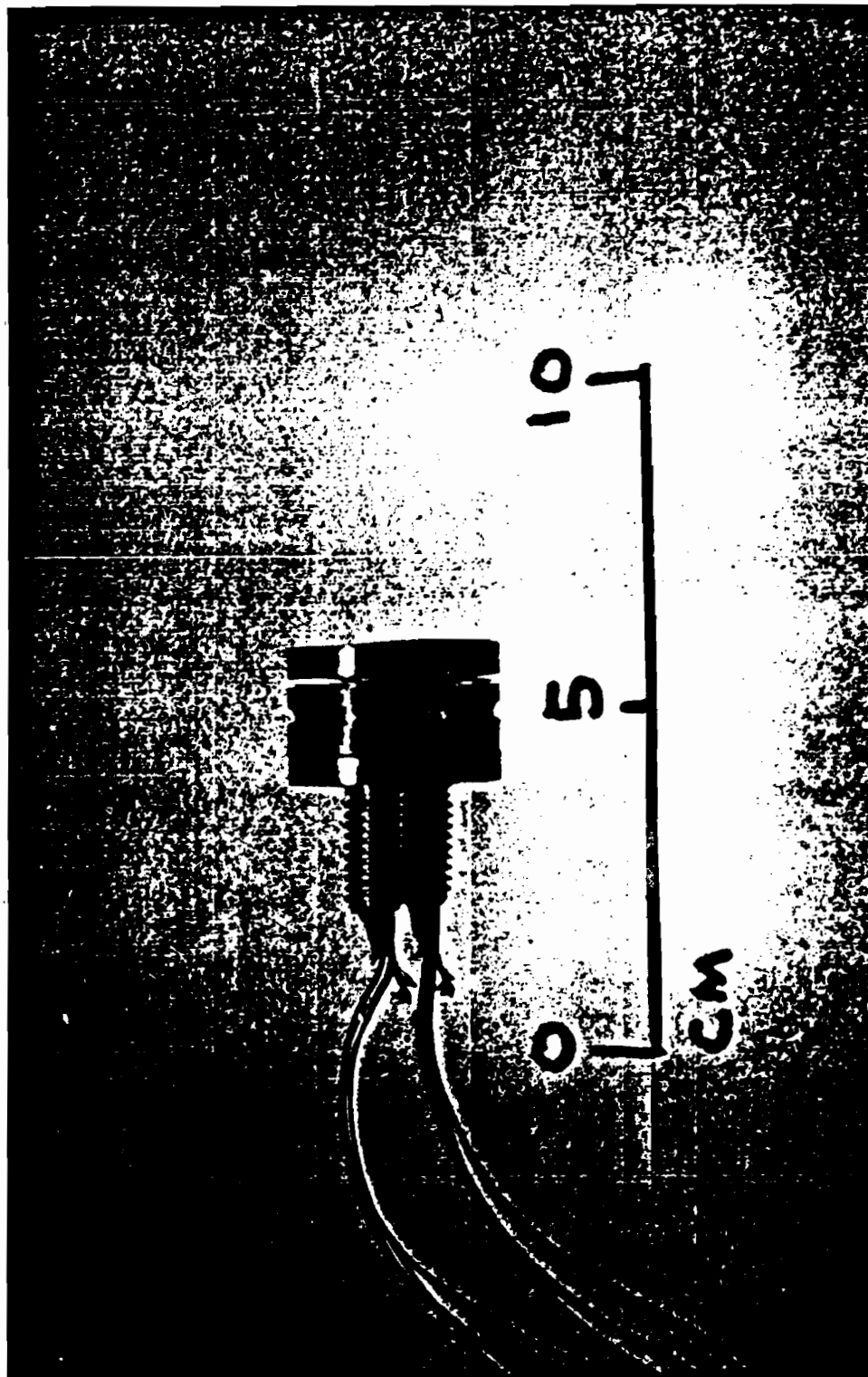
Plate 3:   Model bins without hoppers
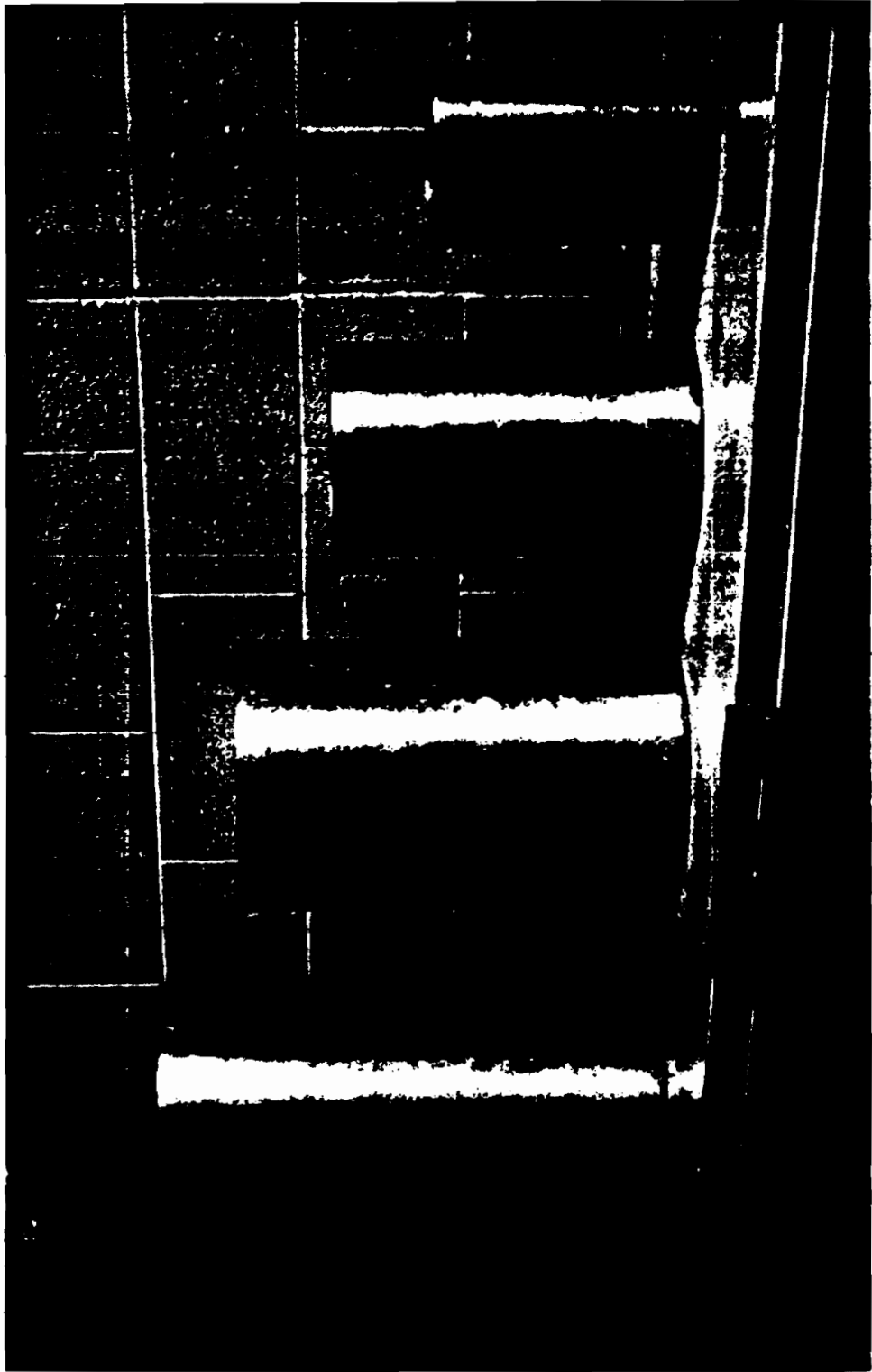
Plate 4: Model bins with hoppers
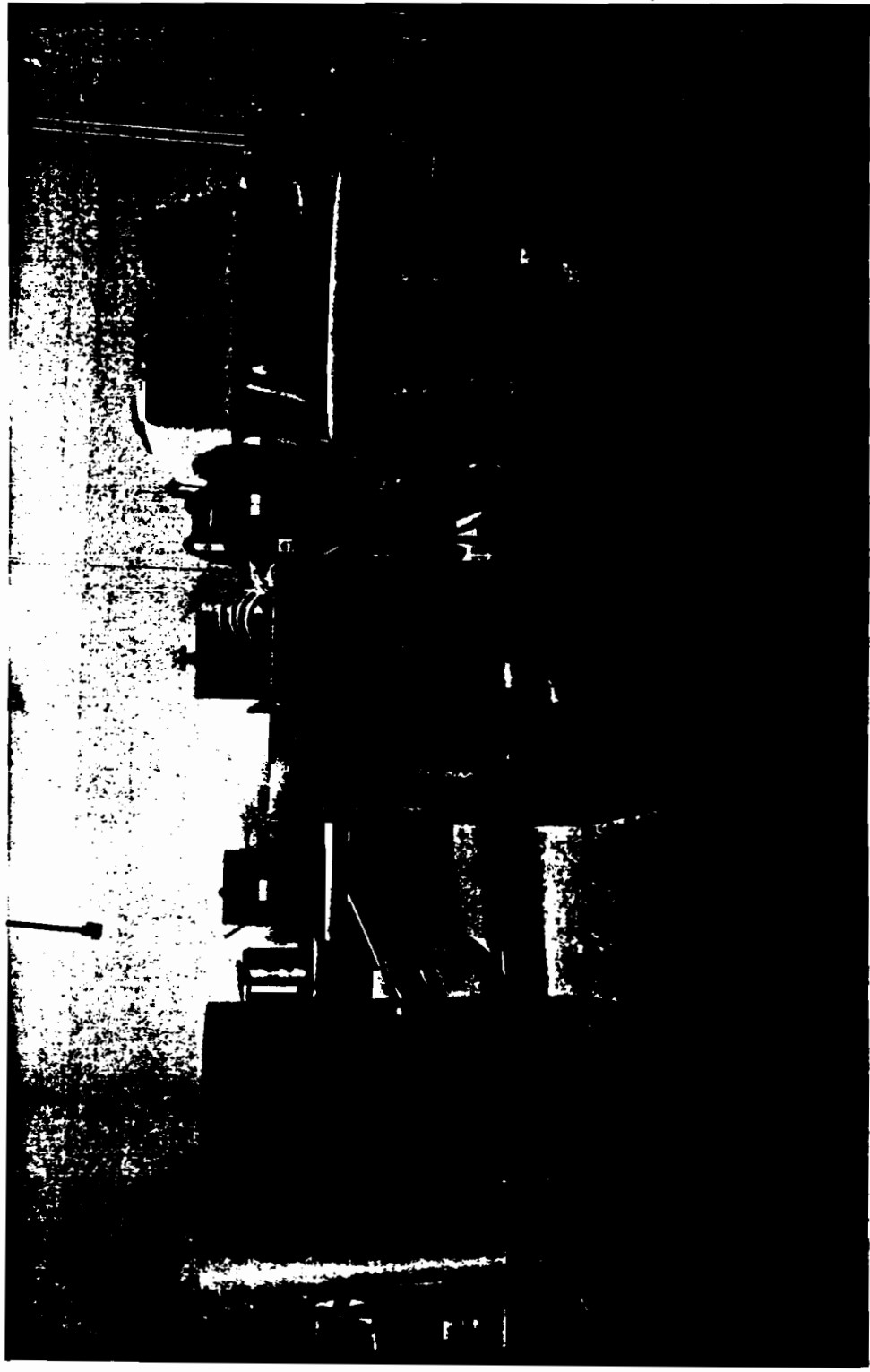
Plate 5: Model bin used for dynamic measurements
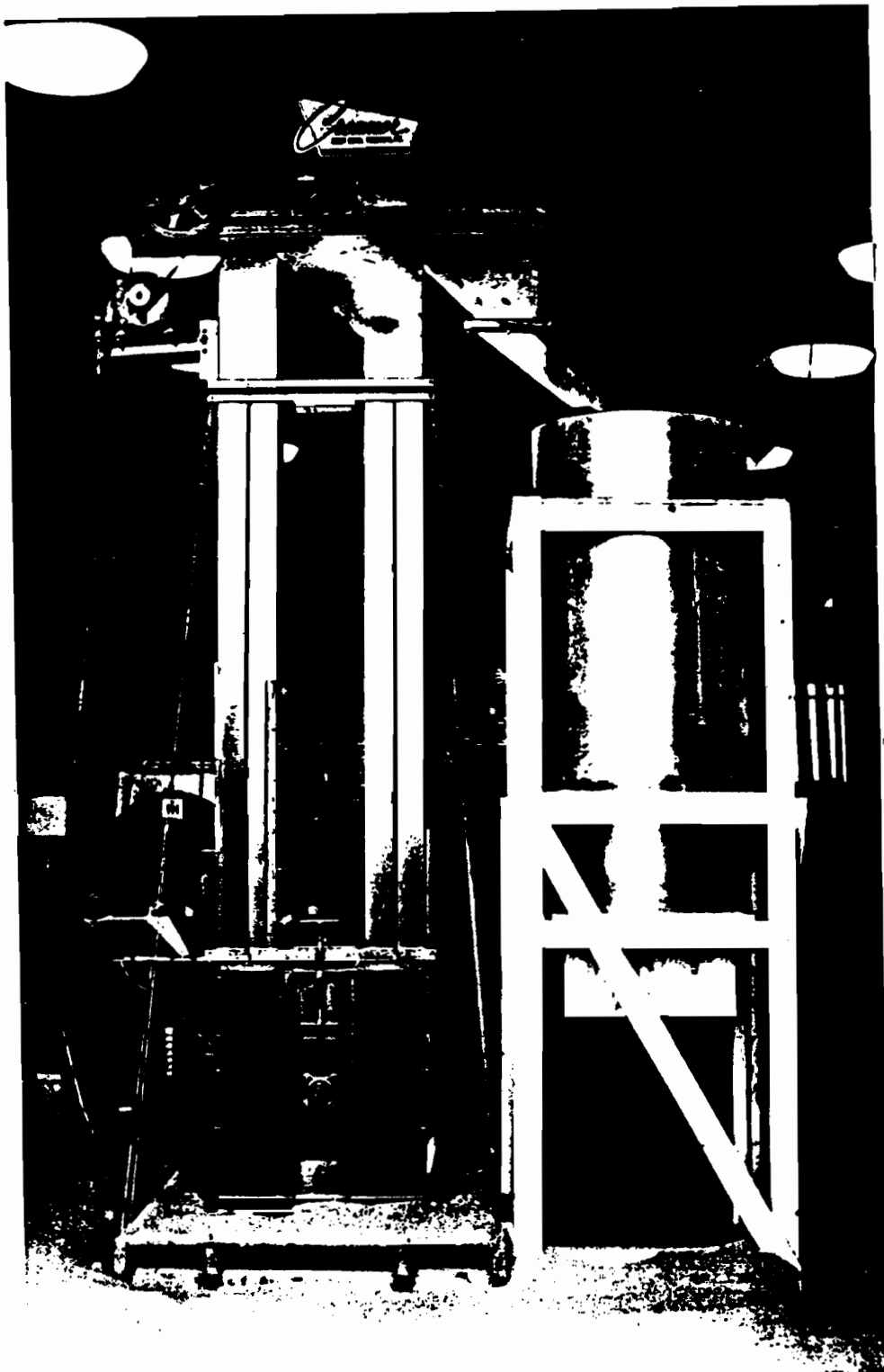
Plate 6: View of a load cell and strain gages mounted on a model bin wall
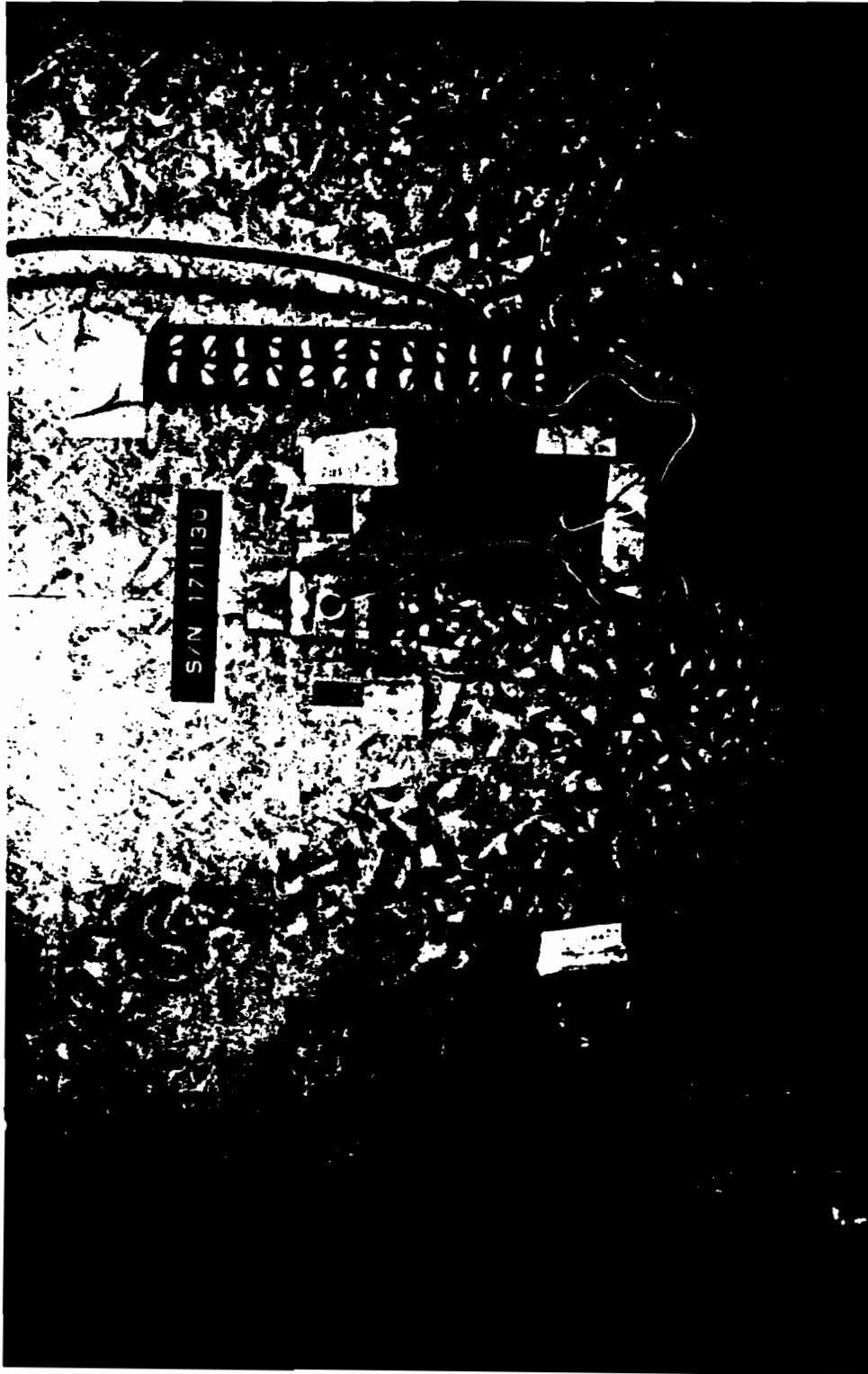
$$\Pi_1 = 0.0024 \ \Pi_{15}^{0.567} \qquad\qquad (4.16)$$

The effect of Π_2 (H_b/D) was studied using four bins with dimensions described in Table 4.12.1. The bins were filled to the top with sand and values of pressure measured using the load cells after 24 hours. Π_8 (Z/H_b) was held constant at 0.8, Π_{11} (λ/D) at 8.27×10^{-4}, Π_{14} (D_h/D) at 7.38×10^{-1}, and Π_{16} (e/D_h) at zero. The rest of the Π-terms were held constant as per Table 4.5. Figures 4.11a and 4.11b are plots of Π_1 ($P_h/\rho G_1$) versus Π_2 (H_b/D). The equation of the plot in Figure 4.11b is:

$$\Pi_1 = 7585.78 \ \Pi_2 \ 0.917 \qquad\qquad (4.17)$$

The effect of Π_8 (Z/H_b) was studied using a bin with the dimensions of Bin 1 in Table 4.12.1. Π_{11} (λ/D), Π_{14} (D_h/D), Π_2 (H_b/D) and Π_{16} (e/D_h) were set at 8.27×10^{-4}, 7.38×10^{-1}, 1.6, and zero respectively. Π_8(Z/H_b) was varied from 0.2 to 0.8 at steps of 0.2. The pressures were measured as described above. Figures 4.12a and 4.12b are plots of Π_1

versus Π_8; the equation of the plot in Figure 4.12b is:

$$\Pi_1 = 11271 \ \Pi_8^{0.904} \tag{4.18}$$

The effects of Π_{12} (Q^2Ne/GD^5) and Π_{13} ($\tau Q/D^2H_b$) were studied using a bin with the dimension of Bin 1 in Table 4.12.1. Different flowrates were achieved by varying the hopper opening (D_h) through four steps, i.e., 0.562m, 0.487m, 0.398m and 0.281m respectively. For studying the effect of Π_{12} (Q^2Ne/GD^5), Π_{13} ($\tau Q/D^2H_b$) was held at 2.56 x 10^{-1} for all the experiments. The flowrates were determined by measuring the emptying times of the bin using a stop watch. For studying the effect of Π_{12}, Π_{13} was held at 6.22 x 10^{-2} and 3.19 x 10^{-3}. The rest of the non-varied Π-terms were held constant as per the preceding paragraph. Figures 4.13 are plots of Π_1 versus Π_{13}. The equations of the log-log plots are:

$$\log \Pi_1 = 1747 + 5.4 \times 10^3 \Pi_{13}$$

$$+ \ 3.8 \times 10^4 \, (\Pi_{13})^2 - 2.37 \times 10^5 \Pi_{13}^3$$

$$- \ 1.8 \times 10^6 (\Pi_{13}2) \, (\Pi_{13})^4 + 2.58 \times 10^6 \Pi_{13}^5$$

$$(D_h/D) = 3.639 \tag{4.19}$$

and

$$\log\Pi_1 = -(4.884 + 5.991(\log\Pi_{13}) + 160.5(\log\Pi_{13})^2$$

$$+ 213.8(\log\Pi_{13})^3 + 140.3(\log\Pi_{13})^4$$

$$+ 35.93(\log\Pi_{13})^5)$$

$$D_h/D = 0.369 \qquad\qquad (4.20)$$

Figure 4.14 is a plot of $\Pi_1 (P_h/\rho G\lambda)$ versus

$\Pi_{12} (Q^2Ne/GD^5)$. An examination of the figure reveals that at

an r^2 value of 0.009, Π_{12} was not significant to the

development of pressure within the range of this study, a

discussion of this finding is in the next section.

Table 4.13   Results of Component Experiments of Π_1 (Ph/ρGλ) Versus Π_{11} (λ/D)

Π_{11} (λ/D) x 10^{-3}	Π_1 (Ph/ρGλ) x 10^3			
	Run 1	Run 2	Run 3	Average
3.4	1.262	1.261	1.2615	1.2615
2.5	2.453	2.491	2.459	2.457
2.0	2.834	2.834	2.836	2.835
1.6	3.228	3.225	3.229	3.227

Table 4.14 Results of Component Experiments for Π_1 (Ph/ρGλ) Versus Π_{15} (E(t)/ρGλ)

Run 1

Π_1 (Ph/ρGλ) x 10^3	Π_{15} (E(t)/ρGλ) x 10^6
5.702	1.353
5.652	1.305
5.630	1.294
5.574	1.287
5.581	1.282
5.561	1.279
5.564	1.276
5.558	1.274
5.542	1.270
5.539	1.267
5.490	1.263
5.482	1.259
5.486	1.251
5.448	1.241
5.422	1.225
5.372	1.208
5.358	1.192
5.212	1.176
5.201	1.160
5.225	1.38
5.249	1.129

Table 4.14, cont.

Run 2

Π_1 (Ph/ρGλ) x 10^3	Π_{15} (E(t)/ρGλ) x 10^6
5.677	1.314
5.643	1.299
5.623	1.290
5.583	1.284
5.578	1.280
5.564	1.278
5.590	1.275
5.558	1.274
5.542	1.272
5.504	1.267
5.588	1.261
5.581	1.258
5.469	1.248
5.456	1.243
5.423	1.219
5.415	1.209
5.372	1.194
5.358	1.175
5.306	1.160
5.201	1.119
5.248	1.129
5.250	1.128

Table 4.14, cont.

Run 3

Π_1 (Ph/ρGλ) x 10^3	Π_{15} (E(t)/ρGλ) x 10^6
5.527	1.351
5.684	1.347
5.771	1.299
5.533	1.287
5.528	1.283
5.525	1.277
5.524	1.266
5.521	1.261
5.377	1.254
5.371	1.248
5.353	1.243
5.350	1.239
5.350	1.236
5.348	1.234
5.313	1.229
5.304	1.226
5.284	1.215
5.282	1.207
5.268	1.194
5.258	1.181
5.239	1.170
5.223	1.130
5.242	1.20

Table 4.15 Results of Component Experiments of Π_1 (Ph/$\rho G\lambda$) Versus Π_2 (H_b/D)

Π_2 (H_b/D)	Π_1 (Ph/$\rho G\lambda$) x 10^3			
	Run 1	Run 2	Run 3	Average
1.6	11.254	11.181	11.236	11.224
1.4	10.800	10.783	10.689	10.757
1.2	9.394	9.22	8.794	9.136
1.0	7.405	7.403	7.299	7.402

Table 4.16   Results of Component Experiments of Π_1 (Ph/ρGλ) Versus Π_8 (Z/H_b)

Π_8 (Z/H_b)	Π_1 (Ph/ρGλ) x 10^3			
	Run 1	Run 2	Run 3	Average
0.2	2.709	2.548	2.899	2.719
0.4	4.331	4.209	4.467	4.336
0.6	8.146	8.091	8.321	8.186
0.8	8.617	8.914	8.743	8.758

Table 4.17a   Results of Component Experiments of Π_1 (Ph/ρGλ) Versus Π_{13} (τQ/D^{2}H$_b$) for Π_{14} (Dh/D) = 0.369

Π_{13} (τQ/D^{2}H$_b$) x 10^{-2}	Π_1 (Ph/ρGλ) x 10^3		
	Run 1	Run 2	Average
6.800	7.726	7.878	7.802
13.420	13.730	12.120	12.925
20.129	13.630	12.640	13.135
26.839	11.710	12.019	11.864
33.549	9.26	10.071	9.639
40.259	7.458	8.248	7.853
46.969	3.192	3.476	3.334
53.678	1.080	1.547	1.314

D_h/D = 0.369

Table 4.17b   Results of Component Experiments of Π_1 (Ph/ρGλ) Versus Π_{13} (τQ/D^{2}H$_b$) for Π_{14} (Dh/D) = 0.522

Π_{13} (τQ/D^{2}H$_b$) x 10^{-1}	Π_1 (Ph/ρGλ) x 10^3		
	Run 1	Run 2	Average
1.71	9.502	10.010	9.756
2.56	8.875	9.436	9.156
3.42	2.941	1.921	2.431

Table 4.17c Results of Component Experiments for Circumferential Strains (ε) Versus Π_{13} ($\tau Q/D^2 H_b$) for Π_{14} (Dh/D) = 0.522

Π_{13} ($\tau Q/D^2 H_b$) x 10^{-1}	Circumferential Strain (ε) x 10^{-5}		
	Run 1	Run 2	Average
1.71	5.347	5.427	5.387
1.92	5.581	5.616	5.599
2.14	6.088	6.112	6.100
2.35	6.166	6.191	6.179
2.56	5.913	6.010	5.962
2.78	5.813	6.001	5.907
2.99	5.018	4.966	4.992
3.21	3.500	3.984	3.742

Table 4.17d   Results of Component Experiments for
Circumferential Strain (ε) Versus Π_{13} ($\tau Q/D^2 H_b$) for Π_{14}
(Dh/D) = 0.369

Π_{13} ($\tau Q/D^2 H_b$) x 10^{-2}	Circumferential Strain (ε) x 10^{-5}		
	Run 1	Run 2	Average
6.800	5.151	5.347	5.249
13.420	5.127	5.996	6.062
20.129	6.283	6.111	6.197
26.839	6.518	6.489	6.503
33.549	6.635	6.711	6.681
40.259	6.557	6.609	6.583
46.969	5.112	4.815	4.964
53.678	3.674	3.714	3.694

Table 4.18 Results of Component Experiments of Π_1 (Ph/ρGλ) Versus Π_{12} (Q^2Ne/GD^5)

Π_{12} (Q^2Ne/GD^5) x 10^{-2}	Π_1 (Ph/ρGλ) x 10^3		
	Run 1	Run 2	Average
12.296 1	10.114	9.814	9.964
8.333 2	6.128	8.927	7.528
4.801 3	9.226	9.116	9.171
1.885 4	9.613	8.943	9.278

1 - D_h/D = 1

2 - D_h/D = 0.866

3 - D_h/D = 0.522

4 - D_h/D = 0.369

Table 4.19   Component Equations for Model Bin Experiments

Component Equation	r^2
$\Pi_1 = 7585\ \Pi_2^{0.917}$	0.956
$\Pi_1 = 1271\ \Pi_8^{0.904}$	0.956
$\Pi_1 = 0.00168\ \Pi_1^{1.227}$	
$\Pi_1^* = 1747 + 5.4 \times 10^4\ \Pi_{13} + 3.8 \times 10^4\ (\Pi_{13})^2$ $- 2.37 \times 10^5\ (\Pi_{13})^3 - 1.8 \times 10^6\ (\Pi_{13})^4$ $+ 2.58 \times 10^6\ (\Pi_{13})^5$	1.0^{***}
$\Pi_1^{**} = -(4.884 + 5.9907\ (\log \Pi_{13})$ $+ 160.5\ (\log \Pi_{13})^2$ $+ 213.8\ (\log \Pi_{13})^3 + 140.3\ (\log \Pi_{13})^4$ $+ 35.93\ (\log \Pi_{13})^5)$	0.996^{***}
$\Pi_1 = 0.0024\ \Pi_{15}^{0.567}$	0.947

* $D_h/D = 0.639$

** $D_h/D = 0.369$

*** R^2
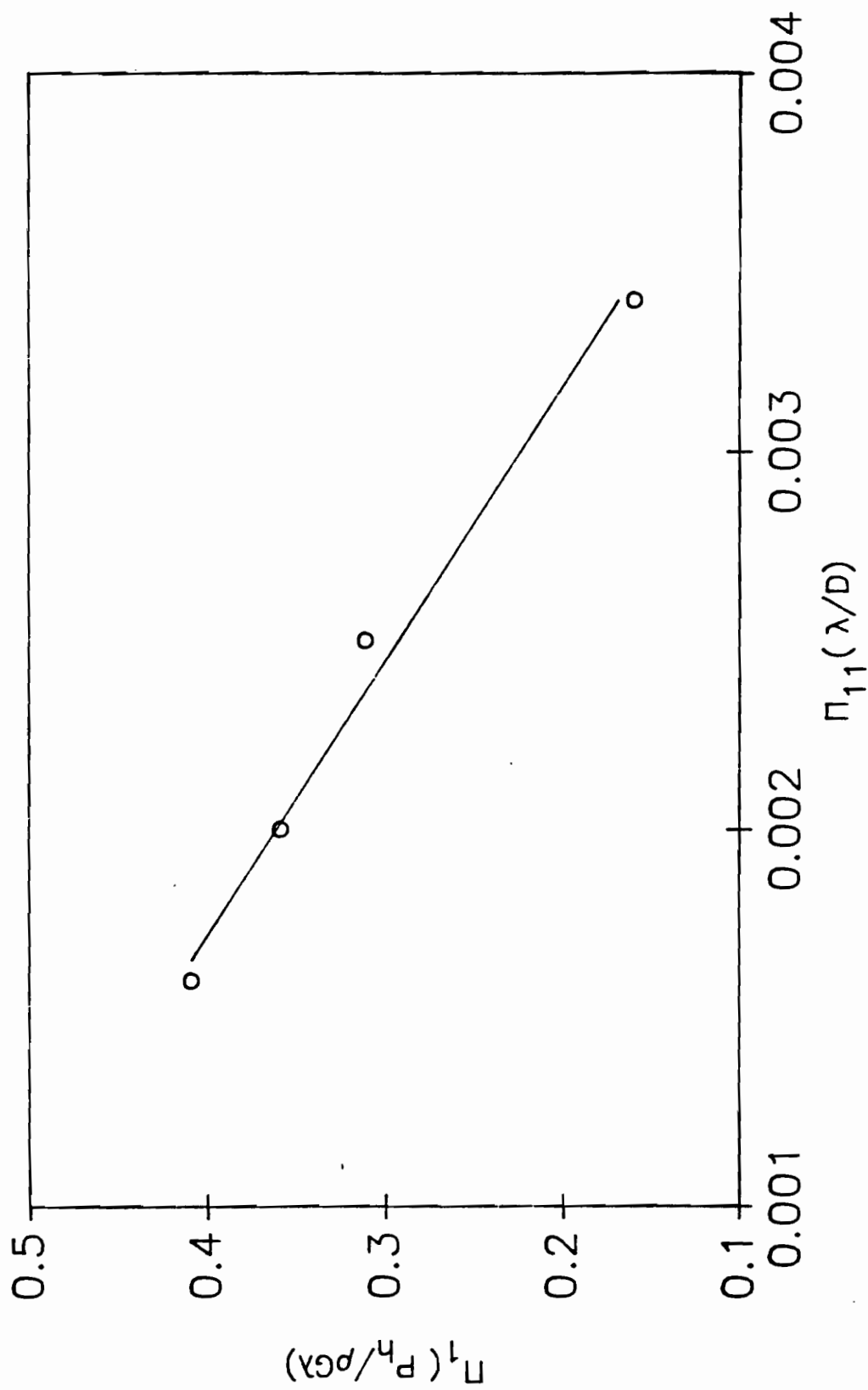
Figure 4.9.1. Linear plot of Π_1 versus Π_{11} for model bin experiments
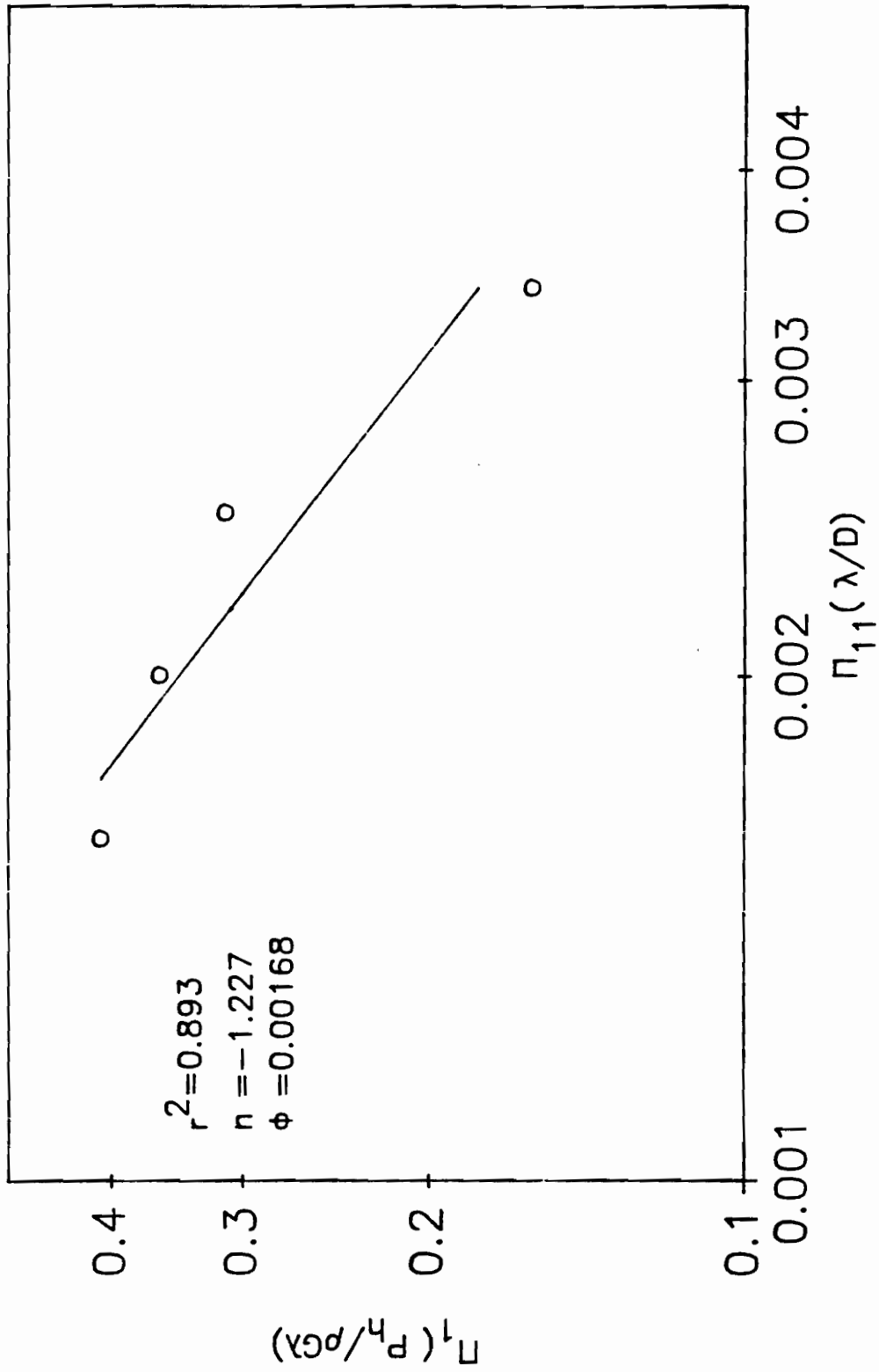
Figure 4.9.2. Log-log plot of Π_1 versus Π_{11} for model bin experiments
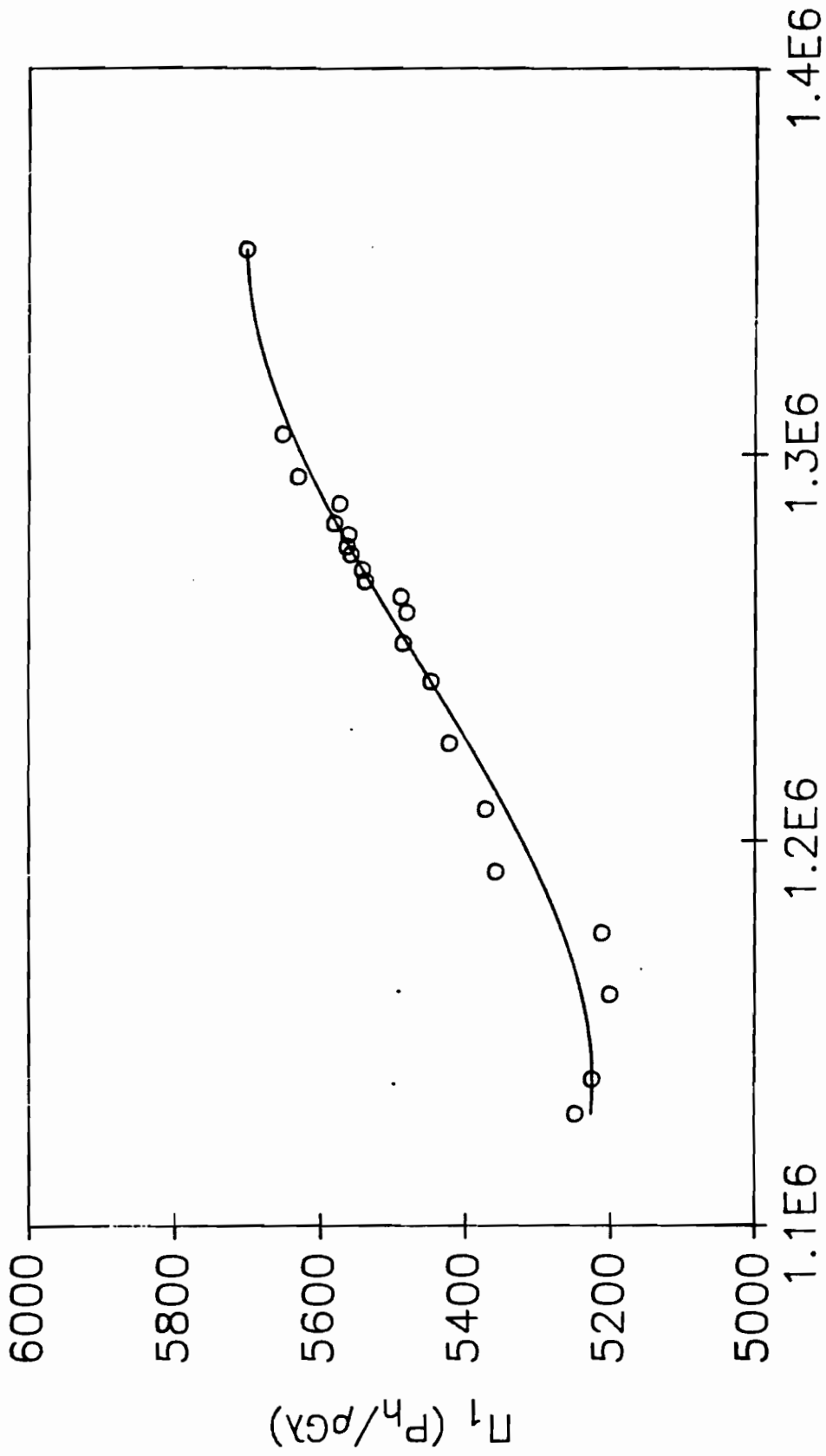
Figure 4.10.1. Linear plot of Π_1 versus Π_{15} for model bin experiments
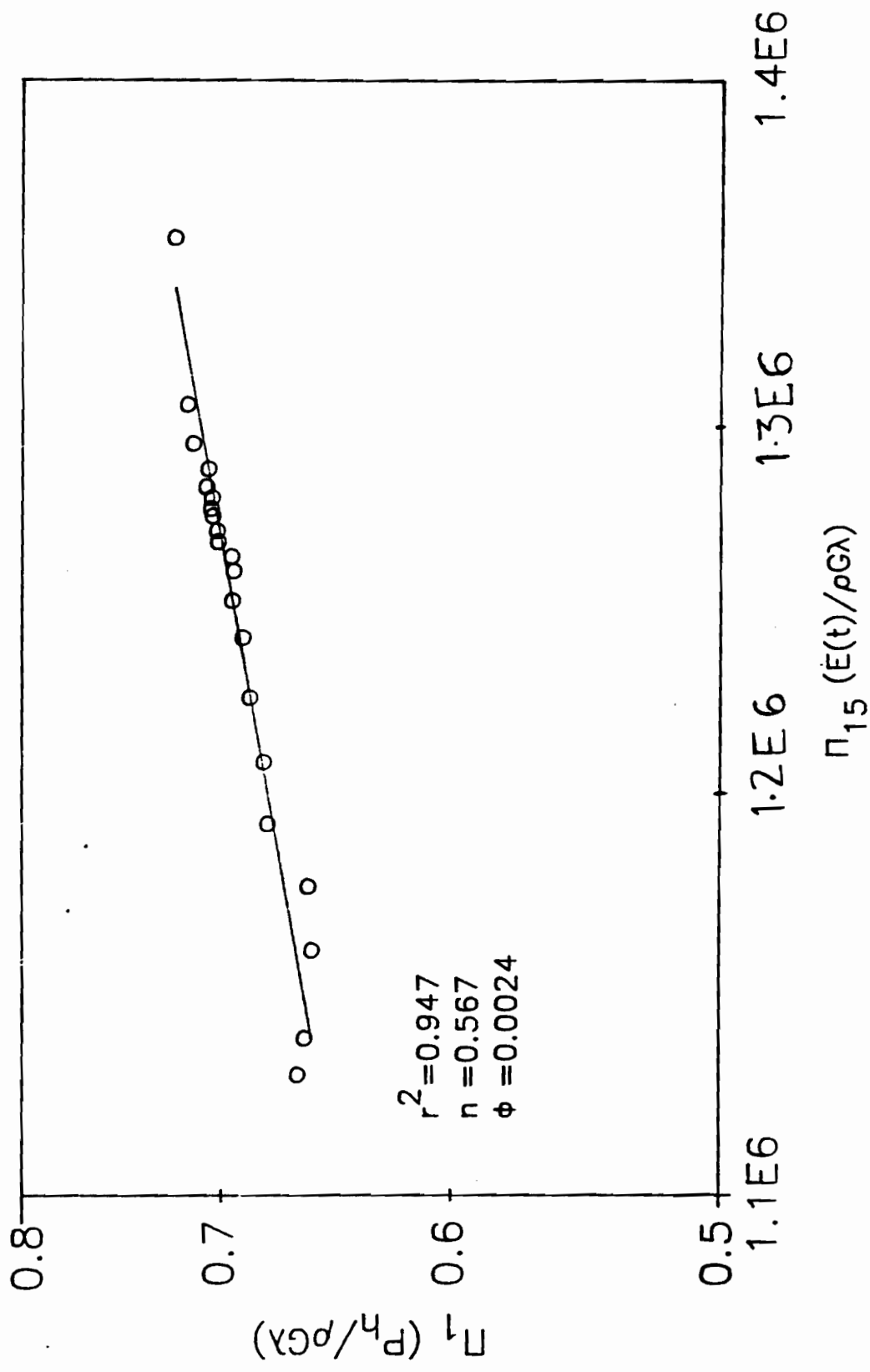
Figure 4.10.2. Log-log plot of Π_1 versus Π_{15} for model bin experiments
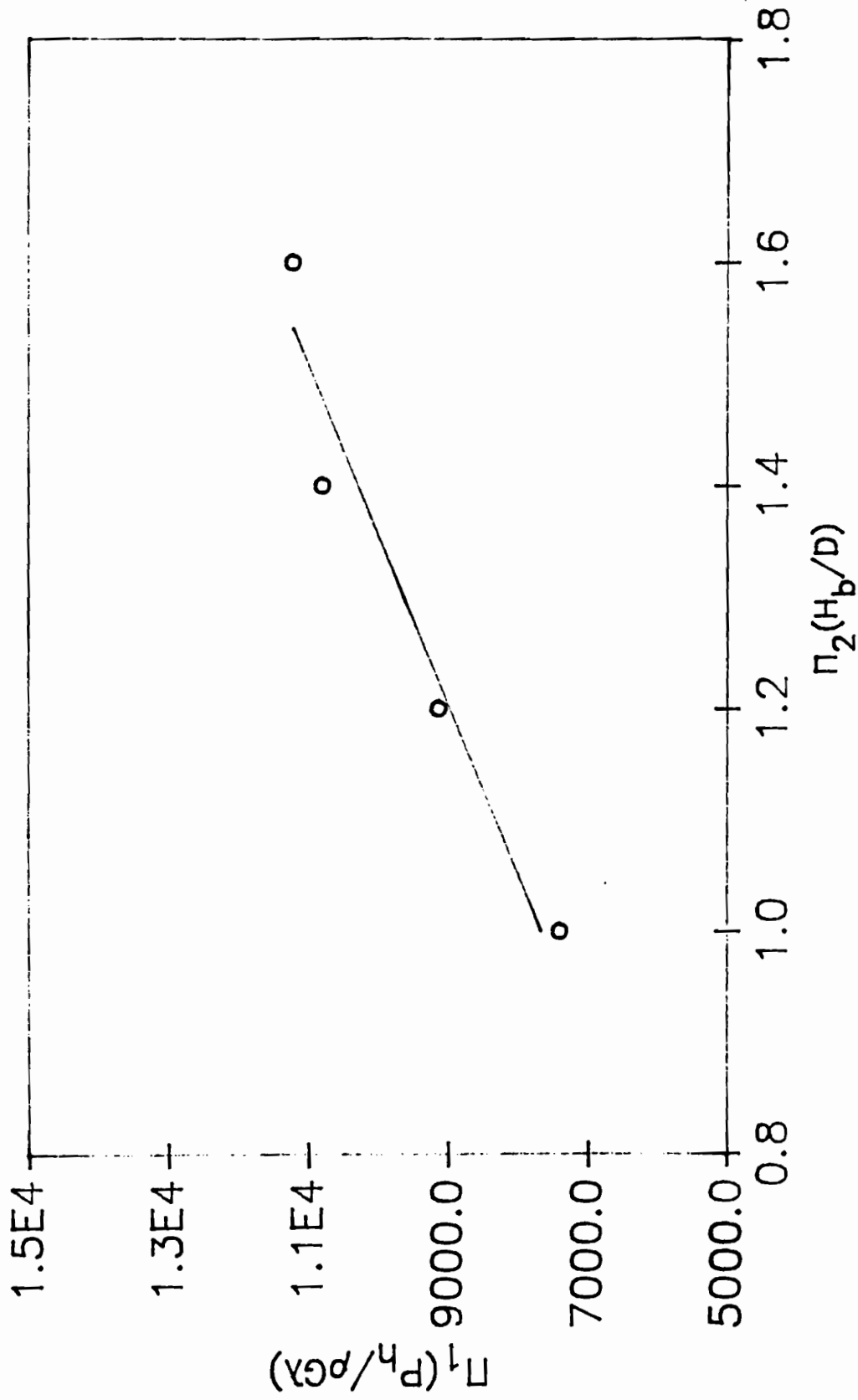
Figure 4.11.1. Linear plot of Π_1 versus Π_2
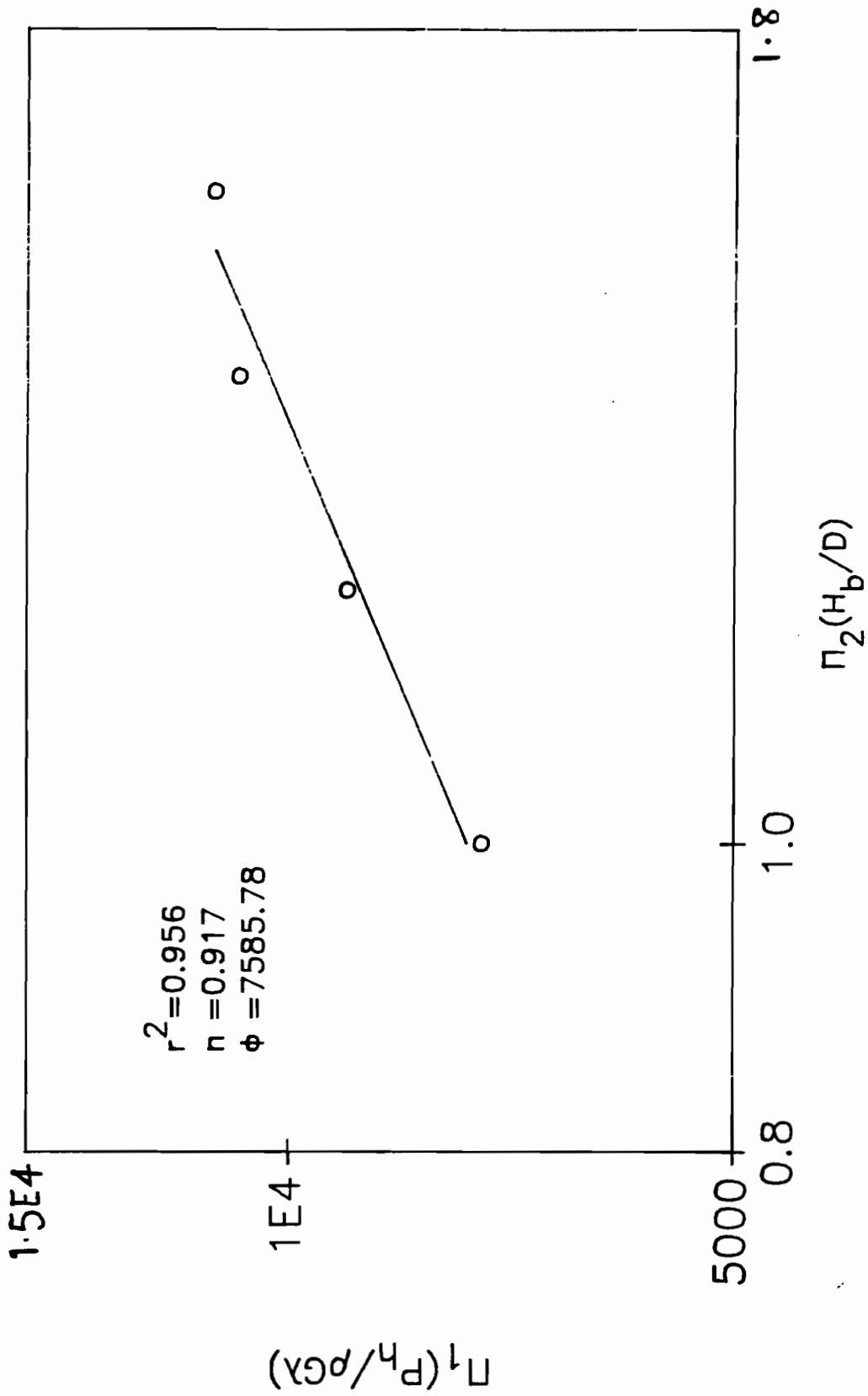
Figure 4.11.2. Log-log plot of Π_1 versus Π_2 for model bin experiments

The plot shows $\Pi_1 (P_h/\rho G A)$ on the vertical axis with values 5000, 1E4, 1.5E4, versus $\Pi_2 (H_b/D)$ on the horizontal axis with values 0.8, 1.0, 1.8.

$r^2 = 0.956$
$n = 0.917$
$\phi = 7585.78$

190
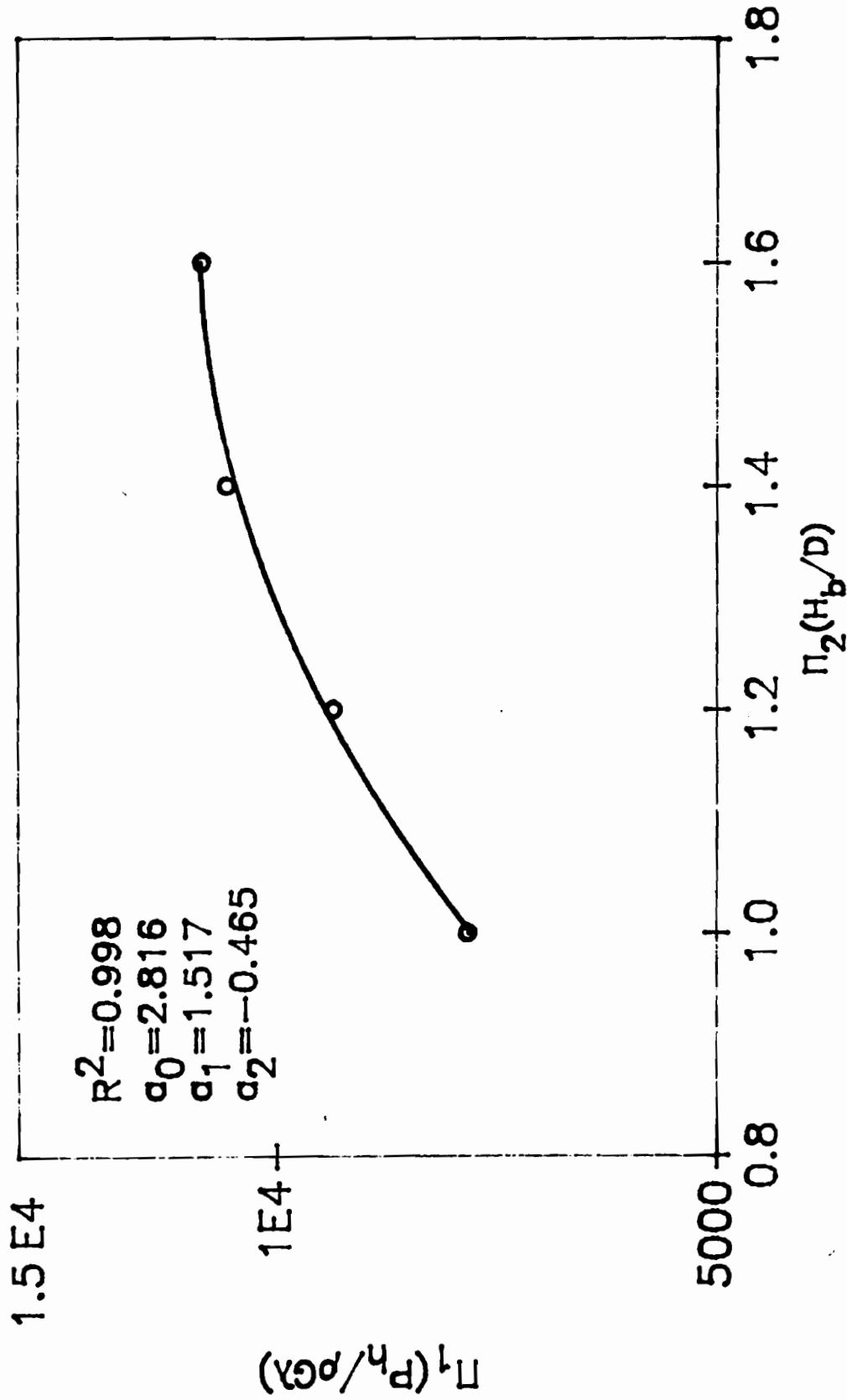
Figure 4.11.3. Semi-log plot of Π_1 versus Π_2

$R^2=0.998$
$a_0=2.816$
$a_1=1.517$
$a_2=-0.465$

$\Pi_2(H_b/D)$

$\Pi_1(P_h/\rho GA)$
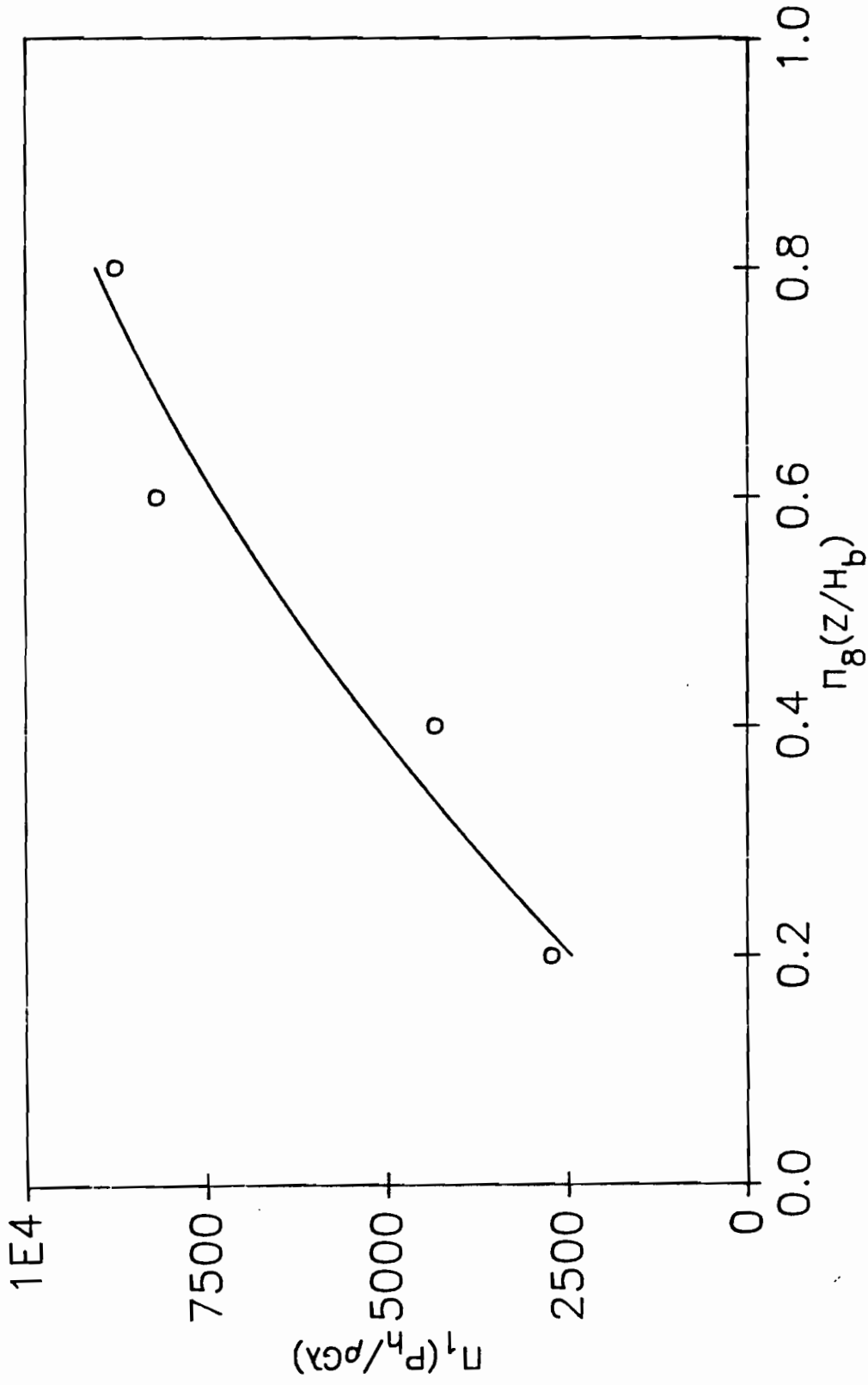
Figure 4.12.1. Linear plot of Π_1 versus Π_8 for model bin experiments
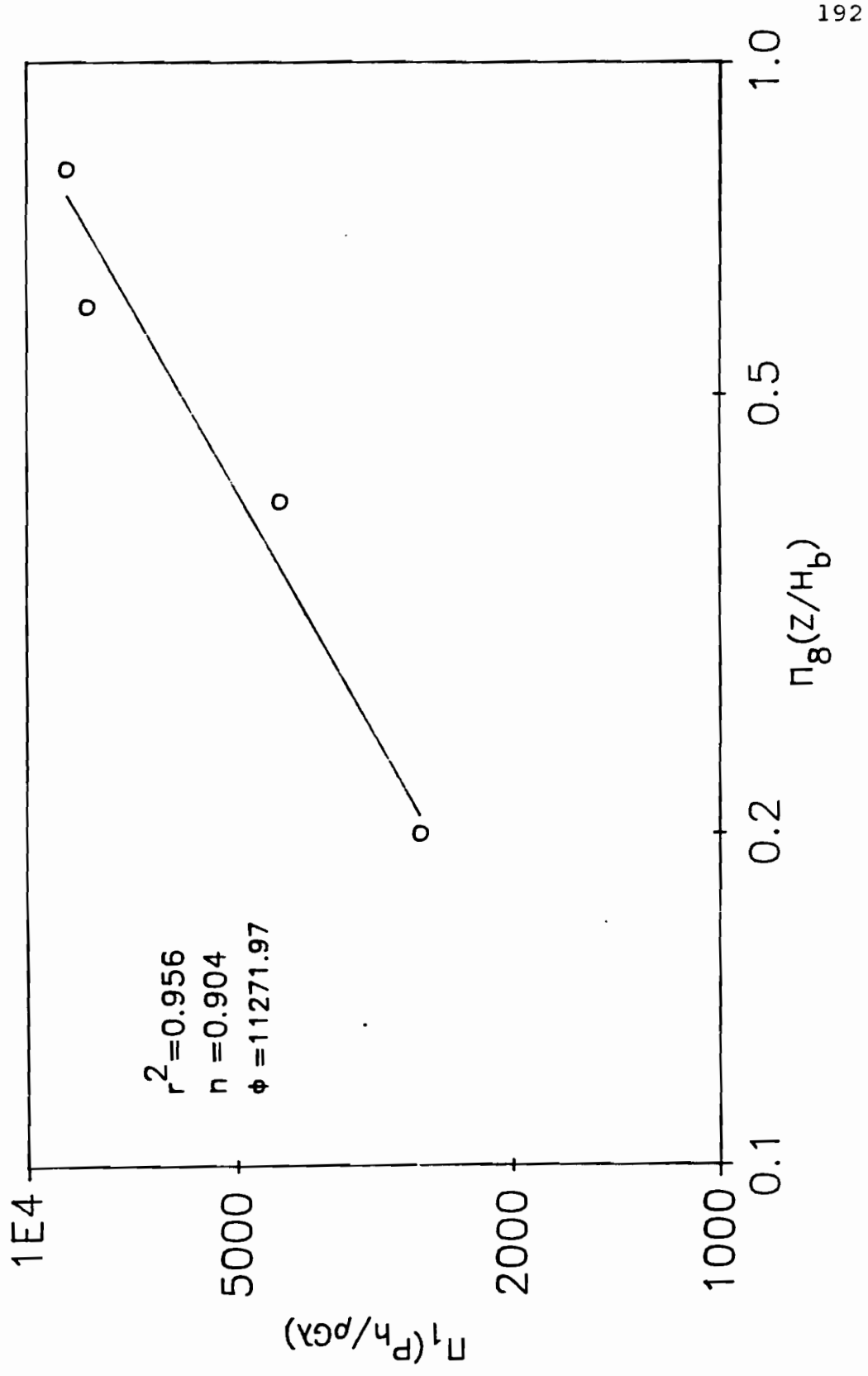
Figure 4.12.2. Log-log plot of Π_1 versus Π_8 for model bin experiments
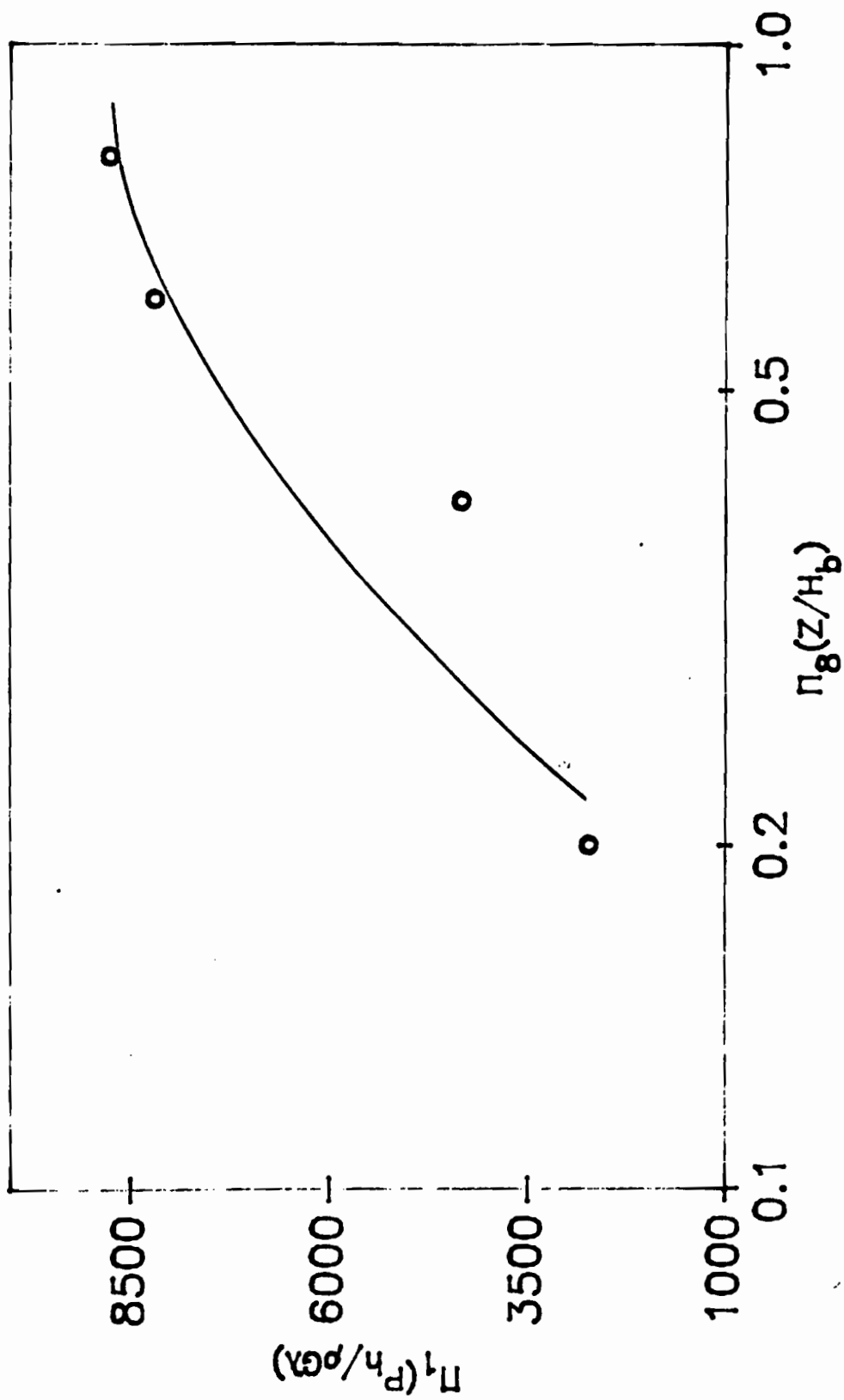
Figure 4.12.3. Semi-log plot of Π_1 versus Π_8
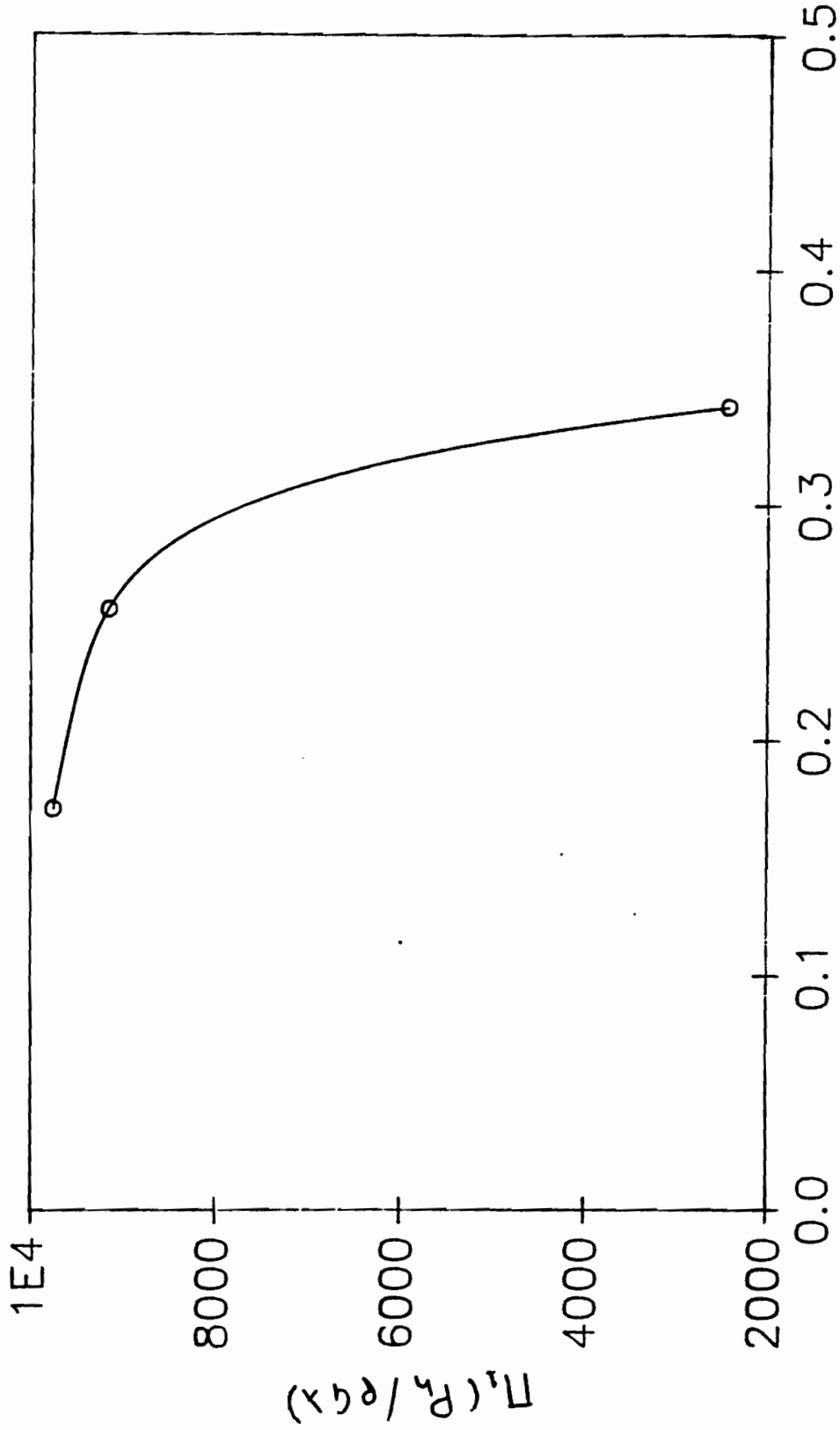
Figure 4.13.1. Linear plot of Π_1 versus Π_{13} for model bin experiments
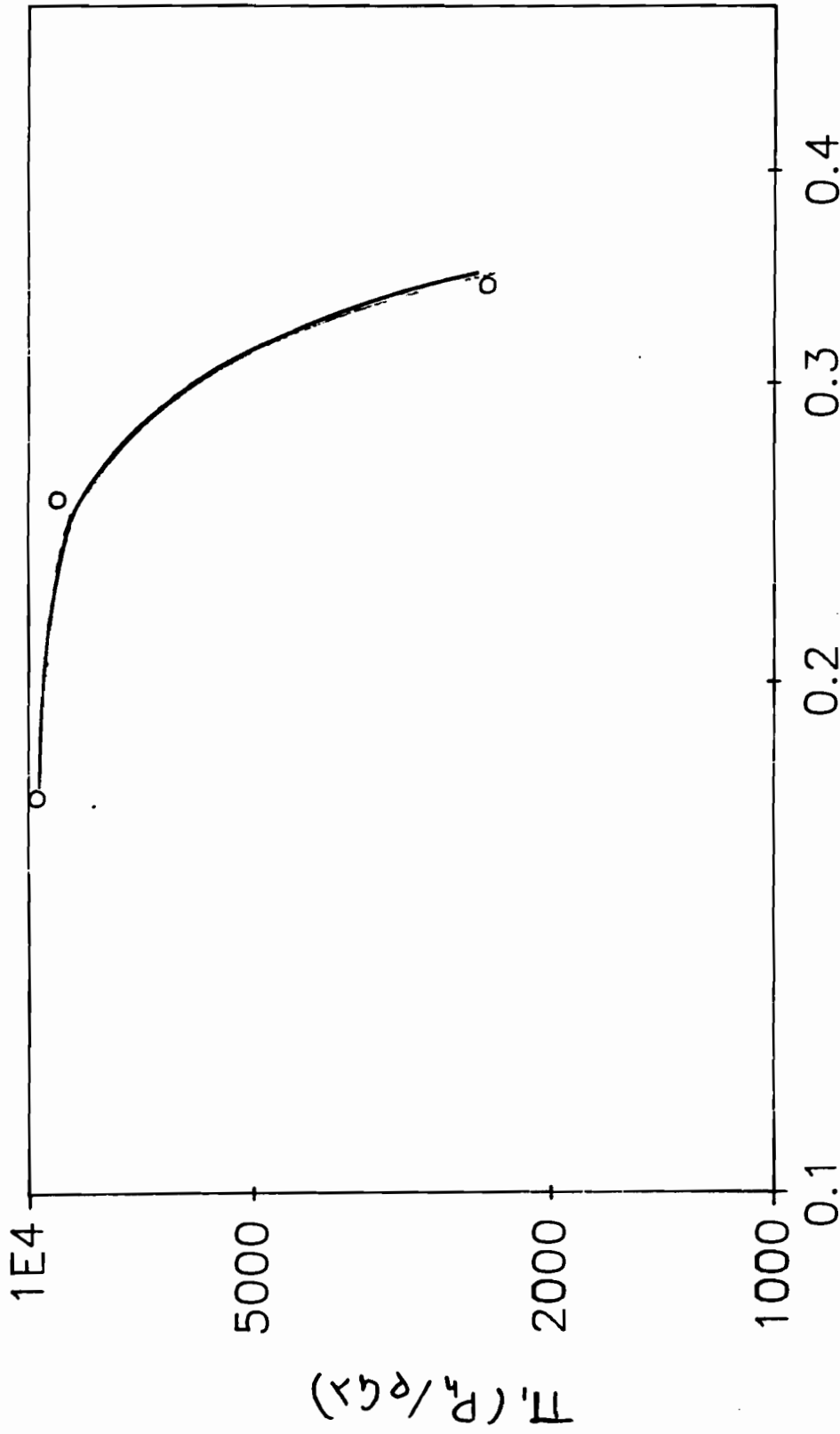
$$\Pi_{14}(\frac{D_h}{D}) = 0.522$$

Figure 4.13.1.2. Log-log plot of Π_1 versus Π_{13} for model bin experiments

$\Pi_{14}(\frac{D_h}{D}) = 0.522$

196
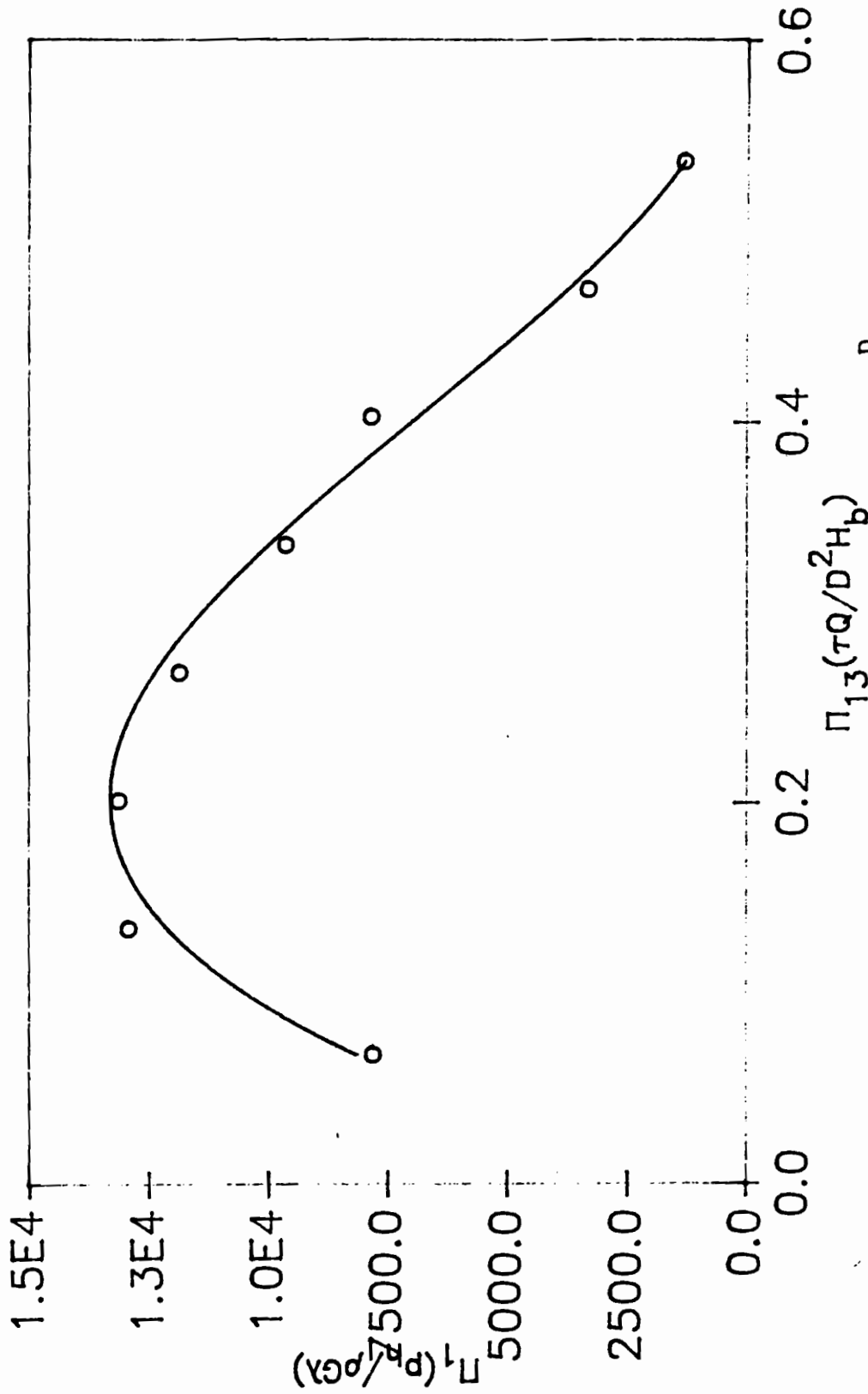
Figure 4.13.2.1. Linear plot of Π_1 versus Π_{13} for $\Pi_{14}(\frac{D_h}{D}) = 0.369$

The plot shows the vertical axis $\Pi_1 (P_R/\rho GA)$ with values 0.0, 2500.0, 5000.0, 7500.0, 1.0E4, 1.3E4, 1.5E4, and the horizontal axis $\Pi_{13}(\tau Q/D^2 H_b)$ with values 0.0, 0.2, 0.4, 0.6.
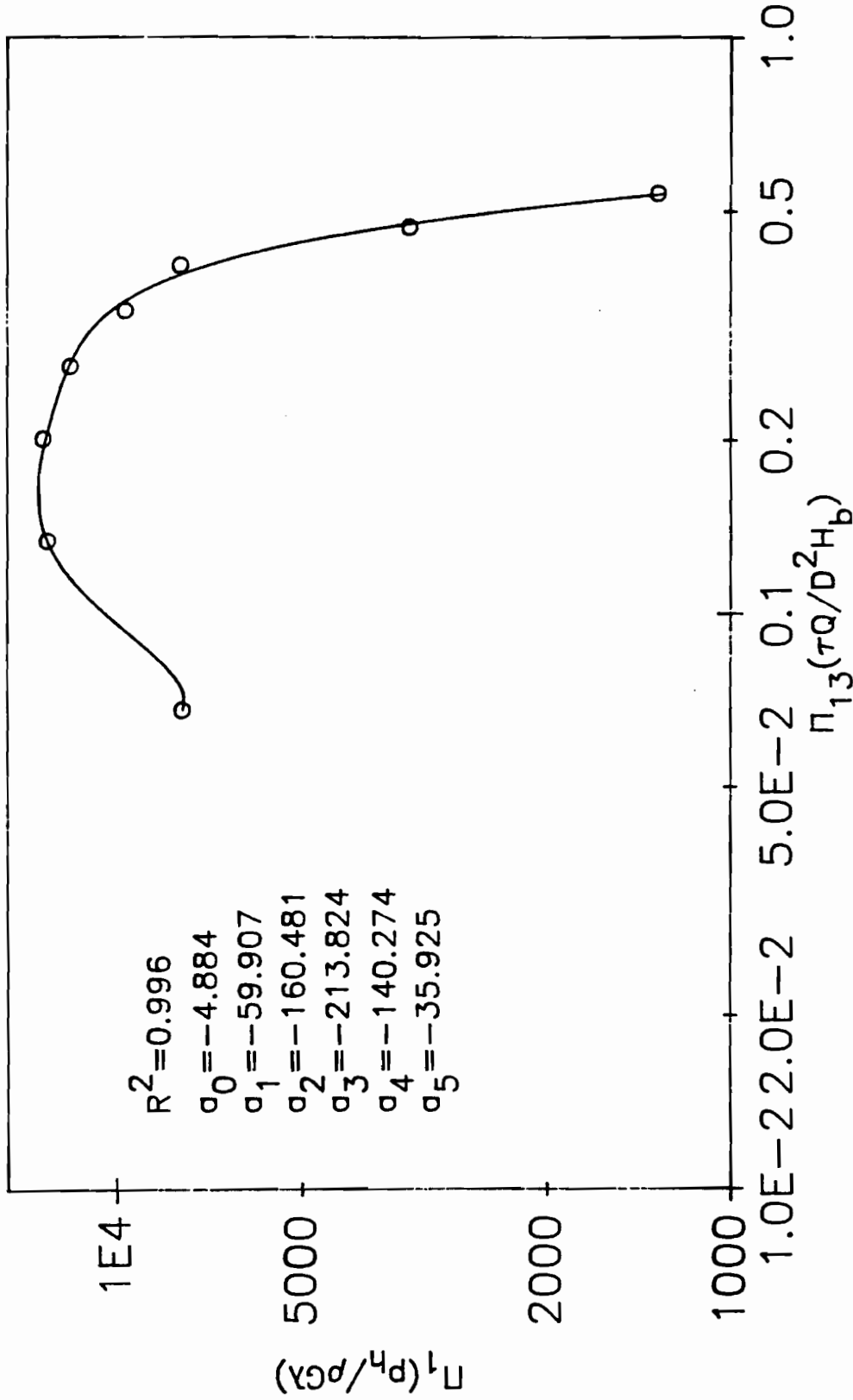
Figure 4.13.2.2. Log-log plot of Π_1 versus Π_{13} for model bin experiments
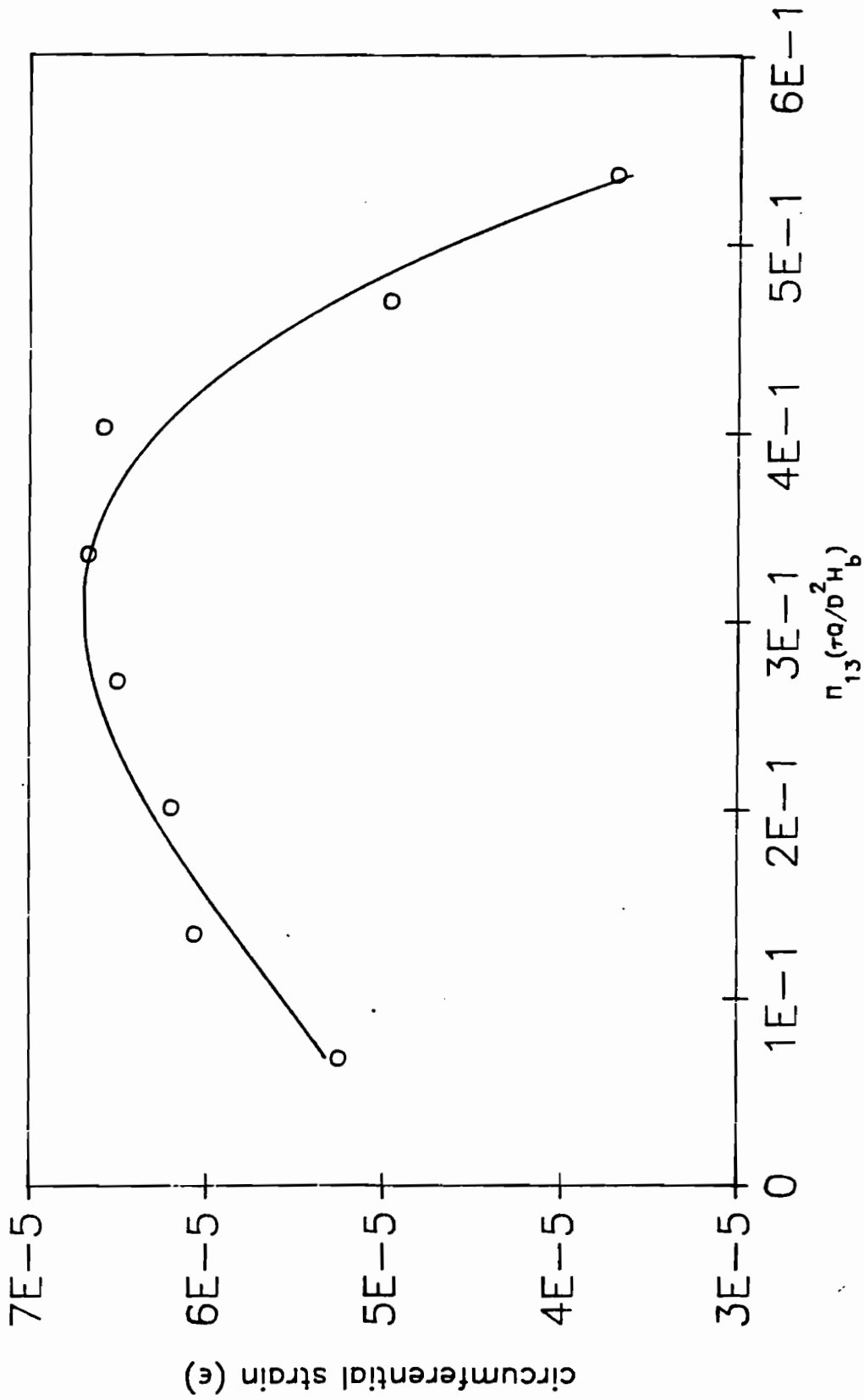
$\Pi_{14}(\frac{D_h}{D}) = 0.369$

Figure 4.13.3. Circumferential strain (ϵ) versus $\Pi_{13}(\tau Q/D^2 H_b)$ for

$$\Pi_{14}(\frac{D_h}{D}) = 0.522$$
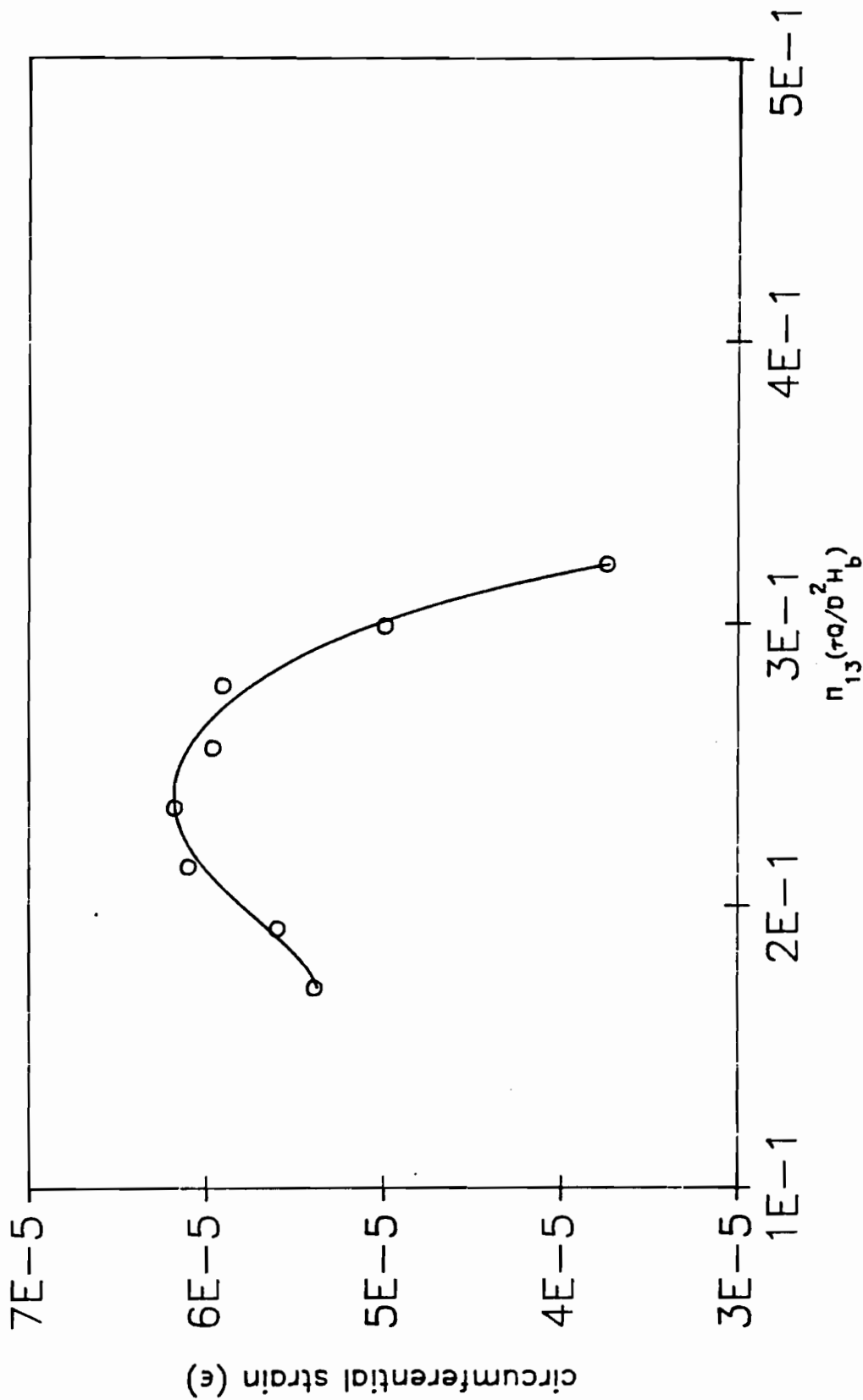
Figure 4.13.4. Circumferential strain (ϵ) versus $\Pi_{13}(\tau Q/D^2 H_b)$ for $\Pi_{14}(\frac{D_h}{D}) = 0.369$
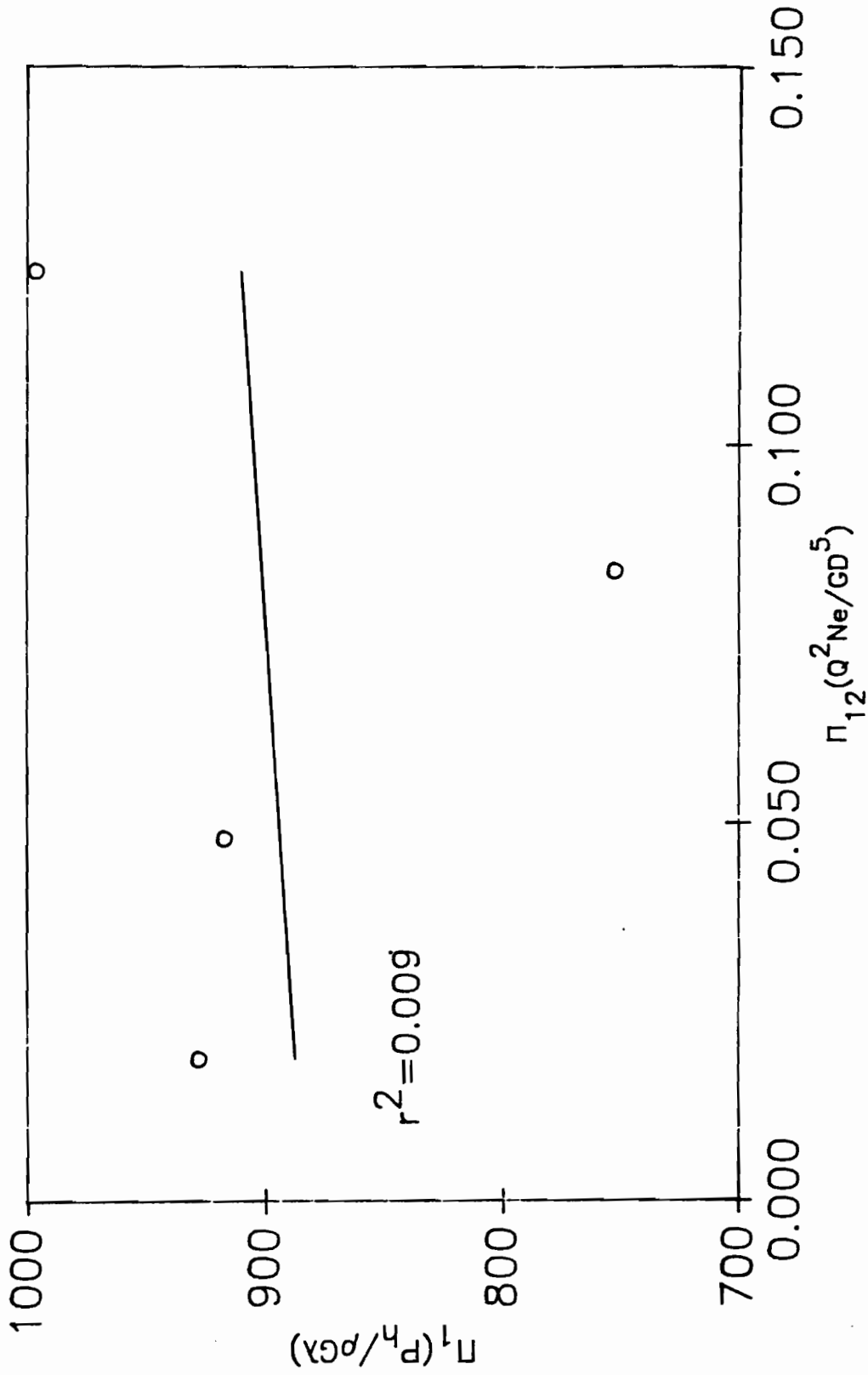
Figure 4.14. Linear plot of Π_1 versus Π_{12} for model bin experiments

5. DISCUSSION OF RESULTS

5.1 Discussion on the Validity of Janssen's Constant "k"

Figures 4.3 to 4.6 and A-4.3 to A-4.6 are graphical representations of Π_1 (k) versus Π_2 ($P_h/\rho G\lambda$). Tables 4.8.1 and 4.8.2 are the equations of Π_1 versus Π_2 for the log-log model and semi-log model respectively. From an examination of the figures for sand, wheat and soybeans the figures can be divided into two sections:

    (i)   a region of increase of Π_1 as Π_2 increases, and

    (ii)   A region in which the value of Π_1 approaches an

         asymptotic value as Π_2 increases.

The implication of the above two observations are that "k" increased with pressure and then subsequently approached a constant value as pressure increased further.

For corn, however, Π_1 decreased with pressure as Π_2 increases and then approached an asymptotic value as Π_2 was further increased.

In Section 4.2.1.10 it was discussed that there are four main schools of thought as to how "k" varies with grain depth in a silo, i.e., with increased pressure:

(i) "k" is constant with depth, Clower et al (1973), Moysey, and Brown (1979) (9).

(ii) "k" increases with depth, Ketchum and Williams (1919), Lenczner (1963), and Kramer (1944) (9).

(iii) "k" decreases with depth Pleissner (Ketchum, 1919) and Caughey et al. (1951) (9).

(iv) "k" varies but with no pattern Jaky (1948), Reimbert and Reimbert (1946).

All the first three trends described above were observed during the experiments. In fact the semi-log (exponential) model which describes phenomena that either increase or decrease approaching some final asymptotic values best described the curves fitted on the data as per Figure 4.3 to 4.6 and A-4.3 to A-4.6; the values of R^2's for the semi-log models were higher than for the log-log model by up to 10.5%. It therefore appears that the pressures involved in the experiments by the above researchers influenced the values of "k" they determined, and also the specific materials tested determined the way "k" varied with pressure.

It has been shown in this research that "k" is a dependent (derived) property of the material and load

system. It is not an independent property of the material as postulated by Janssen.

Manbeck and Nelson (35), using a 0.10 m (4 in.) cubical sample container filled with wheat and means for independently and simultaneously applying principal stress to the three pairs of opposite faces of the container, proved that one could arbitrarily fix any value of k desired. This therefore implies, also, that k is a derived property of the material and loading conditions but not an independent intrinsic property of the material.

The behavior of corn vis-a-vis the rest of the materials tested, i.e., decreasing k as pressure was increased, may be due to viscoelasticity.

The differences in viscoelastic behavior of various biological grains may be due to differences in: moisture content, oil content and internal cell structures. Even for a given species of grain, there may be differences because of differences in climatic conditions of the areas in which they were grown, and differences in cultural practices like irrigation, fertilization, harvesting time and seeding rate. For the purposes of the study, the viscoelastic properties of the materials were idealized as linear and the materials were also idealized as isotropic and homogeneous. However it is evident that biological grains may actually be non-linear viscoelastic, anisotropic and non-homogeneous. Therefore a thorough study and proper

material characterization, in terms of evaluation of all the viscoelastic parameters, elastoplastic parameters and so on, may shed more light on the subject.

5.2 The Effect of the Independent Π-terms on Horizontal Pressures for the Model Bin Experiments.

5.2.1 Effect of Π_3 (μ_w), Π_4 (ϕ), Π_5 (η_1), Π_6 (e_0), Π_7 (v_g), Π_{10} (e/D), Π_{16} (e/D_h) on Horizontal Pressures.

No component experiments were carried out to investigate the effects of the above independent Π-terms on the dependent Π-term Π_1 $(P_h/\rho G\lambda)$, i.e. their effect on horizontal wall pressures.

5.2.2 Effect of Π_{11} (λ/D) and Π_2 (H_b/D) on the dependent term, Π_1 $(P_h/\rho G\lambda)$

Singh (63) has discussed conditions for plug flow patterns as well as the boundaries of four different flows developed within granular material during emptying as proposed by McCabe (1974). McCabe concluded that Π_{11} (λ/D) and Π_2 (H_b/D) determine the type of flow pattern during emptying. Figure 5.1 shows representations of emptying pressure patterns according to McCabe. He concluded that

the particle size and height of material, and hence Π_{11}

(λ/D) and Π_2 (H_b/D), affect the crater formation level and hence the development of dynamic overpressures. Jenike (58) has discussed harmful flow irregularities such as arching, pulsation and shock. Pulsation results from repetitive formation and collapse of an obstruction to flow. The frequency of pulsation is directly proportional to rate of outflow, while the amplitude tends to be higher at low flow rates than at higher rates. According to Jenike pulsation can be reduced by having a low Π_2 (H_b/D), rough cylinder walls, convergent cylinder, silo construction containing a variety of convergent, divergent and rough ledges, and the use of a circumferential shelf.

He also concluded that fine material, i.e., low Π_{11} (λ/D), tend to inhibit pulsation.

This study revealed that increasing the value of Π_{11} (λ/D) results in a reduction of horizontal wall pressures (see Figures 4.9), i.e., Π_1 $(P_h/\rho G\lambda)$. The relationship is linear within the range of the study and can be mathematically represented by equation 4.15. The study also revealed that, within the experimental range, Π_1

varied linearly as Π_2 (H_b/D) (see Figures 4.11). The relationship of the terms is expressed mathematically in Equation 4.17, which shows that increasing Π_2 results in increased Π_1, i.e., horizontal pressures in silos.

The fact that Π_{11} (λ/D) affects static pressure, i.e.,

Π_1 (P_h/$\rho G\lambda$) is significant. Traditional methods of computing static pressures, like the Janssen and Reimbert methods, do not take into account the average particle size of the fill material. This obviously limits the accuracy of such traditional methods. As mentioned above, many authors, like Jenike and McCabe, only considered the effect of average particle size on dynamic conditions, i.e., during flow. This study has therefore revealed that design engineers must take into account the effect of the average prticle size of the fill material on silo pressures, for better accuracy in the estimation of design pressures in silos. Π_2 (H_b/D) has long been recognized as being important to the development of pressures in grain silos (17, 53, 58, 63). It is a factor which must be taken into account in silo design.

5.2.3 <u>Effect of Π_8 (Z/H_b) on the dependent term,</u>

<u>Π_1 ($P_h/\rho G\lambda$)</u>

Figure 4.12a is a linear plot of Π_8 (Z/H_b) versus Π_1

($P_h/\rho G\lambda$). An examination of the figures reveals that it

has the same general form as Figures 2.3 and 2.4 which are

representations of the variations of horizontal silo wall

pressures with grain depth, for the Janssen and Reimbert

equations respectively. Π_1 varied at decreasing rate

tending towards an asymptotic value as Π_8 increased, as

proposed theoretically by Janssen and semi-theoretically by

Reimbert and Reimbert. Equation 4.18 is a mathematical

relationship of Π_1 to Π_8.

As noted in Section 2, early silo designers, not

recognizing the importance of vertical friction between

stored material and the silo wall, assumed that lateral

pressures vary hydrostatically (58). Experiments by

Roberts (17) on models and full sized silos showed that

this was incorrect because some of the weight of the stored

material is transferred to the wall by friction. Janssen7

confirmed this conclusion and in 1895 published his theory

(17). Since some of the weight of the granular mass is

transfered to the silo wall by friction, the shape of the

curve of pressure versus depth is of the general form as
Figures 2.3 and 2.4 discussed above. This has been
experimentally verified by Reimbert and Reimbert (54).
The shape of the curves show increases of pressures with
depths tending towards some asymptotic values. The curve
of Π_1 versus Π_8 is essentially that of pressure variation
with depth and should follow the general shape as described
above; this trend is evident in Figure 4.12a.

5.2.4 Effect of Π_{15} (E(t)/ρGλ) on the dependent term,

Π_1 (P$_h$/ρGλ)

Figure 4.10a is a linear plot of Π_1 (P$_h$/ρGλ) versus

Π_{15} (E(t)/ρGλ). The curve increases at an almost constant
rate and then tends towards an asymptotic value. The
material used (sand) was idealized as being linearly
viscoelastic and its relaxation modulus, E(t), evaluated
(see Table 4.5.1). This study revealed that Π_{15}, the ratio
of viscoelastic forces to gravity forces, is pertinent to
the development of pressures in grain silos. The
relaxation modulus (E(t)) decreases with time to an
asymptotic value (see Figure 4.7.1). It is therefore
logical that the wall pressures become asymptotic if

viscoelastic forces are pertinent to the development of such pressures. This study has revealed that viscoelastic forces are pertinent to the development of wall pressure as evidenced in Figures 4.10. Equation 4.16 is a mathematical expression of the relationship between Π_1 and Π_{15}.

The fact that the study revealed that viscoelasticity is important to the development of pressures in silos is important. As noted in Section 3, Manbeck and Nelson (34, 35) Schott and Britton (60), Mohsenin (38) and Herum (20) are among the researchers who characterize various grains as being viscoelastic. Zhang et al (79, 80) have characterized wheat as being elastoplastic. Bishara (8) characterizes grains as being non-time dependent in behavior. The implications of the findings of this study, that viscoelasticity is important to the development of grain pressures in silos, is that ignoring viscoelasticity in design equations for predicting pressures in silos lead to errors in such prediction. All equations currently recommended by silo design codes from various countries, like ACI Standard 313-77 (1) and the Soviet Code CH-302-65 (58), do not account for viscoelasticity of the grain. The equations are therefore limited in this respect, and new design equations reflecting viscoelastic effects should be developed.

5.2.5 Effect of Π_{12} (Q^2Ne/GD^5) and Π_{13} $(\tau O/D^2H_h)$ on the

dependent term Π_1 $(P_h/\rho G\lambda)$

Figure 4.14 is a plot of Π_1 $(P_h/\rho G\lambda)$ versus Π_{12}

(Q^2Ne/GD^5). The r^2 value of the fitted cuve is 0.009 reveal-

ing that Π_{12} (Q^2Ne/GD^5) has no effect on Π_1 $(P_h/\rho G\lambda)$ within

the range of the study. The implication of this is that

inertial effects have no effect on the development of

horizontal wall pressures in cylindrical silos, a finding

also reported by Singh (63).

Figure 4.13.1a is a plot of Π_1 versus Π_{13} for Π_{14}

(D_h/D) = 0.522. The values of Π_1 obtained show a decrease

as Π_{13} increases. Only three readings could be obtained as

the load cells could not take instantaneous readings and

therefore "lagged" behind the events, the circumferential

strains measured (Figures 4.13.3) however showed some

slight increase with increasing Π_{13}. It is therefore

difficult to conclusively say whether there was an increase

or not. Figure (4.13.2a) is a plot of Π_1 versus Π_{13} for

Π_{14} (D_h/D) = 0.369. The plot shows a definite pattern of

increase of Π_1 with Π_{13}, i.e., the phenomenon of dynamic
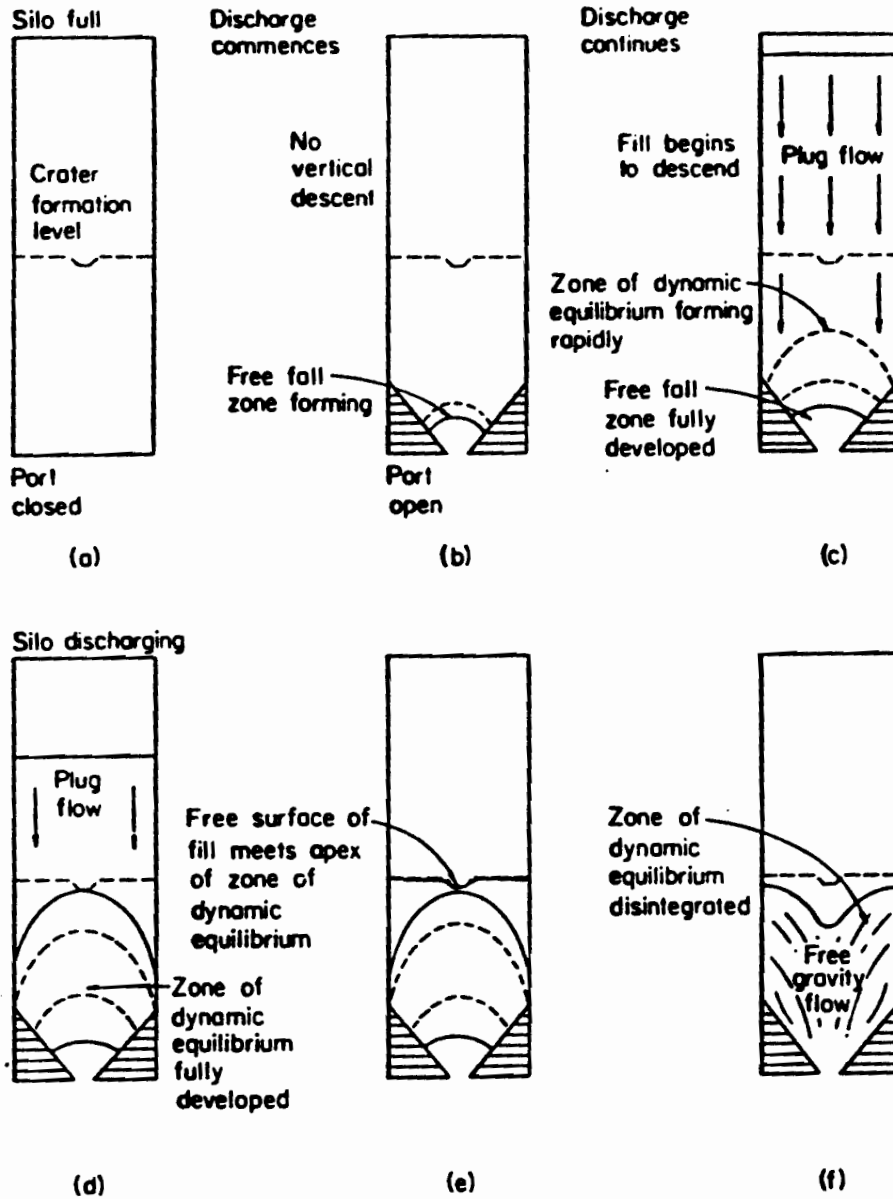
Figure 5.1. McCabe's patterns of emptying (Safarian and Harris, 1985)

overpressures. The maximum dynamic pressure increase was by a factor of 1.7 above static. It was not possible to observe the type of flow taking place as the model bin was made of steel. However, it seemed apparent from the emptying times and rates that there was mass flow rather than funnel flow. It seems reasonable to accept McCabe's explanation, described by Safarian and Harris (58), as to the development of overpressure in bins (see Figure 5.1).

It is interesting and significant that inertial effects are not pertinent to the development of pressures in silos. It would appear to the casual observer that since, during emptying of bins, a large mass of grain is accelerated, i.e., from rest or initial condition to flow and during change in flow velocity as at the silo-hopper interface and at the hopper opening, inertial effect would be pertinent to the development of silo pressures especially dynamic overpressures. However as revealed by this and other studies (Singh (65)), inertial effects are not pertinent to the development of such pressures. McCabe's explanation as to the development of dynamic overpressure as presented by Safarian and Harris (58) seems to adequately describe the development of dynamic overpressures. McCabe made the following observations and conclusions:

(1) Plug flow occurs at all levels above the "mitre of revolution" the apex of which coincides with crater formation level (Figure 5.1d). Materials in the plug flow

zone descend vertically at constant velocity. The crater
formation level and velocity of material depend on silo
diameter, port opening size, and maximum particle size.

(2) Dynamic Equilibrium. This zone is confined to that
of a mitre of revolution that forms above the central port
opening, where the material is in a steady state of
deformation and strain. Indications are that plastic flow
occurs in this zone. Boundaries were determined from
changes in rate of descent of the stored material. The
underside of the mitre of revolution occurred at a height
above the bottom approximately equal to the silo diameter.
The apex occurred at the crater level.

(3) Dead Space is confined to a zone of inert material
that forms a natural hopper approach to the port opening.
It was noted that the upper portion of the hopper surface
was conveniently located to form the springing to the
active zone, referred to above as the mitre of revolution.

(4) Free fall: The zone beneath the soffit of the
mitre of revolution is of open texture with various
particles accelerating freely. This zone is the first to
form, taking the shape of a parachute whose maximum size
remains fixed for any given grading on silo diameter. It
was found that particle acceleration closely approximated
that of gravity. According to McCabe, during plug flow
emptying constant formation and breaking down of arches
causes increased dynamic strain in the bin wall at the arch

formation level (see Figure 5.1). He also concluded that the rate of discharge (Q) for a uniformly graded material, is independent of depth of material and wall surface finish.

Π_{13} ($\tau Q/D^2 H_b$) contains τ, the elapsed time of discharge. It is interesting to note that this term has been constantly ignored by researchers in this area except Singh (63). This study has revealed that time is a pertinent quantity to the development of pressures in silos, a fact which would appear to be obvious, as emptying is a time dependent activity one would have expected researchers to account for time in proposed pressure prediction equations, however, this has not been the case.

CONCLUSIONS

An experimental investigation was conducted to
determine the effects of pertinent independent physical
quantities on horizontal pressures in cylindrical grain
silos. Dry sand was used as a fill material in model silos
mounted with load cells to investigate the effect of perti-
nent independent physical quantities on the development of
horizontal pressures in silos. Another such investigation
was carried out to investigate whether Jannsen's constant k
is a valid independent physical. Four materials, sand,
corn, wheat and soybeans, were used in investigating the
validity of k.   A small cylindrical specimen cell mounted
with strain gages and an Instron testing machine were used
for investigating the validity of k. The principles of
similitude were utilized in organizing and conducting the
experiments, analyses of the data and the development of
the prediction equations. The following conclusions were
drawn from the investigations:

(1) Janssen's "constant" k is a derived dependent
    physical quantity of ensiled granular materials
    en-masse and is therefore not an independent

215

pertinent physical quantity of granular materials en-masse.

(2) Π_{11} (λ/D) is significant to the development of horizontal pressures in ensiled granular materials, i.e., significant to Π_1 ($P_h/\rho G\lambda$). This implies that the particle size (average) of the material influences grain loads. Π_{11} has a linear inverse relationship to Π_1 within the range of the study.

(3) Π_2 (H_b/D) is significant to the development of pressures (Π_1 ($P_v/\rho G\lambda$) in ensiled granular materials en-masse. An increase in Π_2 results in an increase in Π_1.

(4) Π_{15} ($E(t)/\rho G\lambda$) is significant to the development of horizontal pressures ($P_r/\rho G\lambda$) in ensiled materials. There is a positive exponential relationship between Π_{15} and Π_1. This implies that viscoelastic properties of ensiled granular materials en-masse are significant to the development of horizontal loads in silos.

(5) Π_8 (Z/H_b) is significant to the development of

pressures $(P_h/\rho G\lambda)$ in grain silos. Horizontal

pressures increase steadily with depth to an

asymptotic (maximum) value.

(6) Π_{12} $(Q^2 Ne/GD^5)$, the ratio of intertial to gravity

forces (Fronde number), is not significant to the

development of horizontal pressures in grain

silos. This implies that inertial effects are

insignificant to the development of such

pressures.

(7) Π_{13} $(\tau Q/D^2 H_b)$ was found to be significant to the

development of dynamic overpressures in silos.

Flowrate of material Q was found to be

signficant to such pressures as varying Π_{14}

(D_h/D), i.e., diameter of hopper influenced the

development of pressures, since flowrate is

proportional to the hopper opening diameter.

RECOMMENDATIONS FOR FURTHER WORK

As illuminating as this and many other experimental, analytical and numerical studies may be, it is hard to deny that the subject of grain-silo loads is still inadequately explored. There, therefore, remains a need for further experimental studies based on similitude concepts, on the subject. The experimental data obtained should be reduced to dimensionless numbers. Specifically, experiments should be designed to:

(1) Study the influence of Π_3 (μ_w), Π_4 (ϕ), Π_5 (η_1),

Π_6 (e_0), Π_7 (v_g), Π_{10} (e/D), and Π_{16} (e/D$_h$) so that a general prediction equation useful to designers may be obtained.

(2) Rigorously characterize granular material behavior so that component experiments may be designed to correlate loads to elastic, viscoelastic and plastic behavior of materials as may be necessary.

(3) Load cells with faster response times should be used for emptying experiments so as to give a more complete picture of the system behavior.

REFERENCES

1. American Concrete Institute (1977), ACI Standard
    313-77, "Recommended Practice for Design and
    Construction of Concrete Bins."

2. Airy, W. (1897), "The Pressure of Grain," Minutes of
    the Proceedings of the Institution of Civil Engineers,
    131, 347-358.

3. Balastreire, L.A. (1977), "Relaxation Modulus for Corn
    Endosperm in Bending," Transactions of ASAE, Vol. 21,
    No. 4, 767-772.

4. Balastreire, L.A., et al. (1982), "Fracture of Corn in
    Bending Part II: Fracture Analysis by Fractography and
    Optical Microscopy," Transactions of ASAE, Vol. 25, No.
    4, 1062-1065.

5. Balastreire, L.A., et al. (1982), "Fracture of Corn
    Endosperm in Bending Part I: Fracture Parameters,"
    Transactions of ASAE, Vol. 25, No. 4, 1057-1061.

6. Bishara, A.G., et al. (1983), "Static Pressures in
    Concrete Silos Storing Granular Material," ACI Journal,
    May-June 1983.

7. Bishara, A.G. (1985), "Interaction of Bin and Bulk
    Solids," Civil Engineering Department, Ohio State
    University, Columbus, Ohio, Unpublished Manuscript.

8. Briassou, D., and Curtis, J. (1985), "Design and
    Analysis of Silos for Friction Forces," Journal of
    Structural Engineering, Vol. III, No. 6, June 1985,
    1377-1398.

9. Briassou, D., and Curtis, J.O. (1985), "Effect of End
    Restraint and Forces on the State of Stress in Circular
    Silos," Transactions of ASAE, Vol. 28, No. 1, 1985,
    222-231.

219

10. Britton, M.G., and Versavel, P.A. (1985), "Bin Wall Configuration--Bulk Wheat Interaction," ASAE Paper No. 85-4001, American Society of Agricultural Engineers, St. Joseph, Michigan.

11. Britton, M.G., and Hawthorne, C.R.J. (1984), "Dynamic Behavior of Wheat in a Lamellar Bin," ASAE Paper No. 84-501, American Society of Agricultural Engineers, St. Joseph, Michigan.

12. Buyanov, A.I., and Voronyuk, B.A. (1985), "Physical Properties of Plants, Fertilizers and Soils," Kotos Publisher, Moscow, U.S.S.R.

13. Coon, M.D., and Evans, R.J. (1971), "Recoverable Deformation of Cohesionless Soils," Journal of the Soil Mechanics and Foundations Division, SM2, ASCE Journal, February, 375-391.

14. Dickson, R.R., and Jofriet, J.C. (1984), "Wall Pressures in Bottom-Unloading Farm Silos," ACI Journal, Vol. 81, No. 1, January-February.

15. Fahmi, Z.F. (1980), "Experimental Study of Dynamic Loads on Cylindrical Silos," M.S. Thesis, Ohio State University, Columbus, Ohio.

16. Findley, W.N., et al. (1976), "Creep and Relaxation of Non-Linear Viscoelastic Materials," Van Nostrand Publishers, Amsterdam, Netherlands.

17. Gaylord, E.H., and Gaylord, C.N. (1984), "Design of Steel Bins for Storage of Bulk Solids," Prentice-Hall, Inc., New Jersey.

18. Gumbe, L. (1983), "Appropriate Technology and Prospects in Grain Storage," Kenya Institute of Food Science and Technology Journal, Vol. 1, No. 3.

19. Hartlén, J., et al. (1984), "The Wall Pressure in Large Grain Silos: Inventory, Pressure Measurement, Material Investigation," Swedish Council for Farm Building Research, Lund, Sweden.

20. Herum, F.L., et al. (1979), "Viscoelastic Behavior of Soybeans Due to Temperature and Moisture Content," Transactions of ASAE, Vol. 22, No. 5, 1220-1224.

21. Jenike, A.W., and Johanson, J.R. (1969), "On the Theory of Bin Loads," Transactions of ASME, Vol. 91, Series B, No. 2, 339-344.

22. Jenike, et al. (1973), "Bin Loads Part 2: Concepts; Part 3: Mass Flow Bins; Part 4: Funnel-Flow Bins," Transactions of ASME, Vol. 95, Series B, No. 1, 1-16.

23. Jenike, A.W. (1954), "Flow of Bulk Solids," Bulletin 64, Utah Engineering Station, University of Utah.

24. Jenike, A.W. (1962), "Gravity Flow of Solids," Transactions of Institution of Chemical Engineers, Vol. 40, No. 5, 264-271.

25. Jenkins, J., and Satake, M. (1983), "Mechanics of Granular Materials: New Models and Constitutive Relaxation," Elsevier Science Pub. Co.

26. Jofriet, J.C., et al. (1977), "Friction Model for Finite Element Analyses of Silos," Transactions of ASAE, 1977, American Society of Agricultural Engineers, St. Joseph, Michigan.

27. Lawton, P.J. (1980), "Coefficients of Friction Between Cereal Grains and Various Silo Wall Materials," Journal of Agricultural Engineering Research, 25, 75-86.

28. Kondre, R.L. (1963), "Hyperbolic Stress-Strain Response: Cohesive Soils," Journal of the Soil Mechanics and Foundations Division, ASCE, Vol. 89, No. SM1, 115-143.

29. Lade, P.V., and Duncan, J.M. (1975), "Elasto-Plastic Stress-Strain Theory for Cohesionless Soils," Journal of Geotechnical Enginering Division, ASCE, 1037-1053.

30. Lade, P.V. (1977), "Elasto-Plastic Stress-Strain Theory for Cohesionless Soil with Curved Yield Surface," International Journal of Solids and Structures, Vol. 13, 1019-1035.

31. Loewer, O.J., et al. (1977), "Properties of Ground Corn as Related to Forces in Bulk Storage Structures," Transactions of ASAE, 155-156.

32. Mahmoud, M.H. (1972), "Bottom Unloading Farm Silos--Structural Design Considerations," Silo-- Structure, Pressure and Design, National Silo Association, 60th Convention, Minneapolis, Minnesota, 1972, ISA, 62-80.

33. Manbeck, H.B., and Puri, V.M. (1985), "Predicting Thermally Induced Loads in Thin-Walled Grain Bins: State-of-the-Art," International Journal of Bulk Storage in Silos, I (3), 9-13.

34. Manbeck, H.B., and Nelson, G.L. (1972), "Methods and Instrumentation for Evaluating the Stres-Strain Behavior of Wheat En Masse," Transactions of ASAE, 919-922, American Society of Agricultural Engineers, St. Joseph, Michigan.

35. Manbeck, H.B., and Nelson, G.L. (1975), "Three Dimensional Constitutive Equations for Wheat En Masse," Transactions of ASAE, Vol. 18, No. 6, 1122-1127.

36. Manbeck, H.B., et al. (1977), "Dynamic Overpressures in Model Bins During Emptying," ASAE Paper No. 77-4505, American Society of Agricultural Engineers, St. Joseph, Michigan.

37. Mendelson, A. (1968), "Plasticity Theory and Applications," The Macmillan Co., New York.

38. Mensah, J.K., et al. (1981), "Effect of Drying Conditions on Impact Shear Resistance of Selected Corn Varieties," Transactions of ASAE, Vol. 24, No. 6, 1568-1572, American Society of Agricultural Engineers, St. Joseph, Michigan.

39. Mohsenin, N.N. (1968), "Physical Properties of Plant and Animal Materials," Gordon and Breach Science Publishers, New York.

40. Moysey, E.B. (1984), "The Effect of Grain Spreaders on Grain Friction and Bin Wall Pressures," Journal of Agricultural Engineering Research, Vol. 30, No. 2, 149-156, London, England.

41. Moysey, E.B., and Landine, P.G. (1981), "Pressures on Grain Bin Walls During Filling and Emptying," ASAE Paper No. 84-4001, American Society of Agricultural Engineers, St. Joseph, Michigan.

42. Moysey, E.B., and Brown, T. (1979), "Factors Affecting Internal Friction of Grain," ASAE Paper No. 79-303, American Society of Agricultural Engineers, St. Joseph, Michigan.

43. Murphy, G. (1950), "Similitude in Engineering," The Ronald Press Co., New York.

44. Muzzelo, L.M., and Manbeck, H.B. (1984), "Measurement of the Thermally Induced Pressures in Model Bin," ASAE Paper No. 84-8400, American Society of Agricultural Engineers, St. Joseph, Michigan.

45. Mróz, Z., et al. (1979), "Application of Anisotropic Hardening Model in the Analysis of Elastoplastic Deformation of Soils," Geotechnique, No. 1, 1-34.

46. Mróz, Z., et al. (1981), "An Anisotropic Critical State Model," Geotechnique, No. 4, 451-469.

47. Mróz, Z. (1973), "Mathematical Models of Inelastic Material Behavior," University of Waterloo, Canada.

48. Negi, S.C., and Jofriet, J.C. (1985), "Structural Loads for Farm Tower Silos," Paper presented at ASAE Summer Meeting, June 23-26, 1985, East Lansing, Michigan.

49. Prévost, J.H., and Höeg, K. (1975), "Effective Stress-Strain Models for Soils," Journal of Geotechnical Engineering Division, Proceedings of ASCE, Vol. 101, No. GT3, 259-278.

50. Puri, V.M., Manbeck, H.B., and Zhang, Q. (1986), "Predictions of Thermally Induced Stresses in Thin Walled Grain Storage Bins Under Declining Ambient Temperatures," Proceedings of the 9th Conference of Electronic Computation, Committee on Elec. Comp. ST Div./ASCE/Birmingham, AL, Feb 23-26.

51. Puri, V.M., Zhang, Q., and Manbeck, H.B. (1986), "Influence of Granular Material Properties on Thermally Induced Bin Loads," Proceedings of the Powder and Bulk Solids Conference/Exhibition, May 13-15, Rosemont, Illinois.

52. Quadri, M.S. (1986), "Experimental Evaluation of Pressures in Cylindrical Hopper Silos Storing Cohesionless Bulk Solids," M.S. Thesis, Ohio State University, Columbus, Ohio.

53. Reimbert, M., and Reimbert, A. (1980), "Pressures and Overpressures in Vertical and Horizontal Silos," Proceedings of the International Conference on Design of Silos for Strength and Flow, September 1-10.

54. Reimbert, M., and Reimbert, A. (1976), "Silos: Theory and Practice," Trans Tech Publications, 5-A, CH-4711, Aedermannsdorf, Sweden.

55. Roscoe, K.H., et al. (1980), "Model Studies of Grain Bin Failure," American Society of Agricultural Engineers (ASAE) Paper No. 80-4504, St. Joseph, Michigan.

56. Ross, I.J., et al (1980), "Model Studies of Grain Bin Failure," American Society of Agricultural Engineers (ASAE) Paper No. 80-4505, St. Joseph, Michigan.

57. Rumsey, T.R., and Fridely, R.B. (1977), "A Method for Determining the Shear Relaxation Function of Agricultural Materials," Transactions of ASAE, 1977, 386-392.

58. Safarian, S.S., and Harris, E.C. (1985), "Design and Construction of Silos and Bunkers," Van Nostrand Reinhold Company, New York.

59. Schott, R.W., and Britton, M.G. (1985), "Plane Strain of Wheat with Various Moisture Contents," ASAE Paper No. NCR 85-505, American Society of Agricultural Engineers, St. Joseph, Michigan.

60. Schott, R.W., and Britton, M.G. (1984), "Plane Strain Behavior of Bulk Grain," ASAE Paper No. 84-503, American Society of Agricultural Engineers, St. Joseph, Michigan.

61. Schwedes, J. (1984), "Influence of Wall Friction on the Design of Silos--Aspects of Process Technology and Statics," Chem. Eng. 56, No.4, 291-298. In German.

62. Sherif, F.A. (1986), "Analysis of Elastoplastic Continuum at Large Deformation Using Hybrid Description and Finite Element Method," Ph.D. Dissertation, Ohio State University, Columbus, Ohio.

63. Singh, M. (1975), "Experimental Investigation of Changes in Circumferential Strain During Centric Emptying of Flat Bottom Cylindrical Steel Model Bins of Height-to-Diameter Ratios 5:4 and 5:1, Ph.D. Dissertation, Ohio State University, Columbus, Ohio.

64. Smid, J. (1975), "Pressure of Granular Material on Wall of Model Silo," Collection of Czechoslovakian Chemical Commun., Vol. 40, 2424-2436.

65. Smith, A.B.B. (1983), "Lateral Coal Pressures in a Mass Flow Silo, M.Sc. Thesis, University of Alberta, Canada.

66. Spencer, G.C. (1968), "Introduction to Plasticity," Chapman and Hall, London, England.

67. Sugita, M. (1978), "Flow and Pressures of Non-Cohesive Granular Materials in Funnel Flow Bin," American Society of Mechanical Engineers, No. 72-OMH-20.

68. Thompson, S.A. (1980), "Physical Properties of Wheat and its Relationship to Vertical Wall Loads in Grain Bins," University of Kentucky, Lexington, Kentucky.

69. Thompson, S.A., et al. (1985), "Wall Loads as a Function of Discharge Rate in Corrugated Model Grain Bins," ASAE Paper No. 85-40003, American Society of Agricultural Engineers, St. Joseph, Michigan.

70. Thompson, S.A., and Wells, L.G. (1980), "Vertical Wall Loads in a Model Grain Bin," ASAE Paper No. 80-4501, American Society of Agricultural Engineers, St. Joseph, Michigan.

71. Thompson, S.A., and Ross, I.J. (1983), "Compressibility and Frictional Coefficients of Wheat," Transactions of ASAE, Vol. 26, No. 4.

72. Turitzin, A.M. (1963), "Dynamic Pressure of Granular Material in Deep Bins," Journal of Structural Division, ASCE, 49-73.

73. Tüzün, U., and Nedderman, R.M. (1985), "Gravity Flow of Granular Materials Round Obstacles," Chemical Engineering Science, Vol. 40, No. 3, 325-336.

74. Tyson, A.W., and Manbeck, H.B. (1980), "Interaction Between Wall Stiffness and Emptying Pressures," ASAE Paper No.80-4502, American Society of Agricultural Engineers, St. Joseph, Michigan.

75. Vardoulakis, I. (1985), "Calibration of Constitutive Models for Granular Material Using Data from Biaxial Experiments," Geotechnique, 35, 299-317.

76. Vardoulakis, I. (1983), "Rigid Granular Model and Bifurcation in Triaxial Test," Acta Mechanica, 49, 57-79.

77. Versavel, P.A., and Britton, M.G. (1984), "In-Bin Bulk Density of Grain," ASAE Paper No. 84-4004, American Society of Agricultural Engineers, St. Joseph, Michigan.

78. Zhang, Q., et al. (1986), "Determination of Elasto-plastic Constitutive Parameters for Wheat En Masse," ASAE Paper No. 86-4073, American Society of Agricultural Engineers, St. Joseph, Michigan.

79. Zhang, Q., et al. (1985), "Finite Element Modelling of Thermally Induced pressures in Grain Bins Filled with Cohensionless Granular Material," ASAE Paper No. 85-4002, American Society of Agricultural Engineers, St. Joseph, Michigan.

80. Ziolkowski, D.P., and Hardin, B.O. (1985), "Shear Modulus of Wheat at Low Strain Amplitude," Transactions of ASAE, Vol. 28, No. 3.

81. Kepner, R., et al. (1978), "Principles of Farm Machinery," The AVI Pub. Co., Inc., Westport, Connecticut.

82. American Society of Agricultural Enginners 91986), "Agricultural Engineering Stands," St. Joseph, Michigan.

83. De Weist, R.L., (1969), "Flow Through Porous Media," Academic Press, New York.

APPENDIX A

LIST OF SYMBOLS

A   = cross-sectional area

a   = length of a rectangular cross-section

B   = function of ϕ

b   = breadth of a rectangular cross-section

c   = characteristic abscissa; side of a rectangle

C_{ijkl} = stiffness tensor

D   = diameter

D   = d/dt

D_h = diameter of hopper opening

E(t)   = relaxation modulus

E_w = Young's modulus of bin wall

e   = eccentricity of discharge

e_0 = initial voidage

F   = distribution factor

f   = yield function

G   = gravity field strength

G(t)   = stress relaxation modulus in shear

H   = height

H_b = height of bin

H(t)   = Heaviside step function

h	=	height
h	=	thickness
$J(t)$	=	creep compliance
J_1	=	first invariant of stress deviator tensor
J_2	=	second invariant of stress deviator tensor
K	=	modulus number
k	=	ratio of horizontal to vertical pressure
Ne	=	Newton's Second Law Inertial Coefficient
n	=	number of cycles
p	=	pressure
Pa	=	atmospheric pressure
Q	=	vertical force
q	=	static vertical pressure
q_1	=	constant
q_2	=	constant
R	=	hydraulic radius; Linear Spring Constant or Young's modulus
S_{ij}	=	stress tensor
T	=	temperature; tension
t	=	time
t_w	=	wall thickness
U	=	perimeter
V	=	vertical force
W	=	work
W^e	=	elastic work

W^p = plastic work

y = depth

z = depth

α = hopper angle

b = loading rate

g = unit weight

$\delta(t)$ = dirac delta

ε = strain

$\dot{\varepsilon}$ = strain rate

ε^c = creep strain

ε^e = elastic strain

εij_c = strain tensor

εij_p = plastic collapse strain tensor

$\dot{\varepsilon ij}$ = elastic strain tensor; plastic expansive strain tensor

εij^P = plastic strain tensor

η = coefficient of viscosity

η_1 = yield constant

θ_c = hopper angle

K = hardening function

K(t) = hydrostatic or bulk relaxation modulus

λ = geometric mean diameter

μ = material-bin coefficient of static friction

μ' = tan ϕ

V_g = granular material's Poisson's ratio

V_w = bin wall's Poisson's ratio

Π = dimensionless Pi-term

ρ = particle density of granular material

σ = stress

σ_{ij} = stress tensor

τ = elapsed time; shear stress

ϕ = angle of internal friction of granular material

ϕ = constant

APPENDIX B

GLOSSARY OF TERMS USED IN

SIMILITUDE THEORY

1. Adequate model: A model which correctly predicts one dependent pi-term, but does not correctly predict certain other dependent pi-terms.

2. Component equation: A quantitative relationship of the dependent pi-term to a particular independent pi-term of a physical system while all the other pi-terms are held constant.

3. Complete set of pertinent physical quantities: A list of all independent physical quantities pertinent to the behavior of a physical system.

4. Dependent quantity: A secondary physical quantity of a physical system which can be derived from independent primary pertinent physical properties of the system.

5. Distorted model: A model for which one or more of the independent pi-terms in the model does not equal the corresponding pi-terms in the prototype.

6. Dissimilar model: A model which bears no apparent resemblance to the prototype but which, through suitable analogies, gives accurate predictions of the behavior of the prototype.

7. Dimension: The qualitative characteristic of a physical quantity which specifies or characterizes the kind of process used to measure a physical quantity.

8. Dimension (Basic): An independent dimension which, based on human experience and human sensory perceptions, appeals to the sense of how to describe the quantities in a physical system.

9. Independent quantity: A physical quantity of a system which cannot be derived from other physical quantities pertinent to the system.

10. Invalid model: A model which cannot be used to predict accurately the behavior of a prototype.

11. Model: A model is a device which is so related to a physical system that observations on the model may be used to predict accurately the performance of the physical system in the desired respect.

12. Governing equations: Fundamental laws of physics expressed mathematically.

13. Physical quantity: The physical attribute or pertinent quantity which must be measured in identifiable units in order to uniquely describe a physical system.

14. Physical system: An interacting set of physical quantities, finite in number, that responds in a consistent, measurable, and predictable manner to a forcing or disturbing effect.

15. Prediction equation: is an equation relating the dependent pi-term to all the independent pi-terms.

16. Prototype: The physical system for which predictions are made.

17. Redundant experiment: An experiment which does not result in or enhance the knowledge of the relationship between the dependent pi-term and an independent pi-term.

18. Redundant quantity: A quantity whose presence in the analysis does not result in or enhance the accuracy of prediction.

19. Scale model: A model whose design conditions involve indicatives between one or more pertinent physical quantities between the model and prototype.

20. Similitude: The prediction of the behavior of physical systems by observations on physically similar systems.

21. True model: A model designed in such a way that all the independent pi-terms in this model and the prototype are numerically equal.

22. Valid model: A model whose observations can be used to predict the behavior of a prototype.

A Universal Form of Equations

for Physical Systems

Murphy (43) has offered a proof on a universal form of equations for physical systems. In general, any measurable quantity α (the secondary quantity) may be expressed in terms of those appropriate quantities a_i (called primary quantities) which affect the magnitude of the secondary quantity. The general relationship between α and the primary quantities may be written as:

$$\alpha = f(a_1, a_2, \ldots a_n) \hspace{3cm} (A-1)$$

in which α denotes the magnitude of the secondary quantity. $a_1 \ldots a_n$ are numbers denoting the magnitudes of the significant primary quantities involved.

Let β be another magnitude of a similar system which is evaluated in terms of the same primary quantities. Then, in general,

$$\beta = f(b_1, b_2, \ldots b_n) \hspace{3cm} (A-2)$$

235

in which b_1 ... b_n are quantities identical in nature to a_1 ... a_n but different in magnitude. The nature of the function in (A-1) and (A-2) is identical only when numerical values are different.

If the magnitudes of the units in which the primary quantities are changed (e.g., from English to metric), the number representing the magnitude of the first secondary quantity will change from α to another number, α', and β will change to β'. That is,

$$\alpha' = f(x_1 a_1, \ x_2 a_2, \ \ldots \ x_n a_n) \tag{A-3}$$

and

$$\beta' = f(x_1 b_1, \ x_2 b_2, \ \ldots \ x_n b_n) \tag{A-4}$$

in which x_1, x_2, ... x_n represent the ratios of the size of the first set of units to the size of the second set of units.

Now an axiom of the basis of Dimensional Analysis states that: "The ratio of the magnitudes of two like quantities is independent of the units used in their measurement, provided the same units are used for evaluating each."

Therefore,

$$\frac{\alpha'}{\alpha} = \frac{\beta'}{\beta} \tag{A-5}$$

Hence,

$$\alpha' = \frac{\alpha}{\beta} \beta' \tag{A-6}$$

or

$$f(x_1 a_1, \ x_2 a_2, \ \ldots \ x_n a_n)$$

$$= \frac{f(a_1, \ a_2, \ \ldots \ a_n)}{f(b_1, \ b_2, \ \ldots \ b_n)} \ f(x_1 b_1, \ \ldots \ x_n b_n) \tag{A-7}$$

If both sides of equation (A-7) are differentiated partially with respect to each x_i, there will result a series of equations of the form,

$$\frac{a_i \partial f(x_1 a_1 \ \ldots \ x_n a_n)}{\partial(a_i x_i)}$$

$$= \frac{f(a_1, \ a_2 \ \ldots \ a_n)}{f(b_1, \ b_2 \ \ldots \ b_n)} \ b_i \ \frac{\partial f(x_1 b_1 \ \ldots \ x_n b_n)}{\partial(b_i x_i)} \tag{A-8}$$

Let all the x's become unity, then:

$$a_i \ \frac{\partial f(a_1, \ a_2, \ \dots \ a_n)}{\partial a_i}$$

$$= \frac{f(a_1, \ a_2 \ \dots \ a_n)}{f(b_1, \ b_2 \ \dots \ b_n)} \ b_i \ \frac{\partial f(b_1, \ b_2 \ \dots \ b_n)}{\partial b_i} \qquad \text{(A-9)}$$

or

$$\frac{a_i \dfrac{\partial f(a_1, \ a_2 \ \dots \ a_n)}{\partial a_i}}{f(a_1, \ a_2 \ \dots \ a_n)} = \frac{b_i \dfrac{\partial f(b_1, \ b_2 \ \dots \ b_n)}{\partial b_i}}{f(b_1, \ b_2 \ \dots \ b_n)} \qquad \text{(A-10)}$$

Equation (A-10) must hold for all values of a_i and b_i. For any given value of b, the right-hand side of the equation is constant and may be designated c_i. Then,

$$\frac{\dfrac{\partial f(a_1, \ a_2 \ \dots \ a_n)}{\partial a_i}}{f(a_1, \ a_2 \ \dots \ a_n)} = \frac{c_i}{a_i} \qquad \text{(A-11)}$$

An equation of the type (A-11) will exist for each value of b_i and each value of a_i. Each equation is a differential equation of the general relationship between $f(a_1, \ a_2 \ \dots \ a_n)$ and the particular a_i involved. Since $a_1, \ a_2 \ \dots \ a_n$ are independent quantities, Equation (A-11) may be written as:

$$\frac{df(a_1, \ a_2 \ \dots \ a_n)}{f(a_1, \ a_2 \ \dots \ a_n)} = c_i \ \frac{da_i}{a_i} \qquad \text{(A-12)}$$

Equation (A-12) may be integrated directly to:

$$\ln [f(a_1, a_2 \ldots a_n)] = C_i \ln a_i + \text{Constant} \qquad \text{(A-13)}$$

If the same procedure is carried out for each value of a_i, there results the general solution:

$$\ln f(a_1, a_2 \ldots a_n) = C_1 \ln a_1 + C_2 \ln a_2 \ldots C_n \ln a_n + \ln C_\alpha$$

$$= \ln a_1^{C_1} + \ln a_2^{C_2} + \ldots \ln a_n^{C_n} + \ln C_\alpha$$

$$= \ln \left[C_\alpha a_1^{C_1} a_2^{C_2} \ldots a_n^{C_n} \right] \qquad \text{(A-14)}$$

or

$$f(a_1, a_2 \ldots a_n) = C_2 a_1^{C_1} a_2^{C_2} \ldots a_n^{C_n} \qquad \text{(A-15)}$$

from which

$$\alpha = C_\alpha a_1^{C_1} a_2^{C_2} \ldots a_n^{C_n} \qquad \text{(A-16)}$$

Equation (A-16) indicates that the secondary quantity is expressed as a dimensionless coefficeint (C_α) multiplied by the product of the pertinent primary quantities, each raised

to the appropriate power. That is, any measurable phenomenon may be evaluated in terms of the factors causing it in the form of (A-16).

The Buckingham Pi Theorem

In general terms, the Buckingham Pi Theorem states that the number of dimensionless and independent quantities required to express a relationship among the variables in any phenomenon is equal to the number of quantities involved minus the number of dimensions in which those quantities may be measured (generally, the rank of the dimensional matrix). In equation form, the Pi Theorem is:

$$S = n - b \qquad\qquad\qquad (A-17)$$

in which

S = the number of Π-terms

n = the number of basic dimensions involved

b = the number of basic dimensions involved (rank of the dimensional matrix).

Equation (A-16) can be rewritten as:

$$C\alpha a_1^{c_1} a_2^{c_2} a_3^{c_3} \ldots a_n^{c_n} = 1 \qquad\qquad (A-18)$$

The corresponding dimensional equation is:

$$\left(d_1^{x_{11}}, \; d_2^{x_{21}}, \; \ldots \; d_b^{x_{b1}}\right)^{c_1} \left(d_1^{x_{12}}, \; d_2^{x_{22}} \; \ldots \; d_b^{x_{b2}}\right)^{c_2}$$

$$\ldots \; \left(d_1^{x_{1n}}, \; d_2^{x_{2n}} \; \ldots \; d_b^{x_{bn}}\right)^{c_n} = 0 \tag{A-19}$$

in which the d_i terms designate the basic dimensions

involved, b in number. Equation (A-19) may be resolved into

b auxiliary equations

$$x_{11}c_1 + x_{12}c_2 + \ldots + x_{1n}c_n = 0$$

$$x_{21}c_1 + x_{22}c_2 + \ldots + x_{2n}c_n = 0$$

$$\begin{matrix} \cdot & \cdot & \cdot \\ \cdot & \cdot & \cdot \\ \cdot & \cdot & \cdot \end{matrix}$$

$$x_{b1}c_1 + x_{b2}c_2 + \ldots + x_{bn}c_n = 0 \tag{A-20}$$

This set of b simultaneous linear equations contains n
unknowns, but any b of the unknowns may be expressed in terms
of the remaining n-b unknowns, provided that the determinant
of the coefficient of b unknowns selected does not equal
zero. That is, if the n-b terms are treated as constant, the
resulting b equations must be independent.

Therefore, b of the exponents in Equation (A-18) may be
replaced by their equivalents as obtained from Equations
(A-20), and Equation (A-18) will contain n-b unknown

exponents. Terms bearing the same exponent may be grouped, and each group will be dimensionless because each exponent must satisfy the simultaneous equations based on dimensional homogeneity. Obviously, there will be n-b of these

dimensionless groups. Since the C_α term may be a function of the variables involved, the equation formed by substituting in Equation (A-18) reduces to:

$$\Pi_1 = F(\Pi_2, \Pi_3 \ldots \Pi_{n-b}) \qquad (A-21)$$

in which

$$\Pi_i = \text{dimensionless } \Pi\text{-terms}$$

It is noted that the only restriction placed upon the Pi-terms is that they be <u>dimensionless and independent</u>.

Tresca Yield Criterion
(Maximum Shear Theory)

The Tresca Yield Criterion, also called the Coulomb Theory, assumes that yielding will occur when the maximum shear stress reaches the value of the maximum shear stress occurring under simple tension (66). For simple tension, since $\sigma_2 = \sigma_3 = 0$, the maximum shear stress at yield is 1/2

σ_0. The Tresca Criterion asserts that yielding will occur when any one of the following six conditions is reached:

$$\sigma_1 - \sigma_2 = \pm \sigma_0 \qquad\qquad\qquad (A-22)$$

$$\sigma_2 - \sigma_3 = \pm \sigma_0 \qquad\qquad\qquad (A-23)$$

$$\sigma_3 - \sigma_1 = \pm \sigma_0 \qquad\qquad\qquad (A-24)$$

Figure (A-1) is an illustration of the Tresca Criterion for a biaxial state of stress. It should be noted that one limitation of this theory is the requirement that the yield stress in tension and compression be equal. The Tresca Criterion is in fair agreement with experiments and is, therefore, used to a considerable extent by designers. However, it suffers from one major difficulty: it is necessary to know in advance which are the maximum and minimum principal stresses. For the Tresca Criterion, the yield stress in pure shear is half the yield stress in pure tension.
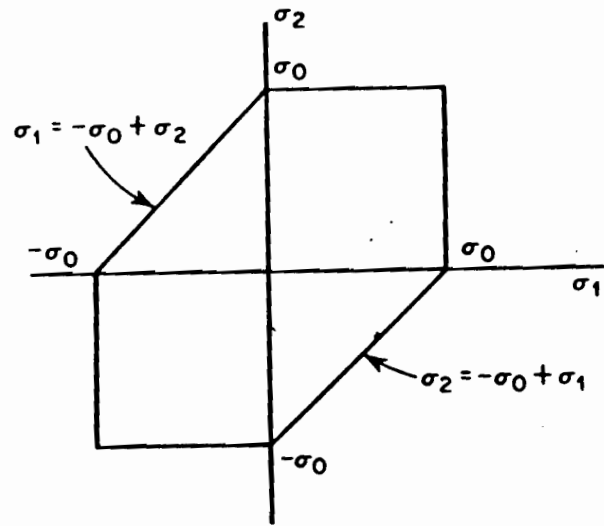
Figure (8-1)   Tresca Yield Criterion
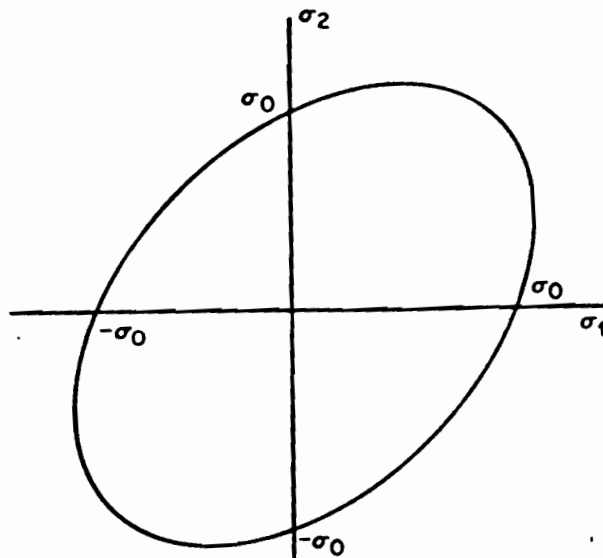
Figure (8-2)   von Mises Yield Criterion

von Mises Yield Criterion

(Distortion Energy Theory)

The Distortion Energy Theory (also associated with Hencky) assumes that yielding begins when the distortion energy equals the distortion energy at yield in simple tension (66), i.e.:

$$U_d = \frac{1}{2G} J_2 = \frac{3}{4G} \tau_{oct}^2 \qquad \text{(A-25)}$$

where

U_d = distortion energy

J_2 = second invariant of strain tensor

G = Shear modulus

τ_{0ct} = octahedral shear stress

At the yield point in simple tension,

$$J_2 = \frac{1}{3} \sigma_0^2 \qquad \text{(A-26)}$$

Therefore, the yield condition becomes

$$\frac{1}{2}\left[(\sigma_1 - \sigma_2)^2 + (\sigma_2 - \sigma_3)^2 + (\sigma_3 - \sigma_1)^2 \right] = \sigma_0^2 \qquad \text{(A-27)}$$

and, for the biaxial case,

245

$$\sigma_1{}^2 - \sigma_1\sigma_2 + \sigma_2{}^2 = \pm \sigma_0{}^2 \qquad\qquad \text{(A-28)}$$

Figure (A-2) is a plot of σ_1 versus σ_2 for the biaxial state of stress for the von Mises Yield Criterion; the plot is called the 'von Mises Ellipse.'

For pure shear the yield stress in 1/ 3 the yield stress in pure tension for the von Mises Yield Criterion. Thus, the von Mises Criterion predicts a pure shear yield stress which is about 15% higher than predicted by the Tresca Criterion. The von Mises Yield Criterion usually fits (but not always) the experimental data better than the other theories, and is usually easier to apply than the Tresca Criterion because no knowledge is needed regarding the relative magnitudes of the principal stresses.

APPENDIX C

Sand First Cycle

$\Pi_2 \ (P_h/P_v)$

$\Pi_1 \ (P_v/\rho G\lambda)$
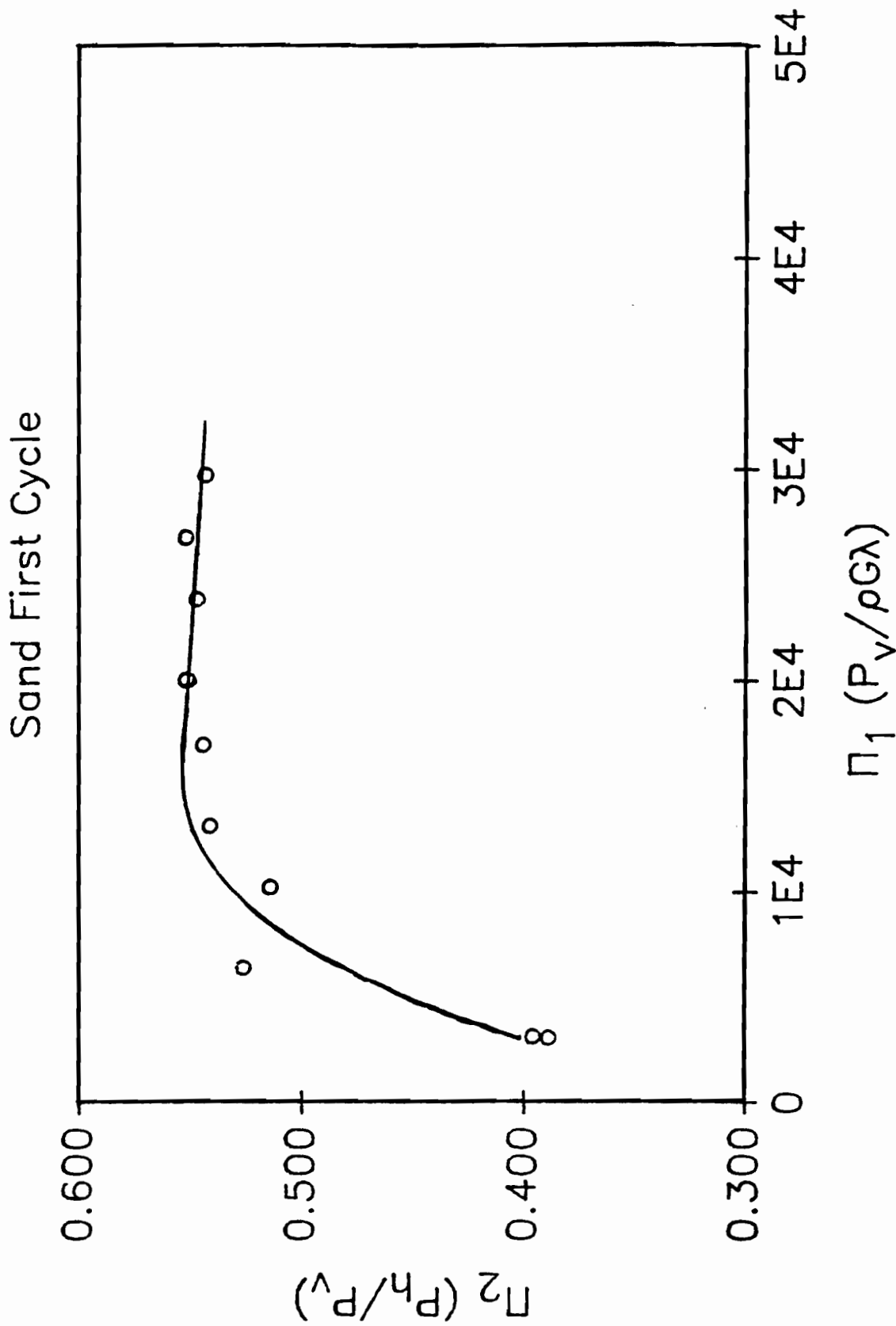
Figure 8.3.1.1.   Linear plot of Π_1 versus Π_2 for first loading cycle of sand
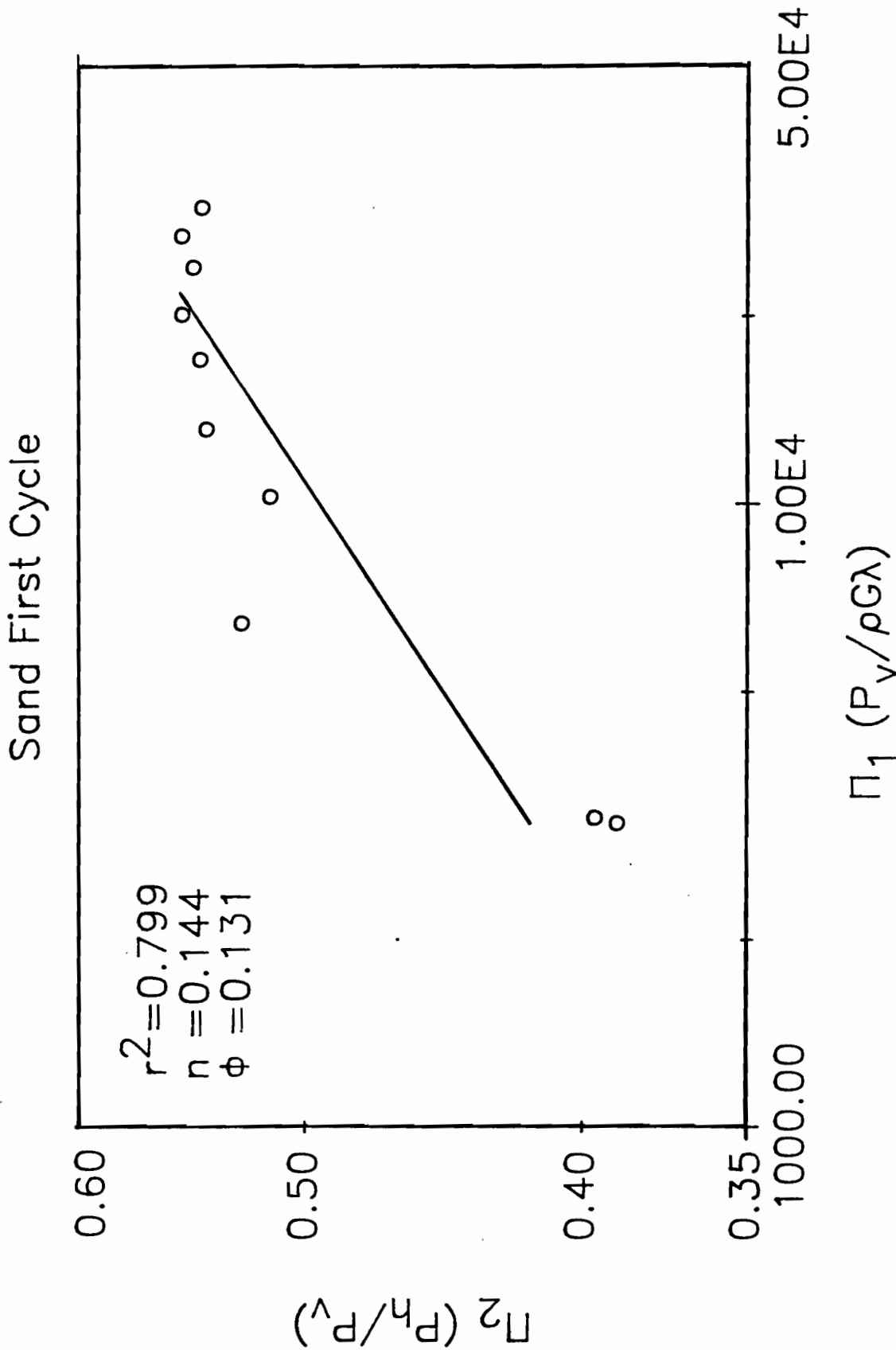
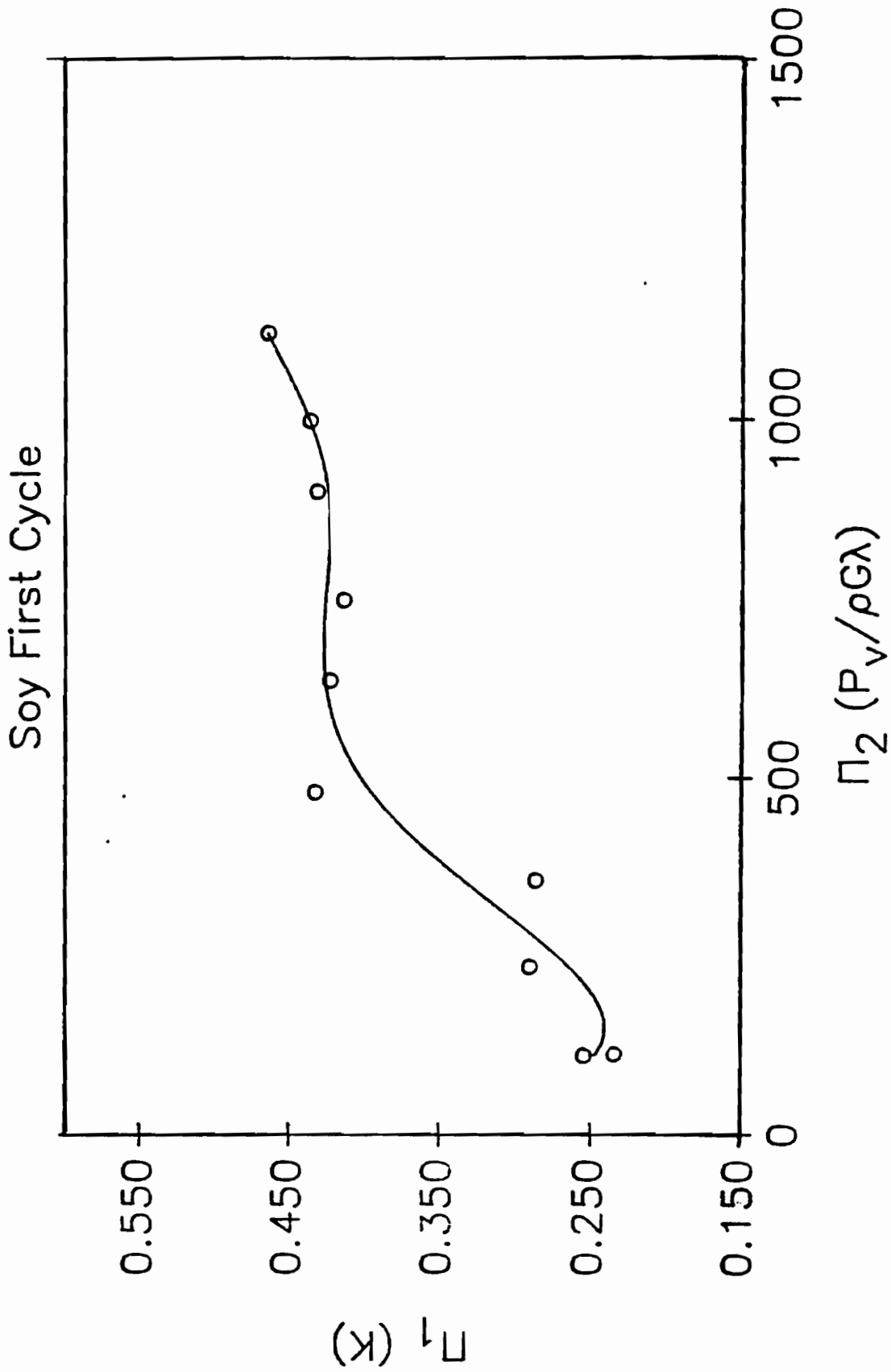Figure 8.3.1.2. Log-log plot of Π_1 versus Π_2 for first loading cycle of sand

Sand First Cycle

$R^2 = 0.976$
$a_0 = -27.209$
$a_1 = 19.740$
$a_2 = -4.683$
$a_3 = 0.371$

Π_1 $(P_v/\rho G\lambda)$

Π_2 (P_h/P_v)
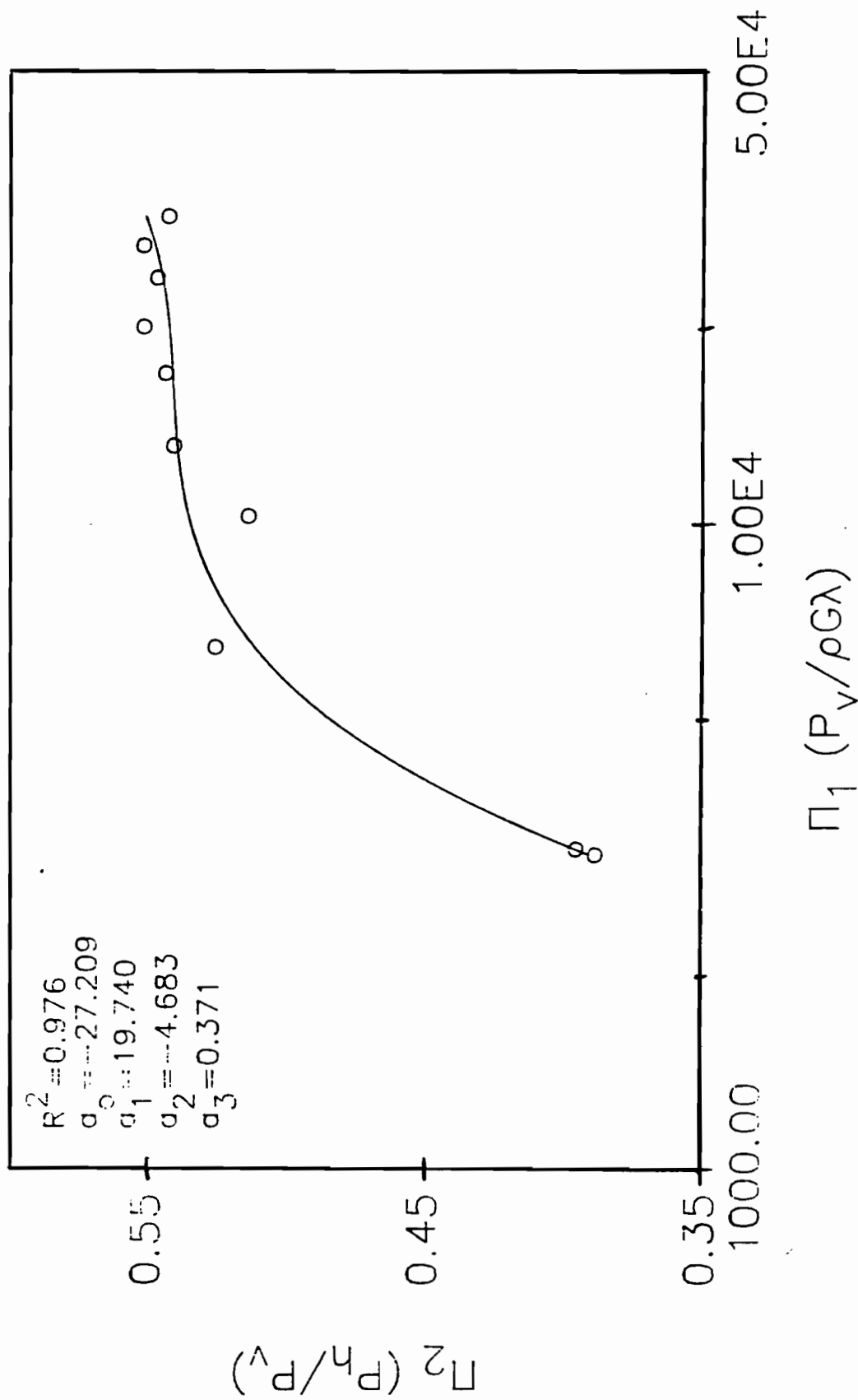
Figure 8.3.1.3. Semi-log plot of Π_1 versus Π_2 for first loading cycle of sand
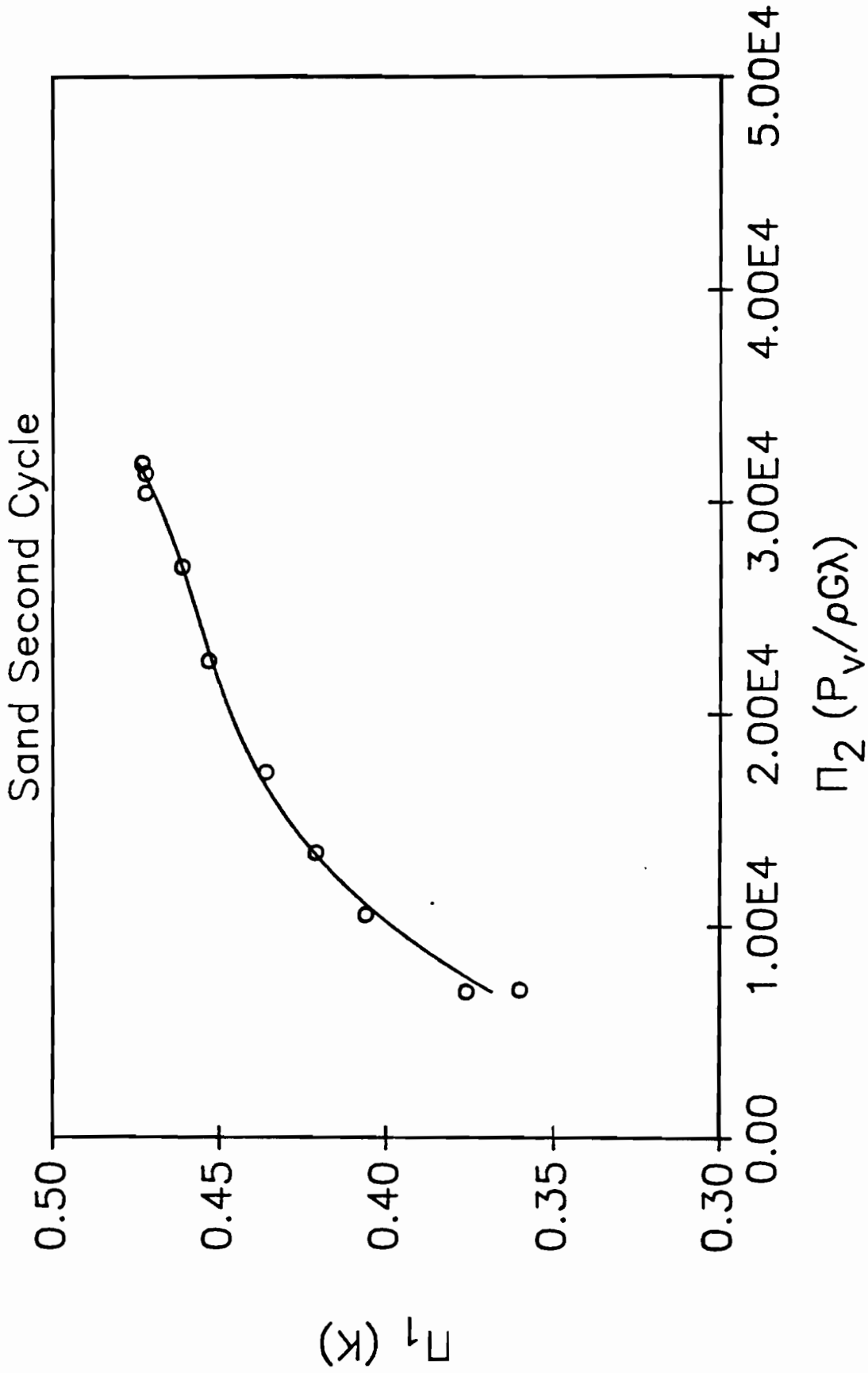
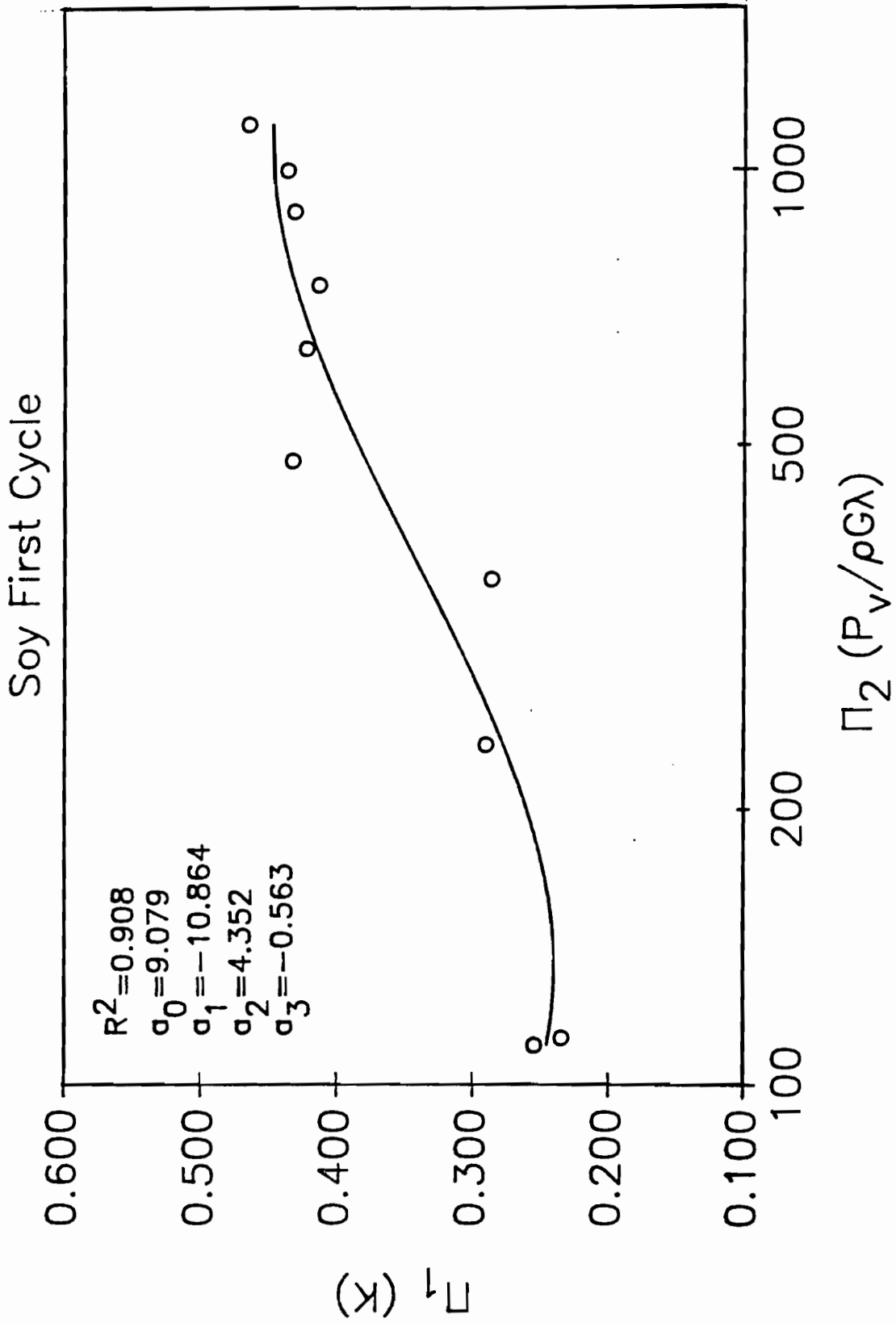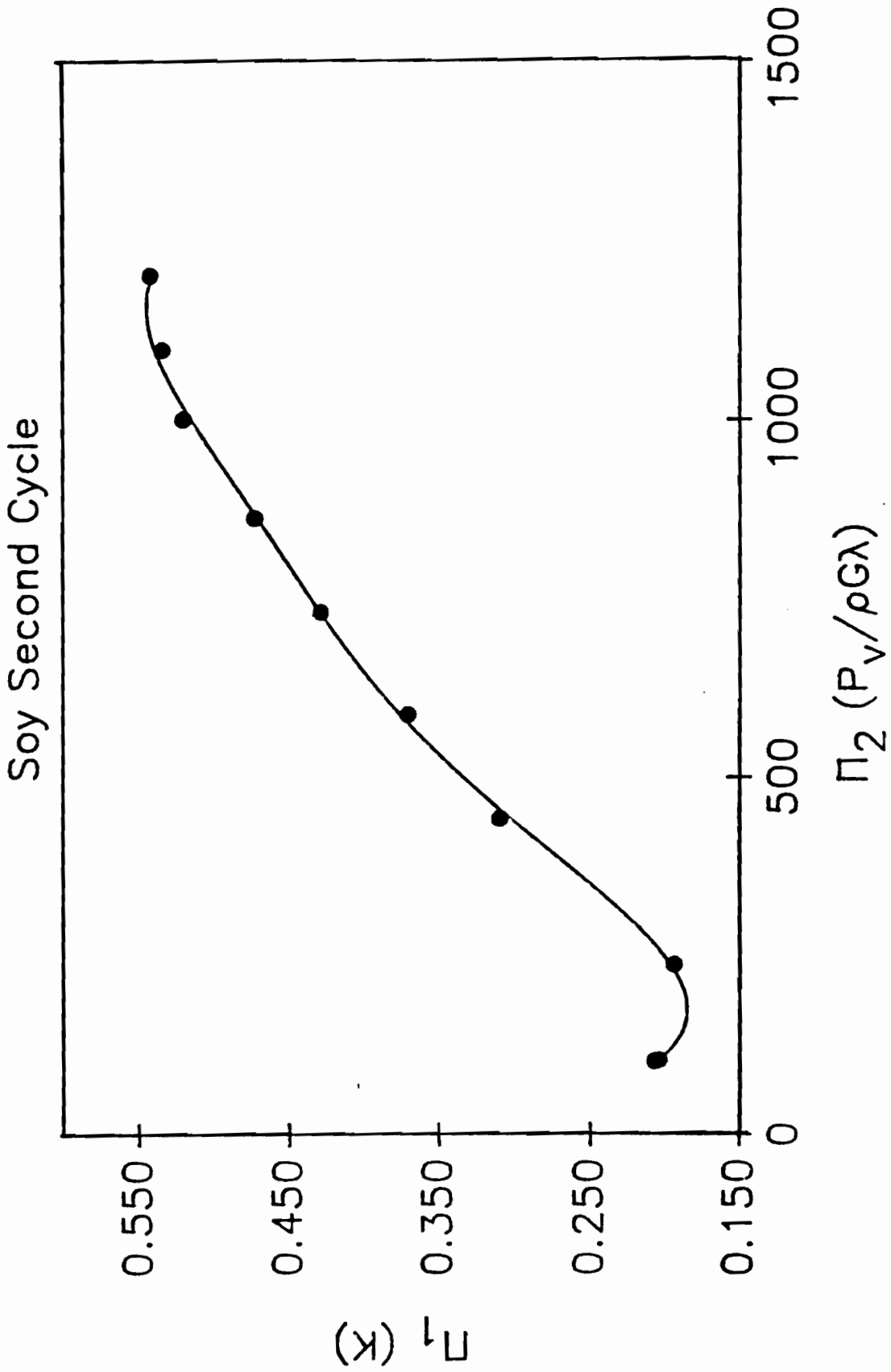Figure 8.3.2.1. Linear plot of Π_1 versus Π_2 for second loading cycle of sand
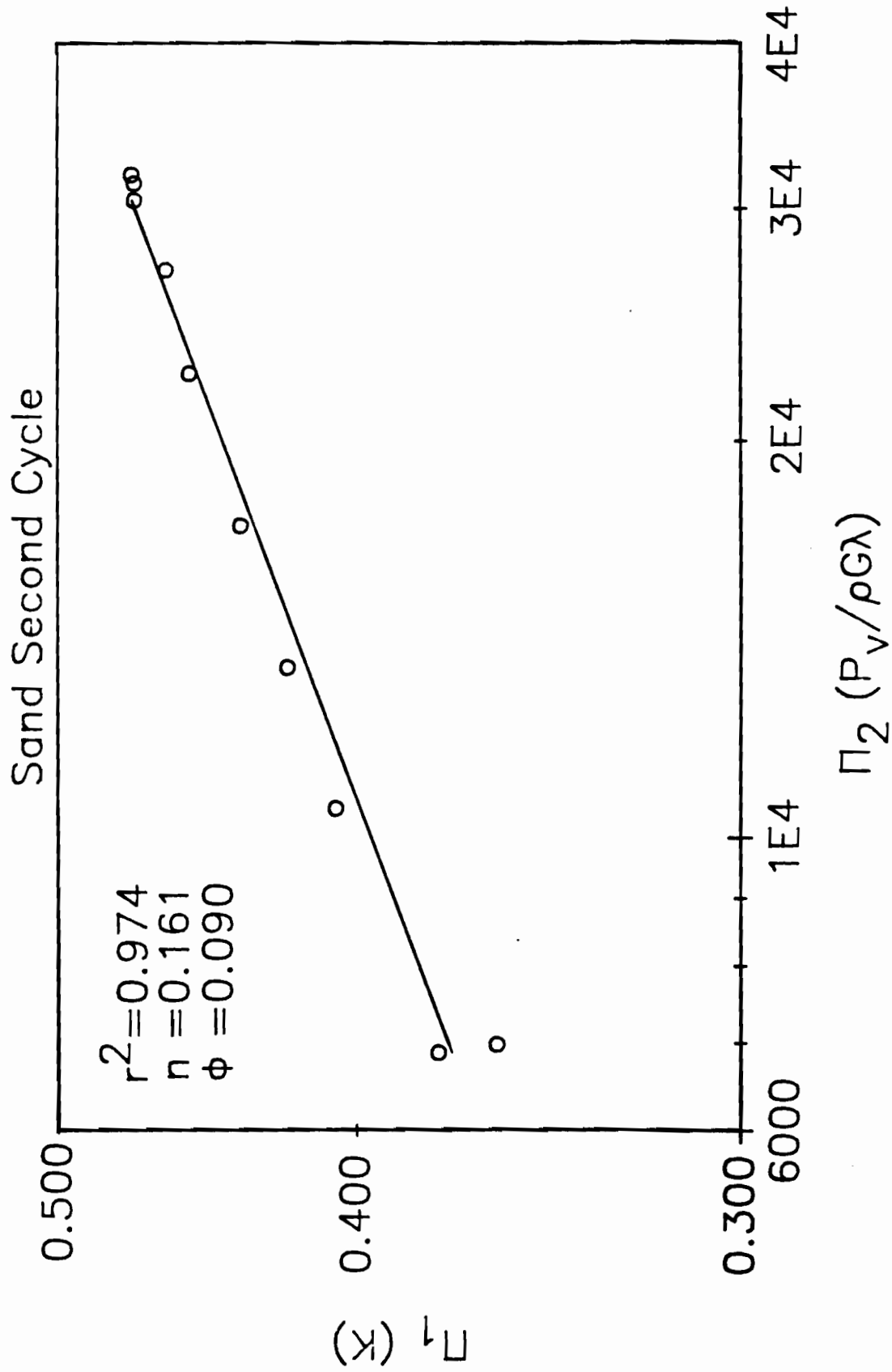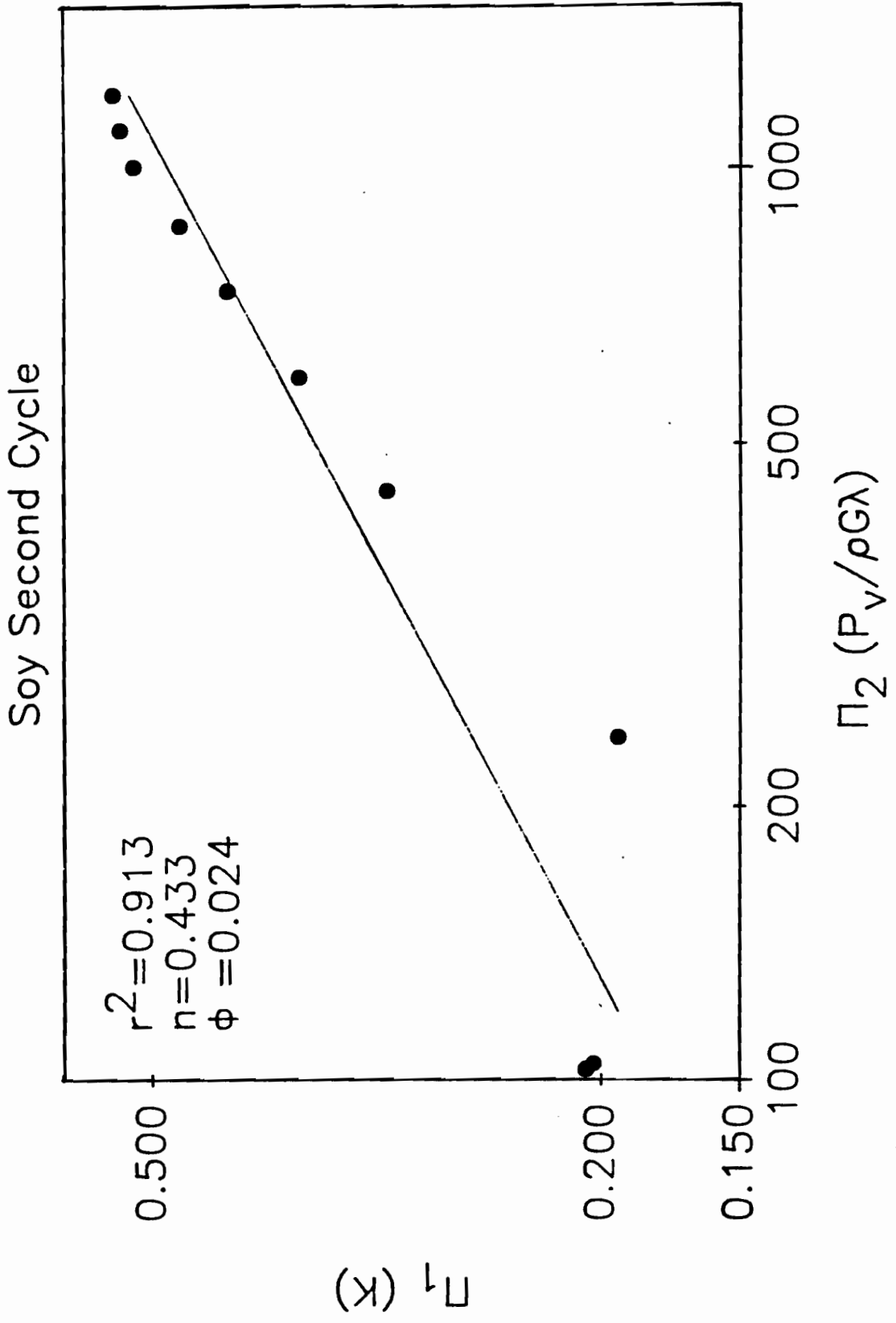
Figure 8.3.2.2. Log-log plot of Π_1 versus Π_2 for second loading cycle of sand
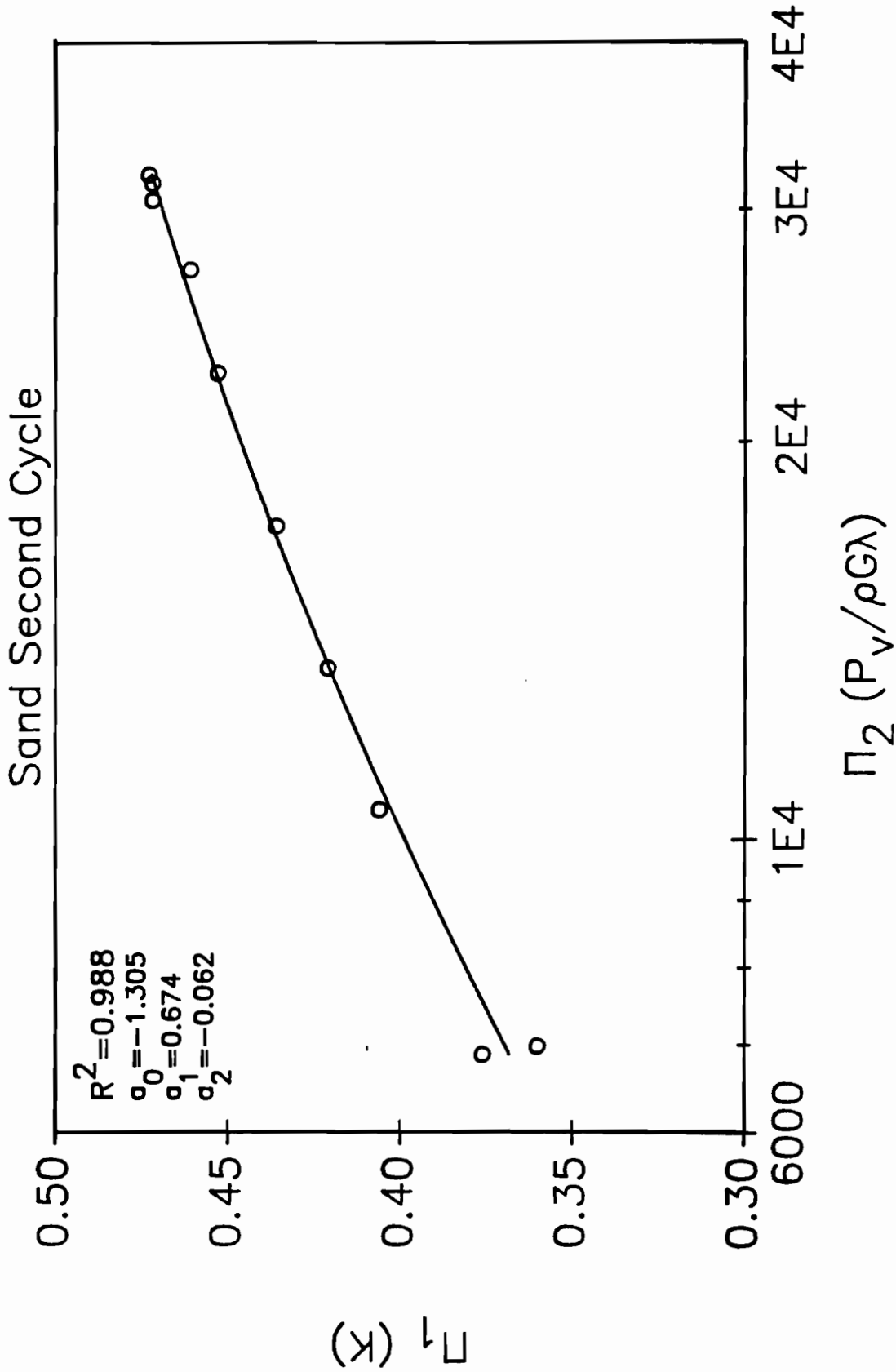
Figure 8.3.2.3. Semi-log plot of Π_1 versus Π_2 for second loading cycle of sand

$R^2 = 0.988$
$a_0 = -1.305$
$a_1 = 0.674$
$a_2 = -0.062$

Sand Second Cycle

Π_2 $(P_v/\rho G\lambda)$

Π_1 (K)
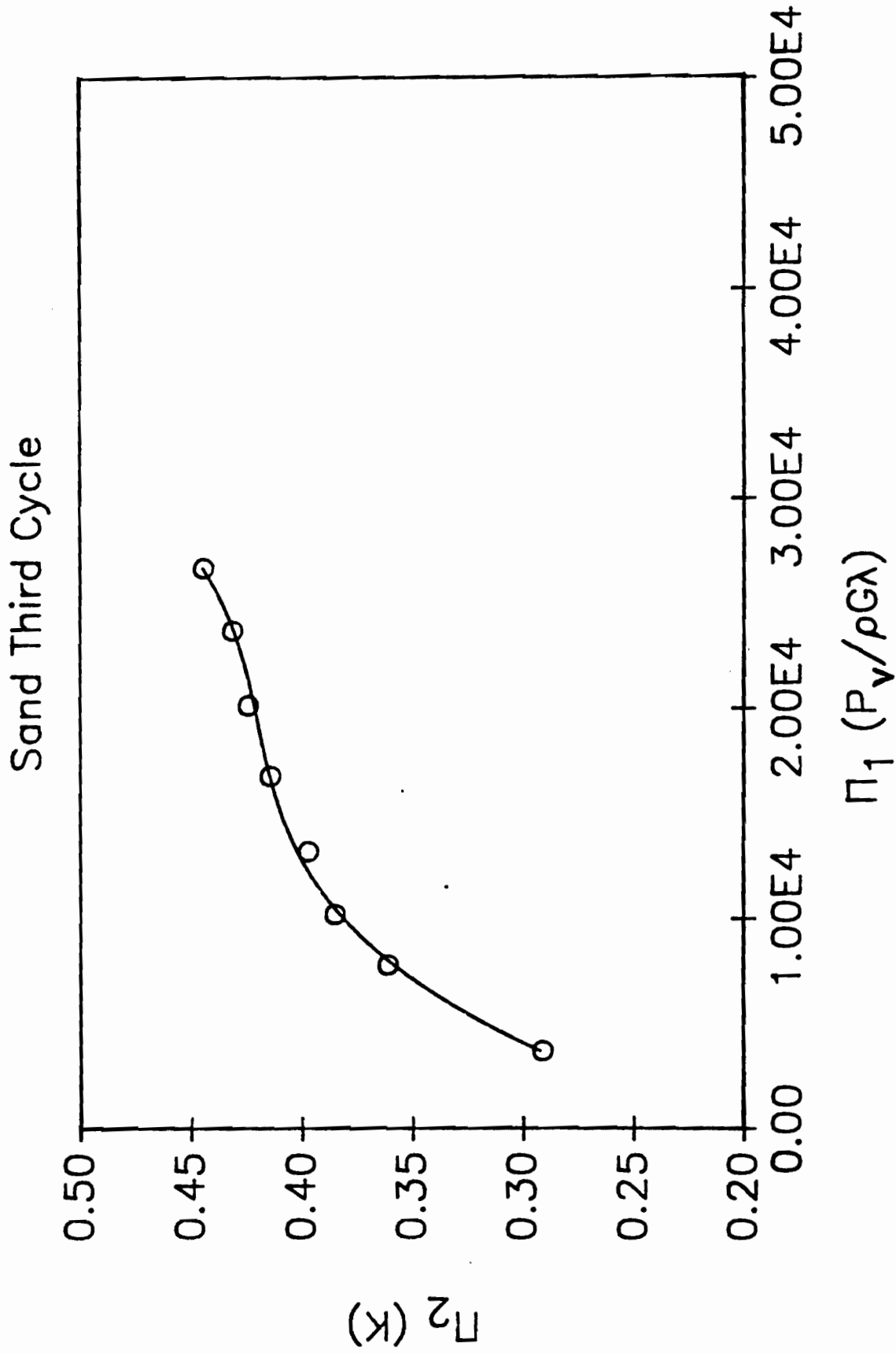
Figure 8.3.3.1. Linear plot of Π_1 versus Π_2 for third loading cycle
of sand

Sand Third Cycle

$r^2 = 0.966$
$n = 0.203$
$\phi = 0.057$

$\Pi_1 \ (P_v/\rho G\lambda)$

$\Pi_2 \ (K)$
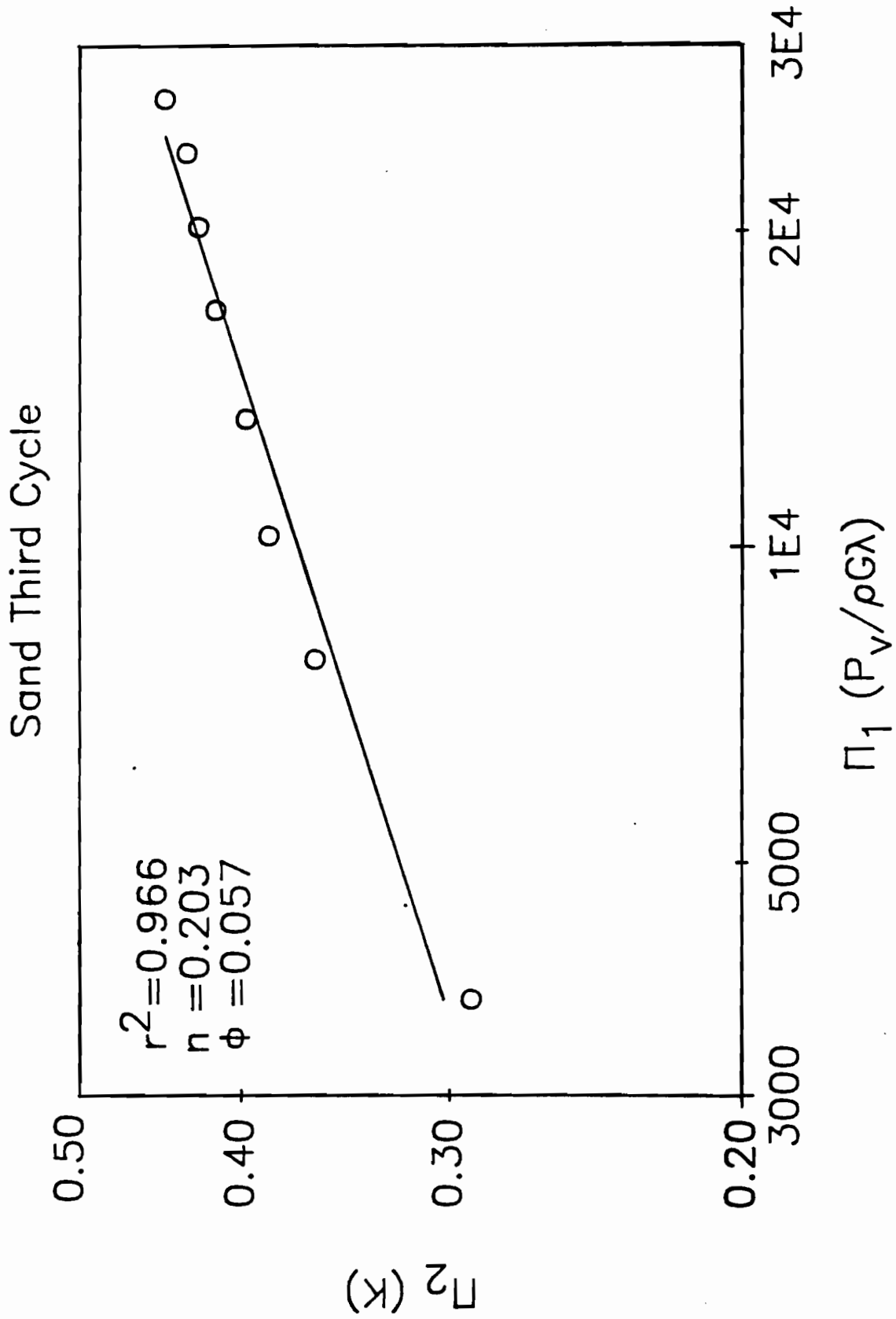
Figure 8.3.3.2. Log-log plot of Π_1 versus Π_2 for third loading cycle of sand
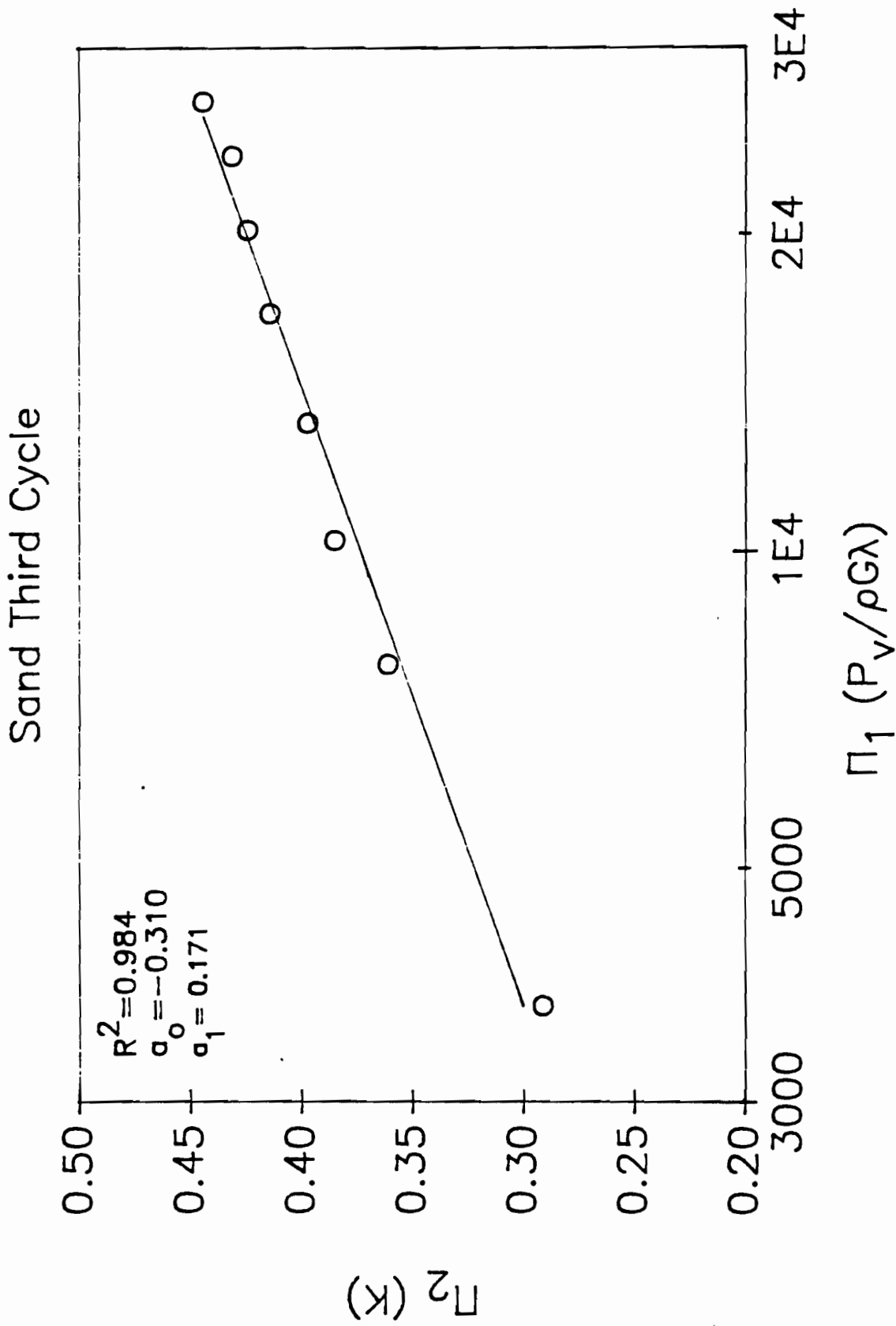
Figure 8.3.3.3. Semi-log plot of Π_1 versus Π_2 for third loading cycle of sand
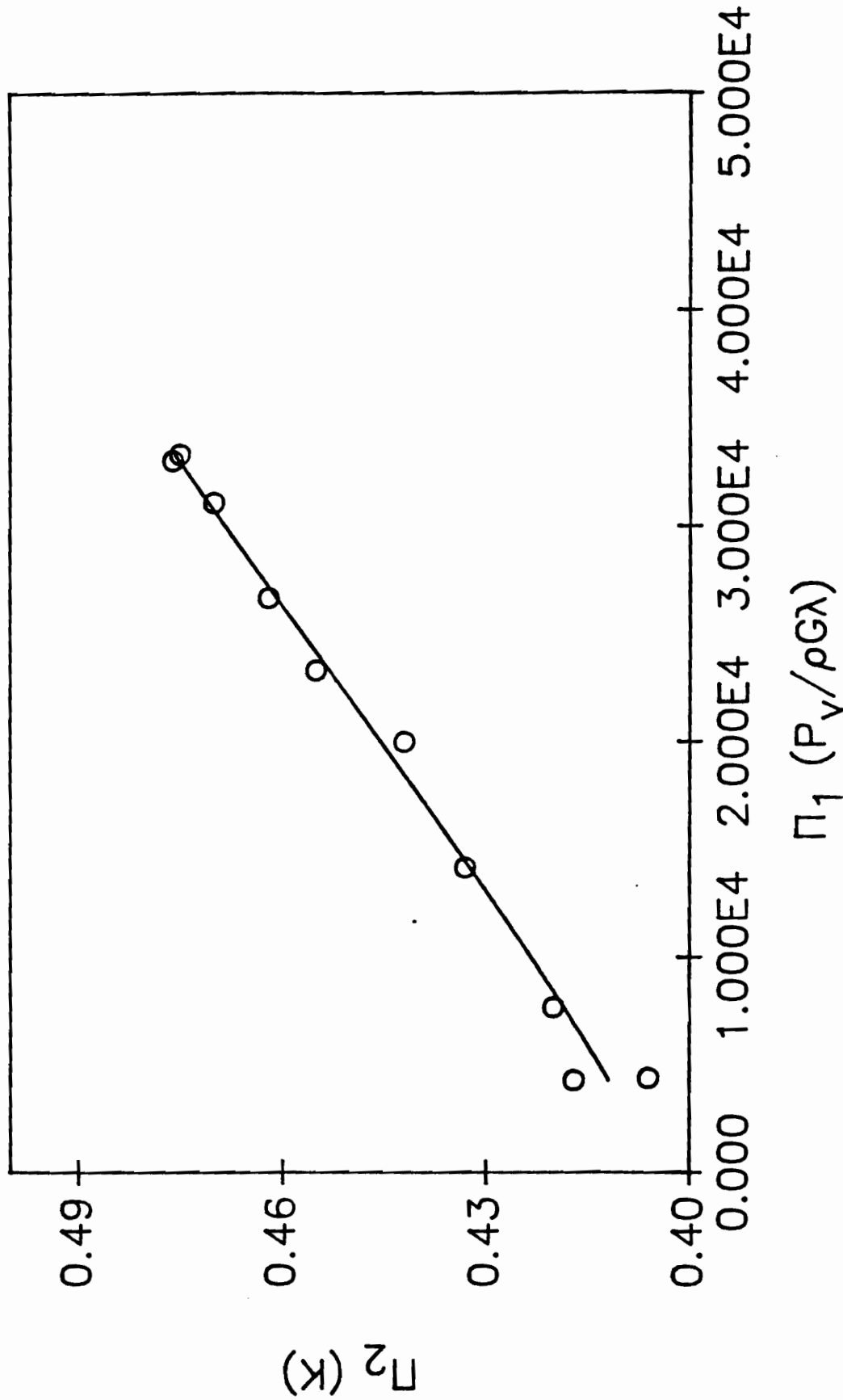
Figure 8.3.4.1. Linear plot of Π_1 versus Π_2 for fourth loading cycle of sand
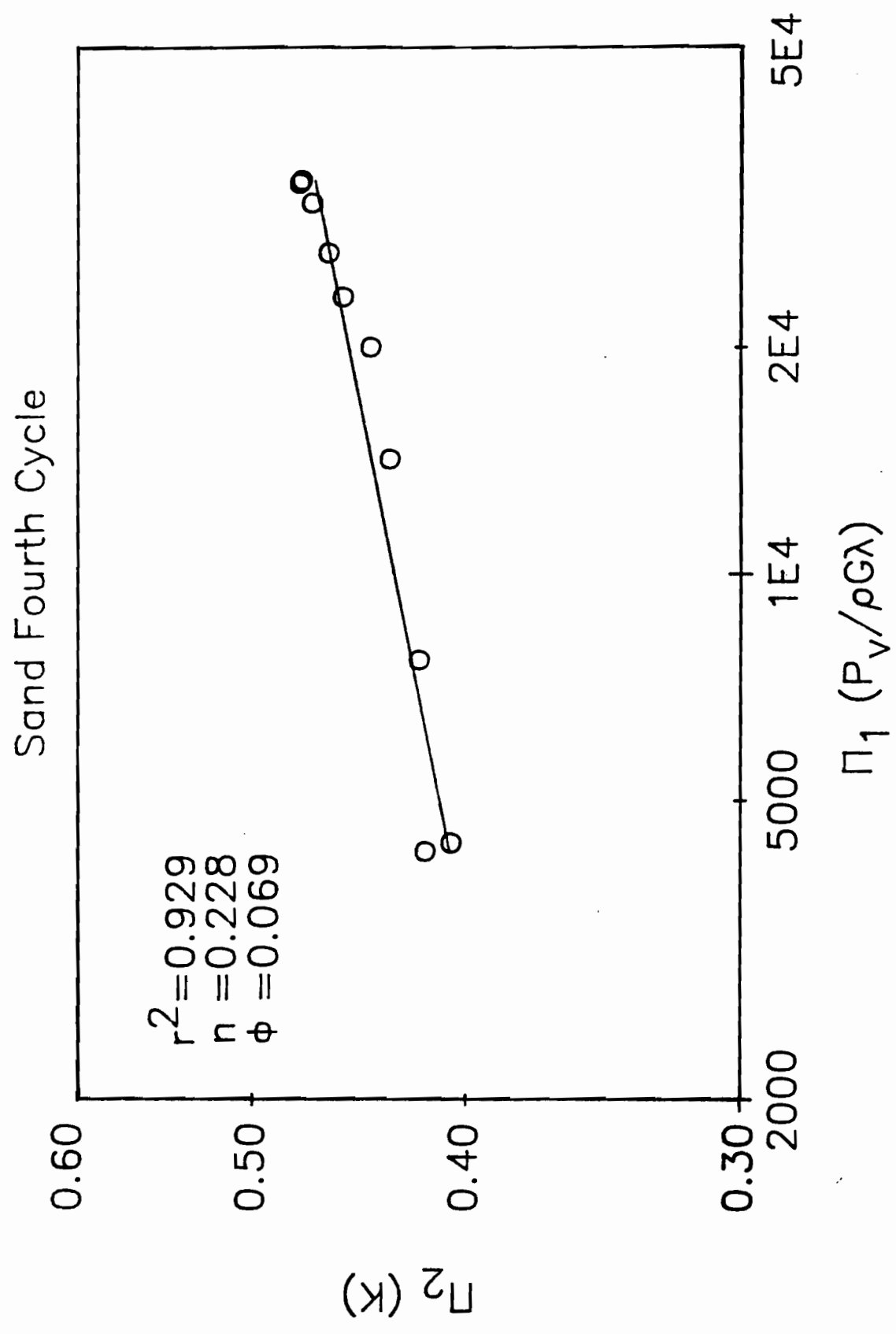
Figure 8.3.4.2.   Log-log plot of Π_1 versus Π_2 for fourth loading cycle of sand
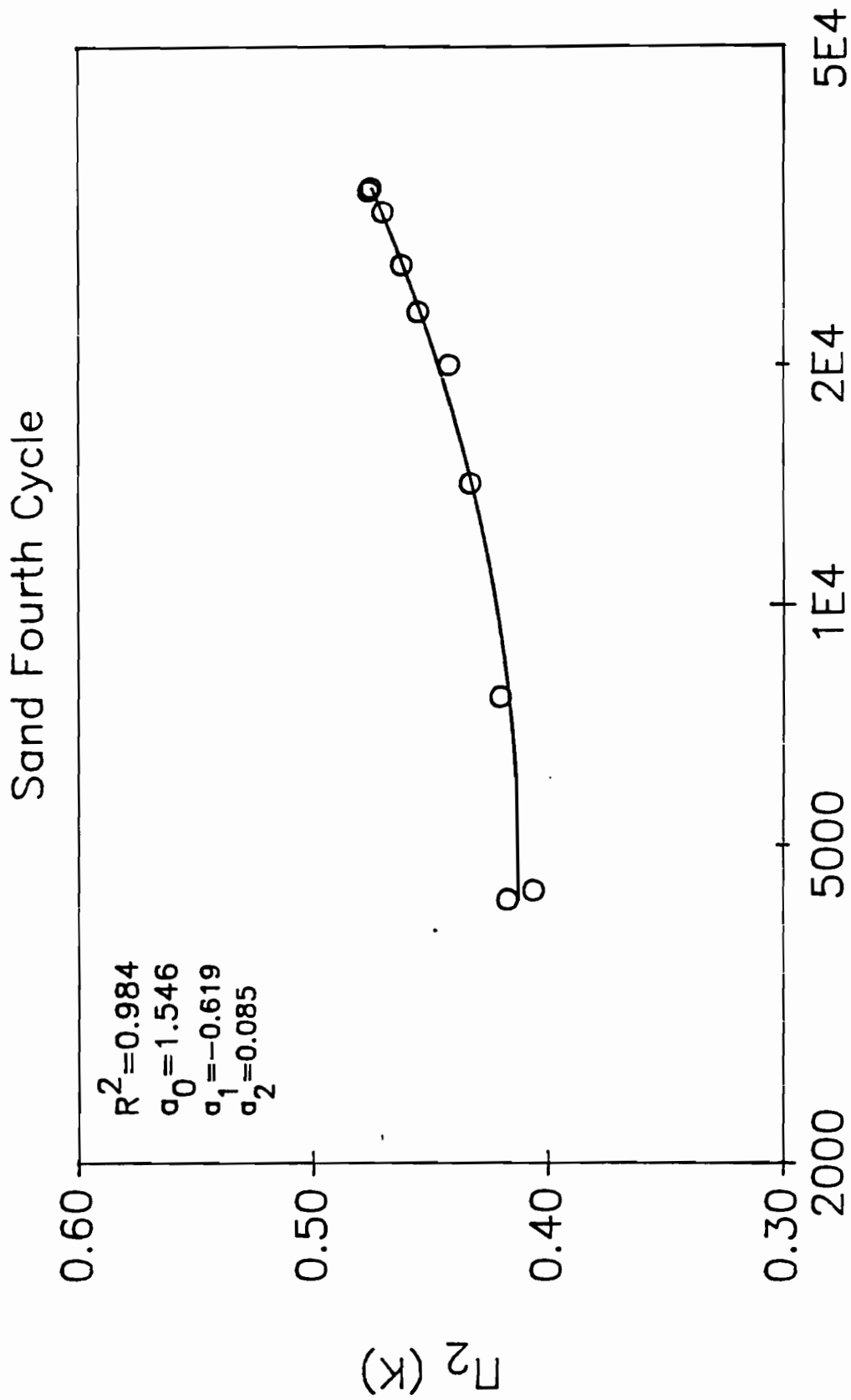
Figure 8.3.4.3.   Semi-log plot of Π_1 versus Π_2 for fourth loading cycle of sand

Sand Fifth Cycle

Π_2 (K)

Π_1 ($P_v/\rho G\lambda$)
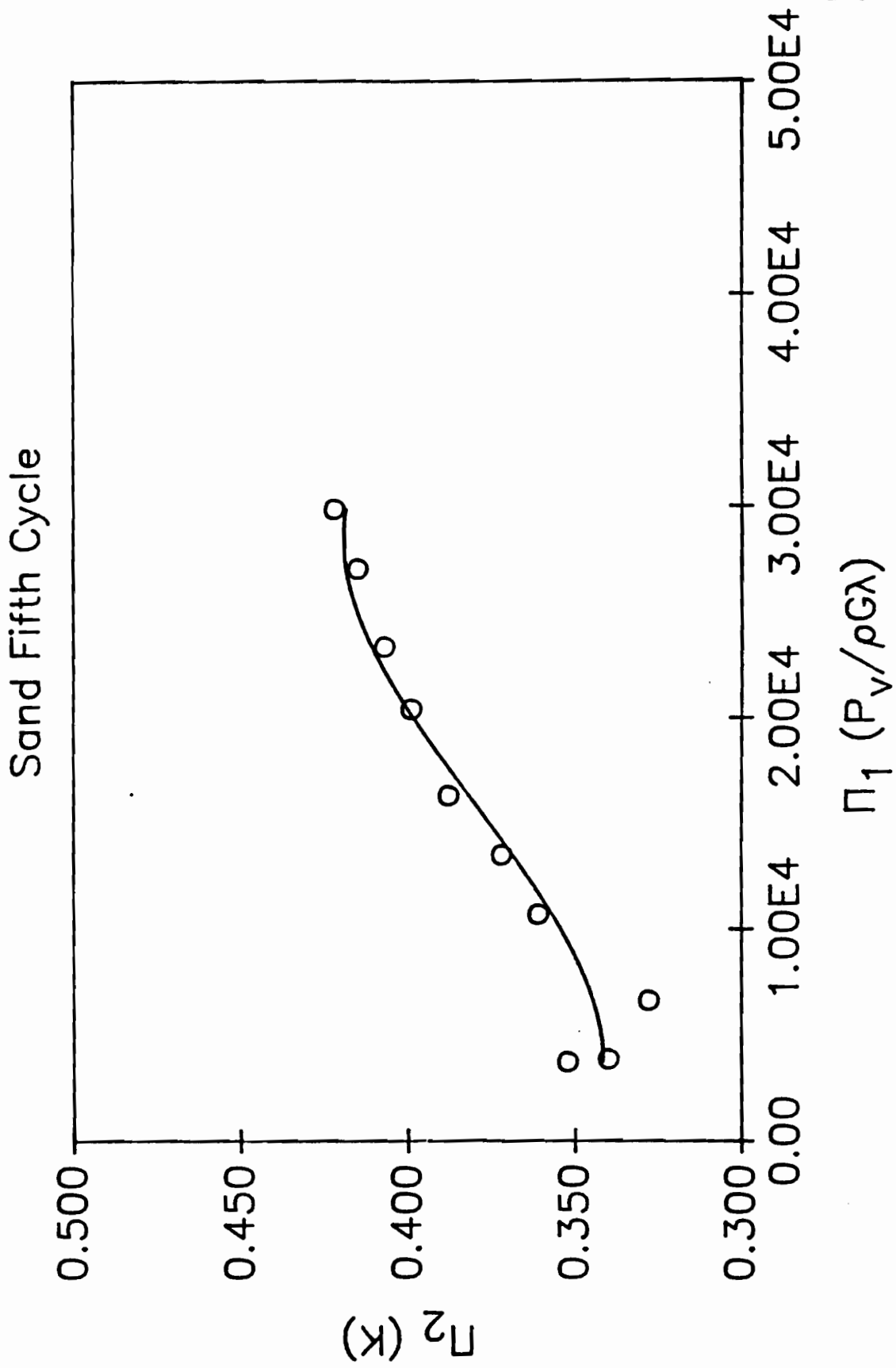
Figure 8.3.5.1. Linear plot of Π_1 versus Π_2 for fifth loading cycle of sand
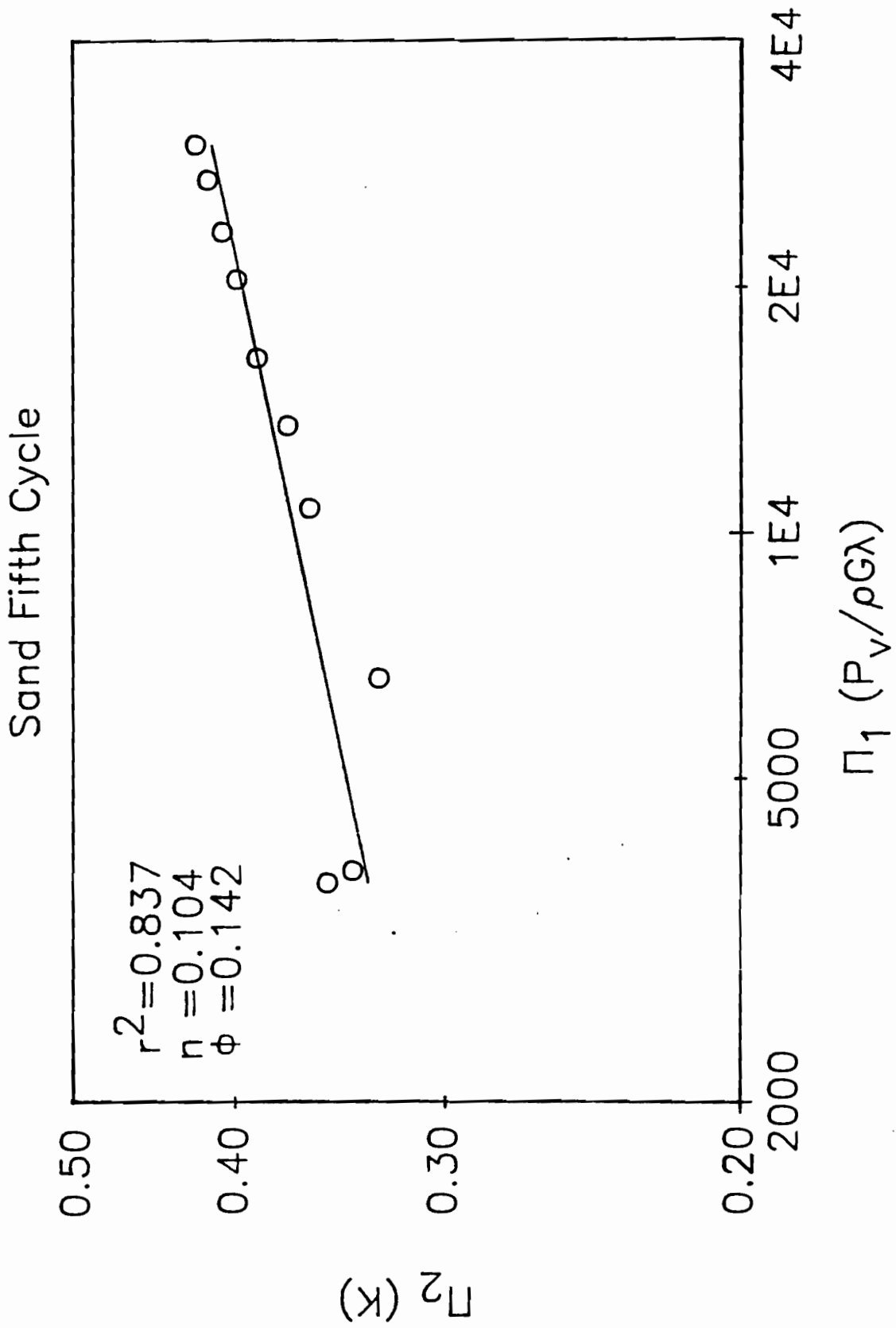
Figure 8.3.5.2.   Log-log plot for fifth loading cycle of sand
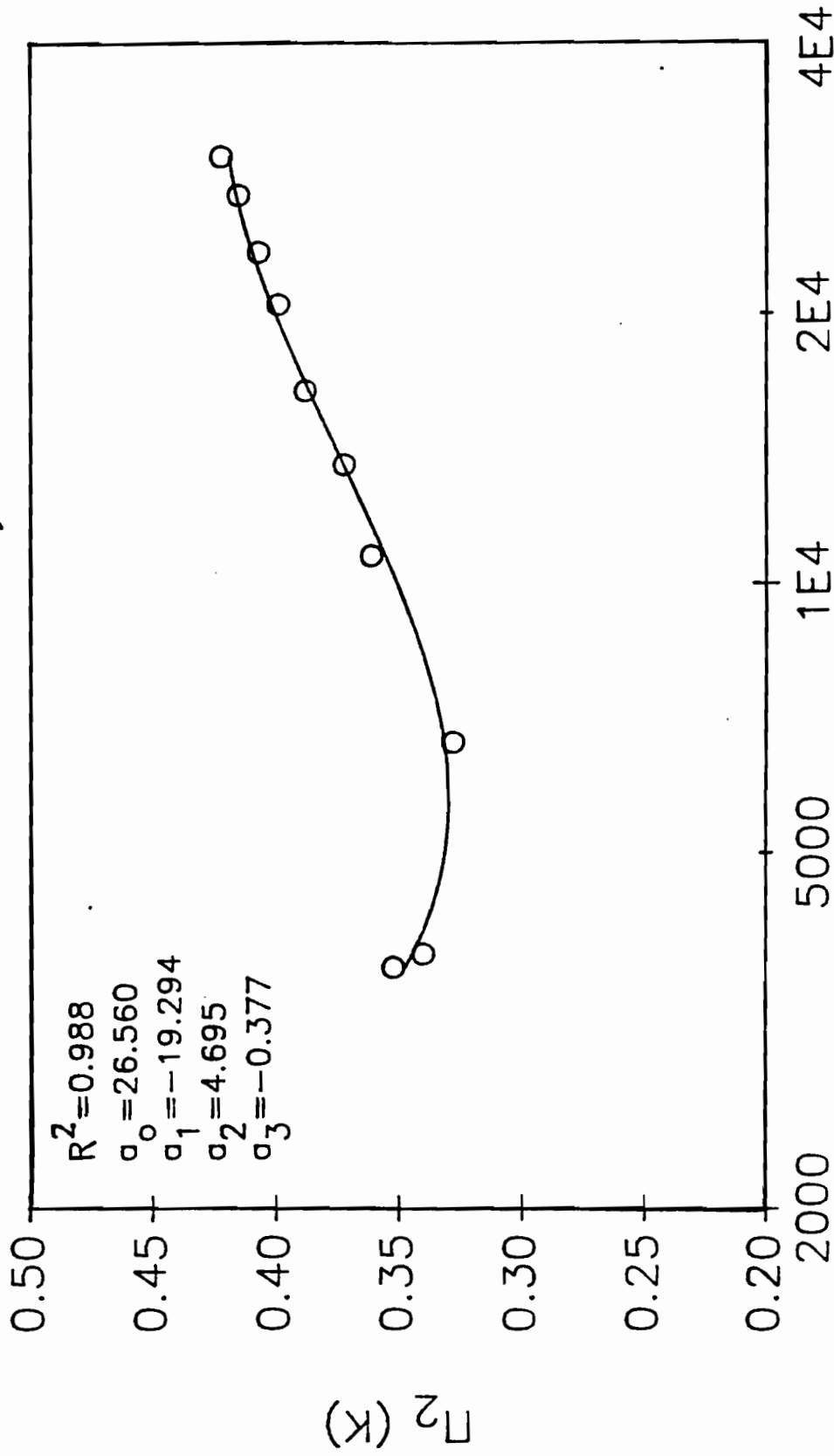
Figure 8.3.5.3.   Semi-log plot of Π_1 versus Π_2 for fifth loading cycle of sand
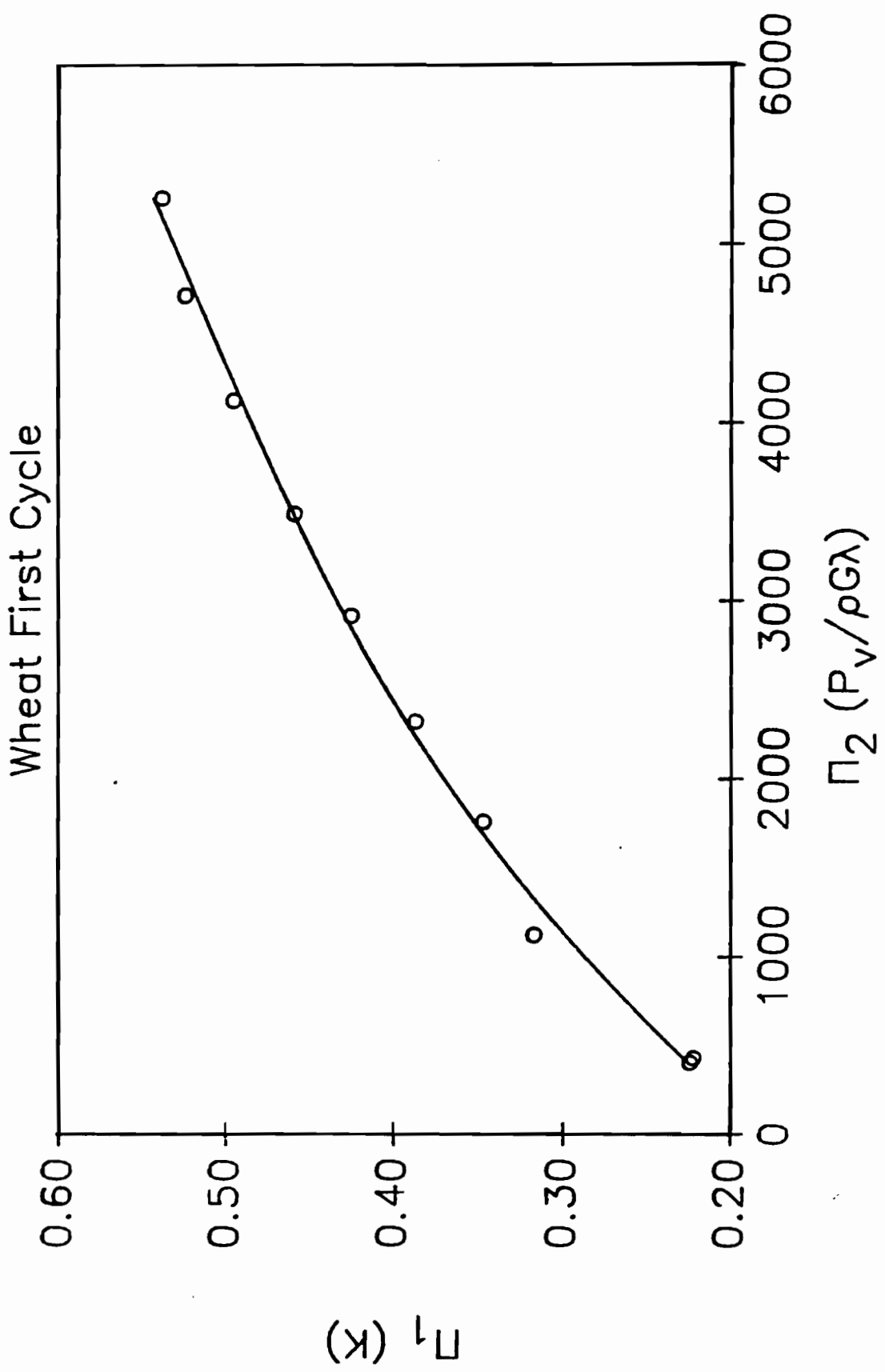
Figure 8.4.1.1. Linear plot of Π_1 versus Π_2 for first loading cycle of wheat

Wheat First Cycle

$r^2 = 0.994$
$n = 0.345$
$\phi = 0.028$

Π_1 (K)

Π_2 (P$_V$/ρGλ)
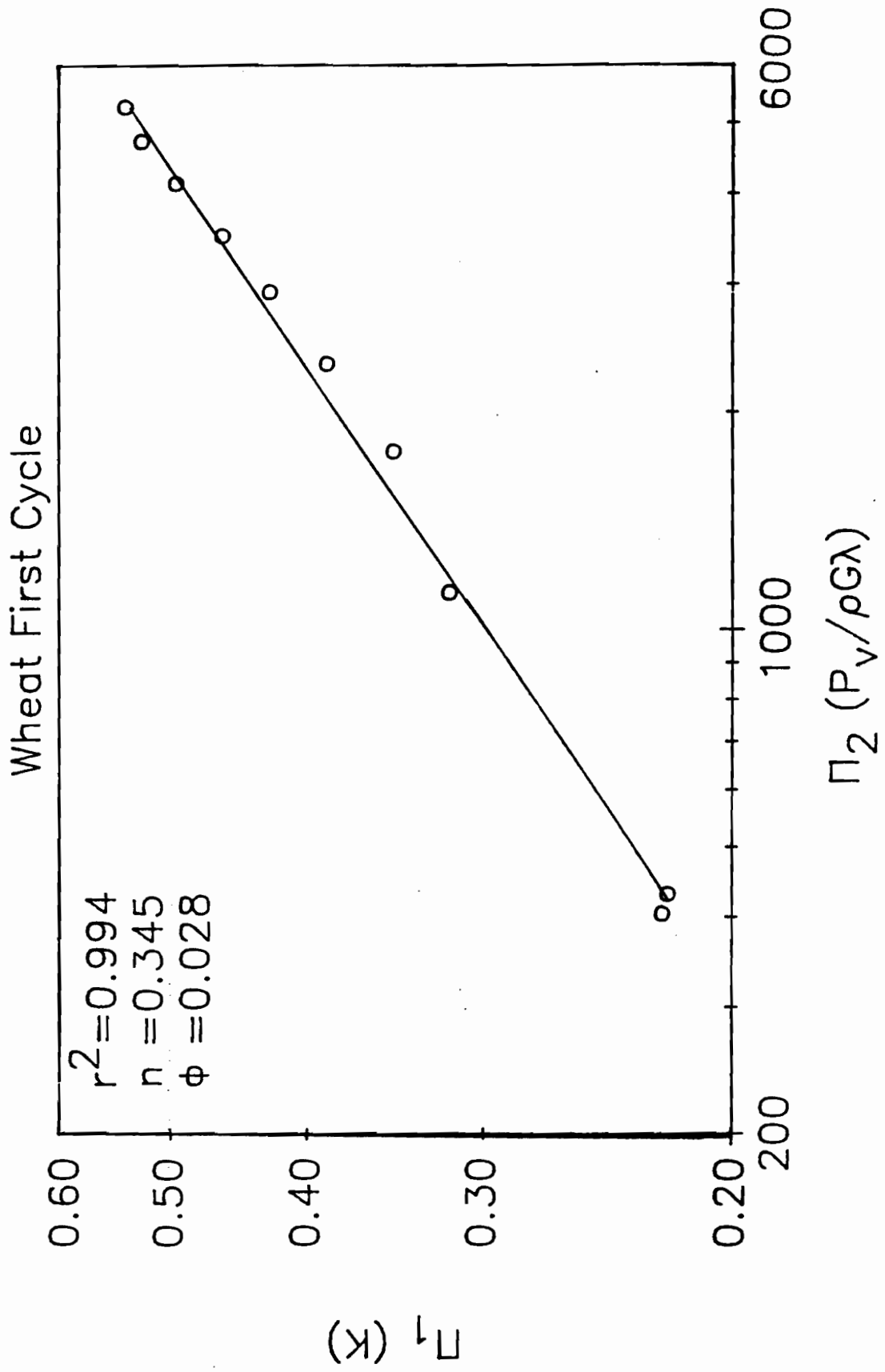
Figure 8.4.1.2. Log-log plot of Π_1 versus Π_2 for first loading cycle of wheat
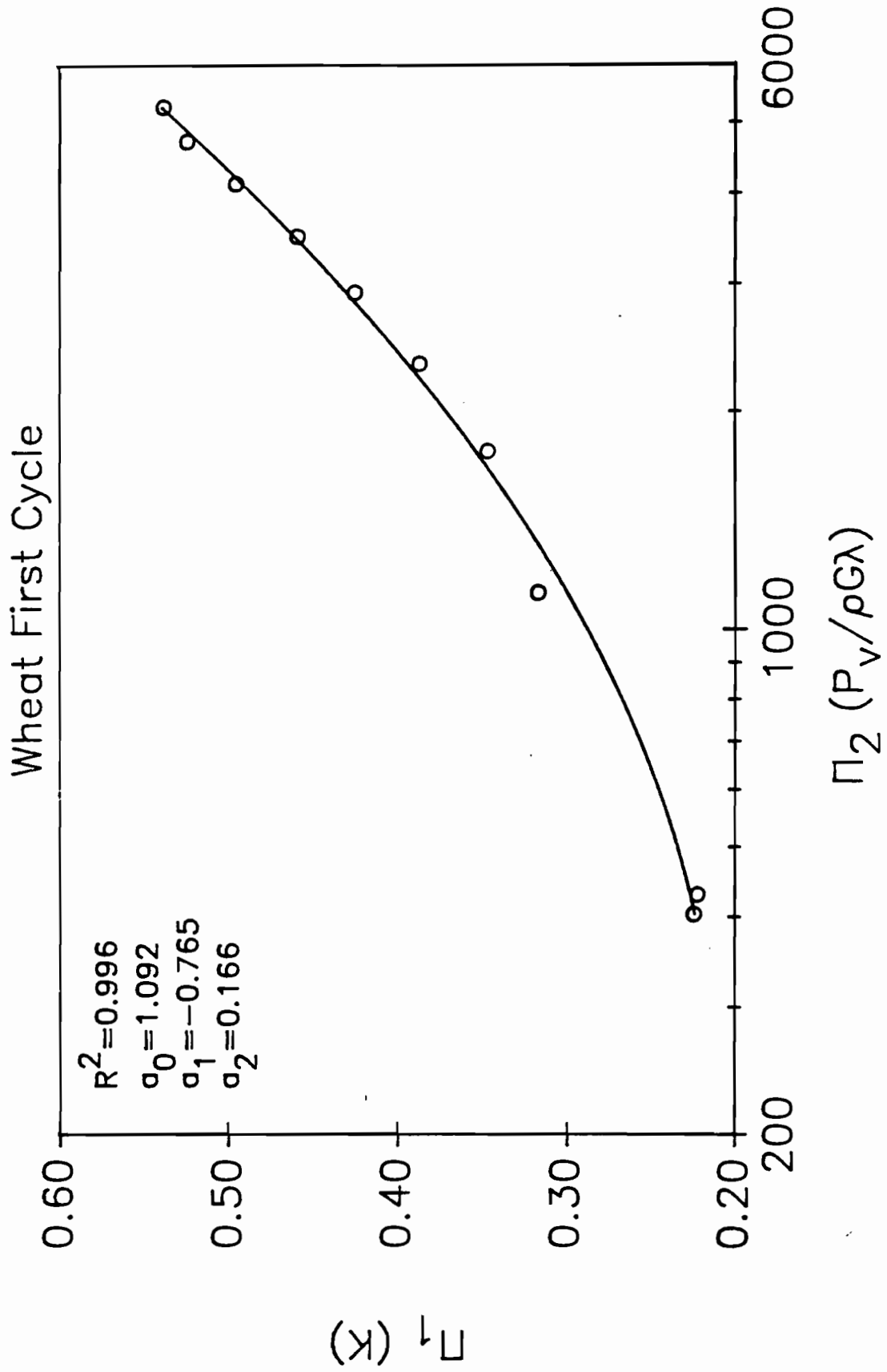
Figure 8.4.1.3. Semi-log plot of Π_1 versus Π_2 for first loading cycle of wheat
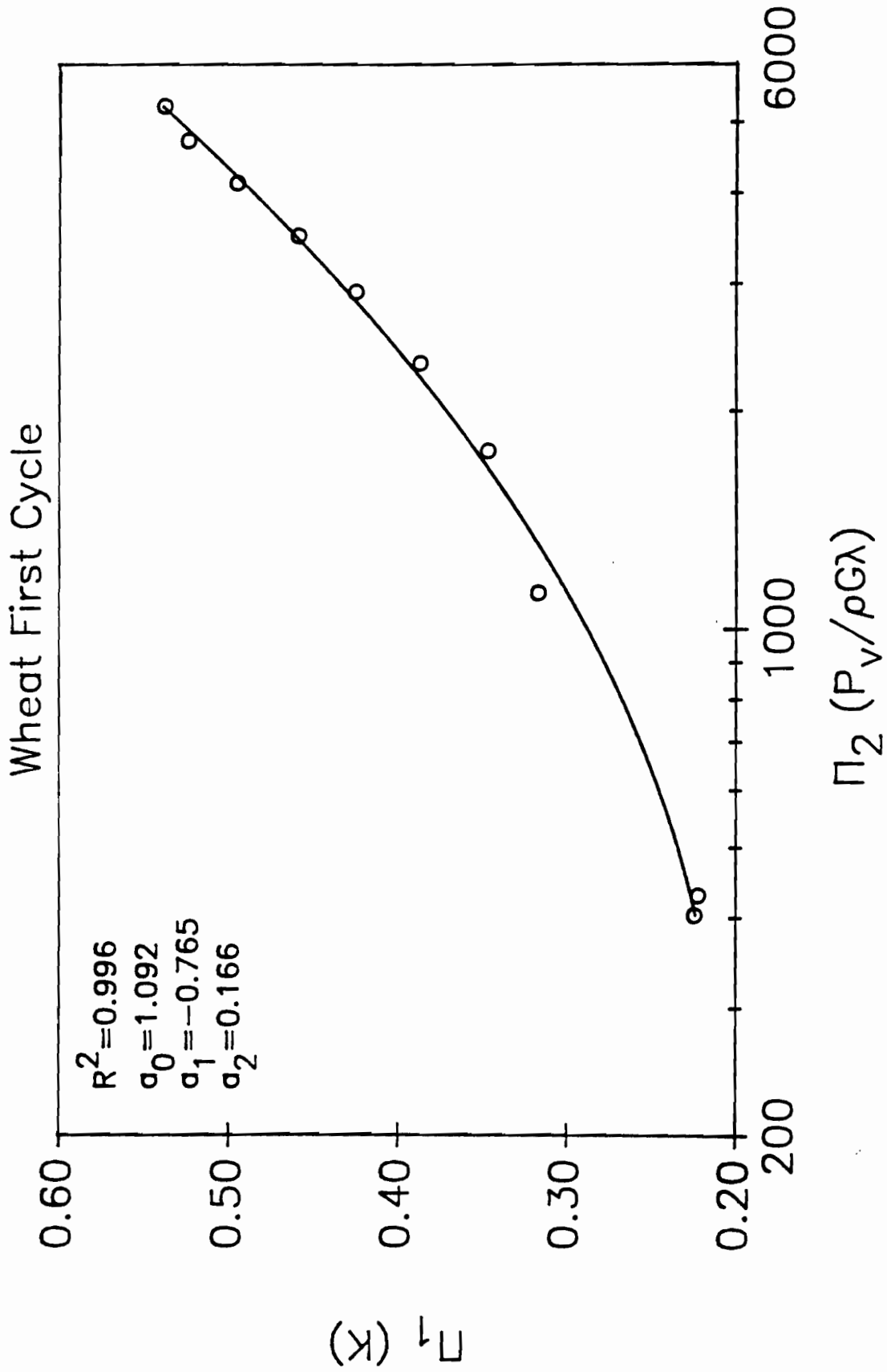
Figure 8.4.1.3. Semi-log plot of Π_1 versus Π_2 for first loading cycle of wheat
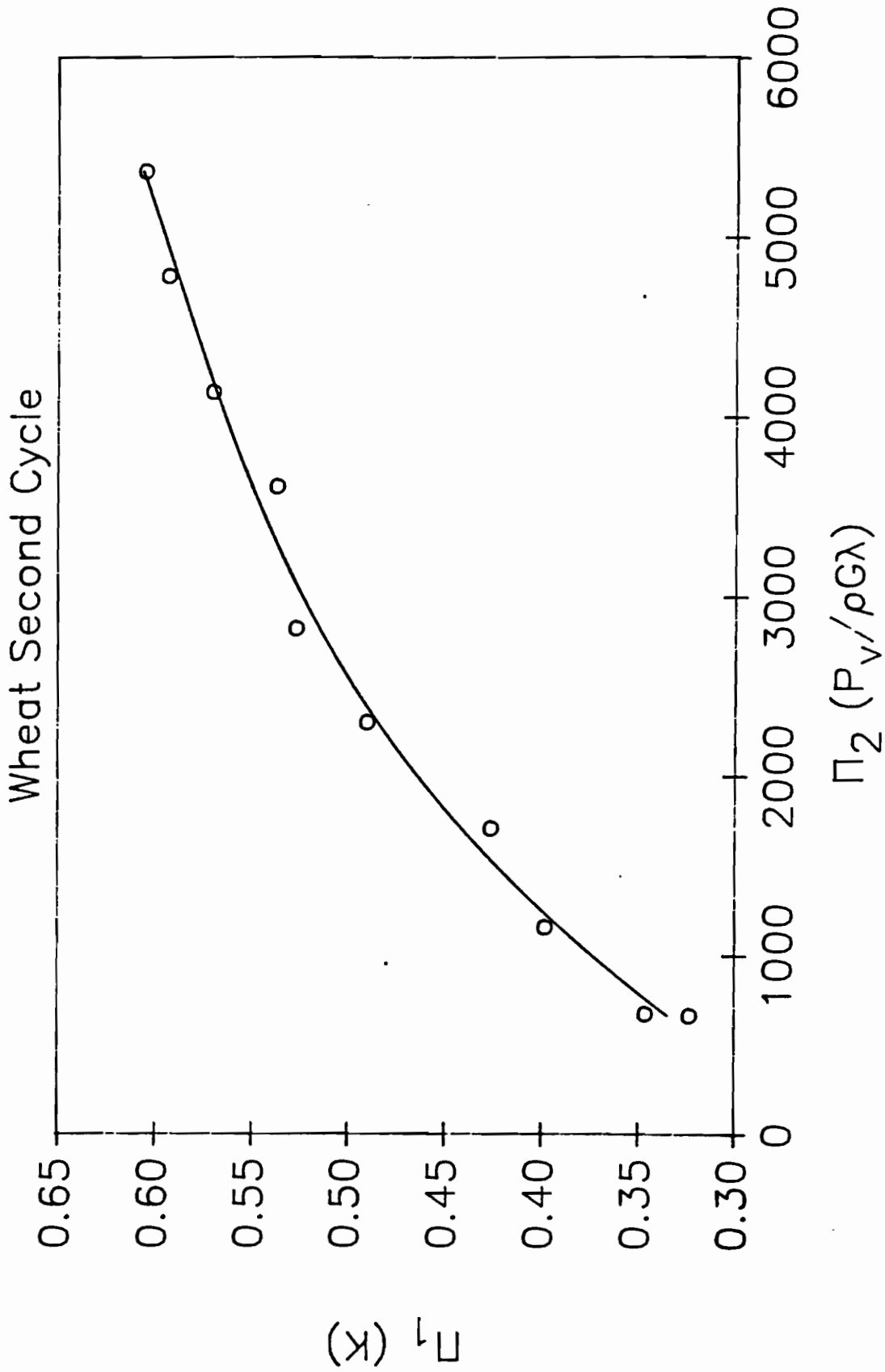
Figure 8.4.2.1.   Linear plot of Π_1 versus Π_2 for second loading cycle
of wheat
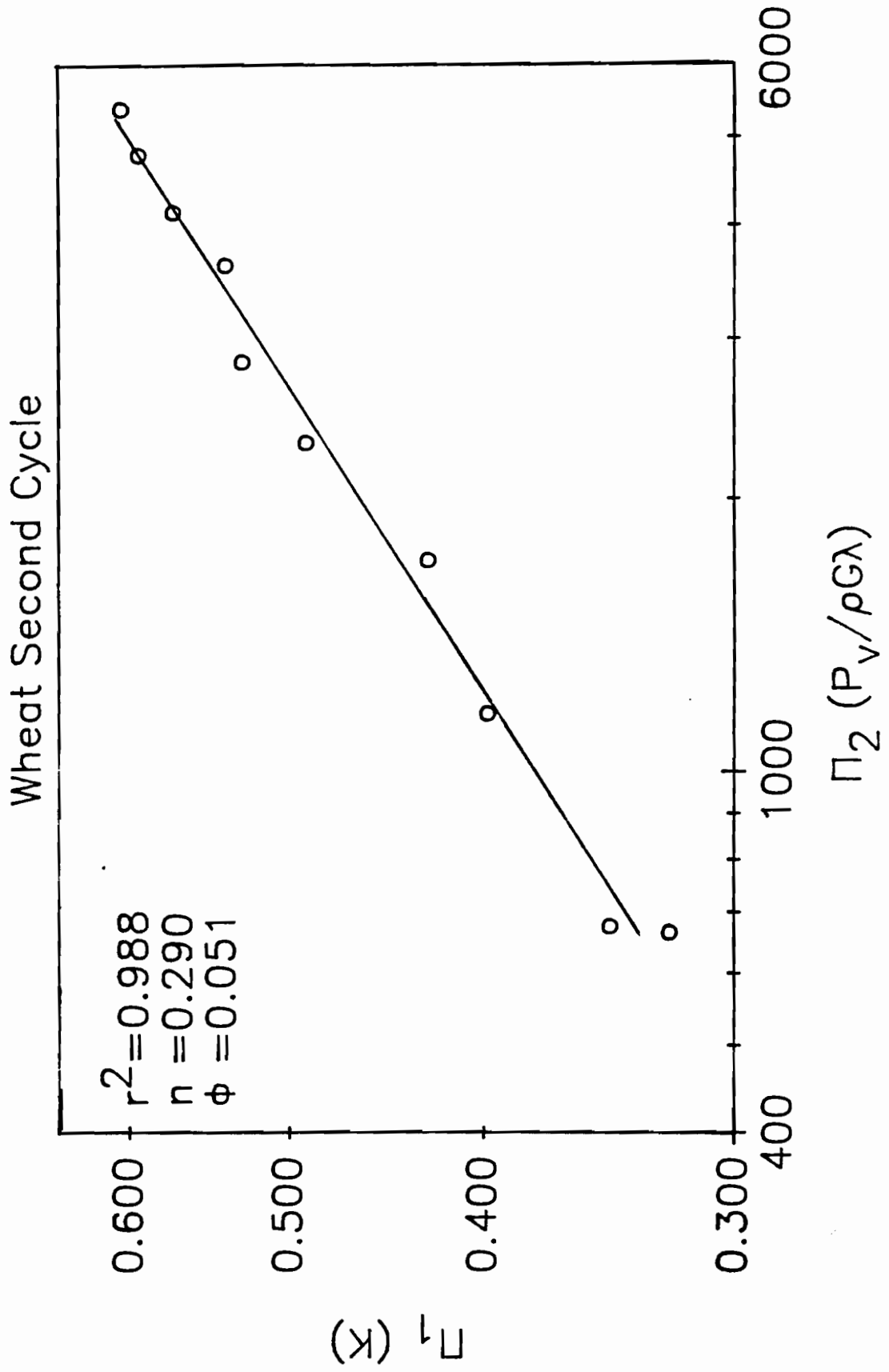
Figure 8.4.2.2. Log-log plot for Π_1 versus Π_2 for second loading cycle of wheat
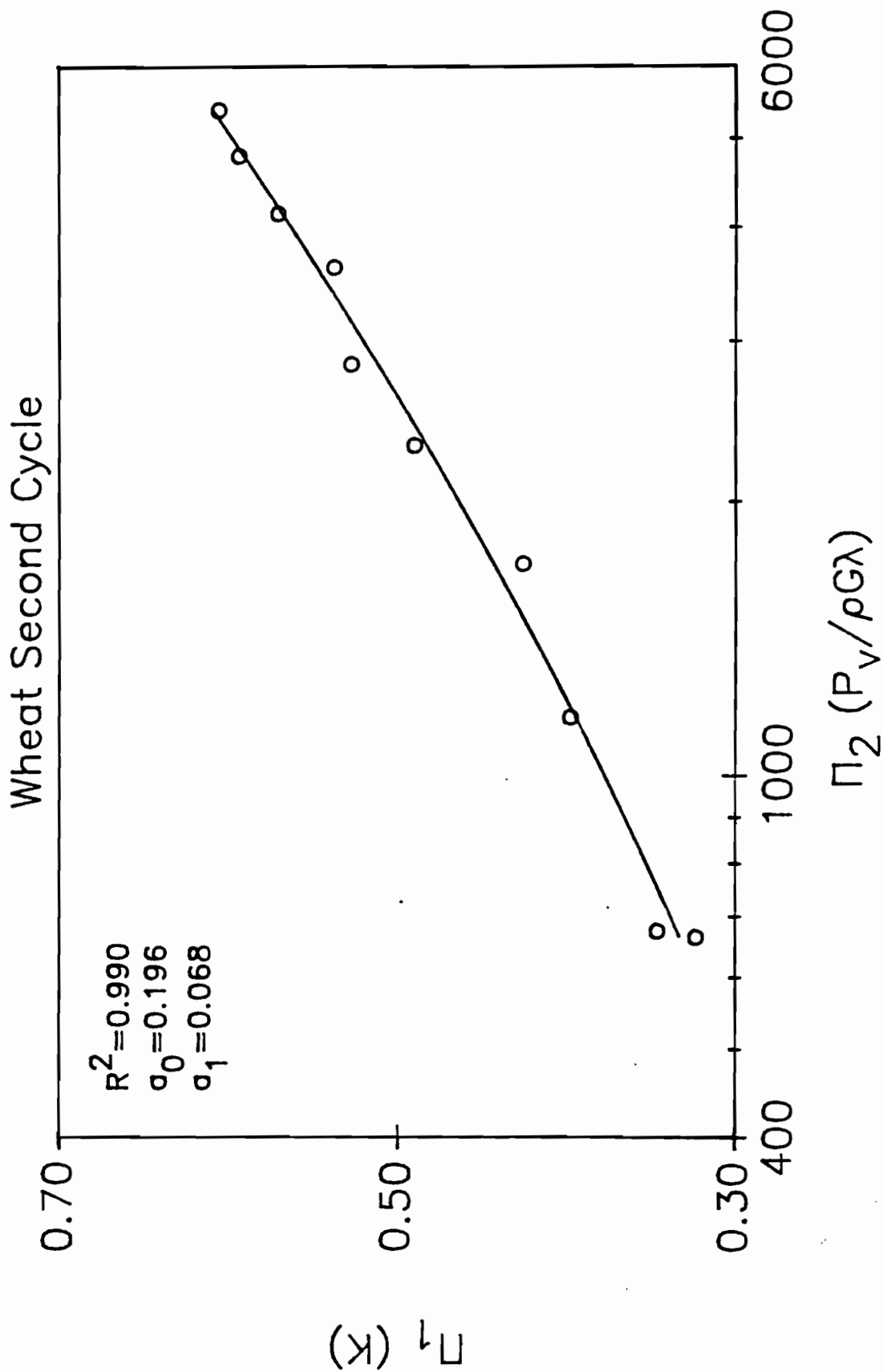
Figure 8.4.2.3.   Semi-log plot of Π_1 versus Π_2 for second loading cycle of wheat

Wheat Third Cycle

Π_1 (K)

Π_2 ($P_v/\rho G\lambda$)
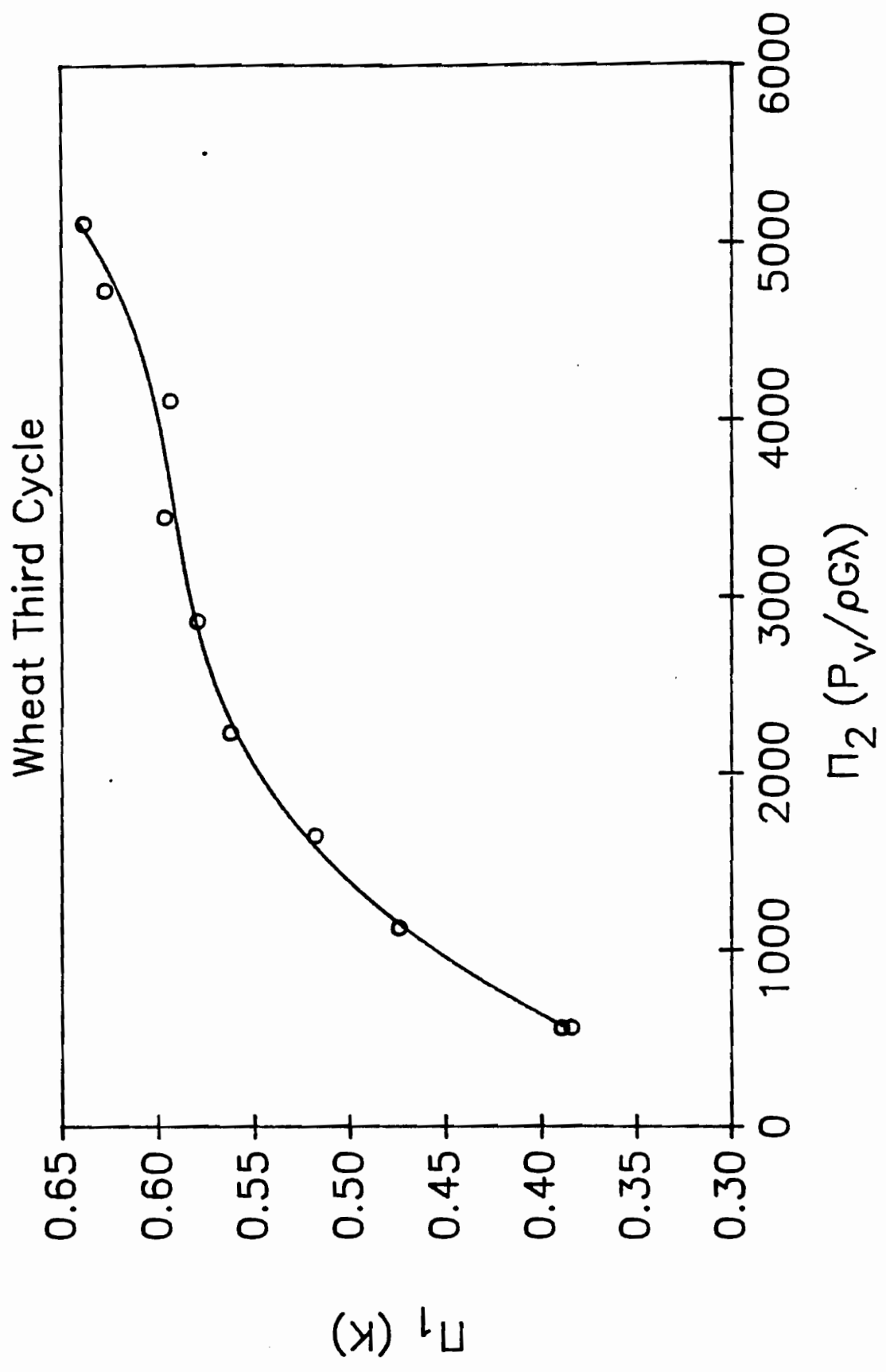
Figure 8.4.3.1.   Linear plot of Π_1 versus Π_2 for third loading cycle of wheat
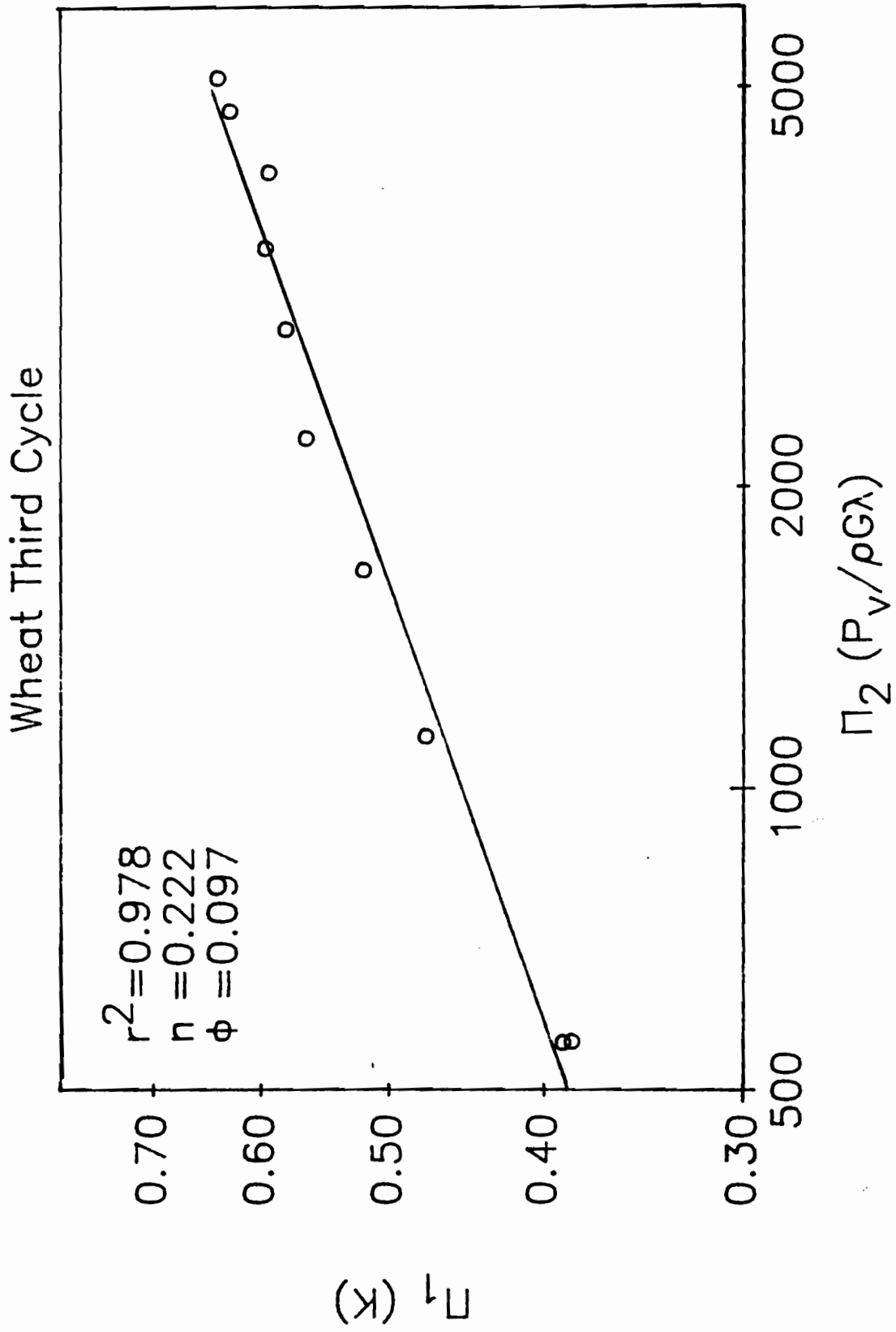
Figure 8.4.3.2. Log-log plot of Π_1 versus Π_2 for third loading cycle of wheat
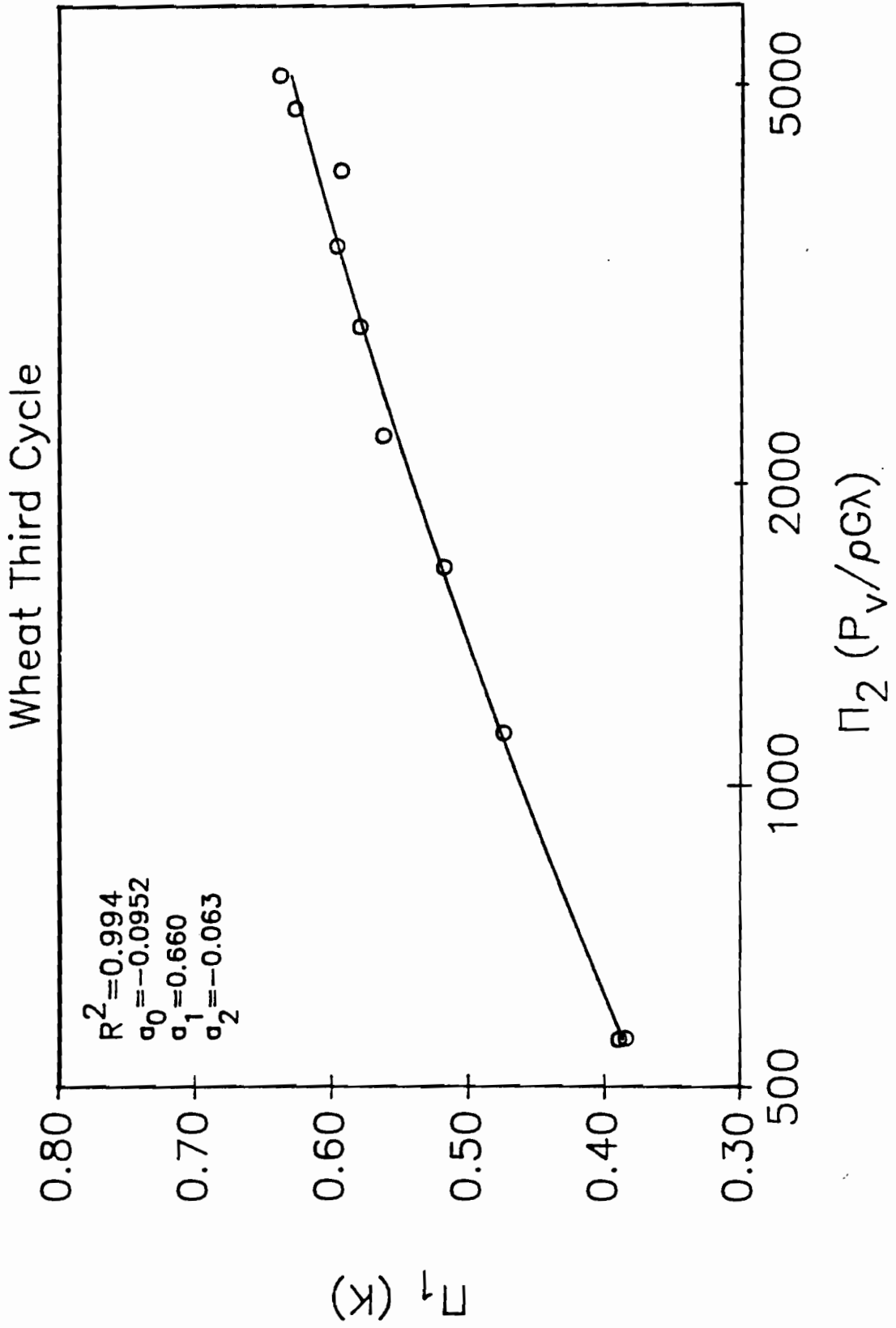
Figure 8.4.3.3. Semi-log plot of Π_1 versus Π_2 for third loading cycle of wheat
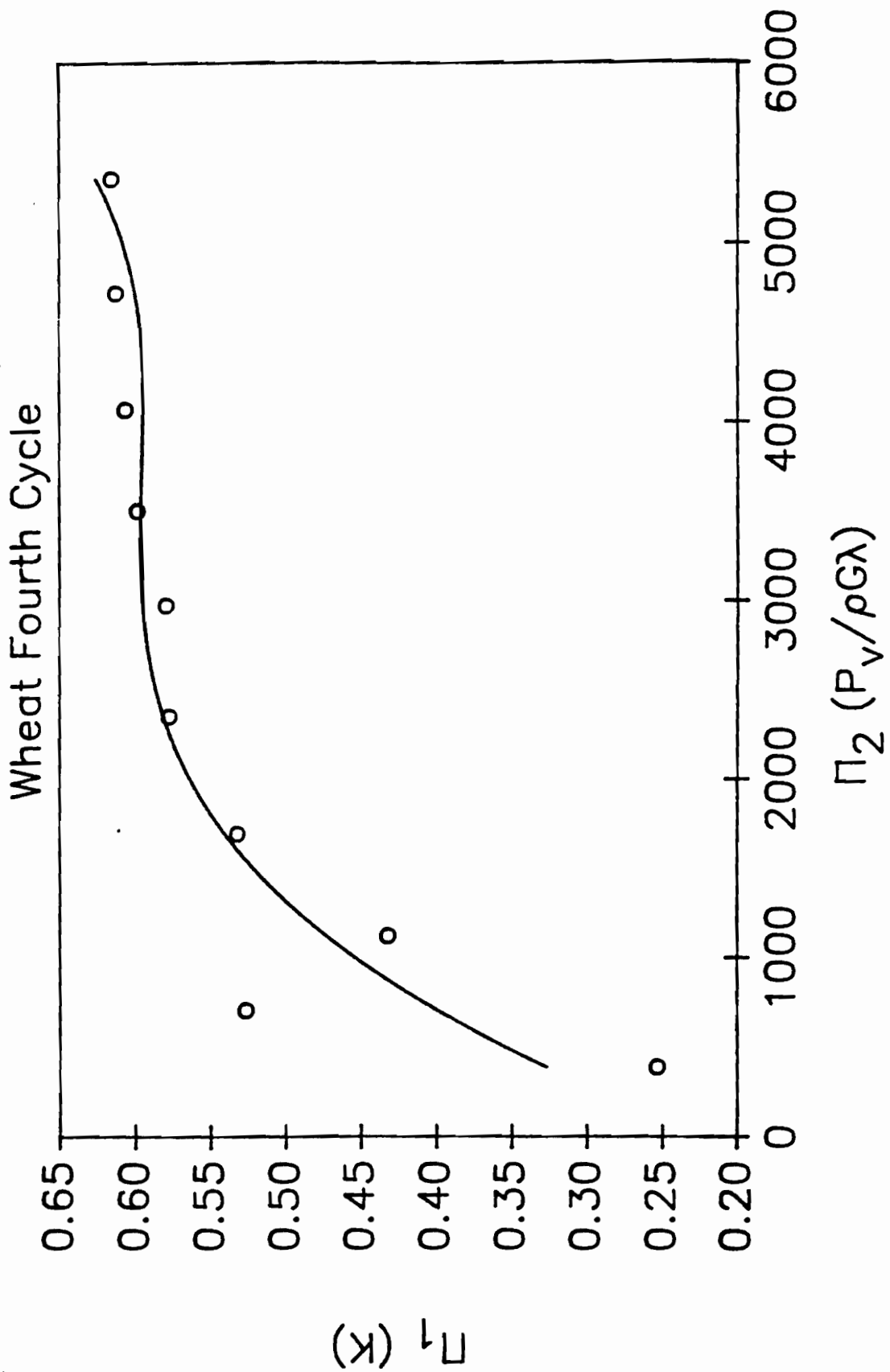
Figure 8.4.4.1.   Linear plot of Π_1 versus Π_2 for fourth loading cycle
of wheat
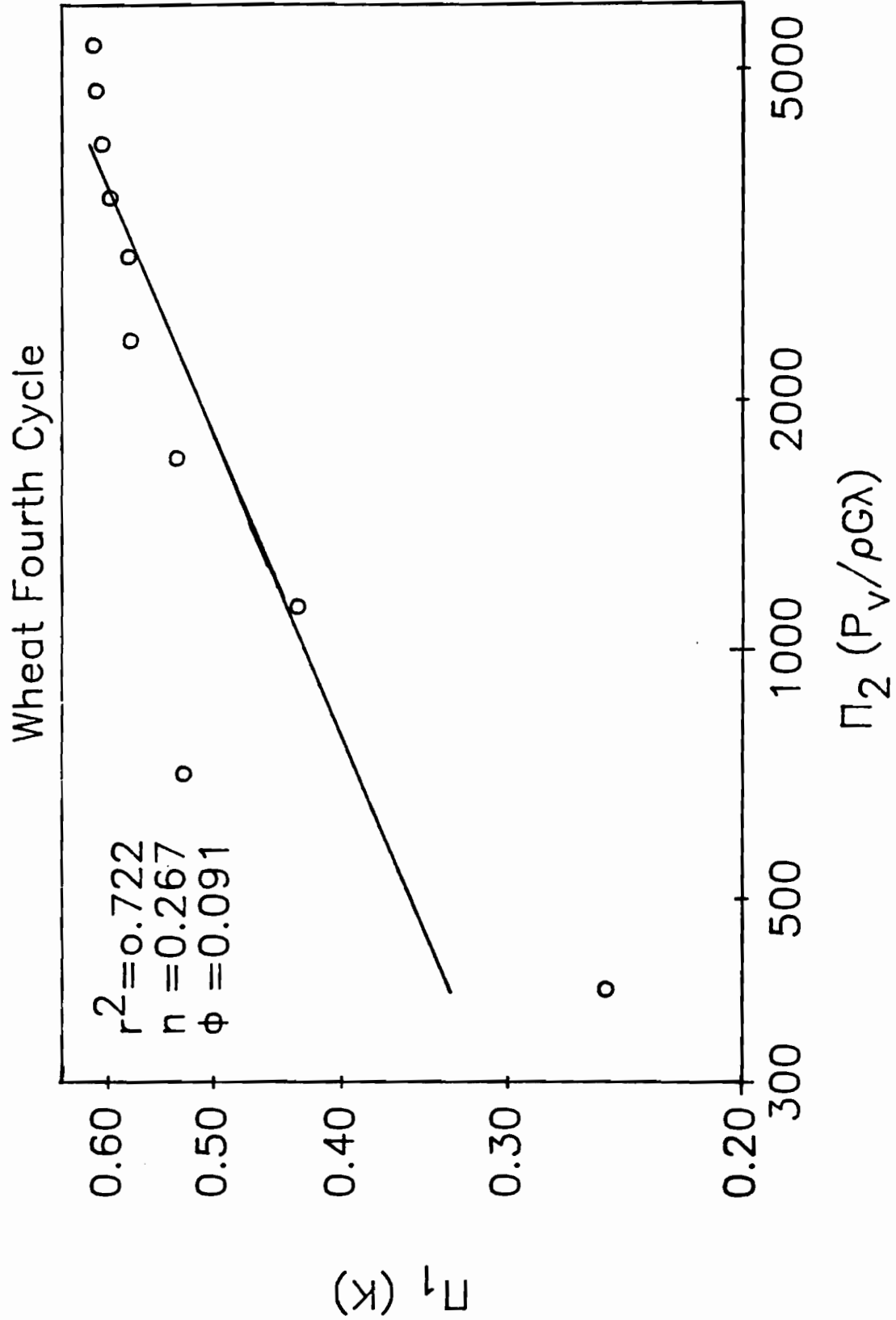
Figure 8.4.4.2. Log-log plot of Π_1 versus Π_2 for fourth loading cycle of wheat
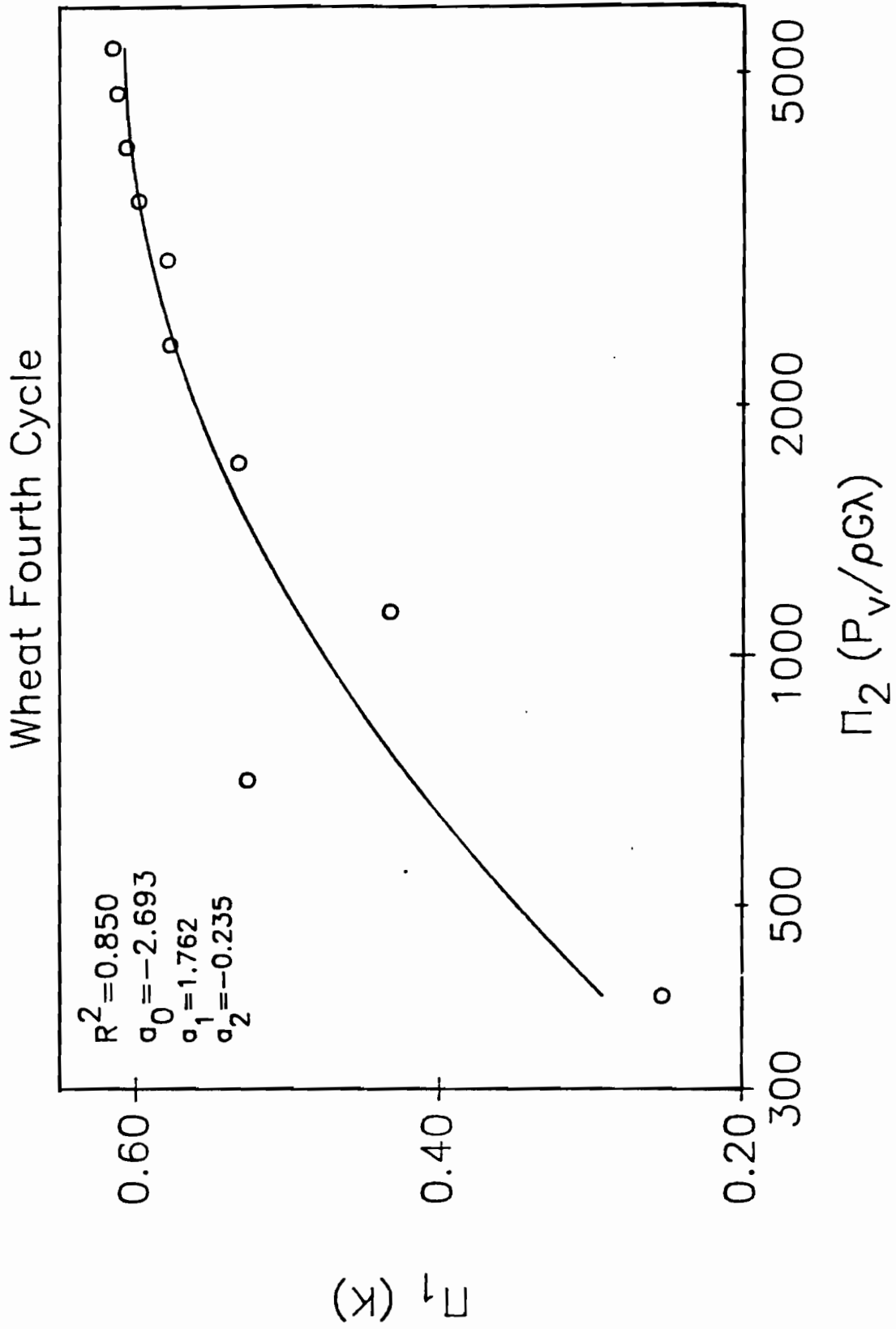
Figure 8.4.4.3.   Semi-log plot of Π_1 versus Π_2 for fourth loading cycle of wheat

Wheat Fourth Cycle

$R^2 = 0.850$
$a_0 = -2.693$
$a_1 = 1.762$
$a_2 = -0.235$

Π_2 $(P_v/\rho G\lambda)$

Π_1 (K)
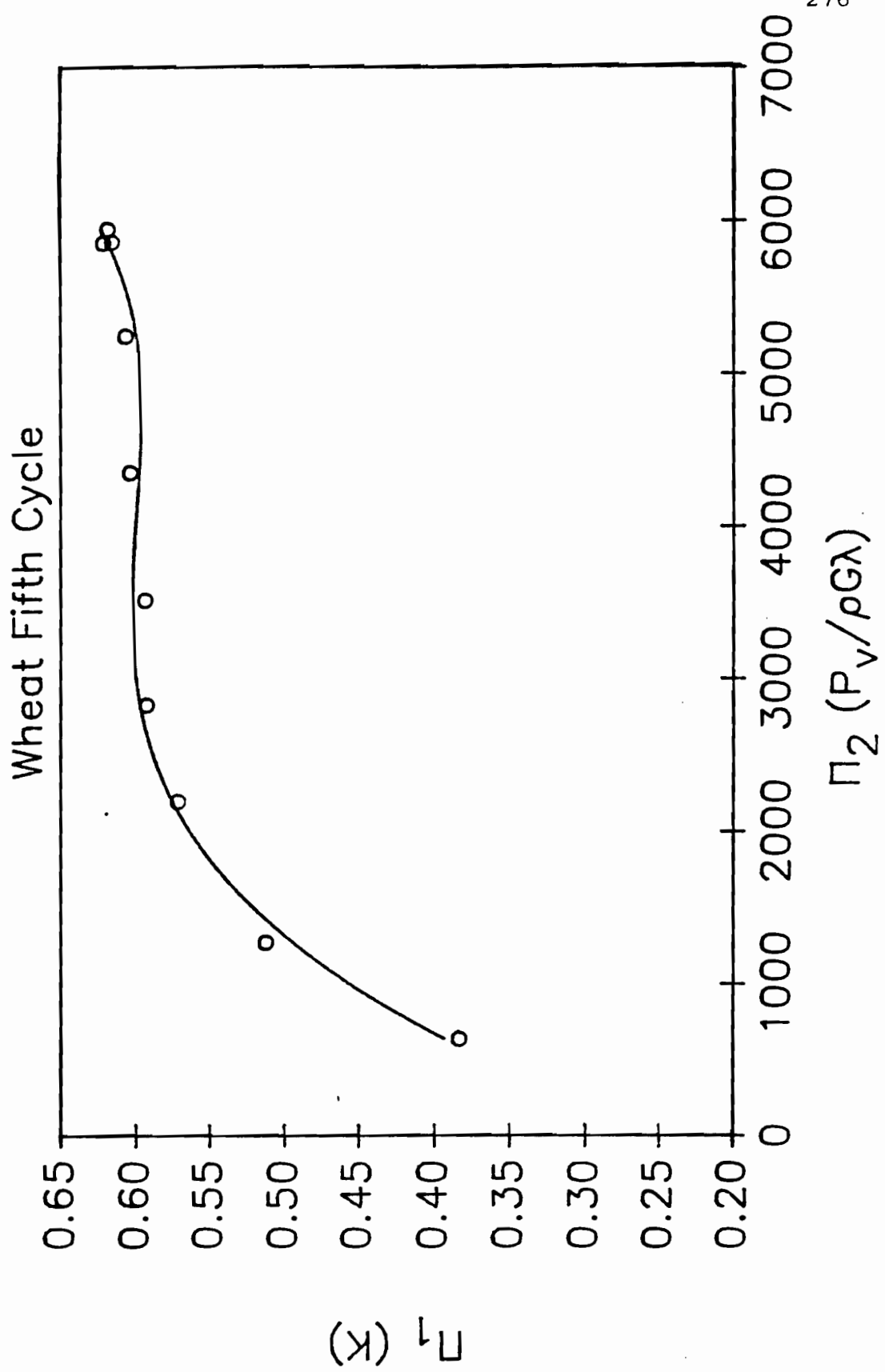
Figure 8.4.5.1.   Linear plot of Π_1 versus Π_2 for fifth loading cycle of wheat
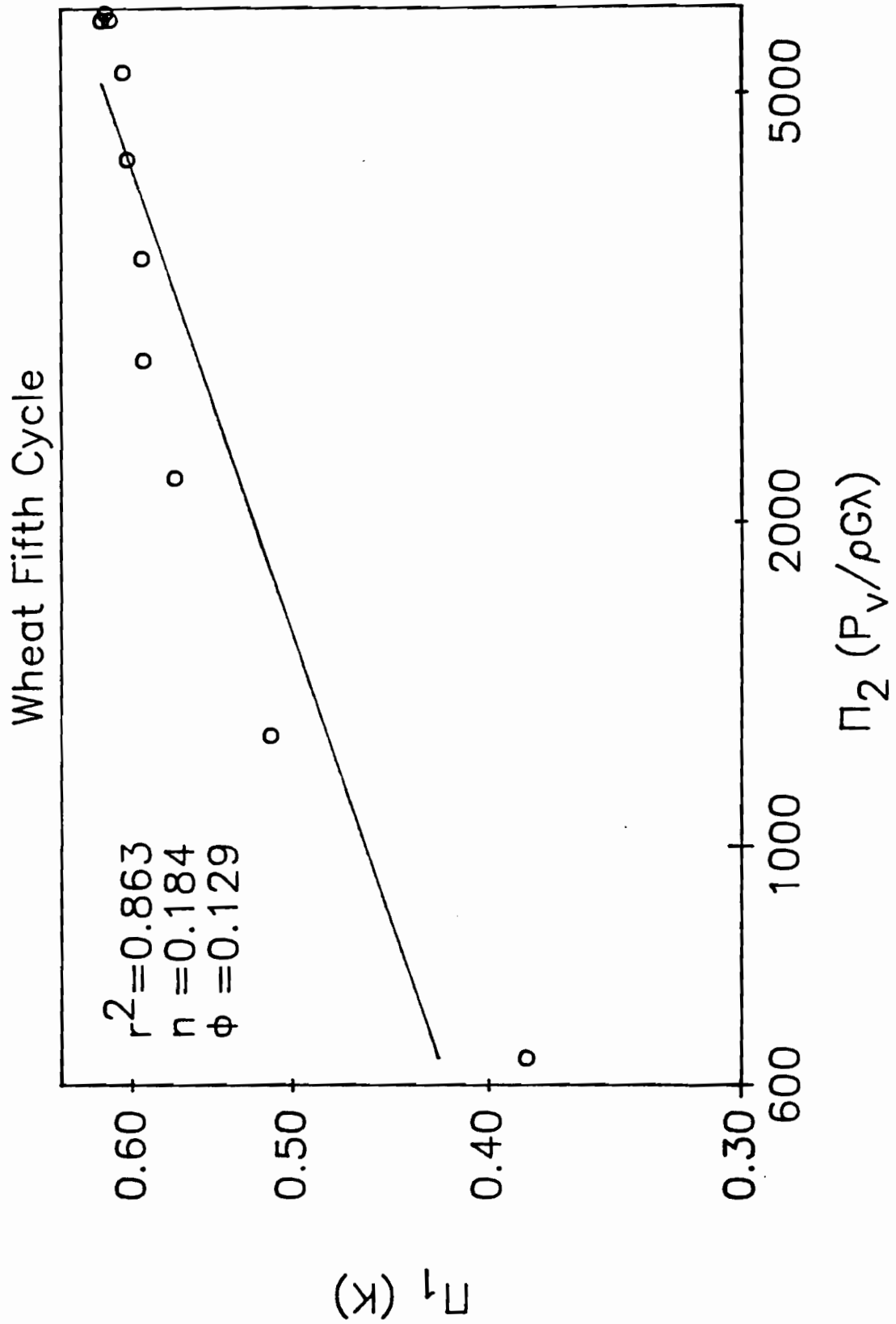
Figure 8.4.5.2. Log-log plot of Π_1 versus Π_2 for fifth loading cycle of wheat
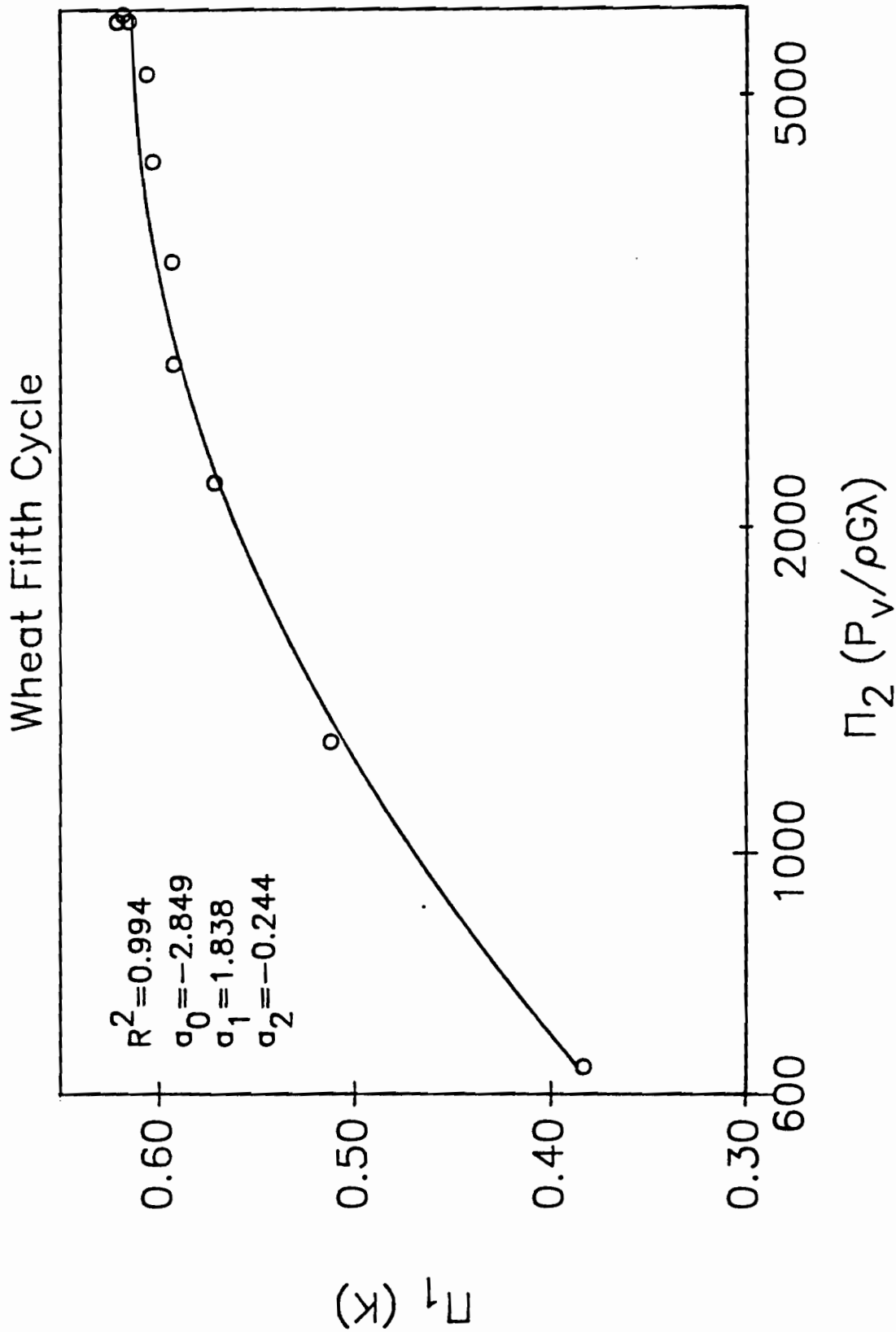
Figure 8.4.5.3.   Semi-log plot of Π_1 versus Π_2 for fifth loading cycle of wheat

Figure 8.5.1.1.   Linear plot of Π_1 versus Π_2 for first loading cycle of soybeans
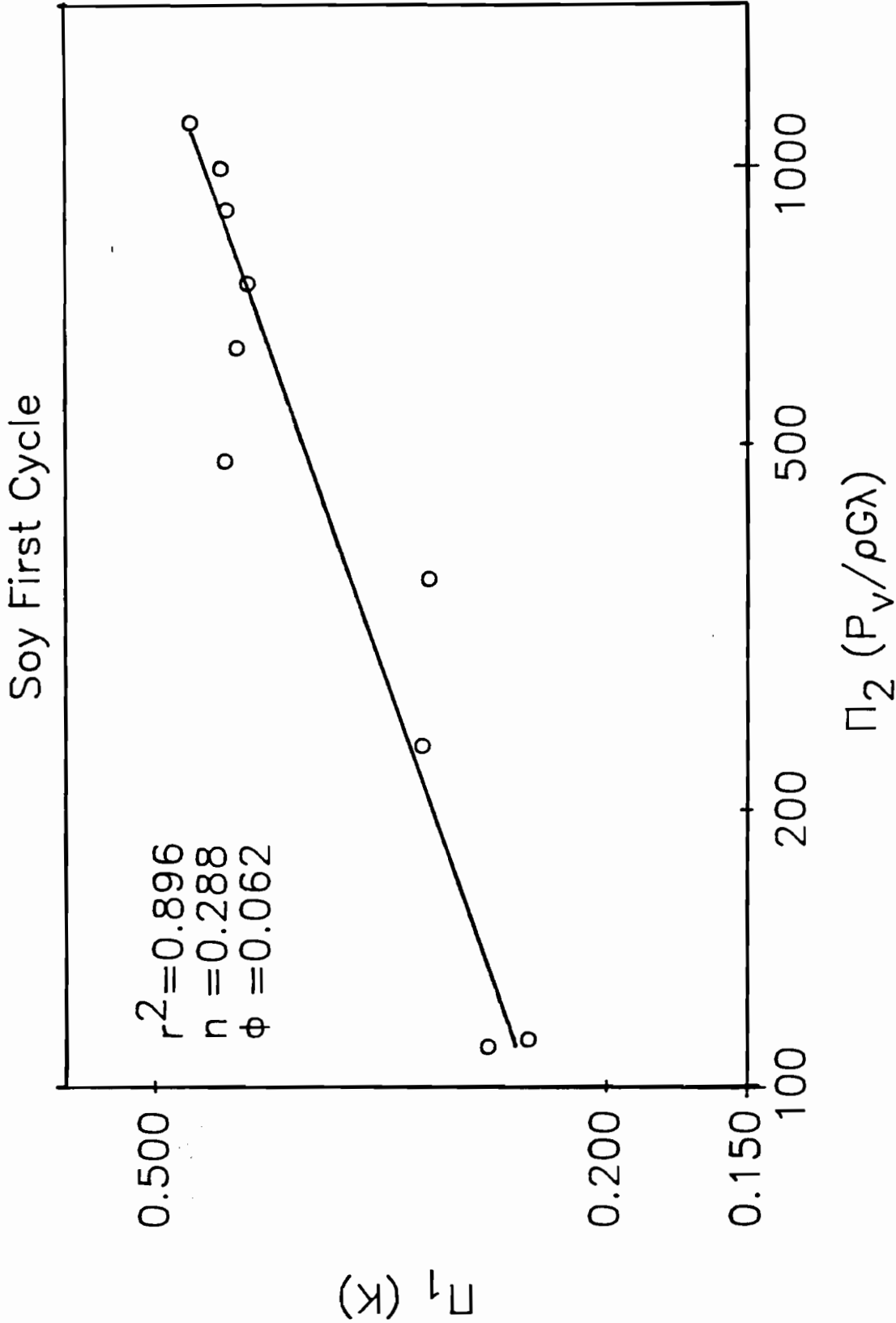
Figure 8.5.1.2. Log-log plot of Π_1 versus Π_2 for first loading cycle of soybeans

Figure 8.5.1.3. Semi-log plot of Π_1 versus Π_2 for first loading cycle of soybeans

Soy Second Cycle

Π_2 $(P_v/\rho G\lambda)$

Π_1 (K)

Figure 8.5.2.1.   Linear plot of Π_1 versus Π_2 for second loading cycle
of soybeans

Figure 8.5.2.2. Log-log plot of Π_1 versus Π_2 for second loading cycle of soybeans
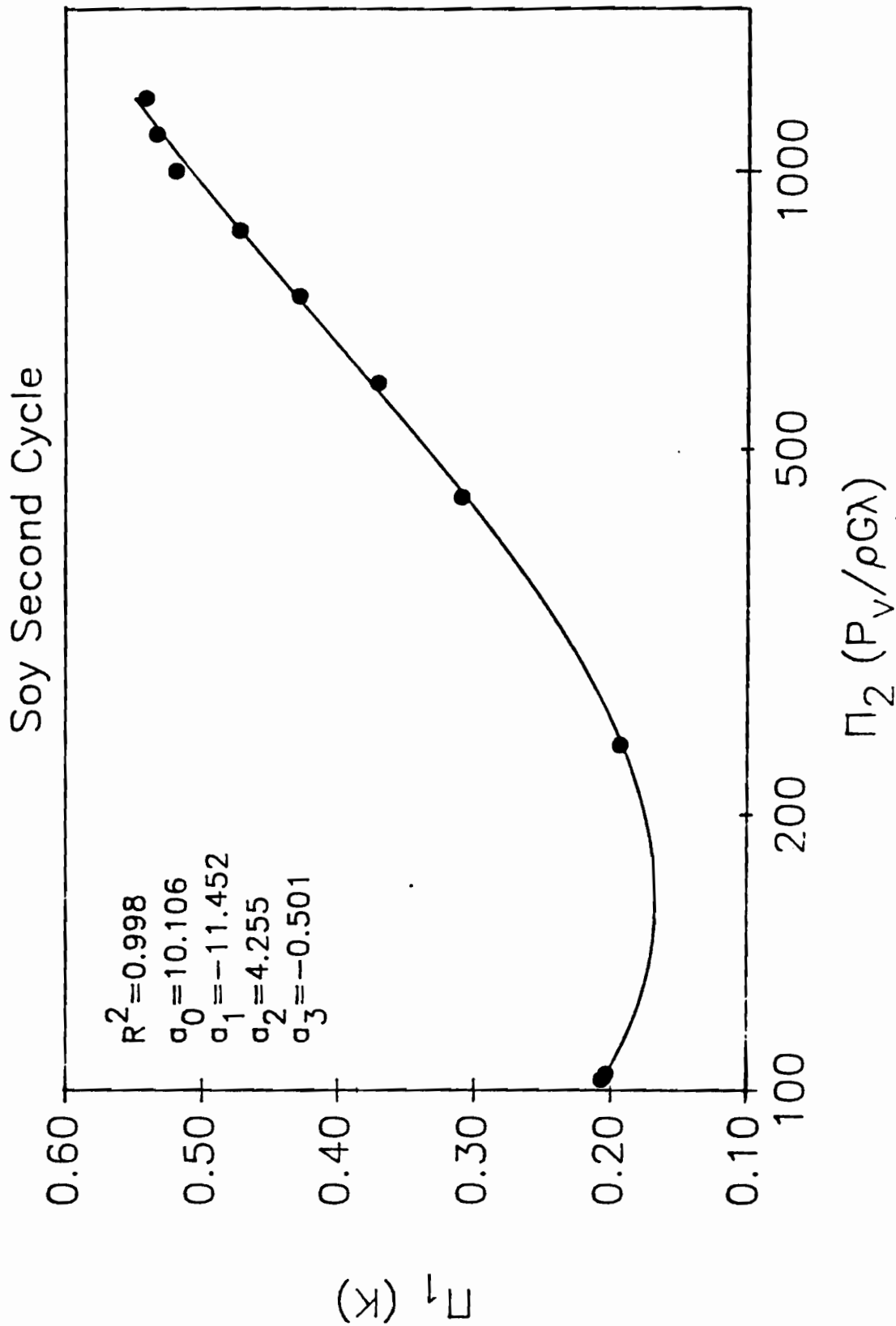
Figure 8.5.2.3.   Semi-log plot of Π_1 versus Π_2 for second loading cycle of soybeans

Soy Third Cycle

Π_1 (K)

Π_2 (P$_v$/ρGλ)
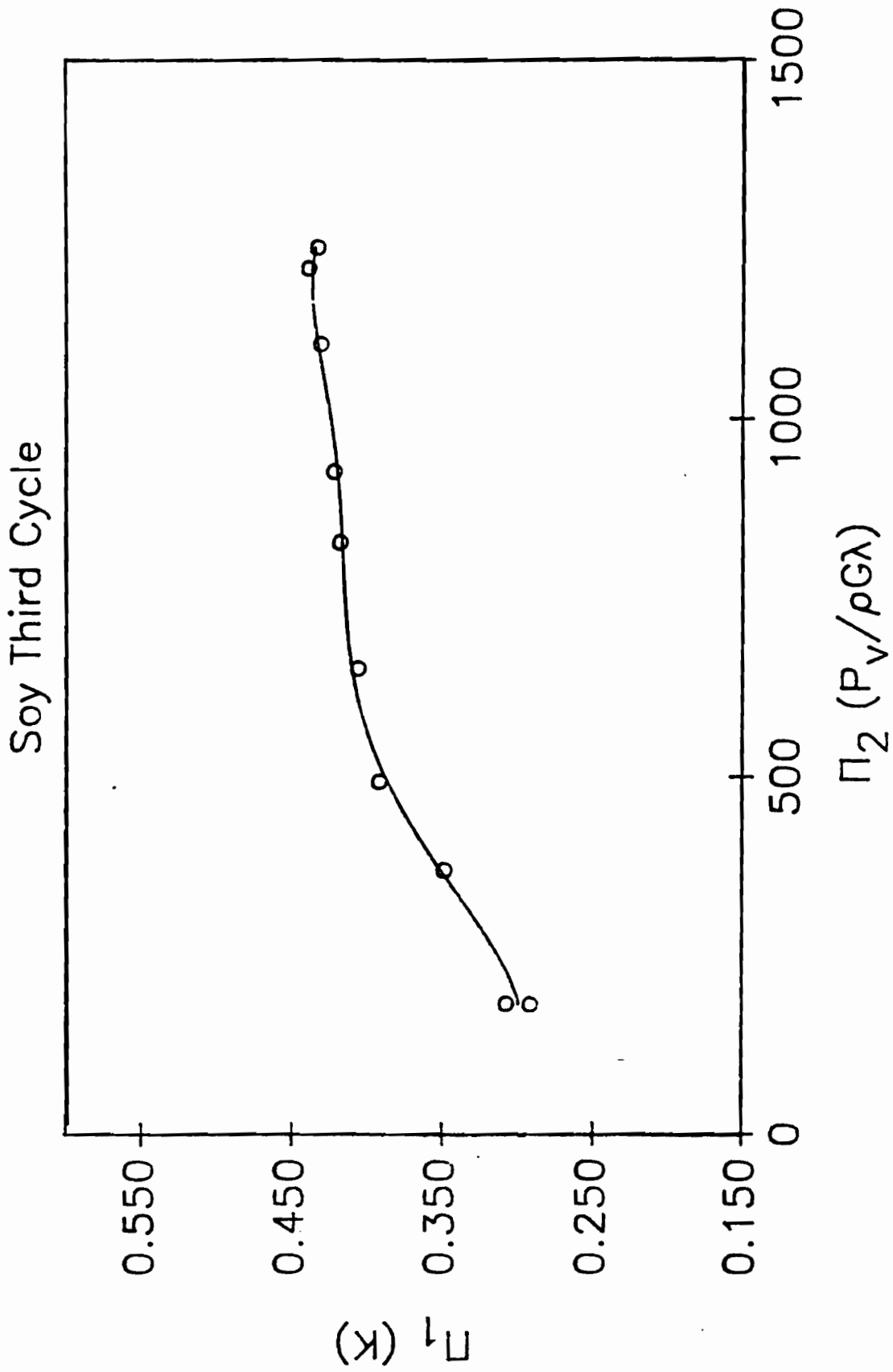
Figure 8.5.3.1. Linear plot of Π_1 versus Π_2 for third loading cycle of soybeans
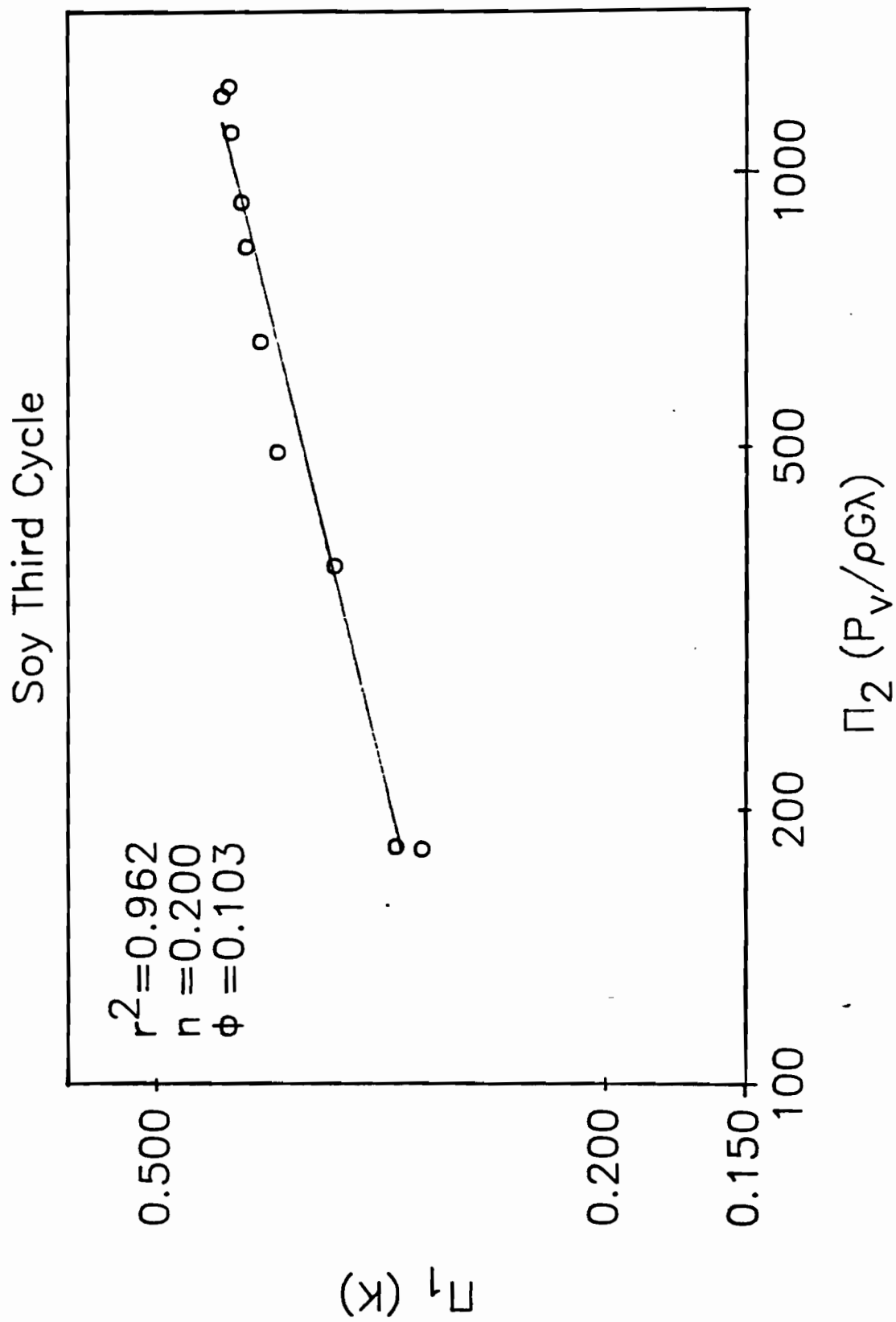
Figure 8.5.3.2. Log-log plot of Π_1 versus Π_2 for third loading cycle of soybeans
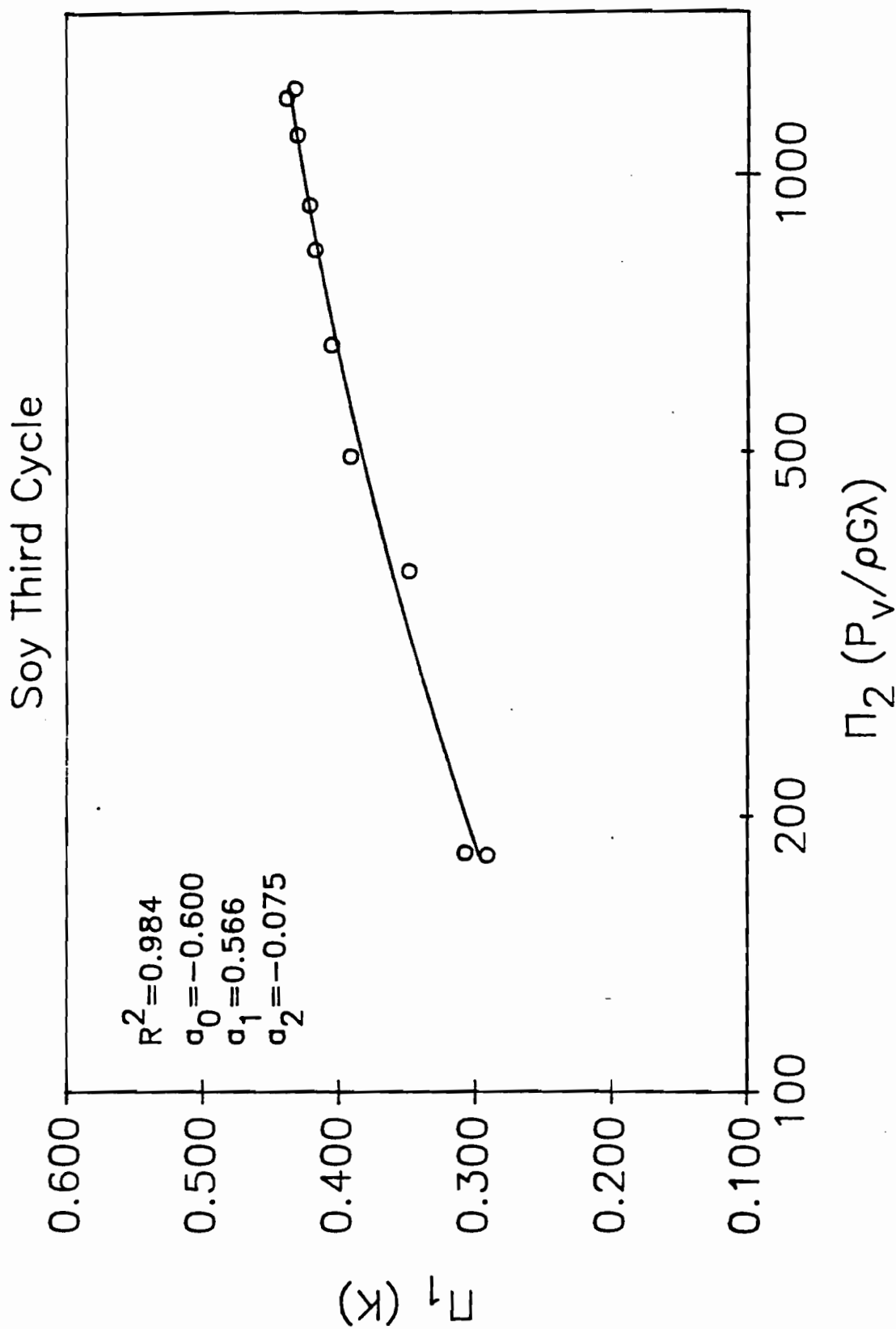
Figure .8.5.3.3. Semi-log plot of Π_1 versus Π_2 for third loading cycle of soybeans

Figure 8.5.4.1. Linear plot of Π_1 versus Π_2 for fourth loading cycle of soybeans

Soy Fourth Cycle

$r^2 = 0.711$
$n = -0.028$
$\phi = 0.527$

Π_2 $(P_v/\rho G\lambda)$

Π_1 (K)
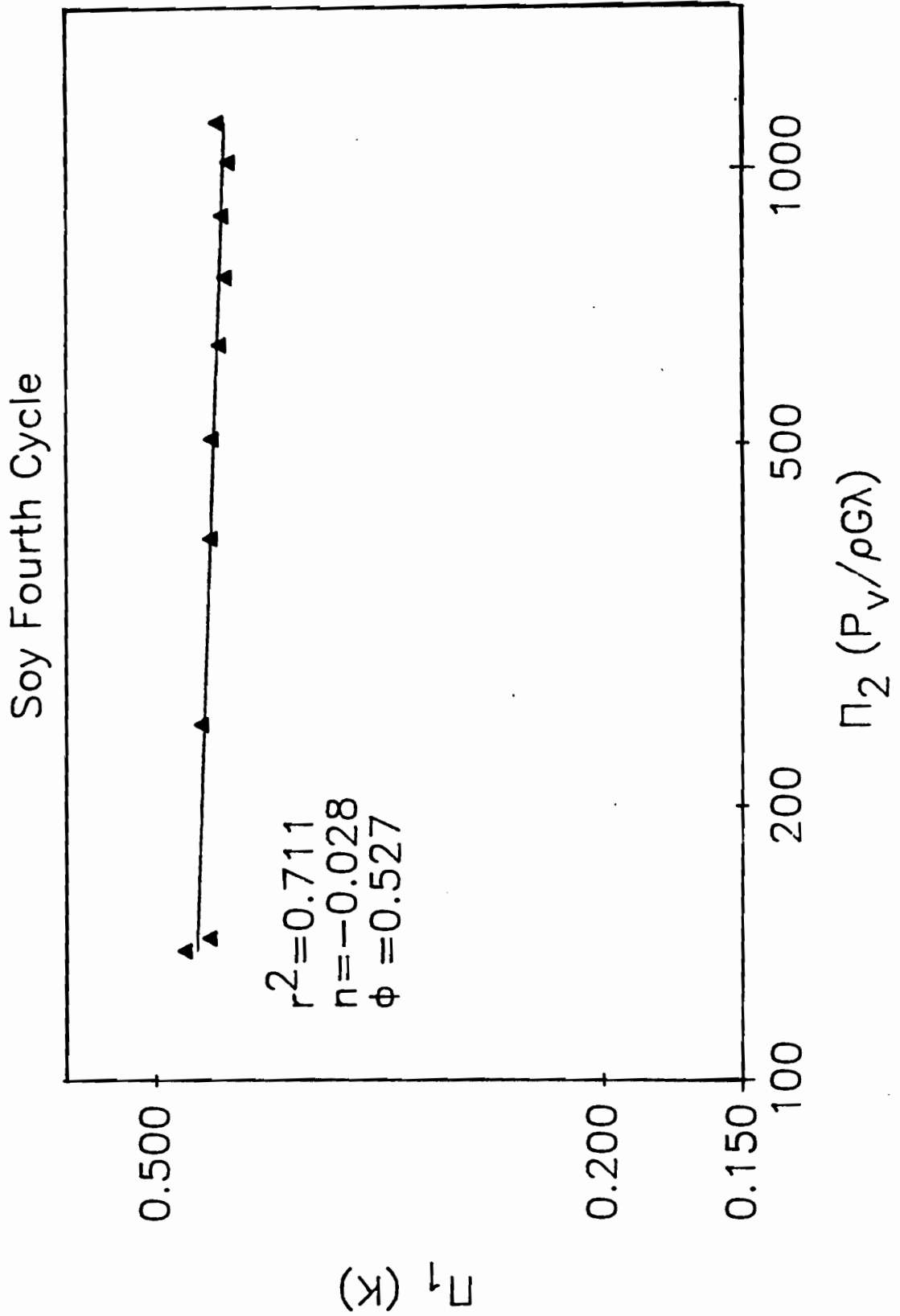
Figure 8.5.4.2. Log-log plot of Π_1 versus Π_2 for fourth loading cycle of soybeans
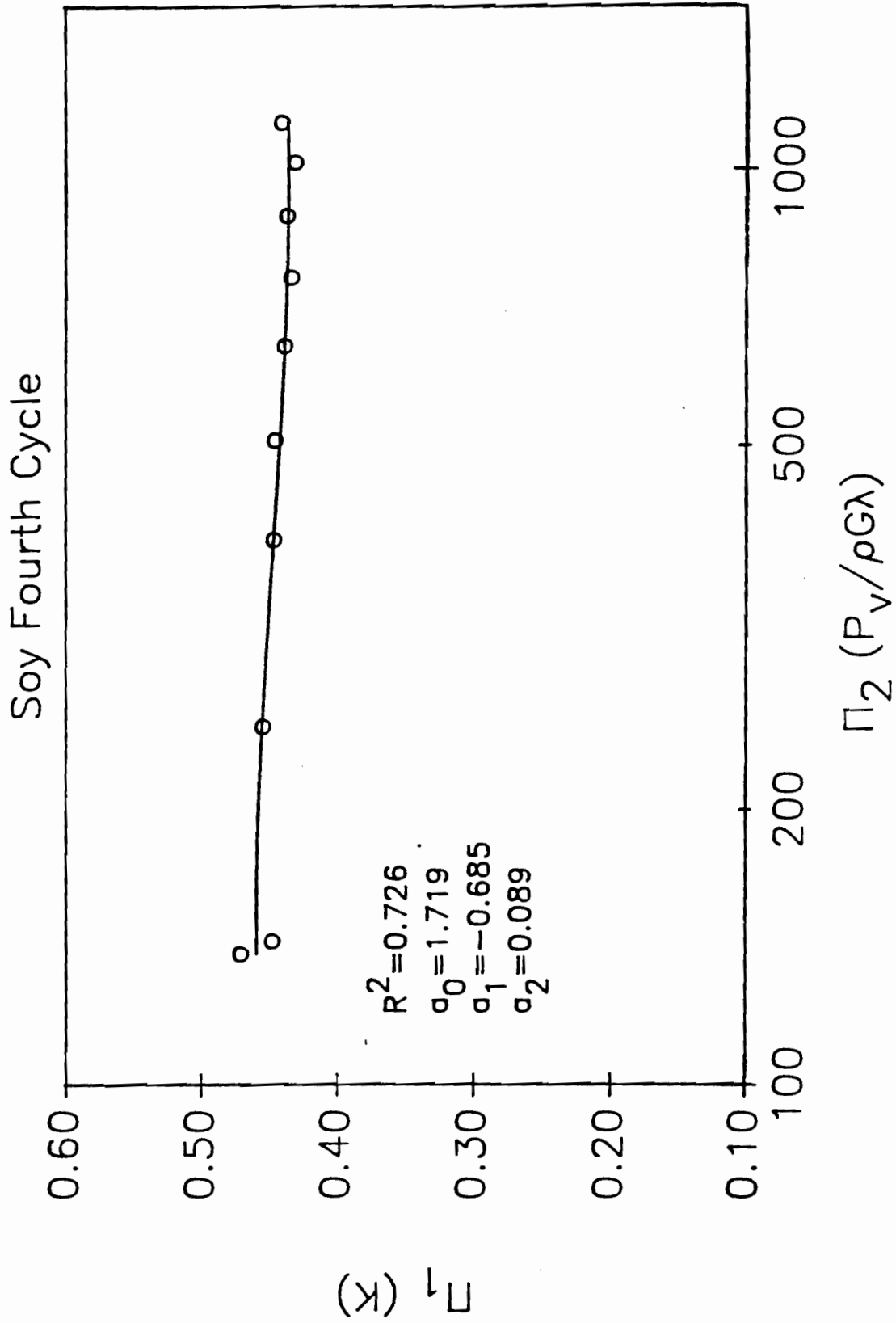
Figure 8.5.4.3. Semi-log plot of Π_1 versus Π_2 for fourth loading cycle. of soybeans
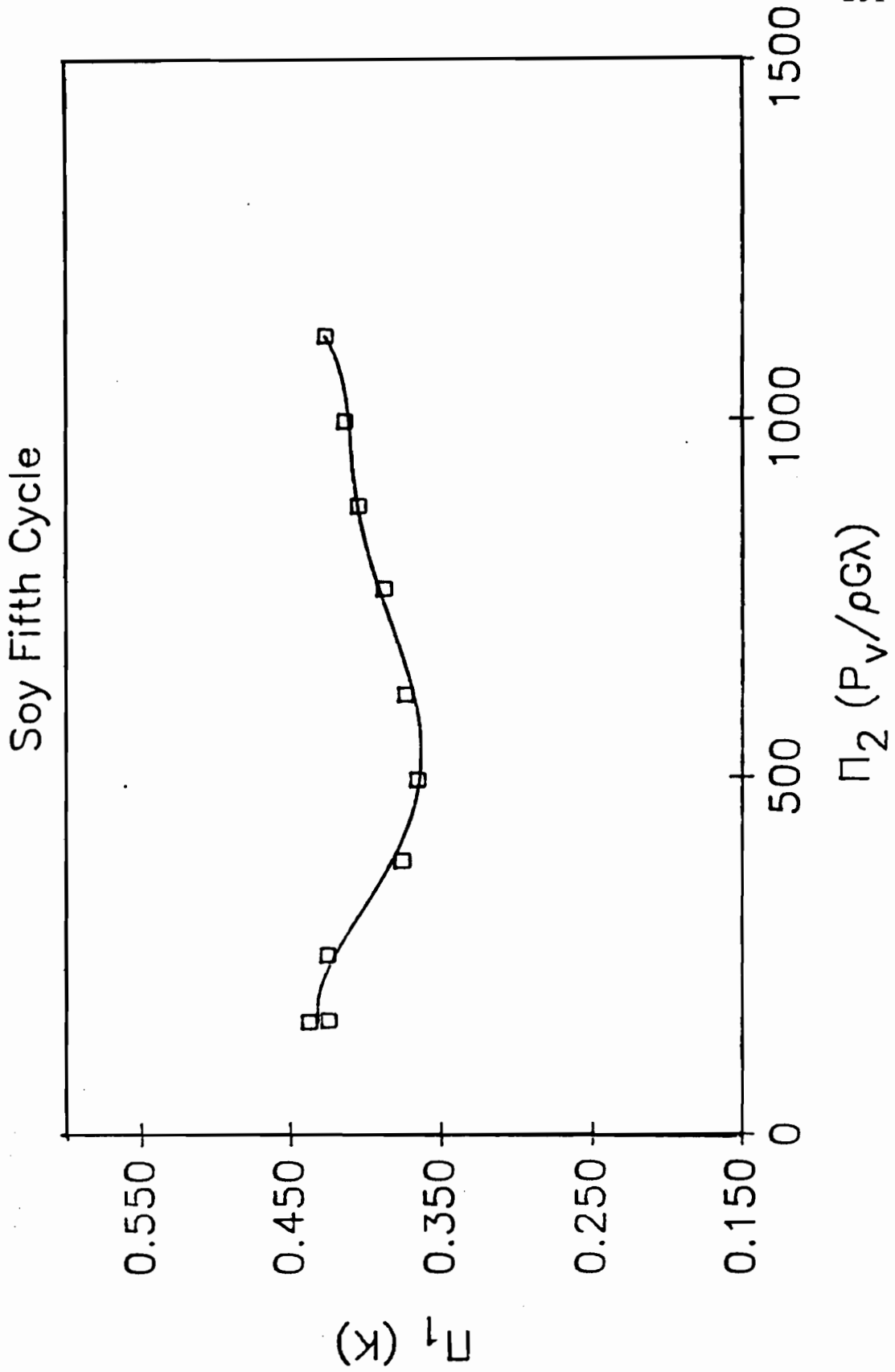
Figure 8.5.5.1.   Linear plot of Π_1 versus Π_2 for fifth loading cycle of soybeans
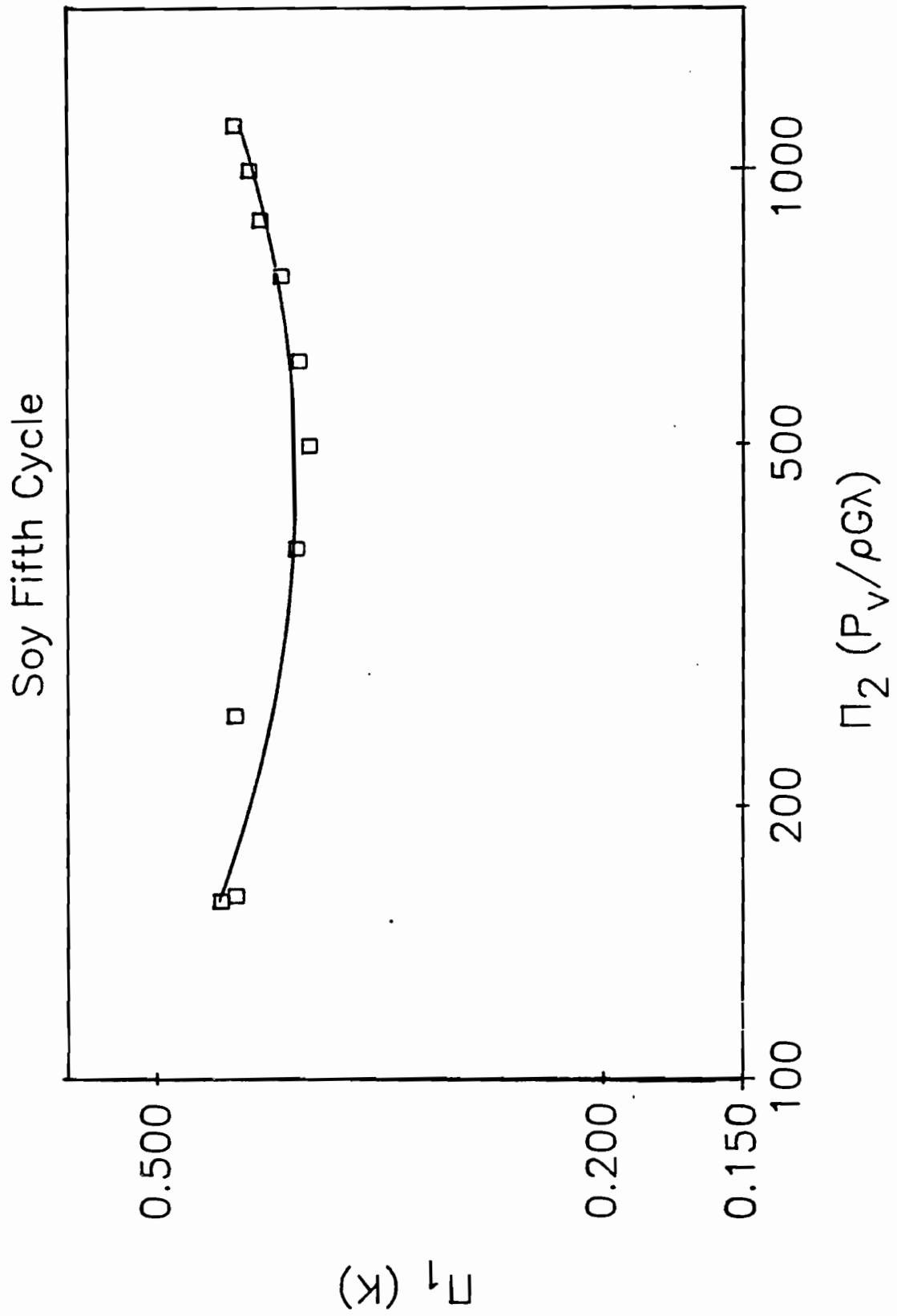
Figure 8.5.5.2. Log-log plot of Π_1 versus Π_2 for fifth loading cycle of soybeans
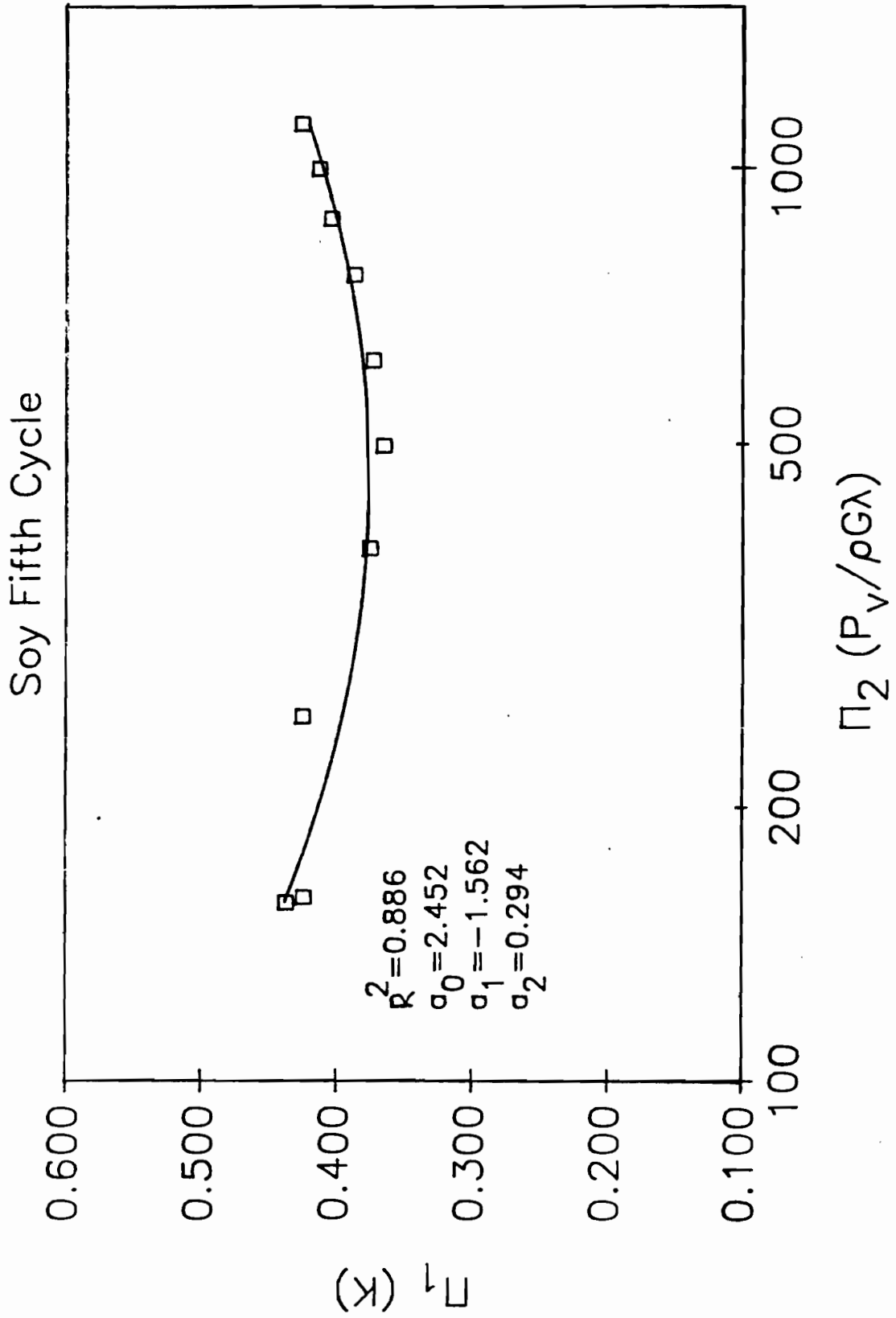
Figure 8.5.5.3. Semi-log plot of Π_1 versus Π_2 for fifth loading cycle of soybeans

Soy Fifth Cycle

$R^2 = 0.886$
$a_0 = 2.452$
$a_1 = -1.562$
$a_2 = 0.294$

Π_2 $(P_v/\rho G\lambda)$

Π_1 (K)
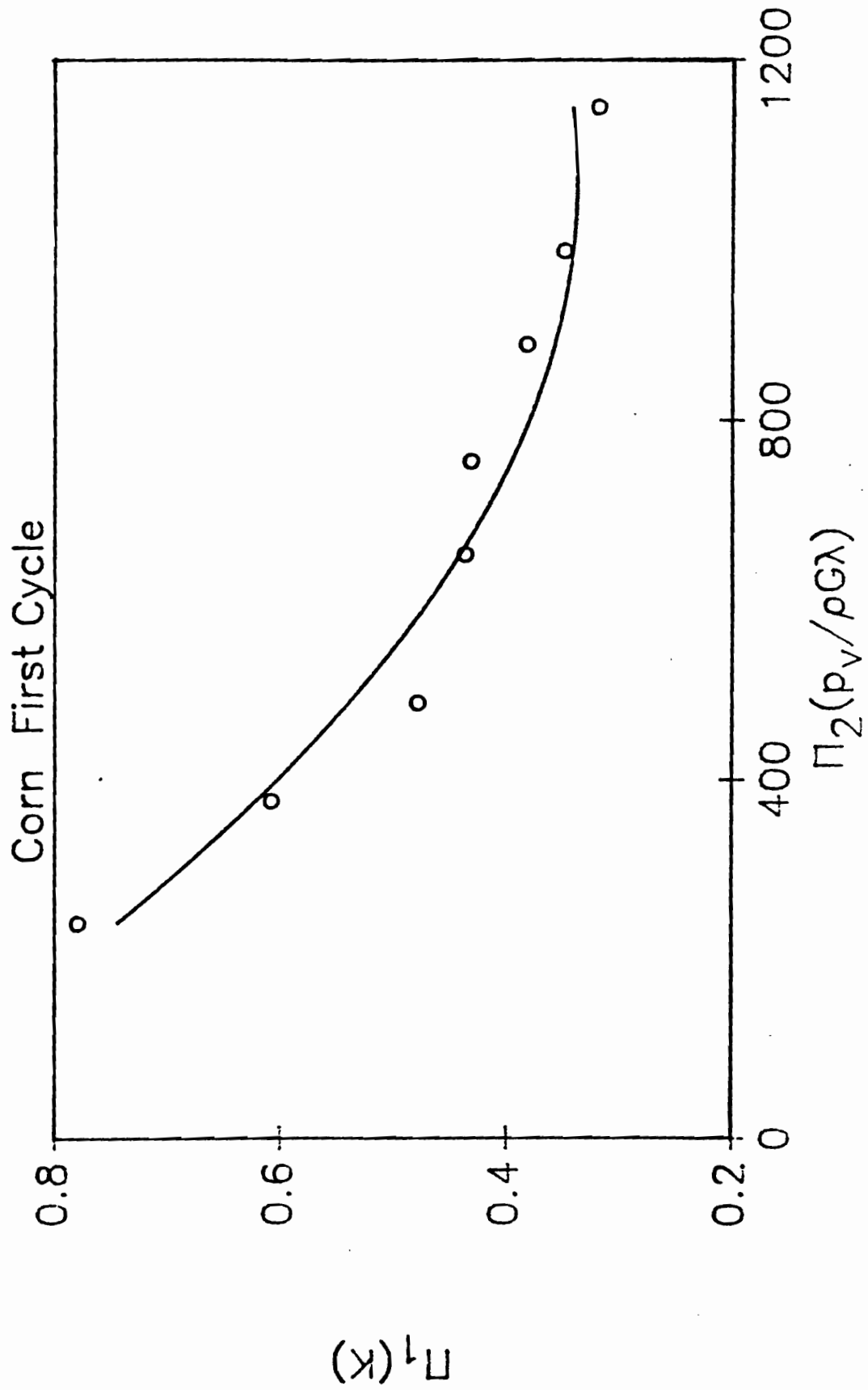
Figure 8.6.1.1.. Linear plot of Π_1 versus Π_2 for first loading cycle of corn
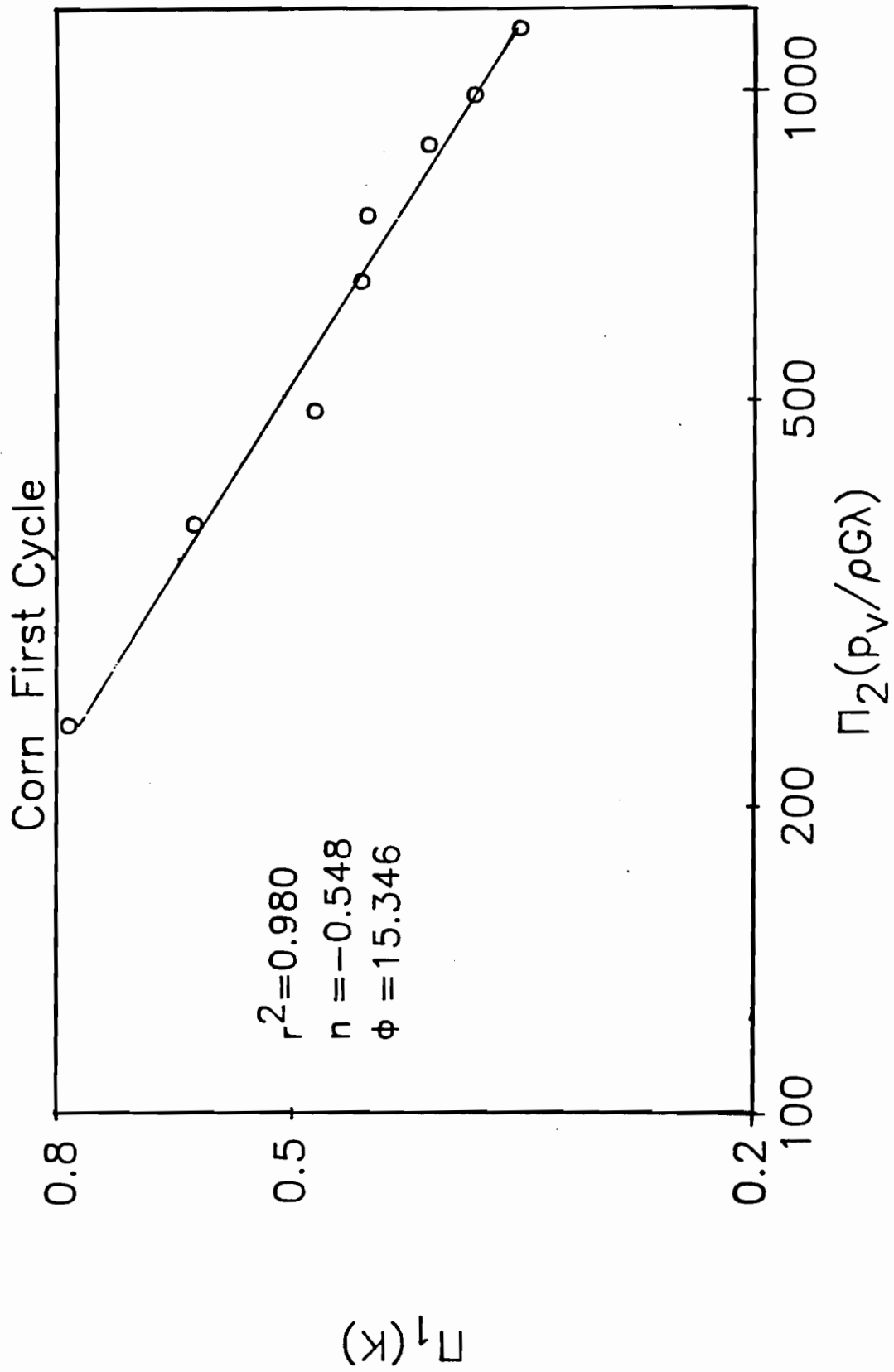
Figure 8.6.1.2. Log-log plot of Π_1 versus Π_2 for first loading cycle of corn
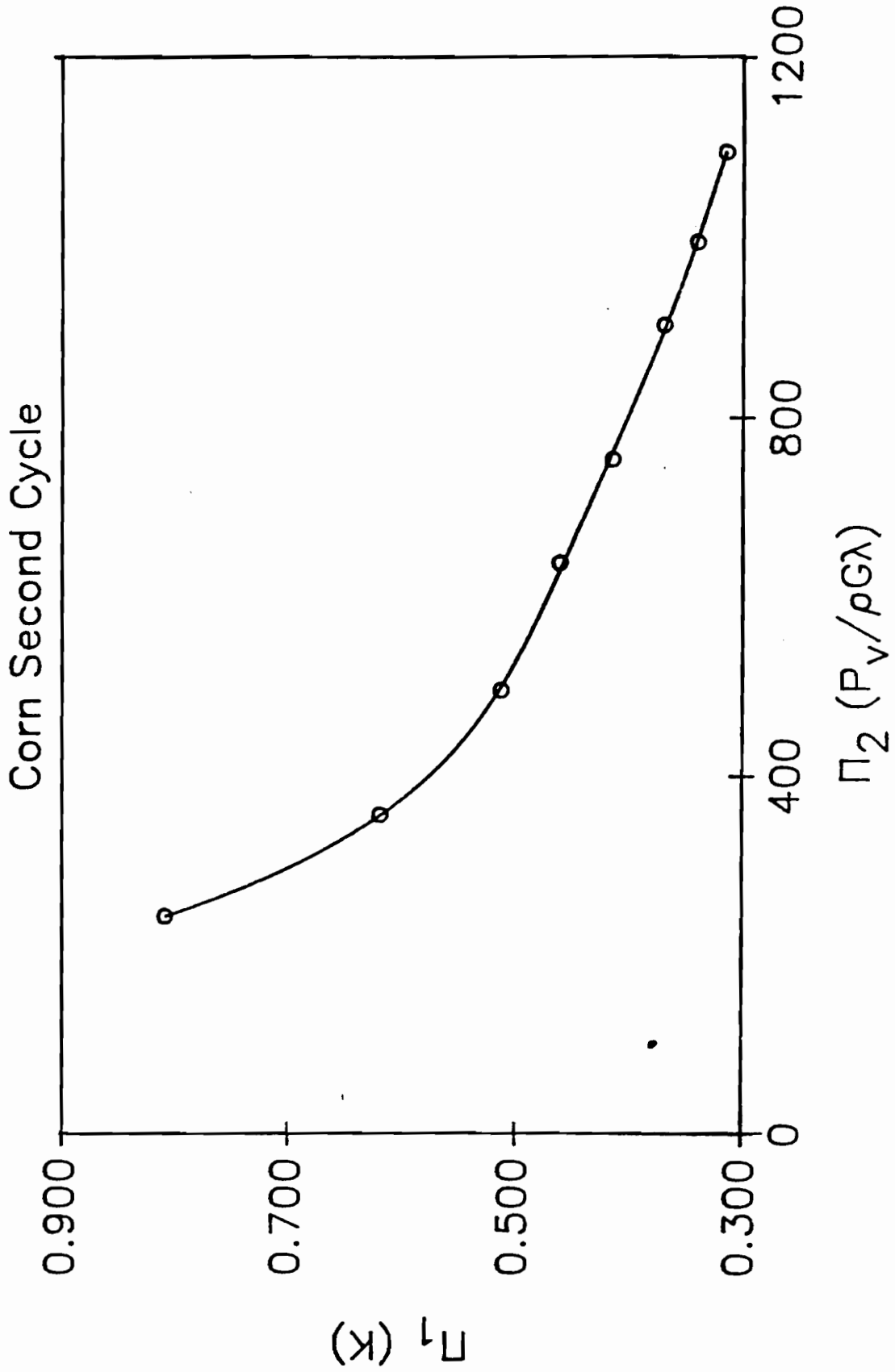
Figure 8.6.2.1.   Linear plot of Π_1 versus Π_2 for second loading cycle of corn
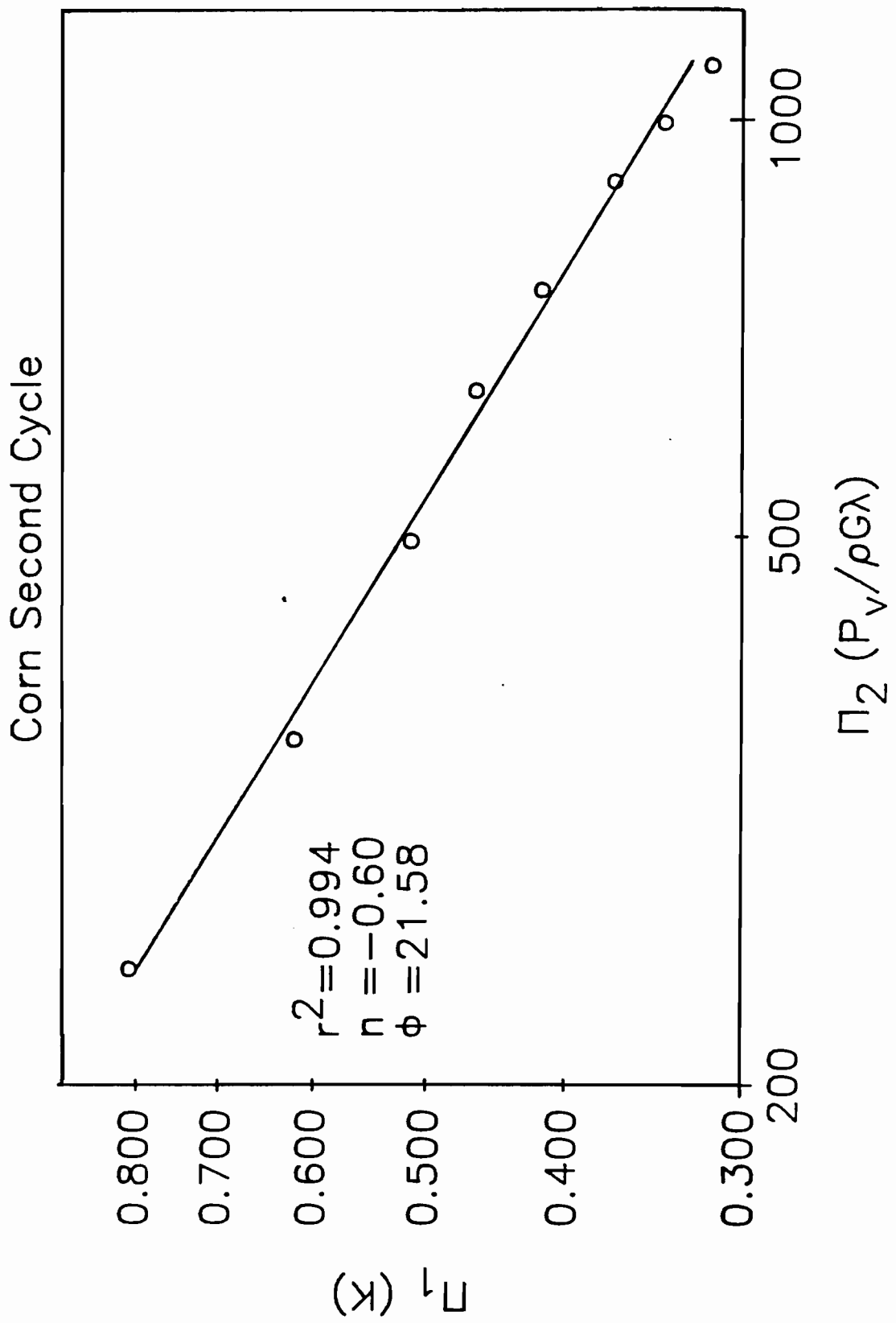
Figure 8.6.2.2.   Log-log plot of Π_1 versus Π_2 for second loading cycle of corn

Corn Second Cycle

$r^2 = 0.994$
$n = -0.60$
$\phi = 21.58$

Π_1 (K)

Π_2 ($P_v/\rho G \lambda$)
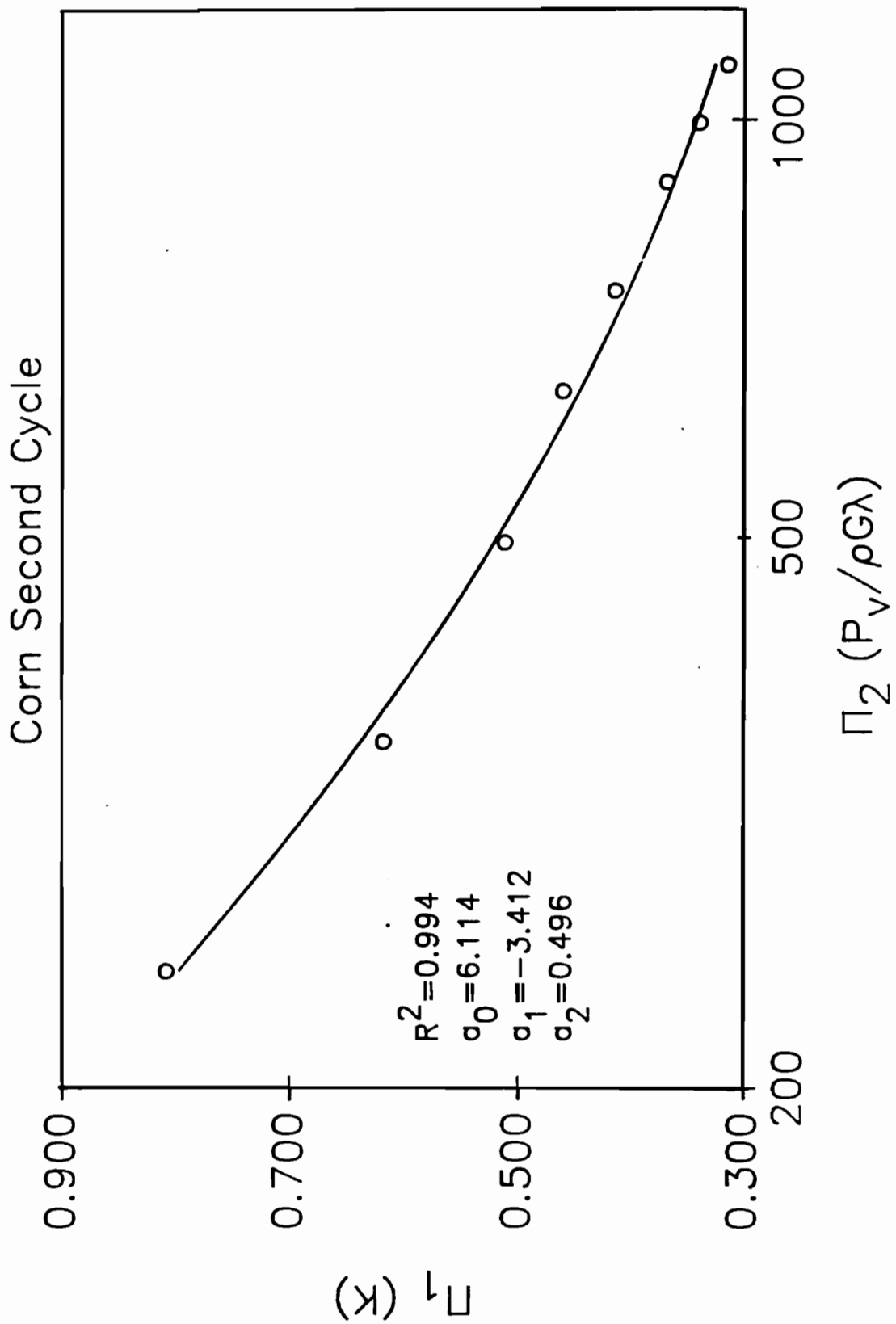
Figure 8.6.2.3. Semi-log plot of Π_1 versus Π_2 for second loading cycle of corn
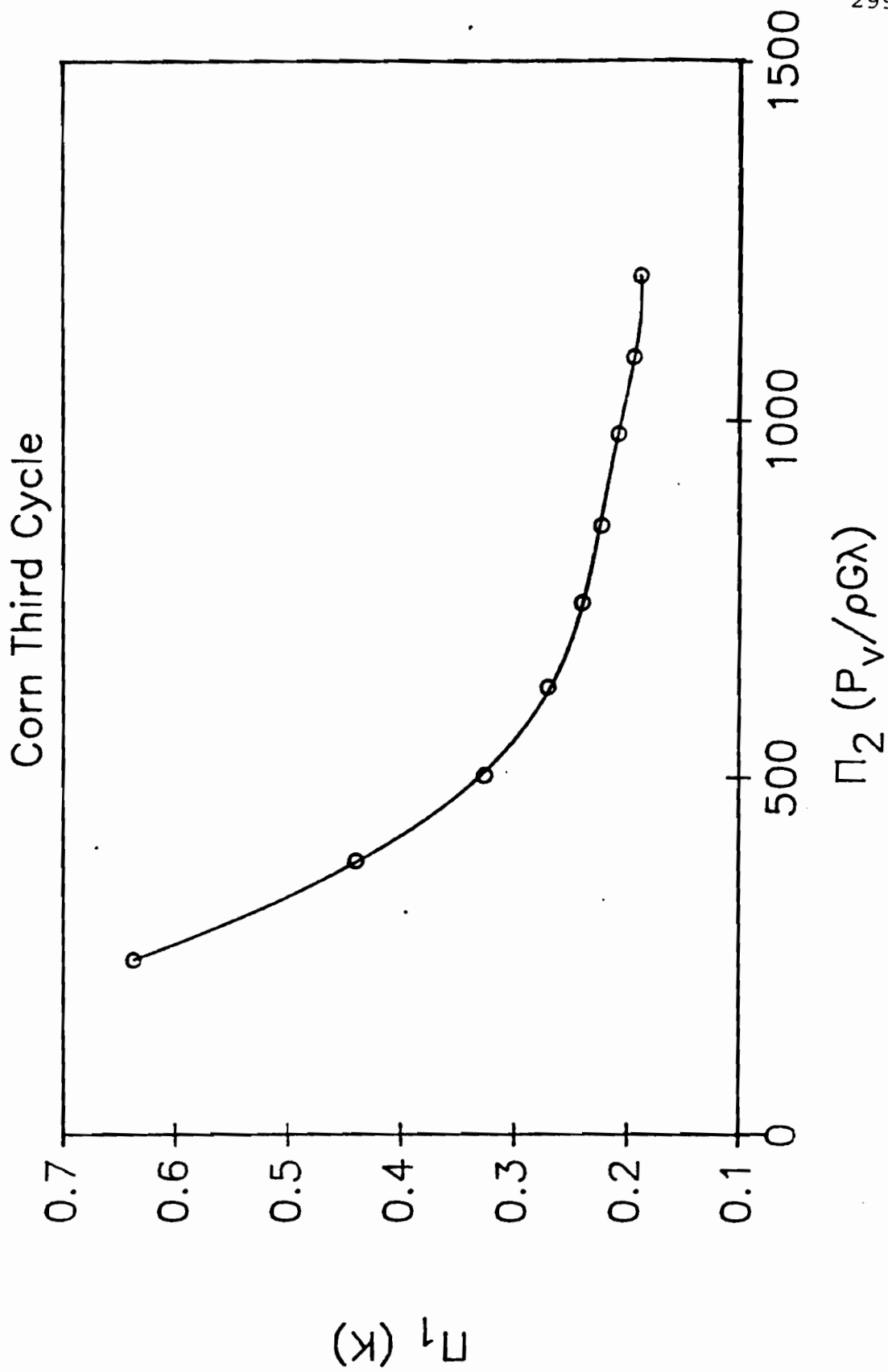
Figure 8.6.3.1. Linear plot of Π_1 versus Π_2 for third loading cycle of corn
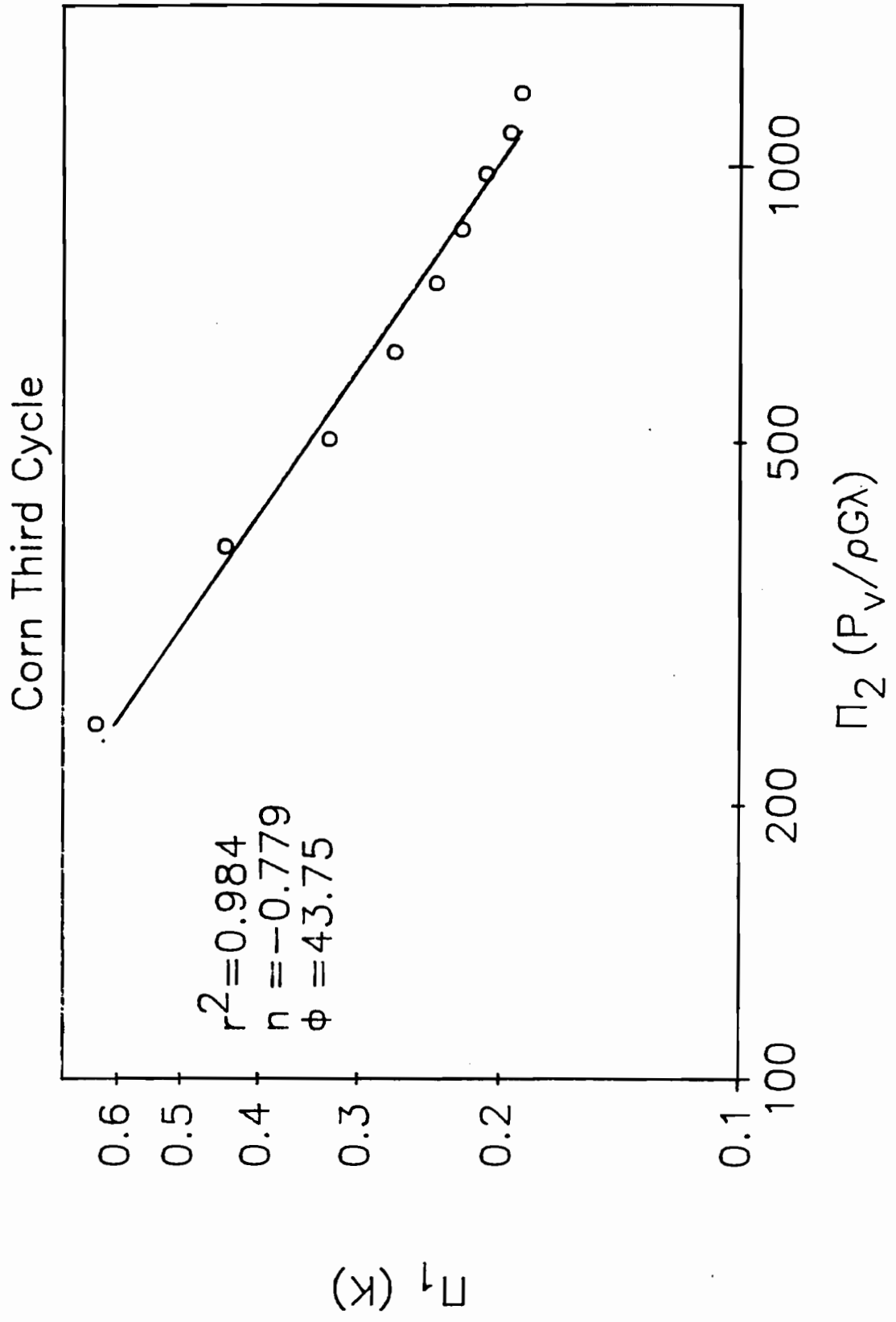
Figure 8.6.3.2. Log-log plot of Π_1 versus Π_2 for third loading cycle of corn
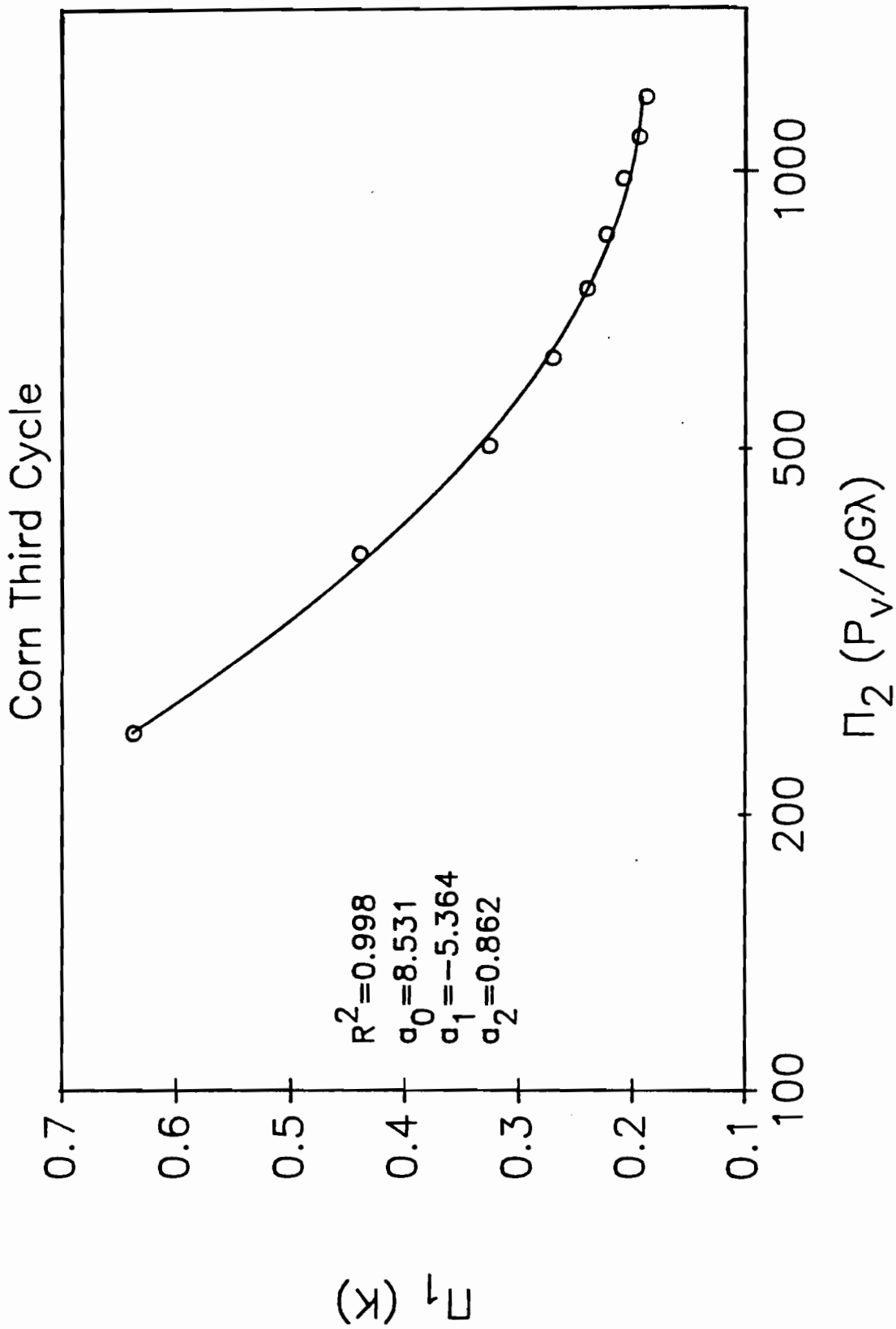
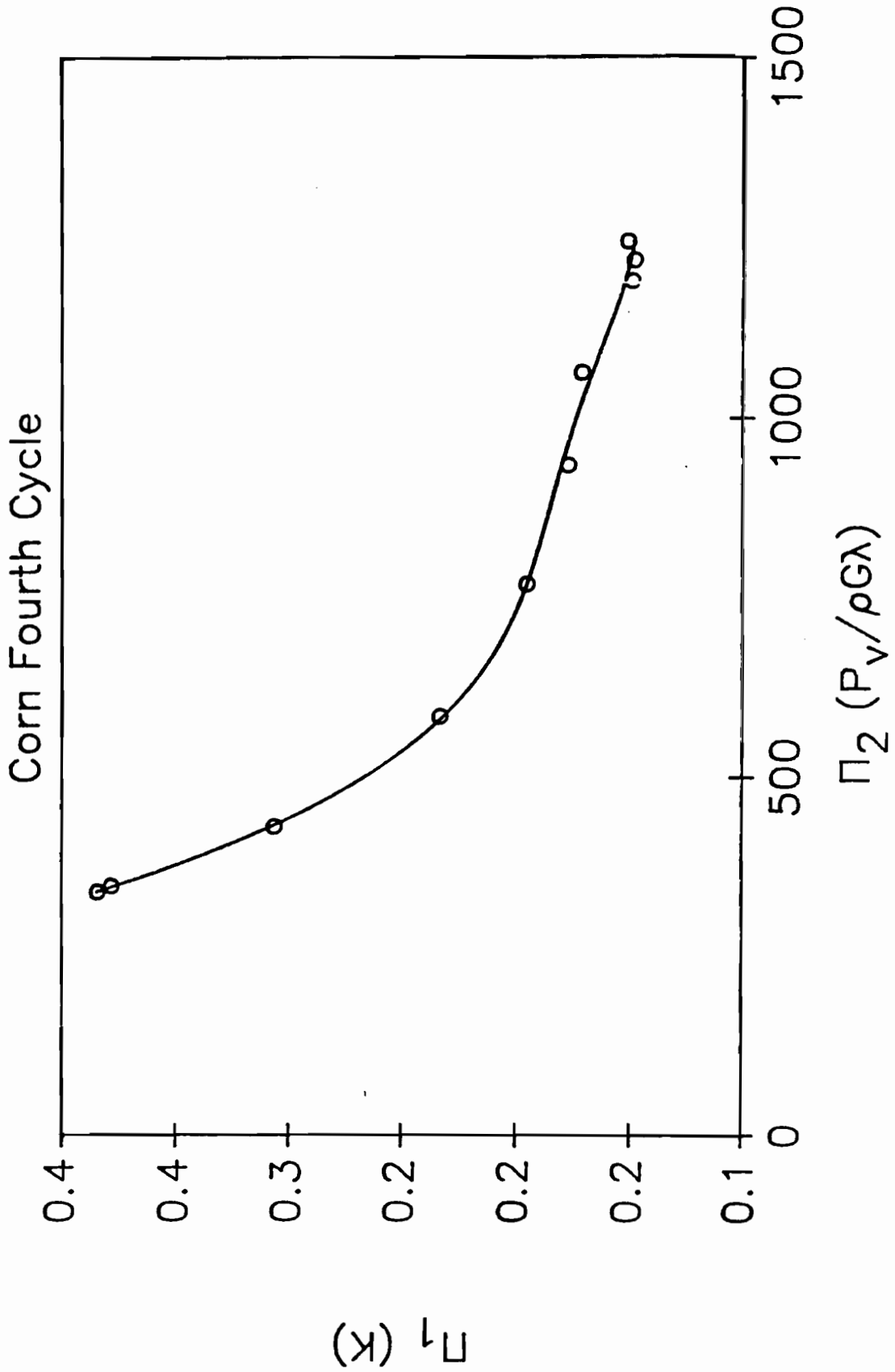Figure 8.6.3.3.   Semi-log plot of Π_1 versus Π_2 for third loading cycle of corn

Corn Third Cycle

$R^2 = 0.998$
$a_0 = 8.531$
$a_1 = -5.364$
$a_2 = 0.862$

Π_2 $(P_v/\rho G\lambda)$

Π_1 (K)

Corn Fourth Cycle

Π_2 $(P_V/\rho G\lambda)$

Π_1 (K)

Figure 8.6.4.1. Linear plot of Π_1 versus Π_2 for fourth loading cycle of corn
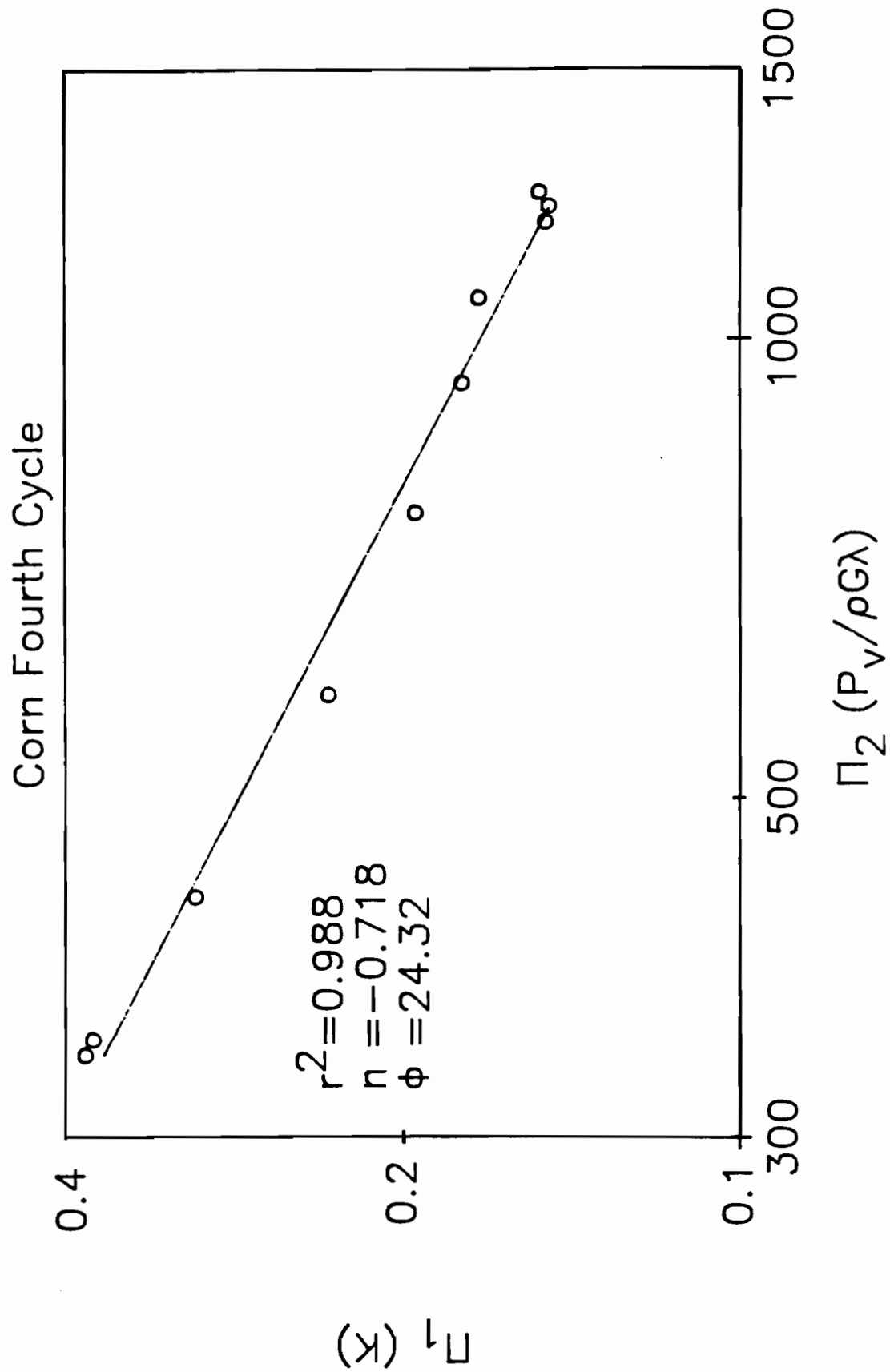
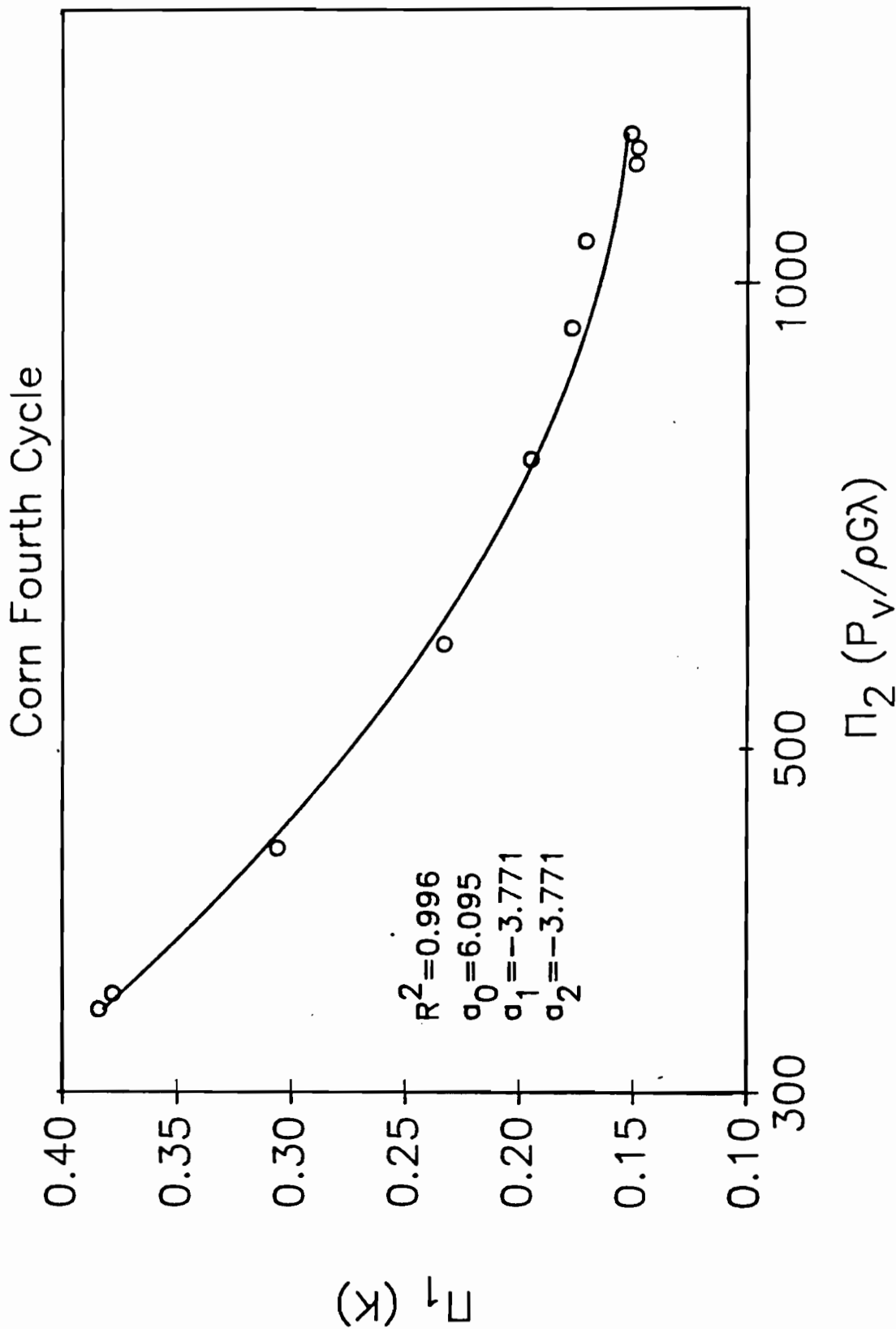Figure 8.6.4.2. Log-log plot of Π_1 versus Π_2 for fourth loading cycle of corn

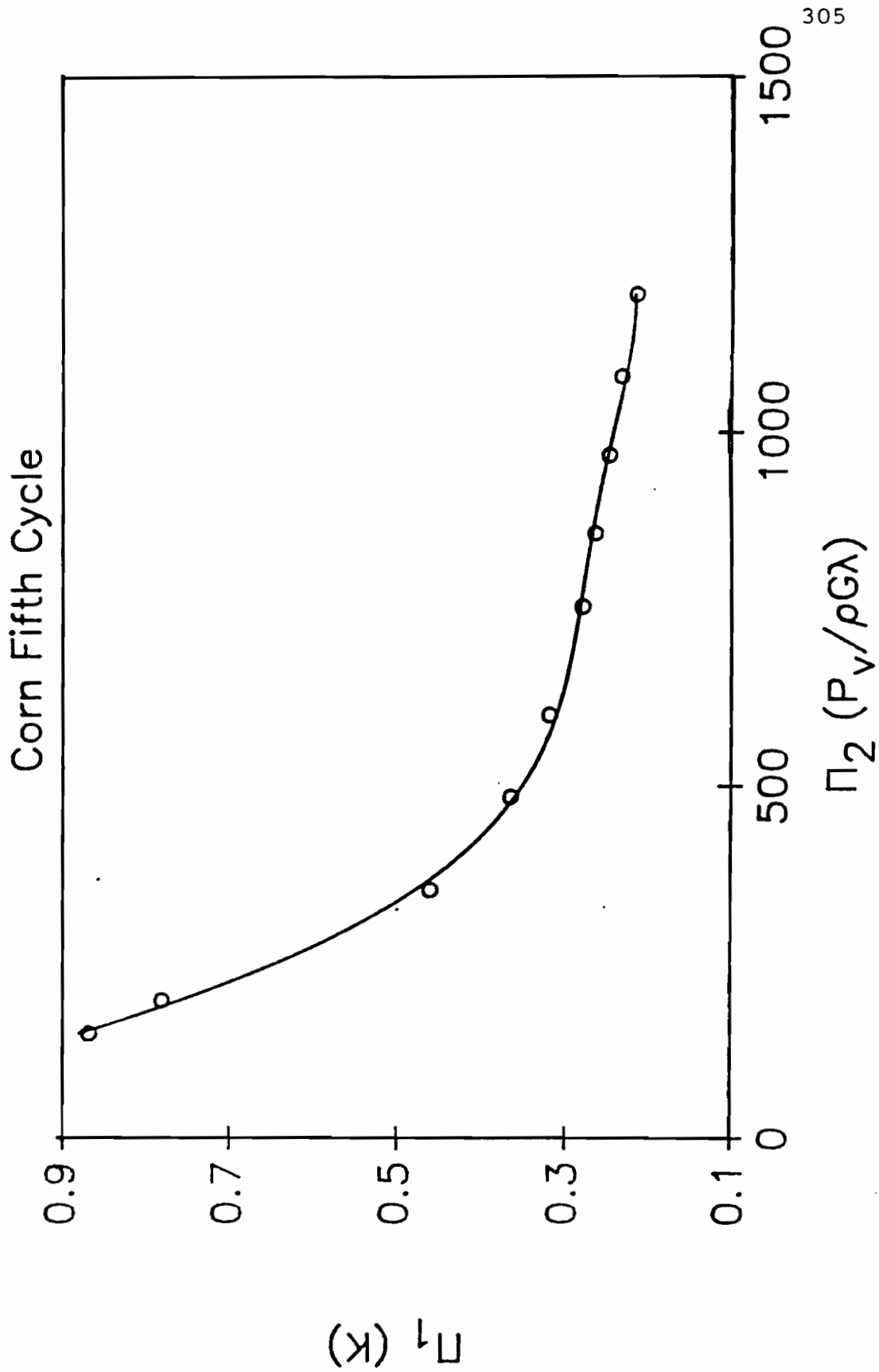Figure 8.6.4.3. Semi-log plot of Π_1 versus Π_2 for fourth loading cycle of corn

The plot is titled "Corn Fourth Cycle" with axes Π_1 (K) versus Π_2 ($P_v/\rho G\lambda$).

$R^2 = 0.996$
$a_0 = 6.095$
$a_1 = -3.771$
$a_2 = -3.771$

Figure 8.6.5.1.　Linear plot of Π_1 versus Π_2 for fifth loading cycle of corn
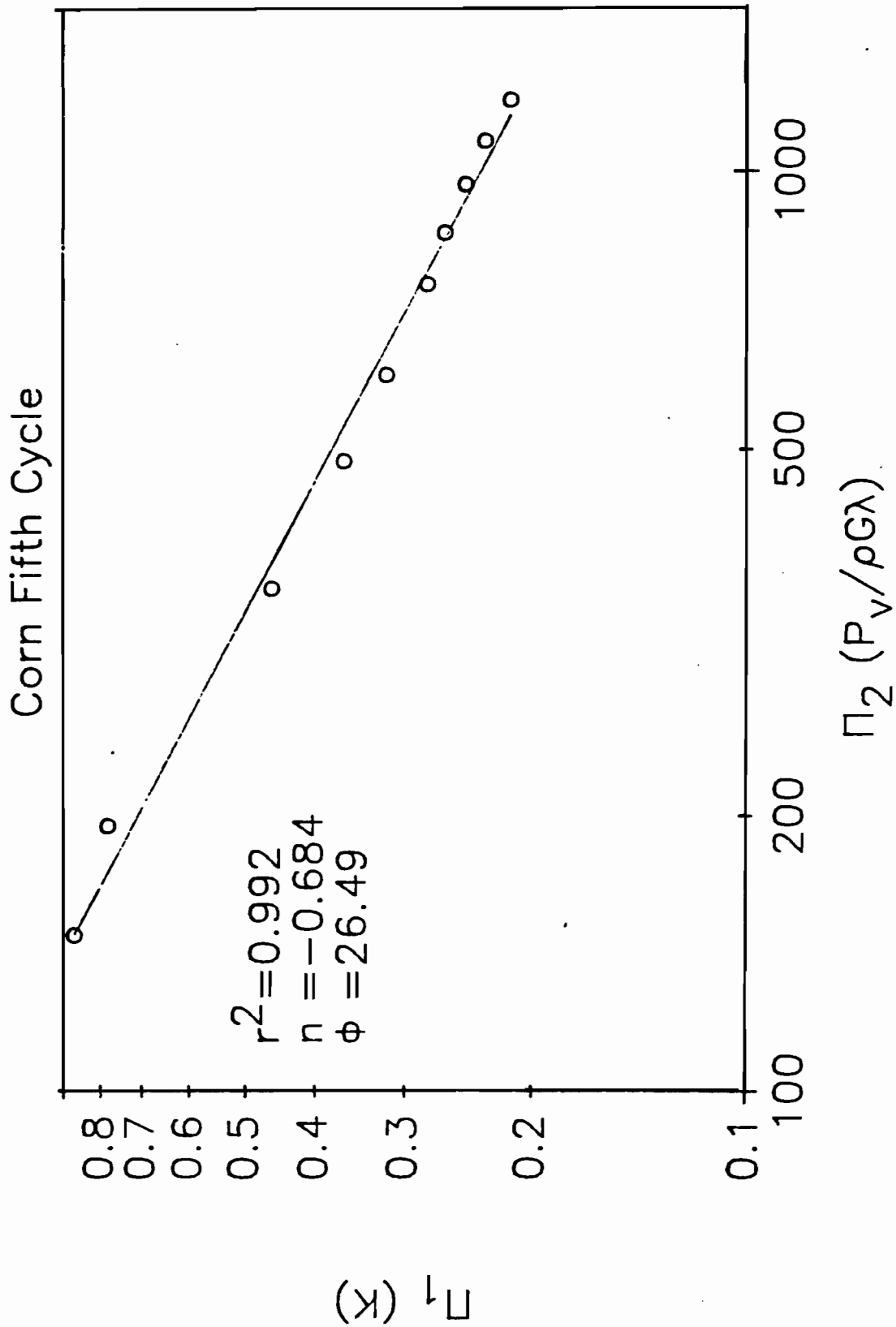
Figure 8.6.5.2. Log-log plot of Π_1 versus Π_2 for fifth loading cycle of corn
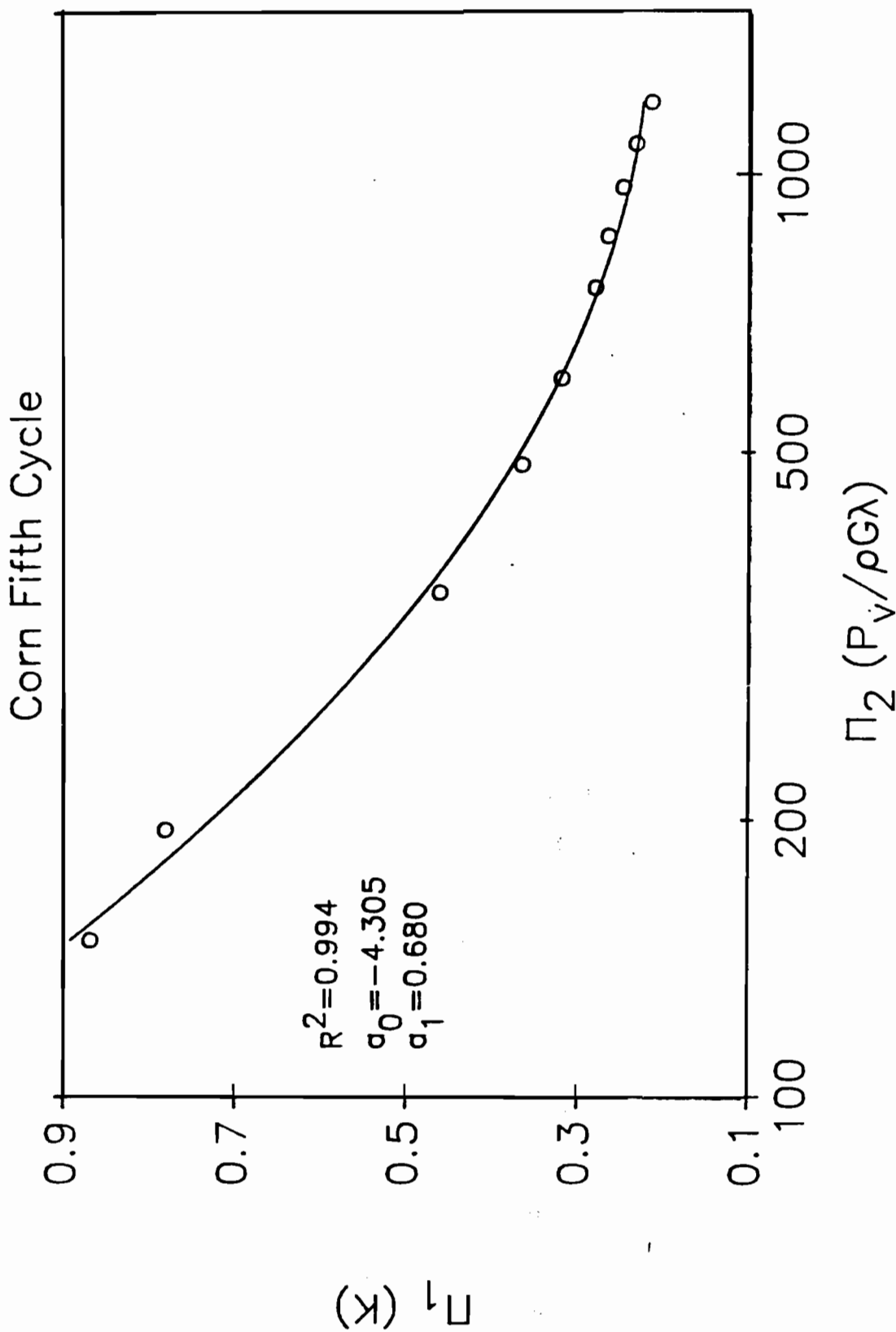
Figure 8.6.5.3. Semi-log plot of Π_1 versus Π_2 for fifth loading cycle of corn